Reactive hydro- and chlorocarbons in the troposphere and lower stratosphere

Sources, distributions, and chemical impact

Reactieve kool- en chloorkoolwaterstoffen in de troposfeer en lagere stratosfeer

bronnen, verdeling en chemische invloed

(met een samenvatting in het Nederlands)

Proefschrift ter verkrijging van de graad van doctor aan de Universiteit Utrecht op gezag van de Rector magnificus, Prof. Dr. W. H. Gispen, ingevolge het besluit van het College voor Promoties in het openbaar te verdedigen op maandag 15 september 2003 des middags te 12:45 uur.

door

Hubertus Augustinus Scheeren

geboren op 12 maart 1966, te Leiden

Promotor: Prof. Dr. J. Lelieveld
Max-Planck-Institut für Chemie, Mainz, Duitsland

Co-promotor: Dr. G. -J. Roelofs
Instituut voor Marien en Atmosferisch onderzoek Utrecht
Faculteit Natuur- en Sterrenkunde, Universiteit Utrecht

Paranimfen: Laurens Ganzeveld
Francesco Spada

Druk / Printed by: Ponsen & Looijen BV, Wageningen.
ISBN 90-393-3466-8

***Omslag**: Overzicht van de campagnestickers van STREAM, LBA/CLAIRE, INDOEX en MINOS.*
Cover: Overview of the campaign stickers of STREAM, LBA/CLAIRE, INDOEX and MINOS.

Stellingen

1) De concentraties van kortlevende koolwaterstoffen en aceton in de lagere stratosfeer zijn gedurende de zomer een factor twee of meer hoger dan tijdens de winter door frequentere en intensievere uitwisseling met de troposfeer (Hoofdstuk 2).

2) Verhoogde concentraties van reactieve chloor- en koolwaterstoffen in vervuilde luchtmassa's uit India en Zuidoost Azië zijn het gevolg van het wijdverbreide gebruik van biomassa (hout, koemest, en landbouwafval) in plaats van fossiele brandstoffen in huishoudens en kleine industrie (Hoofdstuk 3 en 4).

3) Als gevolg van de moessoncirculatie wordt de hogere troposfeer boven het oostelijk Middenlandse-Zeegebied gedurende de zomer in sterke mate beïnvloed door emissies uit India en Zuidoost Azië (Hoofdstuk 4).

4) De concentraties van HFC-134a, afkomstig van lekkende autoairco's, zijn duidelijk lager in vervuilde lucht uit Azië dan in Noord-Amerikaanse lucht. Hieruit blijkt dat HFC-134a een geschikte indicator is voor vervuiling van Westerse origine (Hoofdstuk 4).

5) De rol van fotochemisch ozon als broeikasgas zal naar verwachting deze eeuw veel belangrijker worden door de toename van het gebruik van fossiel brandstoffen in Azië (Hoofdstuk 4).

6) Op mondiale schaal vormen tropische bossen de belangrijkste natuurlijke bron van organische chloorverbindingen in de atmosfeer (Hoofdstuk 5).

7) Helaas is de roemruchte roman "Onder professoren" van W.F. Hermans anno 2003 nog steeds actueel met betrekking tot de perikelen rond het benoemen van een nieuwe hoogleraar.

8) In het Nederlandse klimaatonderzoek is er vaak sprake van onvoldoende "chemie" tussen atmosferisch fysici and chemici.

9) Om de Nederlandse "Kenniseconomie" op de rails te zetten zou de overheid minder geld aan de "Betuwe- en Hogesnelheidslijn" moeten uitgeven en meer aan wetenschappelijk onderzoek.

10) Naast de bekende wijsheid "meten is weten", blijkt in de praktijkdat "meten is zweten" !

Stellingen behorend bij het proefschrift "Reactive hydro- and chlorocarbons in the troposfeer and lower stratosfeer" door Bert Scheeren

Content

1 Introduction

This thesis addresses reactive C_2 – C_7 non-methane hydrocarbons (NMHC) and C_1 – C_2 chlorocarbons with atmospheric lifetimes of a few hours up to about a year. These compounds are part of a wide range of species referred to as trace gases comprising much less than 1% of the atmosphere. Although present at relatively low quantities in our atmosphere (10^{-12} – 10^{-9} mol mol^{-1} of air), they play a key role in atmospheric photochemistry. The oxidation of NMHC plays a dominant role in the formation of ozone in the troposphere, for example, while in the stratosphere the photolysis of (mainly anthropogenic) chlorocarbons leads to enhanced ozone depletion. In spite of their important role, however, their global source and sinks budgets are not yet completely understood. Here an overview is given of the role of NMHC and halocarbons in atmospheric processes. Firstly, the main natural and anthropogenic sources to the atmosphere are described based on emissions estimates for pre-industrial, present, and future conditions. Secondly, the main mechanisms of atmospheric trace gas transport are introduced. The NMHC and chlorocarbon measurement method is introduced, which is described in greater detail in the Appendix. Finally, the research aims and the outline of this thesis are presented.

1.1 Hydrocarbons in the atmosphere

The most abundant hydrocarbon in the atmosphere is methane, CH_4, with a mean global atmospheric concentration of 1.7 μmol mol^{-1} (or 1.7 ppmv = part per million by volume). There are many sources of methane, with the most important being the production by anaerobic bacteria in natural wetlands, rice paddies and domestic ruminants (e.g. cows), and oil and gas production [*Houweling et al.*, 1999]. Methane has a lifetime of about 8 yrs in the atmosphere, before it is oxidized to carbon monoxide (CO) and ultimately to carbon dioxide (CO_2). Non-methane hydrocarbons (NMHC) denote basically all C_nH_m species with a carbon number of two or more, which includes the group of alkanes (e.g., ethane: CH_3-CH_3), alkenes (e.g., ethene: CH_2=CH_2), alkynes (e.g., ethyne or acetylene: CH≡CH) as well as aromatic compounds (e.g., benzene: C_6H_6) and terpenes from higher plants (e.g., isoprene (2-methyl-1,3,-butadiene): CH_2=CH-CCH_3=CH_2). Although typical concentrations of these species are relatively low, between10^{-12} – 10^{-9} mol mol^{-1}, compared to methane, due to their relatively high reactivity they play a key role in global-scale atmospheric chemistry, notably in the formation of tropospheric ozone (O_3) and the oxidative capacity of the atmosphere [e.g., *Houweling et al.*, 1998; *Roelofs and Lelieveld*, 2000]. Their role in atmospheric chemistry will be explained in detail later. In addition, condensation of low-volatile hydrocarbons and aromatic compounds, and their oxidation products, contributes to organic particle formation in the atmosphere. Clearly, improving our knowledge about the NMHC source strengths and their global atmospheric distribution is essential to understand present and predict future atmospheric ozone levels and the role of organic aerosols.

NMHC have a large number of natural and (mostly fossil fuel related) anthropogenic

sources, of which the latter are reasonably well quantified. NMHC have atmospheric lifetimes ranging from hours (e.g. isoprene) to months (e.g. ethane). Their main removal from the atmosphere is through oxidation, which forms secondary compounds such aldehydes (e.g. formaldehyde: CH_2=O), ketones (e.g. acetone: CH_3C=OCH_3) and alcohols (e.g. methanol: CH_3OH) and eventually CO, which itself is oxidized to CO_2. Species like methanol and acetone are observed at the ppbv level throughout the troposphere. In addition to hydrocarbon oxidation, they have large natural sources (vegetation and oceans) as well, and are emitted by biomass burning [*Singh et al.*, 1995; *Jacob et al.*, 2002].

In the next section, the oxidation of NMHC will be treated in detail. Similar as CH_4, atmospheric levels of NMHC, CO and nitrogen oxides (NO_x = NO and NO_2) have increased strongly over the past 15O years mainly due to human activities involving fossil fuels [*Van Aardenne*, 2001]. The main sources of NO_x are fossil fuel and biomass burning related to anthropogenic activities (e.g., biofuel burning, agricultural waste burning) [*Lelieveld and Dentener*, 2000]. Hence, NO_x emissions are often associated with NMHC emissions. In Table 1.1, we present an overview of estimated global annual sources of CO and NMHC for pre-industrial (1860), recent (1993) and future times (2025).

Table 1.1: Overview of estimated annual sources of CO and NMHC in the pre-industrial (1860), Recent (1993) and Future (2025) Period in Tg (10^{12} g) yr^{-1}.

	CO[a], Tg yr^{-1}			NMHC[a], Tg yr^{-1}		
Source category	1860	1993	2025	1860	1993	2025
Energy use						
fossil fuel comb.	2	112	142	1	37	67
fossil fuel prod.				0	26	65
biofuel comb.	22	83	83	8	32	32
aircraft						
Industry	6	15	18	0	56	102
Biomass burning						
savannah burning	24	77	95	5	15	17
trop. deforestation	8	48	71	1	8	12
temperate wildfires	90	46	50	7	4	4
agri. waste burning	36	89	156	5	16	19
Vegetation/soils	115	115	115	403	403	403
All Natural	205	161	165	410	407	407
All Anthropogenic	98	424	565	20	190	314

[a] CO and NMHC data are from *Van Aardenne et al.* [2001].

From Table 1.1 we find that present day anthropogenic sources of NMHC are for ~80% determined by emissions related to the production and use of fossil fuels. Natural emissions, dominated by isoprene and terpenes from vegetation [*Guenther et al.*, 1995], are

estimated to be twice as high as anthropogenic emissions. Isoprene is the most important building block for the formation of plant terpenes and is emitted from a wide variety of vegetation types during day. The emission of isoprene and terpenes strongly depends on temperature. Hence, emissions are highest in the evergreen tropics where isoprene and terpenes are the dominant emitted hydrocarbon species [*Guenther et al.*, 1995].

While natural NMHC emissions are assumed to have remained approximately unchanged over the past 150 years (nobody really knows), it appears that anthropogenic emissions of NMHC have increased almost by a factor of 10 from 20 to 190 Tg yr^{-1} (Table 1.1). In the pre-industrial period, the largest anthropogenic fraction (65%) of NMHC was accounted for by the burning of biofuels and agricultural waste. These emissions increased by almost a factor of four to the present time in concurrence with the strong population increase and consequent biofuel consumption in Africa and Asia. In the “developed” world the increase of anthropogenic NMHC appears to be entirely due to the strong increase in the production and use of fossil fuels. The future emission estimates are based on the Intergovernmental Panel on Climate Change moderate growth scenario (IS92a) scaled to the year 2025, assuming a world population of 8.4 billion. Hence, the rapid economic development and population growth in Asia (notably India and China) is expected to largely account for increases in fossil fuel emissions in the next 25 years.

In this thesis, we analyze measurements of NMHC among other trace gases in the atmosphere at altitudes up to 13 km. The altitude range explored covers different atmospheric layers, determined by the temperature profile of the atmosphere. The lowest part of the atmosphere, the troposphere, extends from the surface to about 10 ± 2 km altitude at midlatitudes and to 16 ± 1 km in the tropics. In the troposphere the temperature decreases with altitude from an average of 288 K at the earth’s surface to ~210 – 220 K at the tropopause. The consequence of the decreasing temperature with altitude is that the troposphere is unstable, which promotes vertical mixing. The troposphere itself can be subdivided in the planetary Boundary Layer (BL), extending from the earth’s surface to 1 – 2 km, and the free troposphere above. The BL represents the lowest part of the atmosphere were most trace gas emissions take place and were turbulence induced by daytime solar heating of earth’s surface is the main mixing process. At night, radiative cooling of the surface leads to a stably stratified BL of only 200 – 300 m thick, which strongly suppresses vertical mixing.

The layer above the troposphere, the stratosphere, extends to about 50 km altitude. Here most of the atmospheric ozone is contained, hence referred to as the “ozone layer”. The absorption of solar radiation by stratospheric ozone leads to a temperature increase as a function of altitude causing a stable stratification, which inhibits vertical mixing. The transition between the troposphere and the stratosphere is called the tropopause. The positive temperature gradient in the stratosphere (temperature inversion) forms a barrier for vertical mixing across the tropopause. Mechanisms of vertical mixing in the troposphere and exchange between the troposphere and stratosphere are described in more detail in Section 1.3.

1.1.1 Removal of hydrocarbons

The gas phase degradation of NMHC is initiated by the reaction with OH radicals, with NO_3 radicals, with O_3 or direct photolysis [e.g. *Jenkin et al.,* 1997; *Atkinson,* 2000], depending on the reactivity of the NMHC species and the ambient conditions (e.g., tropospheric or stratospheric). In the troposphere, only the alkenes are reactive enough to be significantly oxidized by O_3 and NO_3, while photolysis is mainly limited to the products of hydrocarbon oxidation like acetone and organic nitrates.

The most important atmospheric removal mechanism for methane, hydrocarbons, reactive chlorocarbons, as well as CO is reaction with the OH radical. The formation of OH is governed by the photo-dissociation of O_3 in the presence of water vapor [*Levy*, 1971]. The O_3 photolysis of O_3 in the ultraviolet at wavelengths (λ) $\leq$ 330 nm generates the electronically excited $O(^1D)$ atom, which can react with water vapor to form OH:

$$O_3 + h\nu\ (\lambda \leq 330\ \text{nm}) \rightarrow O(^1D) + O_2 \quad (1.1)$$

$$O(^1D) + H_2O \rightarrow 2\ OH \quad (1.2)$$

where $h\nu$ is the product of the Planck constant and the frequency of light at wavelength λ. Although the concentration of the highly reactive OH species appears to be extremely low, being about ~10^6 molecule cm^{-3}, it is the primary oxidant in the troposphere. Hence, changes in the tropospheric ozone concentration influence the oxidative power of the atmosphere. Until the 1950s, it was assumed that the abundance of tropospheric ozone is controlled by exchange between the troposphere and stratosphere [e.g.; *Junge*, 1962]. However, although downward transport from the stratospheric reservoir is important for ensuring a background level of ozone in the troposphere, it cannot explain the high ozone levels, especially those observed over polluted regions. In the 1960s, it was shown that the oxidation of hydrocarbons and CO over polluted urban regions during summer generates O_3 as a by-product [*Haagen-Smit and Fox*, 1956; *Leighton*, 1961].

Photochemical O_3 formation is catalyzed by nitrogen oxides (NO_x), involving organic peroxy (RO_2) and oxy (RO) radicals, and the hydroperoxy radical (HO_2). The main sources of NO_x are fossil fuel and biomass burning related to anthropogenic activities (e.g., biofuel burning, agricultural waste burning) [e.g. *Lelieveld and Dentener*, 2000]. Hence, NO_x emissions are often associated with NMHC and CO emissions. The main hydrocarbon (RH) oxidation sequence in the atmosphere is:

$$RH + OH\ (+O_2) \rightarrow RO_2 + H_2O \quad (1.3)$$

$$RO_2 + NO\ (+O_2) \rightarrow NO_2 + HO_2 + R'CHO \quad (1.4)$$

$$HO_2 + NO \rightarrow NO_2 + OH \quad (1.5)$$

$$2\ [NO_2 + h\nu\ (+O_2) \rightarrow NO + O_3] \quad (\lambda < 424\ \text{nm}) \quad (1.6)$$

$$\text{Net:}\quad RH + h\nu + 3\ O_2 \rightarrow 2\ O_3 + H_2O + R'CHO \quad (1.7)$$

O_3 is produced if NO is converted to NO_2 by reacting with species other than ozone (reaction 1.4 and 1.5). NO_2 can photolyze in the troposphere at wavelengths < 424 nm. The

generated $O(^3P)$ radical reacts with O_2 to produce O_3 (reaction 1.6). Since NO and the OH radical are regenerated, this mechanism forms a catalytic cycle, which is illustrated in Figure 1.1.

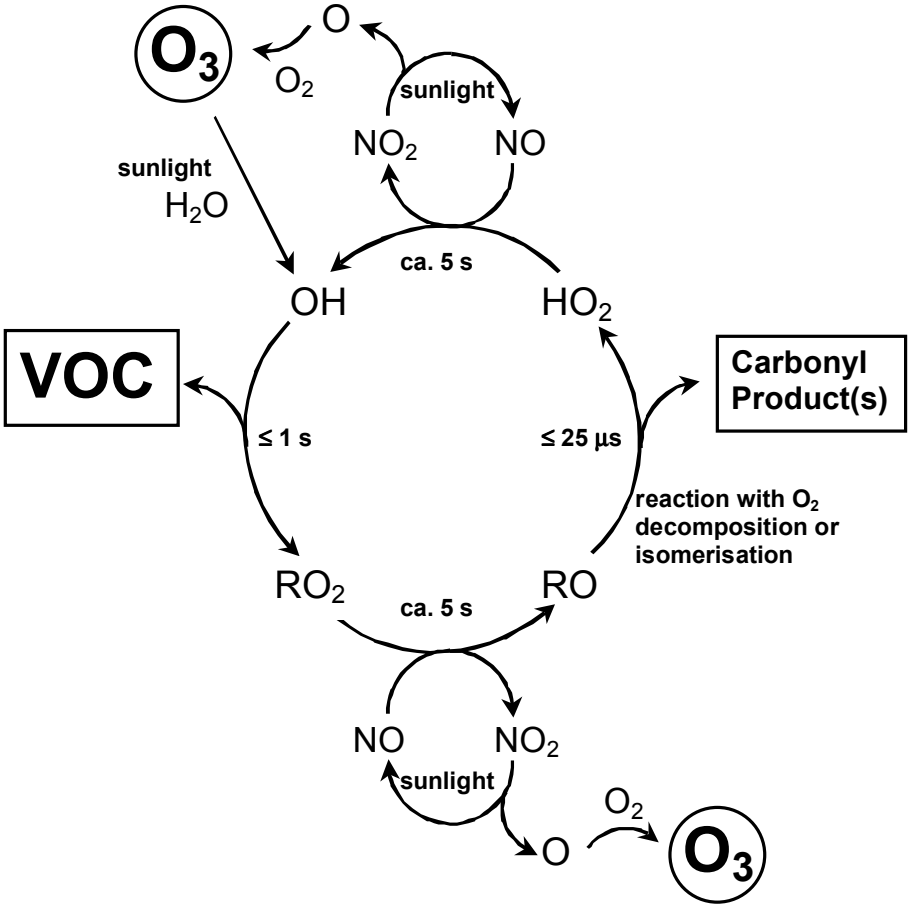

Figure 1.1: Ozone formation reaction cycle of the free radical (OH and HO_2) catalyzed Volatile Organic Carbon (VOC, includes NMHC species) oxidation. Included are typical boundary layer lifetimes of free radicals and organic peroxy (RO_2) and oxy radicals (RO).

Methane, carbon monoxide and NMHC emissions thus supply the "fuel" for tropospheric chemistry. Although methane is more abundant in the atmosphere than NMHC, due to their reactivity the O_3 yield per fully oxidized NHMC molecule, of around 10 – 14 molecules of O_3, is much higher than for CH_4, which is about 3.5 [*Lal et al*., 2000]. Hence, in a global chemistry-transport model study by *Houweling et al.* [1998] the present day contribution of NMHC to the tropospheric net-photochemical ozone production is estimated to be up to 40%.

In the absence of sufficient NO_x the HO_2 radicals formed destroy O_3, or they recombine

into peroxides (mainly H_2O_2), which are removed by wet and dry deposition. This is called a NO_x-limited regime, which appears to be the case in the pollution plume coming from Southern Asia [*Lelieveld et al.*, 2001]. Similarly, under conditions of high NO_x the O_3-production becomes dependent on the amount of available hydrocarbon species (hydrocarbon-limited regime). This regime has been observed in polluted air masses coming from North-America (*this thesis*). Both features are discussed in Chapter 4.

1.2 Organic chlorine in the atmosphere

Organic chlorine species are hydrocarbons with H atoms replaced by Cl, referred to as chlorocarbons. Although more than 200 different chlorinated gases have been identified in air, most of them are so short-lived or produced at such low quantities that they are not important for global atmospheric chemistry [*Khalil*, 1999]. Depending on their chemical reactivity, chlorine species are removed from the atmosphere by oxidation, hydrolysis in clouds and oceans, wet and dry deposition, or by photolysis in the stratosphere [*Khalil*, 1999]. Chlorocarbons have been classified according to their atmospheric lifetimes determined by their reactivity in the troposphere. Species with a tropospheric lifetime of about a year or less are considered to be “reactive” and do not contribute substantially to the stratospheric chlorine loading and ozone destruction. The group of reactive species includes the most abundant atmospheric chlorocarbons species with large natural sources, which are chloromethane (CH_3Cl), dichloromethane (CH_2Cl_2), and trichloromethane ($CHCl_3$), and tetrachloroethylene (C_2Cl_4) with mainly anthropogenic sources. Present atmospheric background concentrations are around 550 pptv, 20 pptv, 10 pptv, and 5 pptv, respectively. Similar to hydrocarbons, they are primarily removed in the troposphere by reaction with the OH radical. As an example, we show the first oxidation step of CH_3Cl by the OH radical:

$$CH_3Cl + OH\ (+O_2) \rightarrow CH_2ClO_2 + H_2O \qquad (1.8)$$

The lifetime of CH_3Cl is long enough to allow about 10% of tropospheric CH_3Cl to be transported to the stratosphere, where it contributes to the natural loading of stratospheric chlorine [*Khalil and Rasmussen*, 1999]. A detailed overview of estimated annual sources of CH_3Cl and $CHCl_3$ in the pre-industrial (1860), recent (1993) and future (2025) period is presented in Table 1.2. The present day global source distribution is based on results presented in Chapter 5 of this thesis and on data from *Lobert et al.* [1999] and has a significant degree of uncertainty. The pre-industrial and future scenarios are obviously highly uncertain and presented as hypothetical data. The pre-industrial and future data for the energy use, industrial processes and biomass burning source categories are extrapolated from the CO emission scenario in Table 1.1 taken from *Van Aardenne et al.* [2001]. Emissions for oceans, wetlands (includes salt marshes) were assumed constant for all periods considered. CH_3Cl emissions from tropical vegetation have been extrapolated on the basis of the FAO/FRA-2000 (FAO, 2000) global forest cover estimates and trends, assuming that the global tropical forest cover decreased by 0.74% yr^{-1} from the year 1940 onward.

Table 1.2: Overview of estimated annual sources of CH_3Cl and $CHCl_3$ in the pre-industrial (1860), Recent (1993) and Future (2025) Period.

	CH_3Cl[a], Gg yr^{-1}			$CHCl_3$[a], Gg yr^{-1}		
Source category	1860	2000	2025	1860	2000	2025
Energy use						
fossil fuel comb.	2	107	136			
fossil fuel prod.						
biofuel comb.	120	451	451	0.17	0.64	0.64
aircraft						
Industry	22	55	66	0	69	83
Biomass burning						
savannah burning	94	303	374	0.23	0.75	0.93
trop. deforestation	9	52	77	0.03	0.19	0.28
temperate wildfires	70	36	39	0.32	0.16	0.18
agri. waste burning	75	185	325	0.10	0.24	0.41
Vegetation/soils	3319	2085	1699	287	180	147
Oceans	477	477	477	360	360	360
Wetlands	211	211	211	24	24	24
All Natural	4077	2809	2426	672	565	564
All Anthropogenic	322	1154	1429	0.5	71	85

[a] The 2000 CH_3Cl and $CHCl_3$ data in Gg = 10^9 g are from Chapter 5 of this thesis and *Lobert et al.* [1999]. The pre-industrial and future CH_3Cl data for the Energy use, Industrial processes and Biomass burning source categories are interpolated using the CO emission scenario from Table 1.1 taken from *Van Aardenne et al.* [2001]. CH_3Cl and $CHCl_3$ emissions for oceans, wetlands (includes salt marshes) were assumed constant for all times. Emissions from tropical vegetation have been interpolated on basis of the FAO/FRA-2000 [*FAO*, 2000] global forest cover estimates and trends (we assumed that the tropical forest cover decreased by 0.74% yr^{-1} from the year 1940 onward).

Table 1.2 shows that the present-day anthropogenic fraction (includes anthropogenic biomass burning) of the annual emissions of CH_3Cl and $CHCl_3$ is of the order of 41% and 13%, respectively (based on Chapter 5 of this thesis). The anthropogenic contribution to annual emissions of CH_2Cl_2 is mainly from industrial activities corresponding to 70% of the total source of 840 Gg per year [*Keene et al.*, 1999]. It appears that emissions of CH_3Cl and $CHCl_3$ are dominated by natural processes. Estimates of future emissions point to an increasing role of anthropogenic emissions from biomass burning and industrial activities. The total CH_3Cl emission trend appears to be slightly negative because the increasing anthropogenic source is counter-balanced by a decreasing vegetation source. The prominent role of (tropical) vegetation as a source of chlorocarbons is investigated and discussed

in detail in Chapter 5 of this thesis.

Species with a lifetime between 1 and 10 years are moderately reactive such as the man-made species 1,1,1-trichloroethane (methyl chloroform, CH_3CCl_3) [*Khalil*, 1999]. Chlorine containing species with a lifetime longer than 10 years are considered to be long-lived, such as the chlorofluorocarbons (CFCs) CFC-11 (CCl_3F) and CFC-12 (CCl_2F_2). They are all man-made and have no significant reactivity in the troposphere. Instead, they are removed in the stratosphere by photo-dissociation. Because of their build-up in the atmosphere, the present-day atmospheric chlorine concentration, in particular in the stratosphere, is dominated by anthropogenic chlorine.

1.2.1 Role of organic chlorine in the stratosphere

The concentration of chlorine in the stratosphere due to natural chlorine species, such as CH_3Cl, is about 0.5 ppbv. Due to the use of CFCs and other anthropogenic halocarbons, this concentration increased to about 3 ppbv from the 1940s to the present. The most important CFCs are CFC-11 and CFC-12, which were used as propellants for spray cans, refrigerants, and blowing agents for the production of foams. Other man-made chlorine species such as methyl chloroform and tetrachloromethane (tetra, CCl_4) were mainly used as solvent and degreasing agent. In the 1970s it was discovered by *Molina and Rowland* [1974] and confirmed by others that these man-made halocarbons slowly photolyze in the upper stratosphere releasing additional chlorine radicals to the natural background. Chlorine radicals react with ozone to form ClO and O_2. Subsequently, ClO can react with an O radical to yield O_2 and recycle Cl, which can destroy another ozone molecule. Thus, following this catalytic loss cycle one Cl radical can potentially destroy up to 10^3 ozone molecules. The photolysis of CH_3Cl (and likewise CFCs) by ultraviolet light (at wavelengths of 185 – 210 nm) releases Cl radicals, which can destroy ozone in a catalytic reaction cycle such as:

$$CH_3Cl + h\nu \rightarrow CH_3 + Cl \quad (1.9)$$

$$Cl + O_3 \rightarrow ClO + O_2 \quad (1.10)$$

$$O_3 + h\nu \rightarrow O_2 + O \quad (1.11)$$

$$ClO + O \rightarrow Cl + O_2 \quad (1.12)$$

$$\text{Net:} \quad 2O_3 \rightarrow 3O_2 \quad (1.13)$$

The reaction cycle can be terminated by reaction of Cl with CH_4 forming the chlorine reservoir species HCl (among other species not discussed here). Inorganic chlorine in the form of HCl is the dominant chlorine species after CH_3Cl in the lower stratosphere present at concentrations up to 1 ppbv [*Khalil*, 1999].

The discovery of the Antarctic ozone hole by *Farman et al.* [1985] made clear that the increasing chlorine concentration due to emissions of man-made chlorine species has an enormous impact on the natural ozone balance in the stratosphere. Later it was discovered that the formation of a springtime polar ozone hole was driven by heterogeneous chemistry

on polar stratospheric clouds (ice clouds formed out of HNO_3 and water vapor) [e.g., *Solomon et al.*, 1986; *Crutzen and Arnold*, 1986]. This environmental threat has given rise to the "Montreal Protocol" in 1987, which regulates the emissions of ozone depleting substances (CFCs, tetra, methyl chloroform, and halons used as fire extinguishers). It was subsequently amended (London 1990, Copenhagen 1992, and Beijing 1999) to respond to the problem of a growing Antarctic ozone hole in the 1990s. An overview of present day anthropogenic chlorocarbons and CH_3Cl concentrations, their atmospheric lifetime and their contribution to stratospheric chlorine is given in Table 1.3.

Since the 1990s, the CFCs have been replaced by the hydrochlorofluorocarbons (HCFCs) HCFC-141b (CH_3CCl_2F) and HCFC-142b (CH_3CClF_2), and by the hydrofluorocarbon (HFCs) HCF-134a (CH_2FCF_3). These compounds include H atoms allowing their degradation in the troposphere by reaction with OH radicals, which prevent them to build-up in the stratosphere. At present, the concentrations of these new halocarbons are still increasing in the atmosphere, but they are to be phased out between 2030 and 2040. In Figure 1.2 the effect of the Montreal protocol on the global industrial production halocarbons is illustrated (upper panel). In addition, we show the global trend in the atmospheric CFC-11 and CFC-12 concentration (lower panel). Due to the long lifetime of these species and the slow mixing between the troposphere and the stratosphere CFC concentrations have only decreased slightly.

Table 1.3: Anthropogenic and natural chlorine species in the atmosphere.

	Atmospheric concentration[a] (pptv)	Atmospheric lifetime[b] (yr)	Contribution to stratospheric chlorine (%)
Man-made			
CFC-11 (CCl_3F)	270	50	25
CFC-12 (CCl_2F_2)	535	100	32
CF-113 ($C_2F_3Cl_3$)	80	90	7
HCFC-22 (CHF_2Cl)	120	11	4
CCl_4	100	42	12
CH_3CCl_3	~35[c]	5	3
Natural			
CH_3Cl	550	1.3	17

[a] Data from this work, *Krol et al.* [2003], and *Khalil* [1999].
[b] Atmospheric lifetime from *Khalil* [1999].
[c] Background concentration of the year 2001 (present day levels are lower).

In this thesis, special emphasis is given to measurements of reactive chlorocarbons to improve our knowledge on their global budgets, notably to reduce uncertainties and to better quantify the contribution of natural sources. Measurements of long-lived man-made chlorine species (notably CFC-11, CFC-12 and methyl chloroform) are being used as air mass tracers of anthropogenic activity for identifying the origin of air masses in the troposphere and lower stratosphere. In the next section, we give a short review of current knowledge regarding the biogenic formation and the role of reactive chlorocarbons.

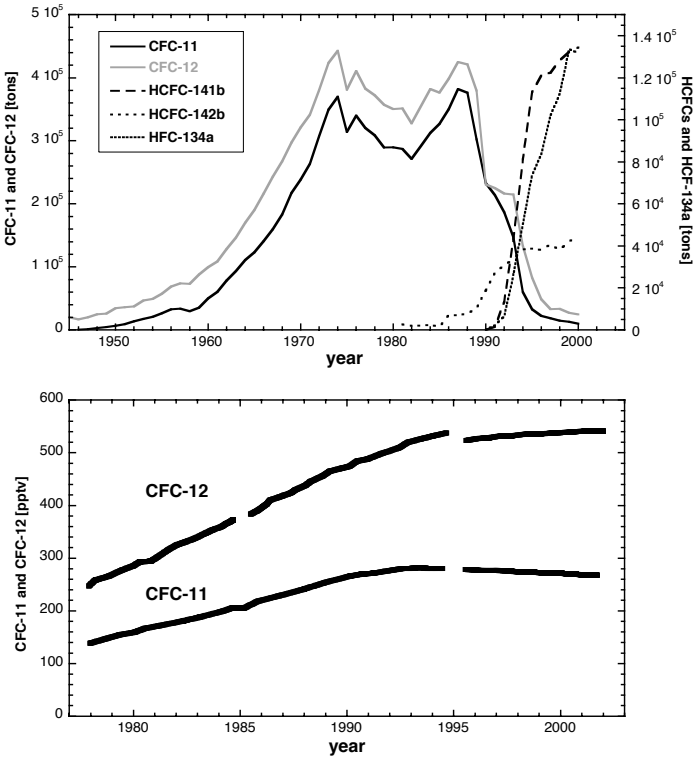

Figure 1.2: The upper panel shows the annual global halocarbon production (metric tons) (Data: *AFEAS* [2003]). The lower panel shows the global average concentrations of CFC-11 and CFC-12 between 1977 and 2001 (Data: *NOAA/CMDL* [2003]).

1.2.2 The biogenic formation of chlorocarbons

Although, thousands of biogenic chlorocarbons species have been identified thus far [*Gribble*, 2003], the natural contribution to atmospheric chlorine is dominated by the chlorinated methanes CH_3Cl, CH_2Cl_2 and $CHCl_3$. Hence, understanding the natural formation of CH_3Cl, CH_2Cl_2 and $CHCl_3$ is of importance for estimating their source strength and ecotoxicological impact [*Urhahn and Ballschmiter*, 1998]. Moreover, it might help us to gain insight in the consequences of global warming on the biogenic chlorine emissions. Here, we briefly review the metabolic role and biogenic formation processes of chlorocarbons in fungi and higher plants.

The utilization of CH_3Cl and other halomethanes (CH_3X, where X = Br or I) in the metabolism of polypore wood-rotting fungi has been intensively investigated and is reasonably well understood [*Harper*, 2000]. The emission of CH_3Cl from a higher plant (potato tubers) was first reported by *Varns* [1982] and later in a more extensive laboratory study by *Saini et al.* [1995] involving herbaceous species and halophytes (plants that prefer a salty soil). The

formation of natural halomethane in fungi and algae appears to be mainly through biomethylation of the respective Cl^-, Br^- and I^- anions by methyl sulfonium compounds [*Ballschmiter*, 2003]:

$$RS^+CH_3 \rightarrow SR + CH_3^+ \quad (R = C_nH_mO_pN_q) \tag{1.14}$$

$$CH_3^+ + Cl^- \text{ (or } Br^-, I^-) \rightarrow CH_3Cl \text{ (or } CH_3Br, CH_3I) \tag{1.15}$$

Similar to fungal metabolism, the study by *Saini et al.* [1995] indicated that higher plants can produce CH_3Cl and other halogenated methanes through a similar methyltransferase reaction. Knowing how plants can produce halogenated methanes, the question rises what could be their metabolic role.

There might be several reasons for fungi and plants to produce and/or release halomethanes. One reason for halomethane formation appears to be the elimination of excess halide ions, which are then released to the atmosphere [*Harper*, 2000]; however, this does not appear to be a prominent process. A study by *Saini et al.* [1995] has indicated that halophyte plants showed relatively low emissions compared to normal plants indicating that a high plant salinity is not an important factor. It is more likely that halomethanes play a more fundamental role in biosynthesis. *Harper et al.* [1981] found that CH_3Cl (as well as CH_3Br and CH_3I) serve as a methyl donor in the methylation of vital aromatic and aliphatic acids during the growth phase of fungus and possibly of higher plants as well:

$$CH_3Cl + RCOOH \xrightarrow{HCl} RCOOCH_3 \tag{1.16}$$

where R can be variety of alkyl or aryl groups.

If, however, halomethanes play a vital role in fungal and plants biosynthesis, it remains unclear why they are released to the atmosphere. It was observed that some wood-rotting fungi release significant quantities of CH_3Cl, whereas other fungi do not, despite their similar metabolic role in methyl transfer [*Harper*, 2000]. Clearly, emission of CH_3Cl is not primarily related to its use as metabolic intermediate. *Harper et al.* [1999] found that about 25% of biosynthesized CH_3Cl in potato tuber was metabolized in-situ rather than released, of which only 7% was fixed in a non-volatile form. This suggests that the majority of the produced CH_3Cl is lost to the atmosphere. Since CH_3Cl is very volatile at normal pressure and temperature conditions, and is poorly soluble in water, it is inevitable that fungi and plants lose CH_3Cl to the atmosphere during respiration.

A more exotic role of halomethane emissions by plants was suggested by *Hutchinson* [1971]. He proposed that the fungal production of halomethanes, notably bromomethane, might serve as insecticides. Another more likely role in fungal metabolism would be that the release of CH_3Cl is a mechanism to reduce the high methoxy content of lignin (in wood), by transferring it into volatile CH_3Cl [*Harper*, 2000]. Summarizing, the biochemical reason for a dominant role of CH_3Cl as methyl donor in fungi, as well as the metabolic role in higher plants remains to be determined [*Harper*, 2000].

In addition to biogenic formation, *Keppler et al.* [2000] have proposed an abiotic route for the formation of CH_3Cl and other halomethane by natural oxidation of organic matter in soils from the demethylation of methoxy phenol involving Fe^{3+} and Cl^- ions. Further

fieldwork is needed to assess the importance of this reaction as a soil source to the atmosphere. Recently, *Hamilton et al.* [2003] proposed another abiotic mechanism for CH_3Cl formation. They show that abiotic conversion of Cl^- to CH_3Cl occurs readily in decaying plant material, with the plant component pectin acting as methyl donor. Significant CH_3Cl emissions were observed from senescent and dead leaves at ambient temperatures between 30° to 40°C, while those emissions rose strongly when temperatures increased up to 350°C. They conclude that the abiotic methylation of Cl^- by pectin not only represents a source of atmospheric CH_3Cl during the weathering of plant material, but also may explain part of the CH_3Cl emissions previously observed in a variety of (tropical) terrestrial ecosystems and during the smoldering combustion of non-woody biomass.

While there are many studies quantifying the natural emission of $CHCl_3$ from forest soils [e.g., *Haselmann et al.*, 2000a, 2000b; *Hoekstra et al.*, 2001], the mechanisms of $CHCl_3$ formation in soils are not completely understood. Several pathways for $CHCl_3$ formation have been reported, such as biosynthesis by fungi or micro-organisms [*Haselmann et al.*, 2000b] and the excretion of exoenzymes like chloroperoxidases by soil organisms, which can lead to production of chlorinated organic compounds such as $CHCl_3$ [*Hoekstra et al.*, 1995]. Another mechanism to form $CHCl_3$ could be the decarboxylation of trichloroacetic acid (CCl_3CH_2COOH) present in conifer needles and rainwater [*Frank et al.*, 1994]. Finally, we mention that the mechanism behind the release of C_2Cl_4 from forest soils reported by *Hoekstra et al.* [2001] remains to be unknown to date.

1.3 Atmospheric tracer transport

In the previous section, we discussed the source distribution, source strength and removal processes of NMHC and chlorocarbons in the atmosphere. Another important aspect in the analysis of trace gas observations are the mechanisms and timescales of vertical and horizontal atmospheric transport, which distributes trace species away from their sources in the boundary layer. In the free troposphere, longer chemical lifetimes and high wind speeds can carry reactive pollutant species such as NMHC and NO_x over large distances, affecting the ozone budget far away from the sources. Here, a general overview is given of the main transport processes in the troposphere and stratosphere relevant for the distribution of trace gases.

1.3.1 Tropospheric transport

The general circulation of the atmosphere is driven by the temperature difference between the tropical regions (30°S – 30°N) and the poles, inducing a continuous energy transfer from low to high latitudes by air and ocean currents. The heating of the earth by the solar radiation is greatest at the equator, causing air to rise more strongly than at higher latitudes. During the poleward flow of the air, it cools and starts to descend around the 30º latitude bands, providing high pressure or anti-cyclonic flow near the surface (e.g., the

"Azores High"). The equatorial upward motion is balanced by a low-altitude return flow from higher latitude bands, known as the "trade winds". This circulation pattern in the troposphere is known as the "Hadley circulation".

In the planetary boundary layer horizontal wind speed and direction are governed by pressure gradients, surface friction, and the Coriolis force (the drag force induced by the rotation of the earth from west to east). In the free troposphere, horizontal winds are driven by pressure gradients and the Coriolis force referred to as geostrophic winds. In the upper troposphere (> 8 km) the general westerly flow maximizes in the so-called "jet streams", which can carry air pollution around the globe on a timescale of a few weeks.

Vertical transport in cumulonimbus clouds (e.g., thunderstorms) or in deep cumulus clouds associated with frontal activity, plays an important role in the redistribution of moisture, heat, trace gases and aerosols from the atmospheric boundary layer to the upper troposphere [e.g., *Dickerson et al.*, 1987; *Lelieveld et al.*, 1994]. Fast vertical mixing in the atmosphere is driven by the release of latent heat during condensation ("moist convection") in thunderstorms, cold and warm frontal system, the tropical monsoons, severe midlatitude storms and tropical cyclones. In the absence of strong convection, the timescale for vertical transport from the surface to the tropopause is about 3 months. In convective clouds, however, vertical mixing is much faster and can take place within hours, redistributing heat, moisture, and pollution from the boundary layer to the upper troposphere. In addition, deep convection can be responsible for the exchange of species between the upper troposphere (UT) and lower stratosphere (LS) [e.g., *Danielsen, 1993*; *Fischer et al.*, 2003].

An important large-scale mechanism for vertical mixing is the passing of warm and cold fronts at midlatitudes (associated with cyclones). A frontal zone is formed when two air masses with different temperatures (or densities) meet (a body of cool air replacing warm air is a cold front and vice-versa). When warm moist air meets colder heavier air, it is pushed upwards in an anticyclonic direction (counterclockwise, due to the Coriolis force), creating a "Warm-Conveyor-Belt" (WCB), in which strong cumulonimbus clouds form. In the WCB boundary layer, air can be transported up to the tropopause. The WCB mechanism is frequently observed over the North American east coast when dry polar air masses meet warm humid sub-tropical air [*Stohl and Trickl*, 1999; *Cooper et al.*, 2001]. As a result, North American pollution from the densely populated (and polluted) east coast is efficiently transported to the UT where it can be carried across the Atlantic by the westerly jet streams. It is believed that frontal systems tracking from west to east over the Atlantic are responsible for the major trace gas transport from North America to the Atlantic Ocean and Europe [*Merryl and Moody*, 1996]. Observations of North-American pollution transport across the Atlantic and chemical impact in the UT over Europe North-American are discussed in Chapter 4.

The meteorological variability in the tropics is largely determined by the "Inter Tropical Convergence Zone" (ITCZ), a "band" of convective clouds of a few hundred km wide that forms near the equator. The convective cloud systems of the ITCZ are driven by convergence of trade winds near the surface, in combination with a strong surface evaporation and condensation in the clouds, causing a strong upward motion and heavy precipitation. The location of the ITCZ varies with season, moving north from January to July, following the sun between the winter and summer solstices. The passing of the ITCZ is known as the rainy season or wet monsoon. The role of the ITCZ in transport of Asian pollution over the Northern Hemisphere and the impact on tropospheric chemistry is highlighted in Chapter 4.

1.3.2 Tracer transport to the stratosphere

In the stratosphere the temperatures generally increases with height, resulting in a temperature inversion at the tropopause and a stable stratification. Thus, exchange across the tropopause is inhibited, while vertical tracer transport in the stratosphere is relatively slow taking place on a timescale of months to a year. The stratosphere and troposphere are coupled by the large-scale meridional “Brewer-Dobson” circulation (named after the two pioneers of stratospheric research [*Brewer*, 1949; *Dobson*, 1956]), following large-scale ascent of warm air at the equator coupled with subsidence of cool air at high latitudes. In addition, smaller scale quasi-horizontal mixing processes on a timescale of days to weeks influence the composition of the lowest part of the stratosphere.

In Figure 1.3, a schematic view of the stratospheric circulation and exchange processes between the troposphere and stratosphere is shown. According to *Holton et al.* [1995], the stratosphere can be subdivided into the “overworld” and the “lowermost stratosphere”. The lowermost stratosphere refers to the volume of air between the local extra-tropical tropopause and a potential temperature level (isentrope) of approximately 380 K (gray area in Fig. 1.3), corresponding to the mean height of the tropical tropopause (thick black line). Horizontal transport mainly occurs along levels of equal potential temperature called isentropes (potential temperature of an air mass is the temperature corrected for temperature changes which are only due to pressure changes). The overworld represents the volume of stratospheric air above the 380 K isentropic surface.

Stratosphere-troposphere exchange (STE) can occur through vertical exchange as part of the large-scale Brewer-Dobson circulation (broad arrows in Figure 1.3). A faster mechanism is the quasi-horizontal exchange along isentropes crossing the tropopause mainly at middle and sub-tropical latitudes (wavy arrows in Figure 1.3). This exchange can take place in both directions. Isentropic exchange is associated with frontal activity in the midlatitude upper troposphere or by exchange in the region of the sub-tropical jet associated with the summer monsoon circulation at lower latitudes [*Danielsen*, 1968; *Hoerling et al.*, 1993; *Dessler et al.*, 1995; *Lelieveld et al.*, 1997; *Hintsa et al.*, 1998; *Vaughan and Timmis*, 1998]. An additional, but probably less important mechanism is vertical exchange across the tropopause induced by deep convective clouds (e.g., thunderstorms) [*Poulida et al.*, 1996; *Fischer et al.*, 2003]. The timescale for quasi-horizontal isentropic transport of the order of days to weeks is much shorter than that of the Brewer-Dobson circulation [e.g., *Holton et al.*, 1995], allowing reactive tracer species with a short photo-chemical lifetime like NMHC and reactive halocarbons to build-up in the lower stratosphere.

Summarizing, we can consider the chemical trace gas composition of the lowermost stratosphere as a mixture of aged stratospheric air descending from the overworld and recent injections of tropospheric air, resulting in a mixing layer above the local tropopause [e.g., *Ray et al.*, 1999; *Fischer et al.*, 2000; *Zahn et al*, 2000]. Model studies indicate that the composition of the lowermost stratosphere may vary with season [e.g., *Chen*, 1995; *Dethof et al.*, 2000], and that isentropic STE is enhanced during summer relative to the winter season. In addition, the seasonality of trace gas abundances in the lowermost stratosphere has been confirmed by observations [e.g., *Fischer et al.*, 2000; *Hoor et al.*, 2002; *Wernli and Bourqui*, 2002]. In Chapter 2 of this thesis, we will investigate the role of isentropic transport on the reactive NMHC, acetone, and methyl chloride budget of the

lowermost stratosphere.

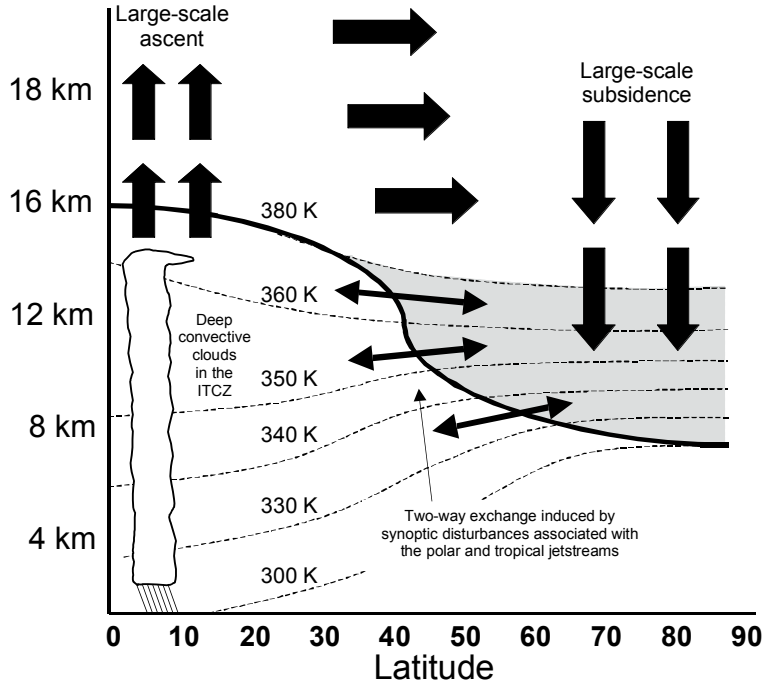

Figure 1.3: Schematic of the major dynamical processes of stratosphere-troposphere exchange according to *Holton et al.* [1995]. The tropopause is shown by the thick line, thin dashed lines are isentropic or constant potential temperature surfaces (in Kelvin). The shaded area represents the "lowermost stratosphere", an area located between the tropopause and the 380 K surface. Broad arrows denote the Brewer-Dobson circulation, with large-scale ascent in the tropics and subsidence in the polar regions. Two-way quasi-horizontal exchange across the tropopause is indicates by double headed arrows.

1.4 Impact on atmospheric chemistry and radiative transfer

Up to now, we addressed the sources, removal processes, and atmospheric distribution mechanisms of reactive NMHC and chlorocarbons. We emphasized the important role of NMHC in tropospheric photochemical ozone formation and the role of chlorocarbons in destruction of stratospheric ozone by chlorine released from chlorocarbon species. Here, we briefly review the impact of NMHC and their oxidation products (e.g., acetone) on atmospheric chemistry and the radiation energy budget.

The abundance of NMHC and acetone has an important impact on the OH radical concentration in the troposphere and lower stratosphere. As described earlier, high NMHC concentrations can lead to increased ozone levels in the presence of sufficient NO_x. As such, in regions that are most polluted in NO_x, NMHC and carbon monoxide (CO), the oxidizing power of the atmosphere is enhanced, preventing an unlimited build-up of pollutants. High ozone levels enhance OH production through the photo-dissociation of O_3 in the presence of water vapor (reaction 1.1 and 1.2). On the other hand, high levels of reactive hydrocarbons (e.g., isoprene from plants) remove OH, decreasing the oxidizing capacity of the atmosphere. Thus over continents, where NMHC concentrations are relatively high, OH removal dominates, whereas over the oceans OH production prevails, where NMHC concentrations are generally lower [*Roelofs and Lelieveld*, 2000].

Oxidized hydrocarbons, like acetone, play an additional role in atmospheric ozone photochemistry in the generation of OH radicals. Acetone can be photolyzed in the troposphere forming methylperoxy radicals (RO_2), which can react with NO forming HO_2 (reaction 1.4) [*Singh et al.*, 2000]. As such, the photolysis of acetone contributes to the HO_x budget, notably in the upper troposphere and lower stratosphere where water vapor concentrations are very low. The role of acetone for the OH budget in the lowermost stratosphere is investigated in Chapter 2.

Next to its key role in atmospheric chemistry, ozone acts as a greenhouse gas through its ability to absorb and emit long-wave infrared radiation reflected from the earth surface. Radiative warming by ozone is most efficient in the tropopause region, where the ambient temperatures reach a minimum and the radiative impact is maximized [e.g., *Lacis et al.*, 1990]. Thus, the tropospheric ozone budget influences the radiative budget of the atmosphere. Hence, it is estimated that since pre-industrial times (from 1860) the contribution of photochemical ozone formation to tropospheric ozone has doubled due to increased precursor emissions [*Lelieveld and Dentener*, 2000]. The increase of tropospheric ozone since pre-industrial times is responsible for an additional significant climate forcing of 0.35 ± 0.15 W m^{-2} comparable to that of methane of 0.57 W m^{-2} (~2.4 W m^{-2} for all greenhouse gases (mainly CO_2)) [*IPCC-TAR*, 2001]. It is expected that future increases in ozone precursor emissions of NMHC and NO_x notably from Asia with the highest population and economic growth, may lead to a future increase of the greenhouse contribution from ozone [*Lelieveld et al.*, 2001; *Hauglustaine and Brasseur*, 2001]. The role of present (and future) ozone precursor emissions from Asia is investigated in detail in Chapter 4.

In addition to the role of chlorocarbons in the catalytic destruction of ozone, they act as greenhouse gases as well. Of importance are the man-made chlorocarbons CFC-11, CFC-12 (responsible for a radiative forcing of 0.06 W m^{-2} and 0.14 W m^{-2}, respectively [*IPCC-TAR*, 2001]), whereas the most important natural chlorine species CH_3Cl plays a minor role.

1.5 Measurements of hydro- and chlorocarbons

Air samples have been collected in custom-build pre-cleaned 2.4 L electropolished stainless steel canisters equipped with *Swagelok* valves. Cleaning of the canisters was

done by heating the canisters at 150 °C, while flushing them with clean N_2 during 12 to 15 hours. For this study, a large number of whole air samples have been collected on-board of two different research jet aircrafts during six measurement campaigns conducted between 1995 and 2001. Detailed specifications about these research aircrafts are provided in the following chapters of this thesis. Ambient air was drawn in through a backward facing stainless steel inlet and compressed to ~4 bar into the canisters by means of a metal bellows pump (*MB-602*). The collection of an air sample took about 5 seconds in the boundary layer, and 3 to 4 minutes at ambient pressures less than 0.2 bar (~12 km altitude). A semi-automated sampling system has been developed and employed, providing for the collection of 9 and later 12 air samples per flight of ~3.5 hour. The air samples were analyzed in the laboratory within a few weeks after collection. The NMHC and halocarbons were detected in 1 – 2 L cryogenically pre-concentrated air samples by gas chromatography equipped with Flame Ionization Detection (FID) and Electron Capture Detection (ECD). In this thesis we present results of the most abundant C_2 – C_7 NMHC being ethane (C_2H_6), acetylene (C_2H_2), propane (C_3H_8), n-butane (n-C_4H_{10}), isobutane (iso-C_4H_{10}), n-pentane (n-C_5H_{12}), isopentane (iso-C_5H_{12}), benzene (C_6H_6)), toluene (C_7H_8), and isoprene, and measurement results of the chlorocarbons CH_3Cl, CH_2Cl_2, $CHCl_3$, C_2Cl_4, CH_3CCl_3, CFC-11, CFC-12, HCF-134a, HCFC-141b, and HCFC-142b. The measurement uncertainty lies between 5 – 15% (species dependent) and is based on calibration with commercial standard gas mixtures. The air sampling system and analysis method are described in more detail in the following chapters and in the Appendix.

Beside the air sampling system, the research aircrafts carried state-of-the-art instrumentation for in-situ trace gas and particle measurements. In the different chapters of this thesis we included measurements of O_3, CO, NO, NO_y (sum of reactive oxidized nitrogen), nitrous oxide (N_2O), CO_2, CH_4, acetone, methanol, acetonitrile (CH_3CN), CFC-12, CFC-11, depending on availability during the specific campaign. The measurement methods and measurement uncertainties for these gases are described in the following chapters.

1.6 Research aims and thesis outline

The overall aim of the research presented in this thesis is to improve our understanding of the sources, distribution, and chemical role of reactive hydrocarbons and chlorocarbons in the troposphere and lowermost stratosphere. To meet this aim, we have analyzed a comprehensive data set of selected NMHC and chlorocarbons derived from six aircraft measurement campaigns with two different jet aircrafts conducted between 1995 and 2001. The measurements were performed at six different locations representing polar, midlatitude, and tropical atmospheres (shown in Figure 1.4). The role of reactive NMHC and chlorocarbon measurements has been investigated with the help of concurrent measurements of O_3, CO, NO, NO_y, N_2O, CO_2, CH_4, acetone, methanol, acetonitrile, CFC-12, CFC-11, HCF-134a, HCFC-141b, and HCFC-142b (when available). These additional trace gas measurements can provide important information about the air mass origin, pollution sources, and chemical age of the analyzed air.

For various reasons, the tropical regions have been of special interest in this research. Firstly, although the tropics are becoming increasingly important in terms of global anthro-

pogenic pollution and climate change, intensive measurement campaigns in tropical regions have been relatively sparse. Secondly, while natural emissions of hydrocarbons (isoprene and terpenes) and reactive chlorocarbons appear to be concentrated in the tropics, large uncertainties still exist with respect to source type and source strength.

Throughout this thesis, the measured C_2 – C_7 NMHC are used as source tracers and indicators of the "chemical age" of an air mass. Uncertainties in the global budgets of the NMHC species investigated here are considerably smaller than those of reactive chlorocarbons and are therefore not a major objective of this study. These NMHC are primarily released from fossil fuel use, of which the production and consumption of fossil fuel are reasonably well documented. The same is the case for long-lived chlorocarbons, which only have anthropogenic sources such the CFCs, and CH_3CCl_3 [*AFEAS*, 2003].

The specific scientific objectives of this study can be summarized as follows:

1. To augment the sparse availability of NMHC and chlorocarbons measurements in the free troposphere and lower stratosphere, in particular in the tropics.

2. To investigate the role of cross-tropopause isentropic transport on the reactive C_2 – C_6 NMHC and acetone budget of the extra-tropical lowermost stratosphere as a function of season (fall, winter and summer).

3. In relation to objective 2: To assess the impact of observed acetone concentrations on the OH radical concentration in the lowermost stratosphere as a function of season.

4. To improve our understanding of isentropic mixing timescales.

5. To improve our insight in the global source budgets of the reactive chlorocarbon CH_3Cl, CH_2Cl_2, $CHCl_3$, and C_2Cl_4, in particular in the role of tropical emissions from biomass burning and biogenic sources.

6. To investigate the role of the ITCZ in the vertical transport and redistribution of Asian pollution over the Northern Hemisphere and the impact of Asian pollution on tropospheric chemistry, with an emphasis on the ozone budget.

The first research objective is addressed by presenting the NMHC and chlorocarbon measurements in the Chapter 2 – 4 of this thesis and by making these data available to the atmospheric chemistry research community.

In **Chapter 2**, we address the research objectives 2 – 4. Here, we present measurement results from the 1995, 1997 and 1998 Stratosphere Troposphere Exchange by Aircraft Measurements (STREAM) campaigns. The STREAM campaigns focused on the region of the upper troposphere and lowermost stratosphere and investigated dynamical exchange processes that affect ozone chemistry. More detailed information about the STREAM campaigns and their objectives is provided in Chapter 2 and references therein. Upper tropospheric air masses, either clean or polluted, are mixed into the lowermost stratosphere, with important potential chemical implications. We investigate in detail the budgets of C_2 – C_7 NMHC, acetone, and methyl chloride in the extra-tropical lowermost stratosphere at different seasons. In addition, the role of acetone photolysis as source of

OH radicals in the summertime lowermost stratosphere is examined. With these NMHC and acetone measurements, we try to contribute to our understanding of the ozone chemistry in the lowermost stratosphere and to provide input for numerical models. Finally, a simple method is presented, which provides new insight in the frequency and quantitative importance of isentropic cross-tropopause exchange processes at midlatitudes.

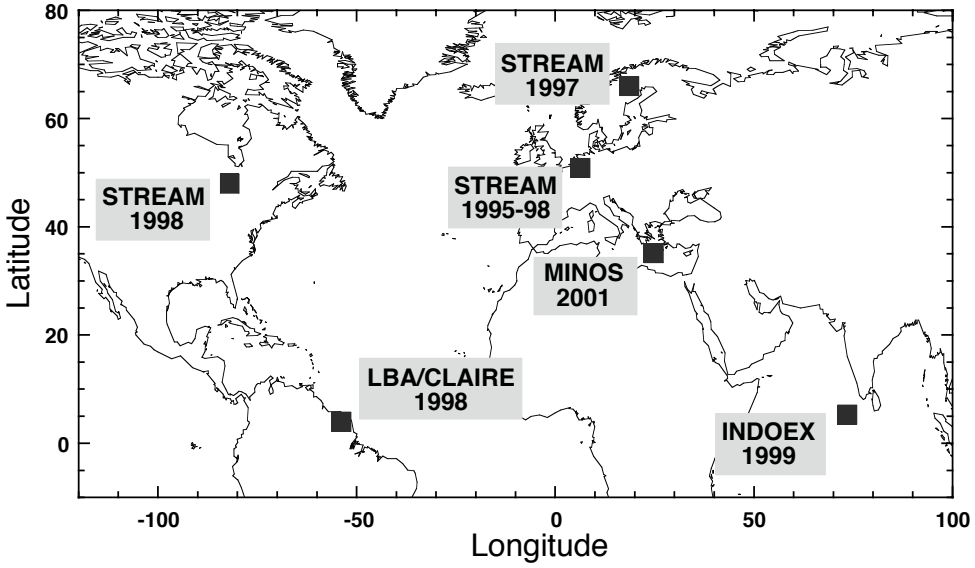

Figure 1.4: Overview of the measurement locations of the different aircraft campaigns described in this study. The campaign acronyms are explained in the text.

Chapter 3 presents measurements of C_2 – C_6 NMHC and selected chlorocarbons from the 1999 Indian Ocean Experiment (INDOEX) campaign, with special emphasis on the most abundant natural chlorocarbon CH_3Cl. In general, the INDOEX study aimed at improving our understanding of the large and increasing role of Asian emissions in global atmospheric chemistry. A general overview of INDOEX results is presented by *Lelieveld et al.* [2001]. We focus on the sources of strongly enhanced levels of CH_3Cl, CH_2Cl_2, and $CHCl_3$, which were observed in highly polluted outflow from India and Southeast Asia over the Indian Ocean (research objective 5). We relate the high chlorocarbon levels to the extensive use of biofuels (wood, dung, and agricultural waste) instead of fossil fuels for household and industrial purposes in the developing parts of Asia. A relatively high emission ratio relative to CO is inferred, which leads to significantly higher biomass burning emissions of CH_3Cl from Asia than previously estimated. Nevertheless, the greater part of the total estimated source budget of CH_3Cl remains to be accounted for. This will be addressed further in **Chapter 5**.

In **Chapter 4**, measurement results from the 2001 Mediterranean Intensive Oxidant Study (MINOS) campaign are presented. The MINOS project was initiated to improve our understanding of the transport processes, chemical mechanisms, and main pollution

sources that determine the chemical composition in the Mediterranean troposphere. We focus on the monsoonal outflow of polluted air from Asia observed in the upper troposphere over the eastern Mediterranean (research objective 6). The work in this chapter continues and extends the research presented in **Chapter 3** on the role of Asian pollution in atmospheric chemistry, by focusing on the large-scale transport and chemical impact of Asian pollution in the troposphere and lower stratosphere. Specific source tracers in combination with back-trajectory analysis and a global chemistry-transport model are employed to elucidate and compare the impact of Asian and Western (mainly North American) pollution in the upper troposphere, with emphasis on the ozone budget. In addition, we investigate chemical impact from the projected increase of Asian NMHC and NO_x emissions in the next 25 years due to the expected strong increase of fossil fuel use (replacing biofuels).

Chapter 5 explores the contribution of natural emission processes to the budgets of the reactive chlorocarbons CH_3Cl, CH_2Cl_2, $CHCl_3$, and C_2Cl_4 from tropical rainforests (research objective 5). We evaluate a unique dataset of these species obtained from air samples collected over the pristine Surinam rainforest spanning from the Atlantic coast to the Brazilian border. The data were obtained during the 1998 Large-scale Biosphere-atmosphere experiment in Amazonia – Cooperative LBA Airborne Regional Experiment (LBA/CLAIRE) campaign. A main objective of LBA/CLAIRE was to investigate exchange of trace gases and aerosols between the pristine tropical rainforest and the atmosphere. The measurements of CH_3Cl, $CHCl_3$, and C_2Cl_4 show a positive gradient as a function of latitude over the forest, in the absence of pollution sources. Hence, it is assumed that the gradients are the result of biogenic emissions from the rainforest, and the data are used to calculate the source strength. In addition, we evaluate vertical profiles of these and other tracer species. We investigate signatures of vertical pollution transport and subsequent outflow in the free troposphere associated with the South American monsoon (objective 1).

Finally, in **Chapter 6**, the main conclusions from the work in this thesis are summarized and recommendations for further research are given.

2 Reactive organic species in the northern extratropical lowermost stratosphere: Seasonal variability and implications for OH

Abstract. We present C_2 – C_6 non-methane hydrocarbons (NMHC) measurements from canister samples obtained in the extratropical lower stratosphere during the fall (November/December 1995), winter (March 1997) and summer seasons (July 1998) as part of the Stratosphere Troposphere Experiments by Aircraft Measurements (STREAM) campaign. The flights were carried out from Amsterdam (the Netherlands, 52°N, 4.5°E) during fall, from Kiruna (Sweden, 68°N, 20°E) during winter, and from Timmins (Canada, 48.2°N, 70.3°W) during summer. The NMHC measurements have been evaluated along with concurrent in situ measurements of acetone (CH_3COCH_3), carbon monoxide (CO), ozone (O_3), nitrous oxide (N_2O), and CFC-12 (CCl_2F_2). The vertical distributions of NMHC and acetone as a function of ozone and potential temperature in the lowermost stratosphere show a strong seasonality. Enhanced concentrations of NMHC + acetone were found during July up to potential temperatures of Θ = 370 K, whereas during March this was limited to Θ = 340 K, in agreement with stronger isentropic cross-tropopause transport during summer. Increasing methyl chloride concentrations with altitude were measured during July, pointing to mixing at the sub-tropical tropopause. During summer and fall, mean NMHC + acetone concentrations were more than a factor of two higher than during winter. Box model calculations indicate that the observed acetone levels of 0.5 to 1 ppbv can explain 30 to 50% of the enhanced OH concentrations in the summertime lowermost stratosphere. Using mass balance calculations, we show that a significant tropospheric fraction (≤ 30%) was present up to Θ = 370 K in the summertime lowermost stratosphere. During winter, the tropospheric fraction approached zero at about Θ = 350 K. The time between selected troposphere-to-stratosphere mixing events and the aircraft measurements has been estimated at 3 – 14 days. Our results emphasize that isentropic cross-tropopause transport can be a fast process occurring on timescales of days to weeks.

Accepted for publication in *Journal of Geophysical Research*, with H. Fischer, J. Lelieveld, P. Hoor, J. Rudolph, F. Arnold, B. Bregman, C. Brühl, A. Engel, C. van der Veen, and D. Brunner as co-authors.

2.1 Introduction

In recent years there has been an increasing interest in the chemical composition of the extratropical lowermost stratosphere, located between the local tropopause and the 380 K potential temperature (Θ) isentrope, the latter coincident with the mean tropical tropopause [*Holton et al.,* 1995]. The lowermost stratosphere has thus been addressed in modeling studies [e.g. *Chen et al.*, 1995; *Holton et al.*, 1995 *and references therein*; *Bregman et al.*, 2000; *Dethof et al.,* 2000; *Rood et al.*, 2000; *Wernli and Bourqui*, 2002] and measurement campaigns [e.g. *Bamber et al.*, 1984; *Kritz et al.*, 1991; *Poulida et al.*, 1996; *Appenzeller et al.*, 1996, *Bregman et al.*, 1997; *Lelieveld et al.*, 1997; *Singh et al.*, 1997; *Hintsa et al.*, 1998; *Flocke et al.*, 1999; *Ray et al.*, 1999; *Fischer et al.*, 2000; *Zahn*, 2001; *Hoor et al.*, 2002] to better understand and quantify cross-tropopause transport processes and their impact on the budget of ozone and other important trace gases. Bi-directional mass transfer across the tropopause can carry pollutants such as halocarbons, with a potential to destroy ozone, into the stratosphere, and on the other hand enrich the upper troposphere with ozone. Ozone near the tropopause acts as an effective greenhouse gas [*Lacis et al.,* 1990]. Hence, understanding the ozone budget in the tropopause region is of great importance for climate change studies.

The lowermost stratosphere can be considered as a distinct region where aged air masses descending from the stratosphere above, defined as 'the overworld' ($\Theta \geq 380$ K) [*Hoskins,* 1991], mix with tropospheric air through several cross-tropopause transport processes [*Holton et al.*, 1995]. Diabatic descent brings aged stratospheric air from the overworld into the lowermost stratosphere, as first proposed by *Brewer* [1949], and studied intensively thereafter both by experimental and modeling work [*e.g. Holton et al.,* 1995 *and references therein*; *Dessler et al.,* 1995; *Appenzeller et al.*, 1996; *Ray et al.*, 1999]. In addition, tropospheric air can enter the lowermost stratosphere adiabatically along isentropic surfaces crossing the subtropical or midlatitude tropopause. Isentropic cross-tropopause transport has been shown to occur from in situ measurements by *Kritz et al.* [1991], *Lelieveld et al.* [1997], *Hintsa et al.* [1998], *Vaughan and Timmins*, [1998], *Fischer et al.* [2000], and *Zahn* [2001], and from modeling work by *Chen* [1995], *Dethof et al.* [2000] and *Seo and Bowman* [2001]. Finally, mixing can occur by diabatic ascent across isentropes at the extratropical tropopause associated with synoptic-scale disturbances (polar fronts) and deep convection in thunderstorms [e.g., *Fischer et al.*, 2003]. Since this process is believed to only affect the region near the tropopause [*Poulida et al.,* 1996; *Lelieveld et al.,* 1997], it can be assumed that isentropic transport is the main source of tropospheric air in the lowermost stratosphere.

Transport from the troposphere to the stratosphere in the extratropics has a strong seasonal dependence, which results in a mixing layer above the local tropopause with a maximum depth in summer and a minimum during winter [e.g., *Chen*, 1995; *Dethof et al.*, 2000; *Hoor et al.*, 2002]. According to modeling work by *Chen* [1995] and *Dethof et al.* [2000] there is very little isentropic transport between $\Theta = 340$ and 360 K across the tropopause during winter due to the strong sub-tropical jet, which acts as a transport barrier. During the northern summer the subtropical jet is much weaker, allowing isentropic transport into the lowermost stratosphere driven by the Asian and Mexican monsoon

circulations. Measurements by *Ray et al.* [1999] demonstrate that most of the air below Θ = 380 K in the lowermost stratosphere during September has entered quasi-isentropically from the sub-tropical troposphere, whereas during May downward advection from the stratospheric overworld (Θ > 380 K) was the dominant source of air. *Hoor et al.* [2002] identified a mixing layer in the lowermost stratosphere from correlations between CO and O_3 observed during the March 1997 and July 1998 STREAM campaigns. They found a significant direct tropospheric influence up to Θ = 330 K during March, while this mixing layer increased to Θ = 360 K during July. This appeared to be caused by a stronger contribution of subtropical tropospheric air mixed in at the subtropical jet.

Thus far, most studies on the chemical composition and dynamics of the lowermost stratosphere have used relatively long-lived tracers (e.g. N_2O, CO_2, CH_4, SF_6, CFC-11, CFC-12) with lifetimes far exceeding typical exchange times between the lowermost stratosphere and upper troposphere, being of the order days to weeks [e.g. *Boering et al.*, 1994; *Lelieveld et al.*, 1997; *Dethof et al.*, 2000; *Andrews et al.*, 2001]. However, to our knowledge little attention has been given to the abundance of short-lived tracers such as non-methane hydrocarbons [*Singh et al.*, 1997; *Flocke et al.*, 1999; *Singh et al.*, 2000] and acetone in the lowermost stratosphere [*Arnold et al.*, 1997; *Wohlfrom et al.*, 1999; *Singh et al.*, 2000]. The occurrence and abundance of NMHC and acetone with relatively short photochemical lifetimes of the order of weeks can give insight into the frequency and timescales of mixing processes, which determine the tracer budgets in the lowermost stratosphere. Moreover, the stratospheric acetone budget is important because acetone photolysis is a source of peroxy and alkoxy radicals, which can enhance OH and HO_2 radical concentrations [*Singh et al.*, 1995].

In this paper we focus on selected C_2 – C_6 non-methane hydrocarbon (NMHC) measurements from canister samples collected in the extratropical upper troposphere and lowermost stratosphere during November/December 1995, March 1997 and July 1998 as part of the Stratosphere Troposphere Experiments by Aircraft Measurements (STREAM) project. In July 1998 methyl chloride (CH_3Cl) has been measured as well. Methyl chloride forms the largest natural source of chlorine in the stratosphere and its relative contribution is increasing due to the decline of man-made halocarbons. The NMHC-data have been analyzed on the basis of concurrent in-situ measurements of ozone (O_3), carbon monoxide (CO), acetone (CH_3COCH_3), nitrous oxide (N_2O) and CFC-12 (CCl_2F_2). The data have been applied to study the seasonality in the NMHC and acetone distributions in the lowermost stratospheric mixing layer. Furthermore, we present estimates of the fraction of tropospheric air transported into the mixing layer. We show results from a photochemical box model study, to investigate the role of observed acetone levels on OH formation in the lowermost stratosphere. Finally, we introduce a simple method to estimate the residence time of air masses in the lowermost stratosphere from elevated NMHC concentrations measured during July 1998, which provides new insight into the timescales related to cross tropopause transport processes.

2.2 Aircraft measurement campaigns

The NMHC measurements from canister samples, as well as the in-situ data presented

here, were obtained during three different STREAM campaigns carried out in the upper troposphere and lower stratosphere between 40° – 80°N. The measurement flights were performed with a twinjet Cessna Citation operated by the Delft University of Technology in the Netherlands. The first campaign, STREAM 95, took place during November and the beginning of December in 1995. Four flights were conducted from Amsterdam (The Netherlands, 52°N, 4.5°E) during which 21 canister samples were collected representing the fall season between 52° – 55°N. Secondly, a late winter campaign (STREAM 97) took place from Kiruna (Sweden, 68°N, 20°E) during March 1997. Here, 4 flights conducted between 68° – 78°N yielded 29 canister samples. Finally, during the summer campaign (STREAM 98) 8 flights were carried out from Timmins (Canada, 48.2°N, 70.3°W) within the 44° – 56°N latitude band, and two flights from Amsterdam (flown between 47° – 57°N). The STREAM 98 campaign yielded 90 canister samples including those collected during the ferry flight from Timmins back to Amsterdam. An overview of the measurement areas covered by the different STREAM campaigns is given in Figure 2.1.

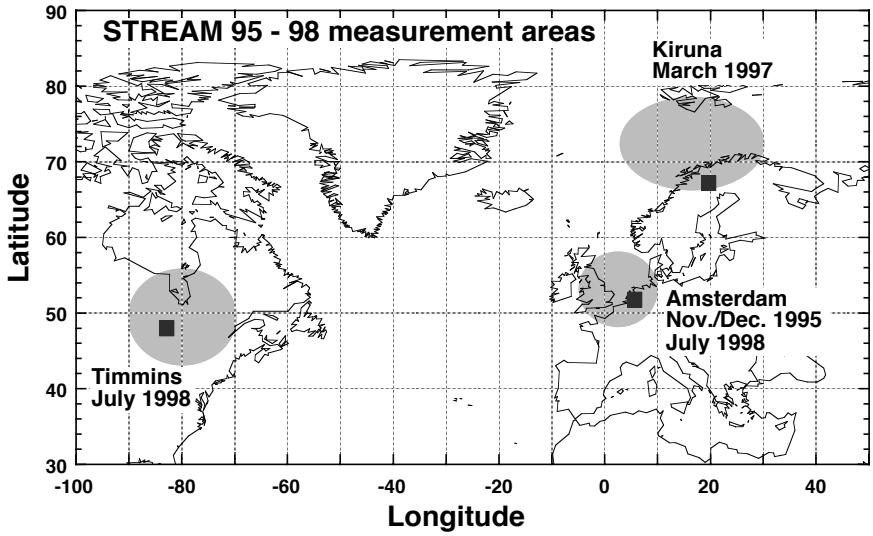

Figure 2.1: Overview of the measurement areas covered by the STREAM campaigns performed in 1995, 1997 and 1998. The squares denote the airport locations from where the flights were conducted.

The major objectives of the STREAM campaigns were (1) to investigate the chemical composition of the upper troposphere and lower stratosphere as a function of season and latitude, (2) to study the extent and role of cross-tropopause exchange processes on the chemical composition of the tropopause region, and (3) to identify the air mass origin (anthropogenic or natural, e.g. biomass burning) and the role of long-range transport therein. The flight duration was typically about 3.5 – 4 hours and consisted of several stacked flight legs up to 13 km altitude (~160 hPa). During most flights the aircraft was able to reach the lower stratosphere at the cyclonic side of the polar jet, north of the polar front.

In Table 2.1 we summarize the approximate Θ-range where the tropopause was located during the different campaigns. Clearly, the tropopause height during summer is located above the winter tropopause, whereas the (late) fall tropopause height marks a transition between both seasons.

Table 2.1: Overview of the Θ-range denoting the local tropopause during the different campaigns and the Θ-range representing the extent of the measurement flights.

Campaign	Period	Lat-range	Θ-range tropopause	Θ-range all flights
STREAM-95	Nov-Dec. 1995	52°-55°N	310-340K	305-360K
STREAM-97	March 1997	60°-78°N	290-320K	260-360K
STREAM-98	July 1998	44°-56°N	320-360K	290-370K

The highest isentropic levels up to Θ = 370 K in the lowermost stratosphere were reached by the aircraft during July 1998. On the anticyclonic side of the jet stream, however, the tropopause height was usually at or above the maximum flight altitude of the aircraft (~13 km). Meteorological forecast and analysis products (e.g. back-trajectories) from the European Center for Medium Range Weather Forecasts (ECMWF), provided by the Royal Netherlands meteorological Institute (KNMI), were used for flight planning and post-campaign data analyses. For more details about the STREAM 1995 – 1997 campaigns as well as measurement results we refer to *Lelieveld et al.* [1999], *Bregman et al.* [2000], and *Fischer et al.* [2000], and for the STREAM 1998 campaign to *Fischer et al.* [2002], *Hoor et al.* [2002], and *Lange et al.* [2001].

2.3 Measurement techniques

NMHC were detected in whole air samples. A semi-automated grab sampling system, developed at Utrecht University, was used to fill 9 pre-cleaned 2.4 L electropolished stainless steel canisters per flight at ~2.5 bar overpressure. Air was drawn in through a backward facing stainless steel inlet by means of a metal bellows pump (*MB-602*). The filling of a canister took up to 3 minutes at ambient pressures of 160 hPa. Canister samples were analyzed in the laboratory by a gas chromatograph (GC) equipped with Flame Ionization Detection (FID) for NMHC and Electron Capture Detection (ECD) for halocarbons in 1 – 2 L cryogenically pre-concentrated air samples. For more details about the GC analysis equipment and methods applied during STREAM 95-97 we refer to *Lelieveld et al.* [1999], and to *Rudolph et al.* [1999] and *Fischer et al.* [2002] for STREAM 98, for which the analyses were done at York University (Toronto, Canada). Part of the GC-analysis during STREAM 98 (ferry flight back and last two flights 9 and 10) was done at Utrecht University for which we refer to *Scheeren et al.* [2002] for technical details. Here we report results for a selected group of C_2-C_6 NMHC, being ethane (C_2H_6), acetylene (C_2H_2), propane (C_3H_8), n-butane (n-C_4H_{10}), isobutane (iso-C_4H_{10}), n-pentane (n-C_5H_{12}), isopentane (iso-C_5H_{12}), benzene (C_6H_6)) and methyl chloride. Routine calibrations with commercial standard gas

mixtures resulted in an accuracy better than 10% for the STREAM 1995 – 1997 results and an accuracy better than 5% for the STREAM 98 results. For the STREAM 95-97 measurement precisions ranged between 2 and 14%, whereas for the STREAM 98 measurements precisions were between 2 and 5%, depending on the species for concentrations larger than 15 pptv (pptv, 10^{-12} mol mol^{-1}). At concentrations ≤ 5 pptv the precision is ≥ 50%. By measuring within a few weeks after collecting the air sample storage artifacts were minimized and stayed within the uncertainty of the measurements.

Ozone was measured at 1 Hz resolution with a modified pressure independent chemiluminescence *BENDIX 8002* monitor with a 1σ precision of 2% [*Lelieveld et al.,* 1997]. The absolute accuracy of the measurement is about 5% based on titration with a NO-standard gas before and after the campaign.

CO and N_2O were measured by Tunable Diode Laser Absorption Spectroscopy (TDLAS) with the TRISTAR (Tracer In-Situ TDLAS for Atmospheric Research) instrument from the MPI Mainz at a 1 Hz resolution, described in detail by *Wienhold et al.* [1998]. Calibrations with secondary standard were performed in-situ during flight resulting in a 1σ precision of ±3.5% for CO and N_2O. Absolute calibration was deduced from cross-calibration with a primary standard resulting in a calibration accuracy of ±2.8% for both compounds, yielding a total uncertainty of 4.5%.

Additional measurements of N_2O, as well as the measurement of CFC-12, were obtained with the Gas cHromatograph for the Observation of Stratospheric Tracers (GHOST) from Frankfurt University at a rate of one sample every two minutes [*Bujok et al.,* 2001]. A precision (2σ) of ±0.90% and ±1.20% and accuracy based on in-flight calibrations of ±2.51% and ±2.39% were obtained for N_2O and CFC-12, respectively. A comparison between the TDLAS and GHOST N_2O measurements showed average deviations of less than ±1.5%, which is within the accuracy range of both measurements [*Hoor et al.,* 1999].

The acetone measurements were performed using a chemical ionization mass spectrometer (CIMS) from the MPI Heidelberg [*Spreng and Arnold*, 1994]. Acetone is chemically ionized by the proton transfer with H_3O^+ ions and the products are detected with a quadrupole mass spectrometer. The precision (1σ) of the acetone measurement is about 15%, whereas the accuracy of the derived acetone concentration is ±30%. Acetone measurements with the CIMS have been compared to GC-measurements, which resulted in an agreement within the uncertainty range of the measurements [*Wohlfrom et al.*, 1999].

2.4 NMHC and acetone in the lowermost stratosphere

2.4.1 Seasonal variability

Previous work has dealt with the abundance and chemistry of NMHC [e.g., *Rudolph et al.*, 1981; *Singh et al.,* 1997; *Lelieveld et al.,* 1999; *Singh et al.*, 2000] and acetone [*Arnold et al.,* 1997; *Bregman et al.,* 1997; *Singh et al.,* 1997; *Wohlfrom et al.*, 1999; *Singh et al.*, 2000] in the midlatitude lower stratosphere, focusing on a particular season. However, to our knowledge seasonal variations in the abundance of reactive organic species in the

extratropical lowermost stratosphere have not yet been studied. *Hoor et al.* [2002] describe a strong seasonality of transport from the troposphere to the stratosphere in the extratropics on the basis of the CO-O_3-relationship from the STREAM 97 and 98 campaigns. They showed that recent tropospheric influence during winter (STREAM 97) does not extend beyond Θ = 20 K above the local tropopause, whereas during summer (STREAM 98) tropospheric influences were found up to a potential temperature interval of Θ = 40 K or more. Here we investigate if a similar seasonality is present in the abundance of reactive organic compounds in the lowermost stratosphere. We examined the depth of the mixing layer for NMHC and acetone in terms of $\Delta\Theta$ relative to the local tropopause. Therefore, the potential temperature of the local tropopause had to be taken into account for each flight. Similar to *Hoor et al.* [2002], we defined the upper boundary potential temperature value of the local tropopause along the flight track by an ozone concentration of 120 ppbv (ppbv = 10^{-9} mol mol^{-1}) in combination with a potential vorticity of 3.5 PV-units (1 PV-unit = 10^{-6} K m^2 kg^{-1} s^{-1}) [*Hoerling et al.,* 1993] as threshold values. PV along the flight track was derived from European Centre for Medium-range Weather Forecast (ECMWF) analyses. Potential temperature at the tropopause was determined from the profile measurements.

Table 2.2 presents an overview of selected C_2 – C_6 NMHC (ethane, acetylene, propane, *n*-butane, isobutane, *n*-pentane, isopentane, and benzene) and other trace gas measurements in the lowermost stratosphere from November/December STREAM 1995, March STREAM 1997 and July STREAM 1998. In addition we show mean results for the upper troposphere (7.5 – 12 km altitude). Note that for STREAM 1997 upper tropospheric measurements were only available for March 23 and 25. For a detailed analysis of NMHC mixing ratios in the upper troposphere during STREAM 1998 we refer to *Fischer et al.,* [2002]. The results in Table 2.2 represent the mean and 1σ standard deviation of a number of measurements performed in the upper troposphere and lowermost stratosphere at $\Delta\Theta$ = 0 – 30 K and at $\Delta\Theta$ > 30 K. The range of $\Delta\Theta$ = 0 – 30 K denotes the average depth of the (summer and winter) stratospheric mixing layer in accordance with *Hoor et al.* [2002].

The values for O_3, CO, CFC-12, N_2O, acetone and meteorological parameters (Θ, and PV from the ECMWF analysis along the flight track) are averaged from time series (and 1σ standard deviations) corresponding with the duration of the canister sampling (~3 minutes). The N_2O measurement results from the GHOST instrument were combined with results from the TDLAS instrument. In addition, we included the sum of total carbon for the selected C_2 – C_6 NMHC and C_2 – C_6 NMHC + acetone in nmol mol^{-1} Carbon (ppbC), as a measure of available reactive organic carbon (ROC). The selected C_2 – C_6 NMHC represent more than 95% of the total NMHC that was detected during STREAM 98 (which included isoprene, 2-methylbutane, 2,2-dimethylpropane, cyclohexane, methylcyclopentane, n-hexane, 2-methylpentane, 3-methylpentane, 2,2-dimethylbutane, toluene, methyl-cyclohexane, n-heptane, ethyl-benzene, o-xylene, p-, m-xylene, n-octane and n-nonane detected close to their detection limit of ~5 pptv). We have to note, however, that the ROC values in this study underestimate the total amount of reactive organic species present in the atmosphere, since they do not include other important organic species such as formaldehyde, methanol and peroxyacetyl nitrate (PAN).

The mean NMHC + acetone concentration in the mixing layer ($\Delta\Theta$ = 0 – 30 K above the local tropopause) of 2.2 $\pm$ 0.5 ppbC (Table 2.2) measured during the fall season (November/December 1995) compares well with the 2.3 $\pm$ 1.7 ppbC found during summer (July 1998), and both are more than a factor of two higher than the 0.9 $\pm$ 0.3 ppbC measured

Table 2.2: Overview of results from STREAM 95, 97 and 98 averaged over the upper troposphere, the lower stratospheric $\Delta\Theta$ = 0 - 30 K mixing layer and the stratosphere at $\Delta\Theta$ > 30 K relative to the local tropopause. Note that the STREAM 1997 free tropospheric concentrations were based on the flights of March 23 and 25 only, while the total $C_2 - C_6$ NMHC (+ acetone) estimate is based on 1 canister sample (March 25). STREAM 1995 upper tropospheric acetone data are only available for the flight of November 29. N denotes the number of canisters. The variability denotes the 1σ standard deviation of the mean.

Species / Campaign	Nov.-Dec. 1995 Upper Trop. *Mean* N = 6	Nov.-Dec. 1995 Lower Strat. $\Delta\Theta$ 0 - 30 K N = 8	Nov.-Dec. 1995 Lower Strat. $\Delta\Theta$ > 30 K N = 3	March 1997 Upper Trop. *Mean* N = 1	March 1997 Lower Strat. $\Delta\Theta$ 0 - 30 K N = 15	March 1997 Lower Strat. $\Delta\Theta$ > 30 K N = 12	July 1998 Upper Trop. *Mean* N = 23	July 1998 Lower Strat. $\Delta\Theta$ 0 - 30 K N = 23	July 1998 Lower Strat. $\Delta\Theta$ > 30 K N = 15
O_3 [ppbv]	61±19	198±55	318±11	46±8	287±65	558±64	69±18	326±84	419±52
P.V. [units]	1.2±0.9	5.9±0.9	7.8±0.3	~1	5.9±1.3	8.4±0.5	0.9±0.8	8.1±2.4	9.2±0.6
Θ [K]	312±5	341±12	351±4	~300	331±9	346±5	333±8	345±8	364±3
$\Delta\Theta$	-14±10	16±9	37±7	-20	20±8	41±7	-10±6	17±9	38±3
N_2O [ppbv]	n.a.	n.a.	n.a.	309±2	297±4	282±6	312±2	293±8	287±5
CFC-12 [pptv]	531±5	506±15	483±9	538±3	505±8	469±13	540±7	494±13	480±9
CO [ppbv]	n.a.	n.a.	n.a.	139±16	37±9	20±3	116±23	35±18	20±7
Acetone [pptv]	790±146	385±112	279±95	315±40	113±42	52±8	2000±509	430±331	203±63
C_2H_6 [pptv]	1101±213	413±100	250±54	n.a.	219±76	73±24	1040±346	303±209	144±106
C_2H_2 [pptv]	140±27	25±11	13±3	n.a.	18±14	1±3	125±38	40±32	11±7
C_3H_8 [pptv]	292±192	24±13	8±4	n.a.	13±7	3±3	210±82	28±27	9±6
n-C_4H_{10} [pptv]	95±60	5±3	3±1	n.a.	1±2	<1	35±25	6±4	4±2
i-C_4H_{10} [pptv]	41±30	2±2	2±2	n.a.	<1	<1	21±11	5±2	3±1
n-C_5H_{10} [pptv]	14±11	4±2	2±1	n.a.	1±2	<1	9±5	3±1	3±2
i-C_5H_{10} [pptv]	19±15	3±3	1±2	n.a.	<1	<1	9±8	3±2	1±1
C_6H_6 [pptv]	34±24	5±4	6±3	n.a.	<1	<1	40±31	10±13	6±3
$\sum C_2$-C_6 [ppbC]	4.27±1.50	1.03±0.27	0.62±0.11	~3.2	0.52±0.20	0.16±0.06	3.45±1.13	0.89±0.57	0.41±0.21
$\sum C_2$-C_6 + acetone [ppbC]	6.64±1.80	2.19±0.54	1.46±0.36	~4.1	0.86±0.32	0.31±0.07	9.5±2.7	2.32±1.7	0.76±0.15

during winter (March 1997). The variability in the ROC mixing ratios during summer, however, was about three times as large as during fall. The variability is strongly dependent on the lifetime and source strength of the compound at the measurement location [e.g., *Jobson et al.*, 1999]. Hence, a higher variability from one location to another (as in the summertime versus the fall lowermost stratosphere) is related to differences in the source and sink strength. The high lowermost stratospheric ROC variability during summer appears not to be reflected in the upper troposphere ("source") ROC variability as presented in Table 2.2. In terms of sink strength, on the other hand, photolysis and OH production are most likely higher in the summertime lowermost stratosphere as compared to fall conditions due to a higher solar zenith angle, thus enhancing ROC variability. In addition, the higher variability during summer suggests a higher frequency of cross-tropopause mixing events, presumably from more intense isentropic exchange at the sub-tropical jet during summer. The role of cross-tropopause transport on the LS ROC variability will be further discussed in Section 2.5.1.

Another point to be considered here is how seasonal variations of NMHC and acetone concentrations in the upper troposphere (UT) contribute to the seasonality observed in the lower stratosphere (LS). NMHC accumulate in the winter troposphere because of much longer photochemical lifetimes than in summer. Acetone, on the other hand, tends to be higher in the extratropical summer due to strongly enhanced terrestrial vegetation emissions and hydrocarbon oxidation processes [*Jacob et al.*, 2002]. Indeed, this seasonality is clearly reflected in the observed upper tropospheric ROC concentrations presented in Table 2.2. This can at least partly explain the high acetone concentrations in the summer LS. When we, however, consider the ratio of total UT to LS NMHC concentrations (in ppbC) we find a ratio of 4:1 for July and of 6:1 for March, while the upper tropospheric concentration equals ~3 ppbC for both seasons. It appears that in spite of the shorter photochemical lifetimes of NMHC during July, the higher NMHC values in the lower stratosphere are in agreement with enhanced and more frequent troposphere-to-stratosphere exchange taking place during summer [*Hoor et al.,* 2002].

The abundances and vertical distributions of ROC-species in the lowermost stratosphere provide a first measure of the extent of troposphere-to-stratosphere mixing and the photochemical age of the mixed air masses in the lowermost stratosphere. Notably the presence of significantly higher amounts of acetone, but also of ethane, acetylene, propane and benzene during the fall and summer period, as compared to the winter, points to mixing timescales of the order of days to weeks based on the photochemical lifetimes of these tracer species in the lowermost stratosphere during summer as summarized in Table 2.3.

The STREAM 97 measurement results for the lowermost stratospheric mixing layer (Table 2.2; $\Delta\Theta < 30$ K) compare well with the PEM West B measurements [*Singh et al.,* 1997] obtained in the lowermost stratosphere over the western/central Pacific (37°N – 57°N) during February/March of 1994. We obtain good agreement within the variability of the mean mixing ratios for O_3, 334 ± 97 ppbv / 287 ± 65 ppbv (PEM West B / STREAM-97); CO, 44 ± 9 ppbv / 37 ± 9 ppbv; ΣC_2-C_3, 209 ±134 pptv / 250 ± 97 pptv; acetone 153 ± 74 pptv / 113 ± 42 pptv. In addition, mean concentrations for the lowermost stratospheric mixing layer during STREAM-95 (November/December) are in accord with mean concentrations in the lowermost stratosphere over the Atlantic during October and November 1997 reported for the SONEX campaign [*Singh et al.*, 2000]. Here, we find for O_3, 191 ± 82 ppbv

/ 198 ± 55 ppbv (SONEX / STREAM-95); ΣC_2-C_3, 461 ± 230 pptv / 462 ± 124 pptv; acetone 336 ± 225 pptv / 385 ± 112 pptv. The comparison between the STREAM and PEM West B and SONEX results is illustrated in Figure 2.2. The good agreement is indicative of the hemispheric-scale seasonality in cross-tropopause exchange intensity with relatively weak exchange during the northern hemispheric winter and enhanced cross-tropopause exchange during fall.

Table 2.3: Estimate of chemical lifetimes, τ, in the lowermost stratosphere based on reaction rate coefficients k_{OH} and k_{Cl} (cm^3 $molecule^{-1}$ s^{-1}), for reaction with OH and Cl radicals, respectively. The chemical lifetime, τ, of a species is defined as $\{k_{OH}[OH] + k_{Cl}[Cl]\}^{-1}$, where [OH] and [Cl] are the daily mean concentrations in molecules per cm^3. We took the following mean ambient conditions in the lower stratosphere of 223 K, 150 mbar, [OH]: 10^6 molecules cm^{-3}; [Cl]: 10^3 molecules cm^{-3}.

Species	k_{OH} (223 K) [a]	k_{Cl} (223 K) [a]	hν	τ
N_2O	n.a	n.a	n.a	122±24[b] yr
CFC-12 (CCl_2F_2)	$<7 \times 10^{-18}$	n.a	n.a.	87±17[b] yr
CFC-11 (CCl_3F)	$<5 \times 10^{-18}$	n.a	n.a	45[b] yr
CO	1.63×10^{-13}	n.a	n.a	95 days
Ethane	6.5×10^{-14}	5.1×10^{-11}	n.a	100 days
Acetylene	3.3×10^{-13}	6.4×10^{-11}	n.a	29 days
Propane	5.0×10^{-13}	1.4×10^{-10}	n.a	18 days
Benzene	1.0×10^{-12}	n.a	n.a	12 days
Acetone	9.5×10^{-14}	n.a	~1.0 x 10^{-6}	11 days
n-butane	1.4×10^{-12}	1.4×10^{-10}	n.a	8 days
n-pentane	1.6×10^{-12}	1.4×10^{-10}	n.a	7 days

[a]Atkinson et al., 2002; [b]Volk et al., 1997.

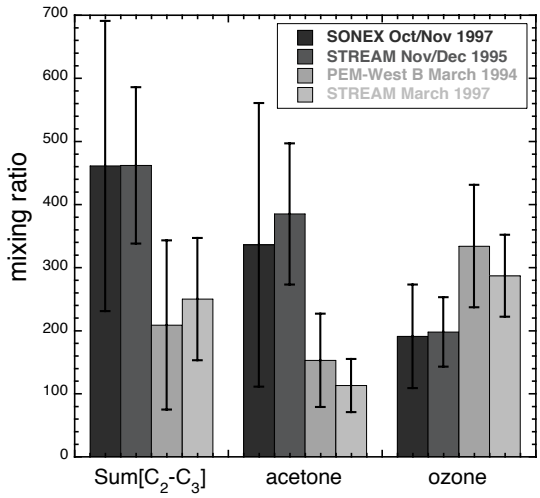

Figure 2.2: Comparison of results from STREAM 1995 and STREAM 1997 with the SONEX 1997 and PEM West B 1994 campaigns for the lowermost stratosphere. The error bars denote the measurement variability.

To further investigate the distribution of NMHC and acetone in the lowermost stratosphere during different seasons we looked at the total NMHC (pptC), acetone (ppbv) and NMHC + acetone (pptC) as a function of ambient ozone, shown in Figure 2.3. *Fischer et al.* [2000] and *Hoor et al.* [2002] used correlations between CO and ozone to show that in the absence of mixing processes across the extratropical tropopause, typically occurring on timescales of weeks, the ozone and CO relationship would approximate an L-shape, representing the 'background' stratospheric and upper tropospheric reservoirs.

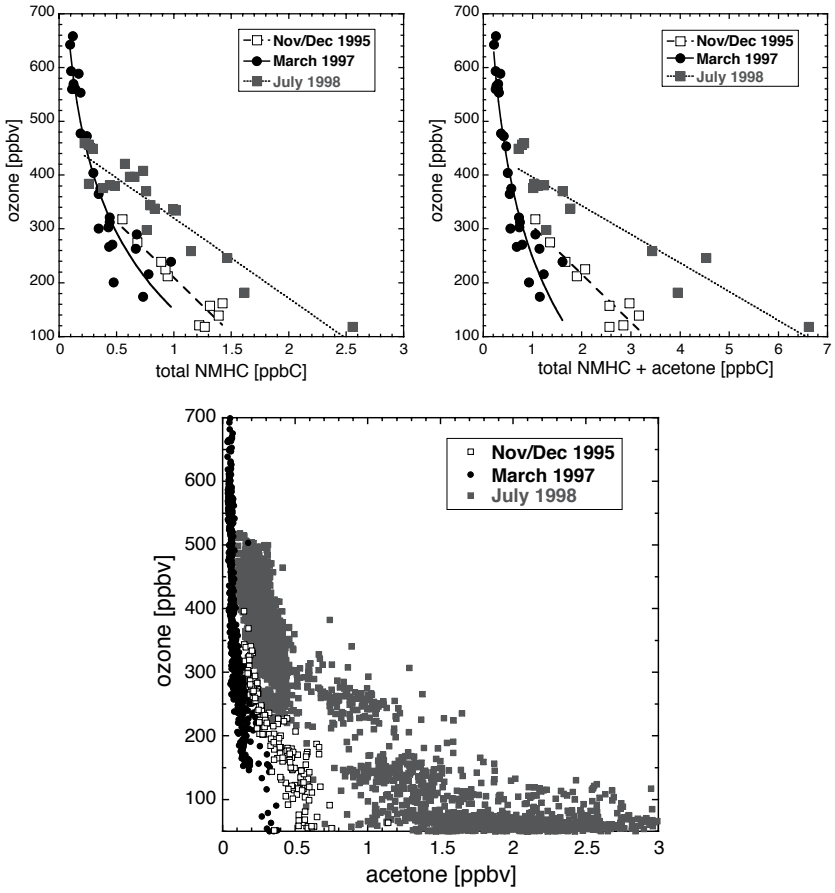

Figure 2.3: Total reactive NMHC in pptC (left panel), NMHC + acetone in pptC (right panel), and acetone in ppbv (lower panel) and in pptC as a function of the ozone concentration in the lower stratosphere for the March 1997, November/December 1995 and July 1998 campaigns. The lower acetone panel includes acetone data in the upper troposphere for ozone concentrations between 50 and 100 ppbv. The curves represent the best fit through the data (r = 0.9), which is logarithmic for March 1997 and linear for November/December 1995 and July 1998. Precision error bars were left out for clarity (~5% for NMHC, 15% for acetone and ~10% for NMHC + acetone).

Irreversible cross tropopause mixing will result in mixing lines connecting both reservoirs with the slope, being a function of the initial tracer mixing ratios and the time since the mixing event took place. The linearity of the ozone to CO relationship in the mixing zone is an indication of the intensity and frequency of the mixing process [*Hoor et al.,* 2002], and the homogeneity of the 'background' stratospheric and upper tropospheric reservoir tracer mixing ratios. A steep slope ($\Delta O_3/\Delta CO$) characterizes aged air masses, in which no recent mixing with tropospheric air has taken place and the major fraction of the ROC tracers has decayed photochemically.

Figure 2.3 shows that a similar relationship between ozone, NMHC (+ acetone) and acetone as for CO [*Fischer et al.*, 2000] is present in the lowermost stratosphere. If we consider the upper part of the March 1997 (winter) branch of NMHC, representative of the 'stratospheric reservoir', the November/December 1995 (fall) and July 1998 (summer) relationships resemble rather compact mixing lines ($r > 0.9$) in the lowermost stratosphere. The summer mixing line lies above the fall mixing line and extends to higher ozone concentrations, which indicates that mixing with tropospheric air extended deeper into the lowermost stratosphere, most likely as a result of intensified isentropic mass transport across the sub-tropical tropopause. The acetone-ozone relationship shows an identical seasonality as for NMHC, emphasizing its similar sources and sinks in the lowermost stratosphere. When acetone is included in the total reactive carbon, the ppbC mixing ratio more than doubles, indicating its important role in the lower stratospheric ROC abundance. The relatively large variability of acetone in the lower stratosphere during July compared to the fall and winter season (Figure 2.3, lower panel) appears to be related to high range in mixing ratios observed in the summertime upper troposphere. An additional probable cause is enhanced isentropic mixing at high potential temperatures in the summertime lower stratosphere.

In Figure 2.4 the relationship between the potential temperature in the stratosphere and the amount of NMHC and NMHC + acetone (in ppbC) is presented for the different seasons. To provide some qualitative information about the depth of the mixing layer we also included the vertical NMHC (and NMHC + acetone) distributions as a function of $\Delta\Theta$ relative to the local tropopause. By using $\Delta\Theta$ instead of Θ the effect of varying tropopause heights is accounted for (as mentioned before, the upper boundary of tropopause is defined by the O_3 = 120 ppbv level and a PV of 3.5). The Θ-NMHC relationship in Figure 2.4 (upper panel) clearly reveals that both the fall and summer NMHC (and NMHC + acetone) gradient lie above the winter gradient, extending to Θ-levels of at least 370 K (the highest flight level). Furthermore, the fall and summer NMHC (and NMHC + acetone) gradient overlap, although it appears that the summer gradient extends deeper into the stratosphere (as function of Θ). However, if we correct for the local tropopause height and plot NMHC (and NMHC + acetone) as a function of $\Delta\Theta$ (Figure 2.4, lower panels) we find an equally deep mixing layer for fall and summer extending to at least 40 K above the local tropopause. Note that during the fall season the tropopause was generally located at lower Θ-levels than during summer, which partly explains the overlap.

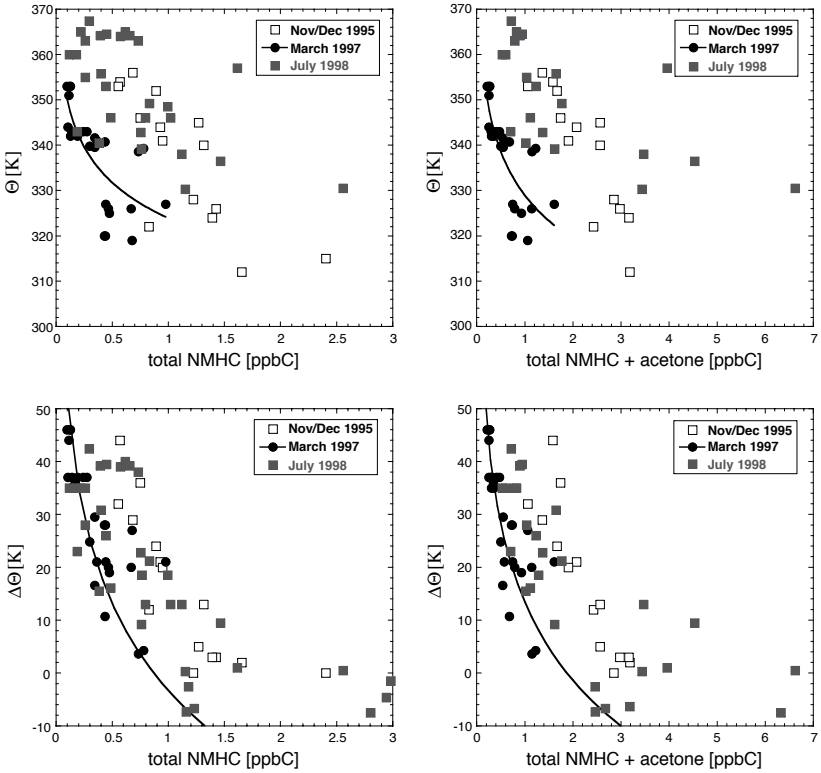

Figure 2.4: The relation between Θ in the stratosphere (upper panels) and ΔΘ relative to the local tropopause (lower panels), and the amount of reactive NMHC in ppbC (left panels) and NMHC + acetone (right panels) in the stratosphere for the different seasons. The logarithmic fit through the March 1997 data (winter) indicates the lower limit reference conditions when cross tropopause transport at higher isentropic levels is reduced. Precision error bars are left out for clarity (~5% for NMHC and ~10% for NMHC + acetone).

From the ΔΘ–ppbC relationship in Figure 2.4 we can furthermore derive that during winter (March 1997) the amount of NMHC + acetone was 0.3 ± 0.1 ppbC at ΔΘ > 30 K above the local tropopause. We consider this as the lower stratospheric "background", which is largely determined by acetone and ethane (~50/50%). These background stratospheric acetone mixing ratios are in agreement with measurements by *Wohlfrom et al.* [1999], who report acetone mixing ratios of 100 to 200 pptv measured in the lower stratosphere over the North Atlantic during the POLINAT-2/SONEX campaigns. During November/December 1995 and July 1998, on the other hand, the amount of ROC (ppbC) was a factor of 3 to 5 higher at ΔΘ > 30 K as a result of intensified mixing with tropospheric air. This difference becomes even more significant by taking into account that the photochemical lifetimes of ROC species in the fall are relatively longer than in summer.

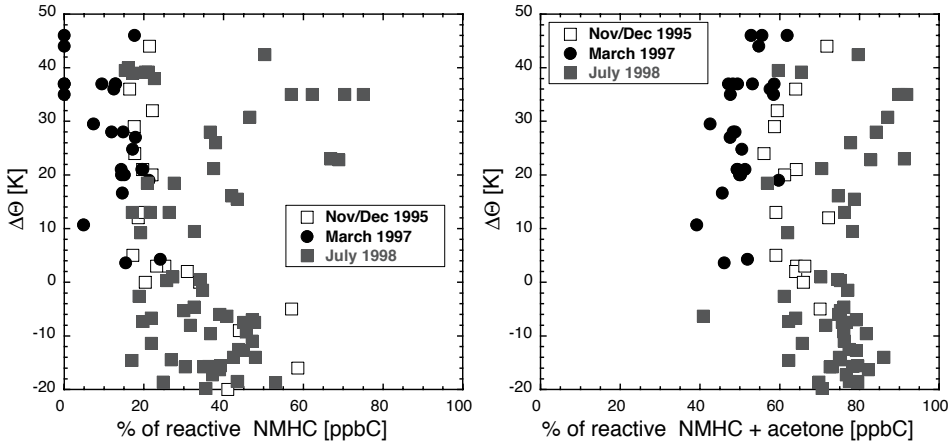

Figure 2.5: The relative fraction of reactive NMHC (minus ethane) and reactive NMHC (minus ethane) + acetone (in ppbC) with chemical lifetimes between 1 and 4 weeks (Table 2.3; all C_3 – C_6 NMHC + acetylene) as a function of $\Delta\Theta$ relative to the local tropopause. Precision error bars are left out for clarity.

Figure 2.5 shows the fraction of short-lived ROC species (in ppbC), which have chemical lifetimes between 1 and 4 weeks in the summertime lower stratosphere (see Table 2.3), relative to the total of ROC species as a function of $\Delta\Theta$. The vertical distribution clearly indicates that the fraction of short-lived ROC tracer species is strongly enhanced during summer, in spite of their shorter photochemical lifetime than in winter. While this fraction remains almost constant during the fall and winter conditions with increasing $\Delta\Theta$ (10 – 20% of NMHC; 40 – 60% of NMHC + acetone), a local maximum appears in the summer data between $\Delta\Theta$ = 20 – 35 K (up to ~70% for NMHC and ~90% for NMHC + acetone). The highest fraction of 'short-lived' ROC tracers was found around the 360 K isentrope ($\Delta\Theta$ = 30), pointing to intensified mixing at these Θ-levels during summer.

2.4.2 Role of acetone

As shown in the previous section, the amount of acetone (in ppbC) equals the sum of NMHC (in ppbC), hence it is the dominant organic tracer species in the lowermost stratosphere after ethane. Recently, *Jacob et al.* [2002] investigated the atmospheric budget of acetone with a 3-D model using extensive atmospheric observations. They found that the principal sources of acetone in the upper troposphere, notably in the tropics and Southern Hemisphere, are the terrestrial vegetation and the oceans. In the extra-tropical Northern Hemisphere winter the oxidation of NMHC (notably propane, isobutane, isopentane) dominates. This implies that acetone can be significantly enhanced over remote regions, such as the tropical Pacific, in the absence of significant anthropogenic NMHC sources. *Dethof et al.* [2000] and *Hoor et al.* [2002] indicated that the summertime stratospheric mixing layer is subject to rapid and frequent mixing with tropospheric air. In fact, enhanced

troposphere-to-stratosphere exchange at the sub-tropical jet over remote areas, where vegetation or oceanic sources of acetone dominate and NMHC-concentrations are low, can explain the relatively high acetone concentrations in the lower stratosphere during summer.

High acetone concentrations can lead to enhanced HO_x (HO_x = OH + HO_2) production from acetone photolysis in the presence of sufficient NO [*Singh et al.*, 1995], substantially enhancing the oxidizing capacity of the lowermost stratosphere during summer. HO_x formation from acetone photolysis begins with the production of methyl peroxy and acetyl peroxy radicals:

$$CH_3COCH_3 + hv + 2O_2 \rightarrow CH_3O_2 + CH_3C(O)_2 \qquad (2.1)$$

In the presence of sufficient NO most of the acetyl peroxy radicals are converted to methyl peroxy radicals forming HO_2 and NO_2 through reaction with NO. Subsequently, methyl peroxy reacts with NO and O_2 forming formaldehyde, HO_2 and again NO_2. The photolysis of NO_2 enhances ozone formation, which can be important in the background upper troposphere. Ultimately, the oxidation of an acetone molecule can lead to the production of $3.2HO_2$ radicals and $3O_3$ molecules [*Brühl et al.*, 2000].

To investigate the impact of enhanced acetone concentrations on the HO_x budget we performed a box model study, which includes detailed acetone chemistry. For technical details of the box model set-up we refer to *Brühl et al.* [2000]. Simulations were performed at the 225 hPa level, a mean temperature of 223 K and chemical conditions in optimal agreement with observed mean conditions in the summertime lowermost stratospheric mixing layer during STREAM 98. As such, CO and H_2O were kept fixed at 50 ppbv and 30 ppmv, respectively. NO_x, HNO_3 and organic nitrates (mainly PAN) were initialized with 0.2 ppbv, 2.0 ppbv and 0.45 ppbv, respectively, adding up to 2.65 ppbv, in good agreement with the mean observed total reactive nitrogen (NO_y) concentration of ~2.5 ± 1 ppbv in the stratospheric mixing layer during STREAM 98 [*Lange*, 2001]. In Figure 2.6 we show simulations of noontime maximum OH concentrations ($[OH]_{max}$) as function of acetone (ranging from 0.5 to 1.5 ppbv) for fixed ozone concentrations of 120, 240, and 360 ppbv. We find that the OH concentration is strongly dependent on available acetone. Under mean conditions of 240 ppbv O_3, the $[OH]_{max}$ ranges from 0.49 pptv at 0.5 ppbv acetone to 0.59 pptv at 1 ppbv acetone and 0.67 pptv at 1.5 ppbv acetone. This corresponds to diurnal mean OH concentrations for July conditions of 1.28, 1.54, and 1.74×10^6 molecules cm^{-3}, respectively. The $[OH]_{max}$ at 'background' conditions of 20 ppbv of CO, 350 ppbv of ozone, and 250 pptv of acetone is 0.4 pptv, corresponding to a diurnal mean OH concentration of ~1×10^6 molecules cm^{-3}. This value is within the range of observed midday OH concentrations in the lowermost stratosphere of 0.2 – 0.5 pptv during the April/May 1996 SUCCESS mission [*Brune et al.*, 1998]. Summarizing, the observed acetone levels of 0.5 to 1 ppbv can explain 30 to 50% of the enhanced OH concentrations in the extratropical summertime lowermost stratosphere up to at least θ = 360 K. Finally, we note that recent laboratory work by *Blitz et al.* [2003] suggests that the present acetone photolysis rates, commonly used in chemical models, might be by a factor of two to high. They indicate that the increase in HO_x production could be reduced by ~25% using their new photolysis rates.

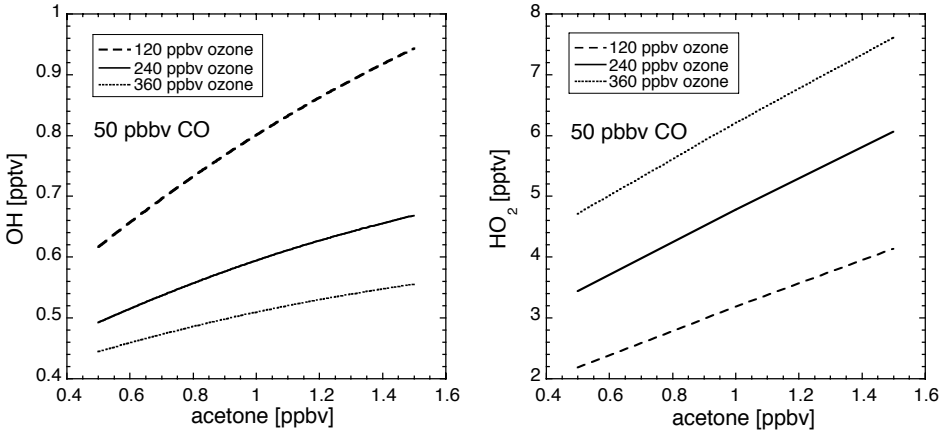

Figure 2.6: Box model noontime volume mixing ratios of OH and HO_2 as a function of acetone mixing ratios for the summertime lowermost stratosphere. Water vapor and CO have been fixed at 30 ppmv and 50 ppbv, respectively.

2.4.3 Indications of (sub-)tropical air mass origin

Hoor et al. [2002] used the CO-O_3 and CO_2-O_3 correlation to indicate that the elevated mixing layer, extending to at least Θ = 360 K in July (STREAM 1998), is caused by a stronger contribution of subtropical air mixed into the lowermost stratosphere at the subtropical jet. Different anti-correlations appear as a result of mixing across the midlatitude and sub-tropical tropopause, respectively, due to the negative gradient of CO and positive gradient of CO_2 during summer towards lower latitudes [*Fischer et al.*, 2002]. We show in Figure 2.7 that the vertical profile of methyl chloride as a function of ozone provides additional evidence for mixing of low latitude air into the lower stratosphere at potential temperatures of 360 – 370 K. It appears that the decreasing tendency of methyl chloride with increasing ozone reverses at about 450 ppbv, corresponding with a potential temperature of $\Delta\Theta \geq 30$ K. A probable explanation for enhanced methyl chloride at high potential temperatures (Θ > 360 K) in the lower stratosphere could be transport across the tropical tropopause followed by fast horizontal mixing (< 1 month) to midlatitudes first proposed by *Boering et al.* [1996]. Methyl chloride shows a global trend of increasing concentrations towards lower latitudes, throughout the tropical troposphere because its main emission sources such as oceans, biomass burning, and vegetation are strongest in the tropics [*Khalil et al.*, 1999; *Scheeren et al.*, 2002, 2003]. Consequently, higher CH_3Cl concentrations can be expected at higher isentropic levels (as was found during July 1998 (Figure 2.7)), for which the tropospheric influence is from (sub)-tropical regions relatively strong.

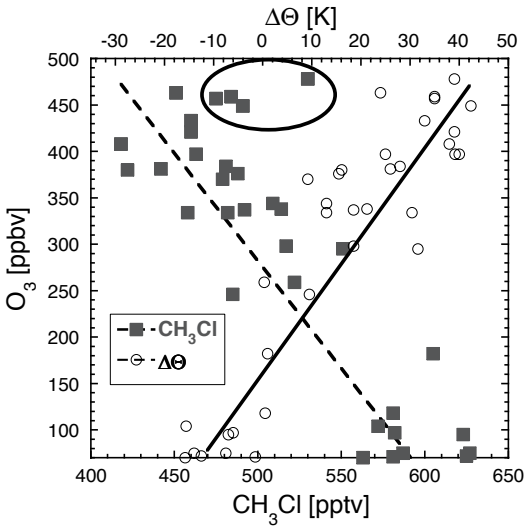

Figure 2.7: The vertical profile of methyl chloride and $\Delta\Theta$ as a function of O_3 for July 1998. The O_3-CH_3Cl relationship shows a decreasing tendency for CH_3Cl up to 450 ppbv of ozone (dashed line; r = 0.83). Above ~450 ppbv of O_3 we find enhanced CH_3Cl values relative to the trend (encircled). The solid line depicts the linear relationship between O_3 and $\Delta\Theta$ (r = 0.93). Precision error bars are left out for clarity (O_3 ≈ 5%, CH_3Cl ≈ 5%; $\Delta\Theta$ ≈ 10%).

2.5 Quantifying troposphere-to-stratosphere transport

2.5.1 Fraction of tropospheric air in the mixing layer

We described the summer lowermost stratosphere as a layer where air from the tropical and extratropical troposphere mixes with air descending from the stratospheric overworld. Since the mixing ratios of long-lived trace gases in the upper troposphere and stratospheric overworld are known (referred to as boundary conditions), along with the trace gas mixing ratio of these species in the mixing layer, the fraction of air from each of these source regions can be approximated by a simple mass balance equation analogous to *Ray et al.* [1999]:

$$\chi_{tse}(\Theta) = \chi_t(\Theta) \times N_t + \chi_s \times (1 - N_t) \qquad (2.2)$$

where $\chi_{tse}(\Theta)$ is the trace gas mixing ratio in the lowermost stratosphere as a function of potential temperature; $\chi_t(\Theta)$ is the upper tropospheric mixing ratio as a function of potential temperature and air mass origin; N_t is the fraction of tropospheric air in the lowermost

stratosphere; χ_s is the stratospheric overworld mixing ratio. A schematic representation of the composition of $\chi_{tse}(\Theta)$ is presented in Figure 2.8 showing the air mass origins and transport pathways that determine the composition of the lowermost stratosphere.

Rewriting equation (2.2) the fraction of tropospheric air, N_t, in the mixing layer can be described by:

$$N_t = \{\chi_{tse}(\Theta) - \chi_s\} / \{\chi_t(\Theta) - \chi_s\} \quad (2.3)$$

The accuracy of N_t depends strongly on the accuracy and representativeness of the boundary conditions, $\chi_t(\Theta)$ and χ_s. Furthermore, trace gases should have a significant difference in mixing ratios between the boundary conditions $\chi_t(\Theta)$ and χ_s in the upper troposphere and stratospheric overworld (larger than their variability). In this study we used the long-lived tracers N_2O and CFC-12 (lifetimes of ~124 yrs and ~87 yrs, respectively, see Table 2.3), which are well mixed in the troposphere with nearly constant tropospheric concentrations over a one-year period. In the stratosphere, however, these species have a strong gradient due to photochemical loss and vertical transport. In addition we have used intermediately long-lived species such as CO and ethane, whose lifetimes of ~3 months far exceed that of reactive organic tracer species such as acetone, acetylene, propane, and benzene (10 – 40 days during summer over the continent; see Table 2.3) in the lowermost stratosphere. Both CO and ethane mixing ratios show a very strong gradient from the upper troposphere to the lower stratosphere, which is significantly larger than their observed variability (see Table 2.2).

In Table 2.4 we present the boundary conditions, which have been derived from the measurement data for calculating N_t-values. The N_t-values have been calculated as the mean of the individual N_t, from hereon referred to as N_t^*, of N_2O, CFC-12, CO and ethane when available, respectively. As such, the N_t^*-values for the November/December 1995 campaign were based on CFC-12 and ethane only because measurement data for CO and N_2O were not available. For the March 1997 campaign upper tropospheric data for CO and C_2H_6 were considered too sparse to determine representative boundary conditions for these species. Here the N_t^*-values were determined on basis of N_2O and CFC-12 alone. The large data set for the July 1998 campaign allowed the determination of N_t^* on the basis of all selected long-lived tracer species. We found that using different tracer combinations has no significant effect on the N_t^* estimates. N_t^*-values for STREAM-98, based on CFC-12 and ethane or on CFC-12 and N_2O alone, show an excellent 1:1 correlation ($r = 0.99$) with the N_t^*-values based on all long-lived tracers.

The accuracy of the mean N_t^*-values is approximated by the variability (1σ standard deviation) of the long-lived tracer concentrations in the upper tropospheric and stratospheric reservoirs used to calculate N_t^* (see Table 2.2 and 2.3). As such, a mean accuracy of ~10% for November/December 1995, ~1% for March 1997, and ~14% for July 1998 was determined. The precision, taken as the 1σ standard deviation of the mean of N_t^*-values (based on the different long-lived species), was on average ~16% for November/December 1995, ~5% for March 1997, and ~6% for July 1998.

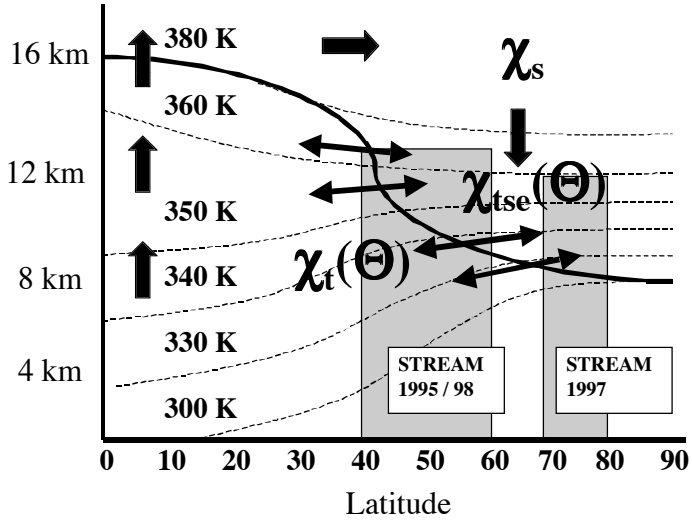

Figure 2.8: Schematic representation of the trace gas mixing ratio $\chi_{tse}(\Theta)$ in the lowermost stratosphere. The $\chi_{tse}(\Theta)$ mixing ratio is composed by air masses descending from above the 380 K surface with mixing ratio χ_s and tropospheric air masses with mixing ratio $\chi_t(\Theta)$. The solid line denotes the tropopause, whereas the thin dashed lines represent potential temperature isentropes. The gray boxes mark the areas covered by the STREAM campaigns. Large-scale transport from the tropics to high latitudes (Brewer-Dobson-circulation) is shown by single headed arrows. Two-way exchange along isentropes associated with the subtropical and polar jet streams is shown as double headed arrows. Upward transport across isentropes (diabatic ascent) can take place at mid-latitudes (not shown).

Table 2.4: Overview of the boundary conditions as used to calculate the Nt-values for the different campaigns. The variability denotes the 1σ standard deviation of the mean.

Campaign	Boundary conditions	N_2O ppbv	CFC-12 pptv	CO ppbv	C_2H_6 pptv
Nov./December 1995	Upper Troposphere	n.a.	531±5	n.a.	1101±213
	Stratosphere θ ≥ 360 K	n.a.	464[a]	n.a.	40[b]
March 1997	Upper Troposphere	309±2	538±3	n.a.	n.a.
	Stratosphere θ ≥ 353 K	275±4	458±10	18±2	54±7
July 1998	Upper Troposphere	312±2	540±7	116±23	1040±346
	Stratosphere θ ≥ 360 K	283±3	474±5	15±4	40±20

[a] From interpolation to 360 K potential temperature. [b] Adopted from STREAM-98.

In Figure 2.9 we show the calculated N_t^*-values as a function of the total amount of ROC from NMHC and NMHC + acetone in ppbC in the upper troposphere and lower stratosphere for the different campaign seasons (precision error bars were left out for clarity). The data can be approximated by a logarithmic fit (r = 0.95) depicted in Figure 2.9, although the stratospheric data at N_t^* < 80% show a rather linear relationship as well, in agreement with equation (2.3). Figure 2.9 further shows that during July 1998 (summer) the amount of NMHC was a factor of 2 to 3 higher than in March 1997 (winter) for a similar fraction of tropospheric air (N_t^* < 80%) in the lowermost stratosphere. When we include acetone the difference is even a factor of 4 to 5. The results for the fall conditions (November/December 1995) appear to lie in between the winter and the summer case, being a transition between both annual extremes.

In addition to the role of the upper tropospheric reservoir conditions (discussed in Section 2.4.1), the seasonal difference in the stratospheric ppbC distributions as a function of N_t^* can also be interpreted in terms of differences in mean air mass age. Closer to the tropopause seasonal differences are smallest where cross tropopause exchange can take place throughout the year, initiated by synoptic disturbances associated with the polar jet [*Chen*, 1995; *Dethof et al.*, 2000]. Thus, depending on the mixing frequency, source strength and photochemical age of the organic species, their mixing ratios are maintained well above their background. Deeper in the mixing layer, at isentropic surfaces > 340 K, the exchange frequency becomes seasonally dependent and the fraction of aged stratospheric air increases. In addition, there is also a latitudinal effect to take into account. During summer troposphere-to-stratosphere exchange (TSE) appears to be strongest at the subtropical tropopause. Tropospheric air masses mixed into the lowermost stratosphere that are transported poleward undergo chemical breakdown of reactive tracer species. Therefore, air sampled at lower latitudes in the mixing layer can be less photochemically processed and contain more reactive trace gases as compared to air masses sampled at higher latitudes with a similar tropospheric fraction.

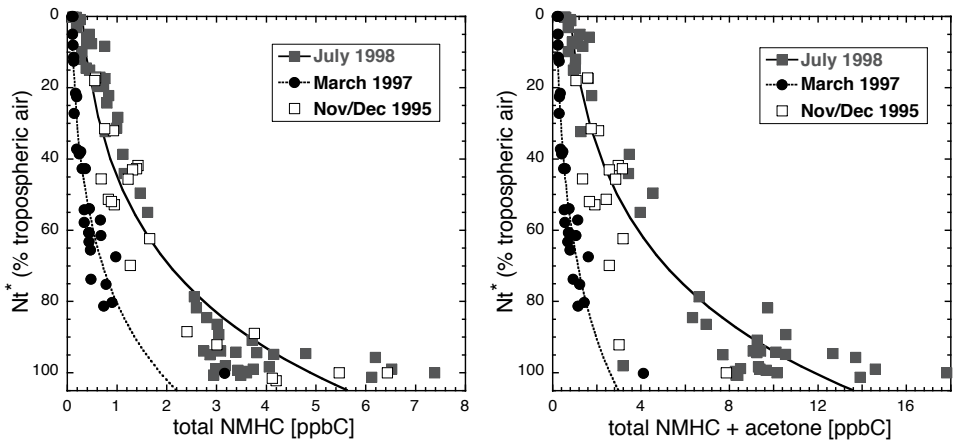

Figure 2.9: The total amount of measured reactive NMHC in ppbC as a function of the fraction of tropospheric air (N_t^*) in the upper troposphere and lower stratosphere for the different seasons. The curves represent the best fit (logarithmic; r = 0.95). Precision error bars are left out for clarity (~5% for NMHC and ~10% for NMHC + acetone; ~16% for N_t^*-1995, ~5% for N_t^*-1997, and ~6% for N_t^*-1998).

In Figure 2.10 the N_t^* in the upper troposphere and lower stratosphere as a function of potential temperature (Θ) and potential vorticity (PV) is shown for March 1997 and July 1998. Complementary to the results shown in Figure 2.9, Figure 2.10 (left panel) indicates that the tropospheric fraction, N_t^*, approaches zero at the Θ = 350 K level during winter, whereas during summer mixing appears to extend to at least the Θ = 370 K level. In agreement with this finding, the N_t^* as function of PV (Figure 2.10; right panel) emphasizes that enhanced ROC mixing ratios were found during winter up to about 9 PV-units, and up to at least ~12 PV-units during summer.

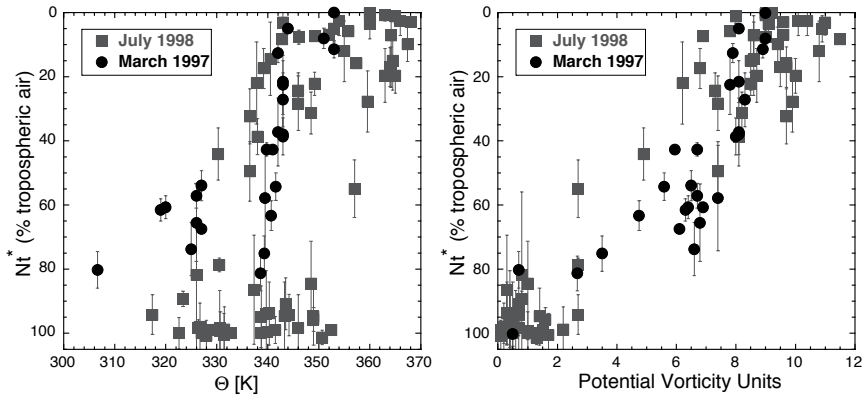

Figure 2.10: The fraction of tropospheric air (N_t^*) in the upper troposphere and lower stratosphere as a function of potential temperature (Θ) and potential vorticity (PV) is shown for March 1997 and July 1998. The data points correspond to the average conditions during canister sampling. The error bars denote the 1σ standard deviation of the mean N_t^*-value (precision error bars of ~10% for Θ and PV are left out for clarity).

2.5.2 Transient times of tropospheric air masses

Significantly enhanced NMHC mixing ratios of ethane, acetylene and propane, as well as acetone, in the stratospheric mixing layer points to recent troposphere-to-stratosphere mixing events on timescales shorter than the estimated photochemical lifetimes of these species. A tropospheric filament in the lowermost stratosphere slowly dissipates by the photochemical decay of these reactive NMHC species and mixing with ambient air, while the long-lived species remain virtually unaffected. As a result, the tropospheric fraction (N_t), determined from mixing ratios of the reactive NMHC species, becomes smaller than the tropospheric fraction calculated from the long-lived species (N_t^*) as a function of time (equation 2.3). Since we know the boundary conditions $\chi_t(\Theta)$ and χ_s for the reactive organic species, their concentrations in the mixing layer $\chi_{tse}(\Theta)$ and the fraction of tropospheric air N_t^* (from long-lived species), we can estimate the time Δt a tropospheric air parcel spent in the stratospheric mixing layer from the moment the mixing event took place at t_0 and the

encounter by the aircraft at t_1 ($\Delta t = t_1 - t_0$). Hence, by introducing photochemical decay from the reactions with OH and Cl radicals into equation (2.2), we can describe the concentration of a reactive organic species in the mixing layer ($\chi_{tse}(\Theta)$) as follows:

$$\chi_{tse}(\Theta) = (N_t^*\{\chi_t(\Theta) - \chi_s\} + \chi_s)\, e^{-(k_{OH}[OH] + k_{Cl}[Cl])\Delta t} \quad (2.4)$$

where k_{OH} is the rate coefficient for the reaction with OH, [OH] is the diurnal mean number density of OH in radicals cm^{-3}; k_{Cl} is the rate coefficient for the reaction with Cl; [Cl] is the diurnal mean number density of Cl in radicals cm^{-3}; Δt is the transient time of the encountered air parcel in the lowermost stratosphere. From equation (2.4) we can write Δt as:

$$\Delta t = \ln\{\chi_{tse}(\Theta) / (N_t^*\{\chi_t(\Theta) - \chi_s\} + \chi_s)\} / -\{k_{OH}[OH] + k_{Cl}[Cl]\} \quad (2.5)$$

The transient time Δt can be considered as the period between a discrete TSE-event bringing tropospheric air masses into the lowermost stratosphere and the encounter with the measurement aircraft. As such, Δt provides a measure of typical timescales of mixing processes in the lowermost stratosphere. Clearly, only recent mixing events provide conditions with NMHC mixing ratios in the mixing layer well above the detection limit of ~5 pptv. We chose the 3σ-precision of the stratospheric background concentration as lower limit excess value, considering mixing ratios $\geq$ 25 pptv as being significantly enhanced. In the following sections we apply the above transient time estimate method to a number of TSE-events encountered during July 1998 over Canada and discuss the uncertainties involved.

2.5.3 Indications of recent TSE-events

The vertical distribution of the CO/C_2H_6 ratio appears to be a useful indicator of air masses with a strong tropospheric signature in the lowermost stratosphere due to a TSE-event. Emissions of ethane and CO are highly correlated as a result of their common natural and anthropogenic sources [e.g., *Olivier et al.,* 1996]. Furthermore, the chemical lifetimes of both gases are of similar magnitude in the upper troposphere (~3 months) in the absence of a high (> 1000) diurnal mean number density of Cl (in radicals cm^{-3}). As a result, the CO/C_2H_6 ratio is not very variable in the upper troposphere and appears to be not very dependent on location and season, as was shown earlier by *Lelieveld et al.* [1999]. They found a value of 0.11 $\pm$ 0.04 (ppbv $pptv^{-1}$) as arithmetic mean for the northern hemispheric upper troposphere from various measurements and campaigns. While the upper tropospheric concentrations of ethane and CO are typically around 1 and 100 ppbv, respectively (Table 2.2), concentrations in the background stratosphere are photochemically reduced to about 40 pptv or less of ethane and 15 ppbv of CO (θ > 360 K; Table 2.3) resulting in a CO/C_2H_6 ratio $\geq$ 0.4. Because of this large concentration gradient, the CO/C_2H_6 ratio does not change significantly after mixing with stratosphere air depleted in C_2H_6 and CO for a certain period of time (< the photochemical lifetime of ethane and CO). Eventually, the CO/C_2H_6 ratio slowly increases from further photochemical depletion of C_2H_6 due to

reaction with Cl radicals and mixing with aged stratospheric air from aloft (with < 40 pptv of C_2H_6). Thus, an air mass with a CO/C_2H_6 ratio within the range of the upper tropospheric mean points to a recent tropospheric origin. How recently this air mass has entered the lowermost stratosphere can be estimated from higher hydrocarbons like acetylene, propane and n-butane (next section). The CO/C_2H_6 ratio as function of the N_2O mixing ratio and $\Delta\Theta$ above the local tropopause is plotted in Figure 2.11 showing the encountered mixing events (in total 18) as a separate linear branch.

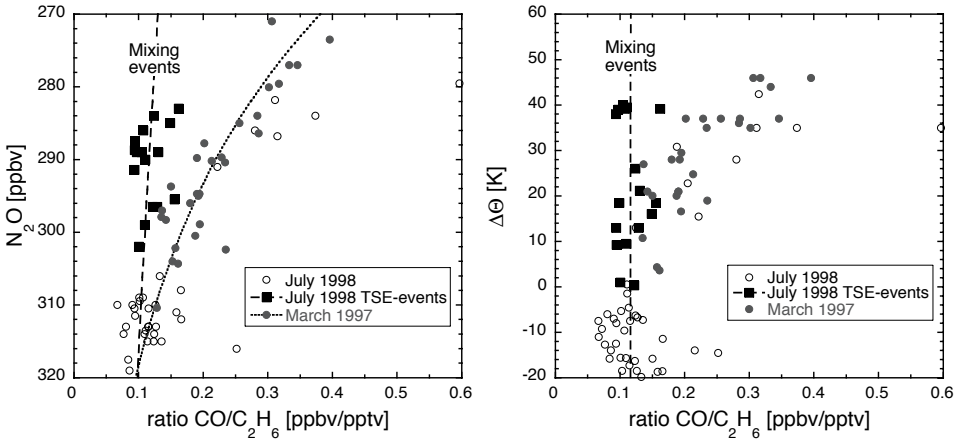

Figure 2.11: The ratio CO/C_2H_6 as a function of N_2O and $\Delta\Theta$ relative to the local tropopause. The STREAM 1997 'reference data' denote the March 1997 conditions with suppressed cross tropopause transport (left panel exponential fit; r = 0.9). The recent STREAM 1998 TSE-events stand out with a CO/C_2H_6 ratio closely related to values found in the upper troposphere (linear fit).

Note that Figure 2.11 includes only data from STREAM 97 and 98 due to missing CO data for STREAM 95. Ratios within the 1σ variability of the tropospheric mean were detected up to N_2O values of 283 ppbv, which corresponded to the Θ = 370 K isentropic level in the lowermost stratosphere during the July 1998 measurements.

2.5.4 Transient times from STREAM 1998 TSE-events

We selected nine TSE-events from the STREAM 98 campaign, for which the concentrations of acetylene and/or propane were sufficiently high (≥ 25 pptv) to calculate a transient time Δt (equation 2.5). Acetone, although abundant enough, has not been included in this analysis because its variability in the upper troposphere is too large (2.5 ± 1.5 ppbv; see Figure 2.3, middle panel) and possible acetone formation in the mixing layer from NMHC precursor species (mainly propane) cannot be excluded. The tropospheric fraction N_t^* has been calculated based on N_2O, CFC-12, CO and ethane mixing ratios in the mixing layer

(χ_{tse}) and boundary conditions for the upper troposphere ($\chi_t(\theta)$) and stratospheric overworld (χ_s). Reaction rate coefficients for reaction of acetylene and propane with OH and Cl radicals in the lower stratosphere were determined for mean ambient conditions of 223 K and 150 hPa (see Table 2.3). We used diurnal mean OH and Cl number densities of [OH] = 1.3×10^6 molecules cm^{-3} and [Cl] = 1000 molecules cm^{-3} for the mid-latitude summertime lowermost stratosphere, estimated with the photochemical box model (Section 2.4.2). The selected TSE-events, upper tropospheric and stratospheric boundary conditions and the calculated transient times based on acetylene ($\Delta t\_C_2H_2$) and propane ($\Delta t\_C_3H_8$) are presented in Table 2.5.

The $\Delta\Theta$-values in Table 2.5 show that all but one (Ferry flight a3) of the selected TSE-events occurred below the $\Delta\Theta$ = 25 K isentropic surface. Hence, with the assumption that isentropic transport of upper tropospheric air into the stratosphere below $\Delta\Theta$ = 25 K took place in the region of the polar jet [*Hoor et al.*, 2002], we have used the mean of all data related to air masses with a mid- to high-latitude origin to define the upper tropospheric reservoir conditions shown in Table 2.5. *Fischer et al.* [2002], who investigated upper tropospheric tracer gradients during STREAM 1998, indicated that the highest concentrations of NMHC, which have strong anthropogenic sources (notably ethane, acetylene, propane), were detected in air masses of mid- to high-latitude origin. Lowest concentrations were found in air masses originating over the (sub-)tropical Pacific with acetylene and propane mixing ratios as low as 40 and 20 pptv, respectively. Air mass origins in the upper troposphere, described in detail by *Fischer et al.* [2002], were based on 10-day backward trajectories (ECMWF). Although the CO/C_2H_6 ratio as a function of $\Delta\Theta$ (Figure 2.11) indicated in total seven more TSE-events at $\Delta\Theta$ > 25 K, the mixing ratios of acetylene and propane were mostly < 25 pptv for these events and are therefore not included in Table 2.5. The low acetylene and propane mixing ratios above the $\Delta\Theta$ = 25 K isentropic level suggest that these TSE-events most likely took place over the (sub-)tropical Pacific during July 1998.

We find Δt-values between 3 and 14 days in the mixing layer below $\Delta\Theta$ = 30 K at a fraction of 20% to 60% of tropospheric air in the lowermost stratosphere during summer (Table 2.5). The variability of the Δt-values denotes the estimated absolute precision. The precision is defined as the mean of the measured variability (1σ standard deviation of the mean) of the $\chi_t(\Theta)$ and χ_s mixing ratios and the 1σ standard deviation of the mean N_t^*-value. The calculated fraction of tropospheric air for the mixing layer (July 1998) is in agreement with the range of 5 – 55% estimated by *Hintsa et al.* [1998] from water vapor, CO_2 and O_3 aircraft measurements performed during May 1995. Our estimates for Δt support results from the model by *Dethof et al.* [2000]. They deduced that isentropic cross-tropopause exchange is a fast process occurring on a timescale of days. Furthermore, they found that the typical transition time for irreversible transport of a tropospheric filament into the lowermost stratosphere is 4 – 5 days.

2.5.5 Uncertainty of the transient time estimates

The results for $\Delta t\_C_2H_2$ and $\Delta t\_C_3H_8$ presented in Table 2.5 are not in perfect agreement. An important potential cause for erroneous results are wrongly defined tropospheric

boundary conditions ($\chi_t(\Theta)$). A too low estimated $\chi_t(\Theta)$ can result in a N_t-value higher than the mean N_t^*-value from stable tracers, which then results in a too low or even negative Δt-value. The latter is the case for the first two examples of flight 1 (F1) and flight 2 (F2) in Table 2.5 for $\Delta t\_C_2H_2$ (written as *n.a.*). A too high estimated $\chi_t(\Theta)$, on the other hand, will result in an overestimated Δt-value. This might be the case for the difference in $\Delta t\_C_2H_2$ and $\Delta t\_C_3H_8$ for flight F4 and F6. The TSE-events of F4 and F6 were encountered very close to the tropopause ($\Delta\Theta \approx 1$ K) and have a high tropospheric fraction ($N_t \approx 50\%$), pointing to a relatively recent mixing event in favor of the $\Delta t\_C_2H_2$ estimate. Furthermore, 10-day trajectories trace back to the mid-latitude (F4) and (sub)tropical (F6) Pacific where lower propane mixing ratios are expected. Hence, by applying the lower-range mixing ratio of 128 pptv for the propane tropospheric boundary condition for F4 and F6 we calculate a $\Delta t\_C_3H_8$ of 8.6 ± 2 and 3.6 ± 1 days, respectively, which is in much closer agreement with the $\Delta t\_C_2H_2$-values.

Another uncertainty in the Δt estimate is the assumed [OH] and/or [Cl] radical number densities. It was shown earlier (Section 2.4.2) that the acetone abundance strongly influences the OH concentration in the summertime lowermost stratosphere. The temperature dependence of the rate coefficients k_{OH} and k_{Cl} poses a potential uncertainty as well. The sensitivity of the transient time estimates to ambient temperature, [OH] and [Cl] is depicted in Figure 2.12 using the selected mixing event of flight 1 (Table 2.5) as a starting point (gray dot). Both graphs indicate that an ambient temperature range of about ±10 K, encountered during the July 1998 flights (shown in the graphs by the vertical bar) causes an uncertainty in Δt of the order of a day (or an uncertainty of <10%). The calculated value for Δt is inversely proportional to the OH and Cl radical concentrations weighted according to the rate constants (equation 2.5). Figure 2.12 shows that the Δt result could vary by ±2 days within the expected range of [OH] of ~1 – 1.5 molecules cm^{-3} as discussed in Section 2.4.2. Varying the [Cl] concentration by a factor of 2 results in a variation of ±1.5 days.

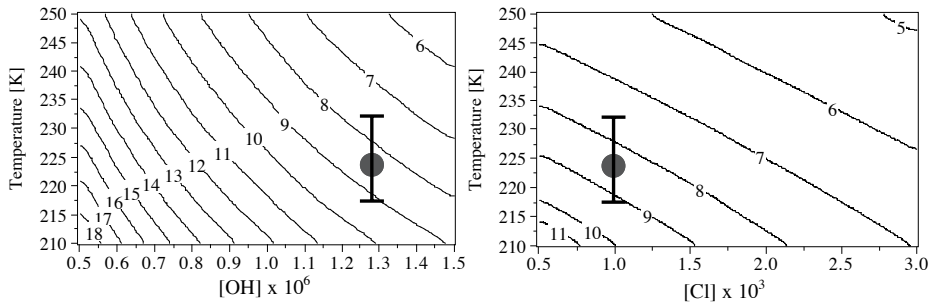

Figure 2.12: Contour plots showing the sensitivity of the calculated residence time in days of the STREAM 1998 TSE-event of flight 1 (F1 in table 2.5) to ambient temperature and an increasing [OH] concentration (in 10^6 molecules cm^{-3}) in the left panel and to an increasing [Cl] concentration (in 10^3 molecules cm^{-3}) in the right panel. In the left panel the [Cl] concentration is fixed at 10^3 molecules cm^{-3}, whereas in the right panel the [OH] concentration is set at 1.3×10^6 molecules cm^{-3}. The gray dot is the residence time calculated with the mean conditions chosen for the STREAM 1998 TSE-events. The vertical bar denotes the ambient temperature range during the selected TSE-events.

Table 2.5: STREAM 98 boundary conditions and selected TSE-events. The TSE-events relate to measurements of C_2H_2 and C_3H_8 concentrations in the lowermost stratosphere, which are larger than the 3σ variability range of the stratospheric background conditions at $\Delta\Theta$ > 35 K above the local tropopause. The variability denotes the measurement variability; except for N_t^*, $\Delta t\_C_2H_2$ and $\Delta t\_C_3H_8$, where the variability indicates the precision. N denotes the number of canister samples.

STREAM-98 TSE-events [OH]: 1.28×10^6 molecules cm^{-3}; [Cl]: 1000 molecules cm^{-3}

Source (Mid-Lat/Polar)	O_3 ppbv	P.V. r.u.	Θ K	ΔΘ K	N_2O ppbv	F-12 pptv	CO ppbv	C_2H_6 pptv	C_2H_2 pptv	C_3H_8 pptv	N_t^* %	$\Delta t\_C_2H_2$ days	$\Delta t\_C_3H_8$ days
Upper Trop. (N = 23)	69±18	0.9±0.8	333±8	0	312±2	540±7	116±23	1040±346	125±38	210±82	0	n.a.	n.a.
Stratosphere (N = 8)	457±15	9.3±0.7	362±4	>35	283±2	474±5	15±4	40±20	11±5	10±6	100	n.a.	n.a.
Mixing Layer F1	338	8.5	349	21	289	492	34	260	48	31	22±4	n.a.	8.5±1.8
Mixing Layer F2	246	7.4	337	10	299	513	54	493	76	60	50±9	n.a.	9.0±2.2
Mixing Layer F4	259	4.9	330	1	296	510	52	427	50	35	44±8	4.8±0.9	15.6±3.7
Mixing Layer F5	n.a.	8.1	338	13	297	496	53	412	34	45	39±5	11.4±2.0	10.0±2.2
Mixing Layer F6	182	3.0	357	1	302	511	59	587	65	59	55±9	2.9±0.6	10.7±2.6
Mixing Layer F8	298	9.7	337	19	295	497	43	276	31	33	32±8	10.3±2.0	12.3±2.9
Mixing Layer Ferry-a1	336	7.4	346	13	289	497	38	362	25	26	27±8	12.3±2.3	13.5±3.2
Mixing Layer Ferry-a2	337	8.2	349	19	n.a.	497	39	393	31	29	31±7	10.1±1.9	13.8±3.1
Mixing Layer Ferry-a3	408	8.7	363	38	291	483	27	283	29	20	20±8	3.7±0.7	n.a.

2.6 Conclusions

We presented data of selected C_2 – C_6 NMHC and acetone, which were collected during November/December 1995 (late fall), March 1997 (late winter) and July 1998 (summer) as part of STREAM in the extratropical lowermost stratosphere. The data augment the sparse reactive organic tracer measurements in the lowermost stratosphere. The NMHC and acetone measurements have been correlated with O_3, N_2O and potential temperature revealing a strong seasonal variability in the abundance of reactive organic species in the extratropical lowermost stratosphere. We found enhanced concentrations of NMHC and acetone up to potential temperatures of 370 K during July 1998. During March enhanced NMHC and acetone concentrations extended up to the Θ = 340 K isentrope. The vertical distributions of MNHC and acetone follow the seasonal variations in mixing layer depth determined by *Hoor et al.* [2002] on the basis of correlations between CO and O_3. During summer and fall mean NMHC + acetone concentrations in the mixing layer equaled (2.3 $\pm$ 1.7 ppbC and 2.2 $\pm$ 0.5 ppbC, respectively) and were more than a factor of two higher than measured during winter (0.9 $\pm$ 0.3 ppbC).

We note that the limited number of campaigns performed in different locations at different times requires caution in extrapolating our results to the whole lowermost stratosphere at all seasons and latitudes. Nevertheless, good agreement was found between mean results of STREAM (March 1997 and July 1998) and the February/March 1994 PEM West B campaign and the October/November 1997 SONEX campaign. In addition, our results cannot reveal possible effects from interannual variability in isentropic cross-tropopause transport on the organic tracer distributions in the lowermost stratosphere. Model work by *Dethof et al.* [2000] and *Sprenger and Wernli* [2002] indicated, however, that the interannual variability of stratosphere-troposphere exchange is relatively small compared to its seasonal variability.

The amount of acetone (in ppbC) equaled the sum of NMHC (in ppbC) making it the dominant organic tracer species in the lowermost stratosphere after ethane. The relatively large acetone concentrations in the lowermost stratosphere as compared to NMHC, especially during summer, emphasize the dominance of terrestrial and oceanic sources in the upper troposphere as suggested by *Jacob et al.* [2002]. We used a box model to indicate that these acetone sources can explain 30 to 50% of the enhanced OH concentrations in the summertime lowermost stratosphere up to at least Θ = 360 K, through enhanced isentropic transport at the sub-tropical tropopause.

A simple mass balance calculation was used to estimate the transport of tropospheric air into the lowermost stratospheric mixing layer. It was found that a significant tropospheric fraction ($\leq$ 30%) was present up to Θ = 370 K during July 1998, while the tropospheric fraction during March 1997 approached zero at about Θ = 350 K. Increasing methyl chloride concentrations at higher isentropic levels (360 – 370 K) in the lowermost stratosphere during July 1998 were found, pointing to a tropospheric fraction with a (sub-)tropical origin.

The decay of reactive organic species in the mixing layer with photochemical lifetimes of a few weeks during summer (notably propane and acetylene) was used to demonstrate a simple method based on a modified mass balance calculation to estimate timescales of troposphere-to-stratosphere mixing. A number of troposphere-to-stratosphere mixing

events, encountered during July 1998, with acetylene and propane concentrations of 25 – 80 pptv well above their detection limit could be used to calculate mixing timescales of 3 to 14 days, indicating the transit time between the mixing event and the encounter with the aircraft. These results corroborate the studies of *Dethof et al.* [2000] and *Hoor et al.* [2002], demonstrating that the summertime midlatitude lowermost stratosphere is subject to intense and frequent mixing with tropospheric air. Our analysis of mixing timescales in the lowermost stratosphere during the 1998 summer is hampered, however, by the low number of encountered mixing events due to the limited canister sample frequency. By greatly increasing the number of NMHC measurements a better representation of the reservoir conditions could be achieved. At the same time, a larger number of TSE-events will be encountered, allowing a more quantitative analysis.

Acknowledgements

We gratefully acknowledge the outstanding collaboration with all members of the STREAM team and the Citation crew from the Delft University of Technology. The STREAM project was funded by the European Union, Utrecht University, and the Max Planck Society.

3 Methyl chloride and other chlorocarbons in polluted air during INDOEX

Abstract. Methyl chloride (chloromethane, CH_3Cl) is the most abundant natural chlorine containing gas in the atmosphere, with oceans and biomass burning as major identified sources. Estimates of global emissions suffer from large uncertainties, mostly for the tropics, partly due to a lack of measurements. We present analyses of whole air canister samples for selected non-methane hydrocarbons and chlorocarbons. The samples were collected from an aircraft during the INDOEX campaign over the northern Indian Ocean in February and March 1999. The CH_3Cl results are correlated to selected non-methane hydrocarbons, and in-situ measurements of carbon monoxide (CO) and acetonitrile (CH_3CN). We relate high mixing ratios of ~750 pmol mol^{-1} of CH_3Cl to biomass burning, as observed in polluted air masses from India and Southeast Asia. We infer a relatively high enhancement ratio relative to carbon monoxide, $\Delta CH_3Cl/\Delta CO \approx 1.74 \pm 0.21 \times 10^{-3}$ mol mol^{-1}. The CH_3Cl levels relate to the extensive biofuel use in India and Southeast Asia, notably the burning of agricultural waste and dung with a comparatively high chlorine content. It appears that CH_3Cl emissions from biofuel consumption in India and Southeast Asia have been underestimated in the past. Furthermore, we observed enhanced dichloromethane (CH_2Cl_2) and trichloromethane ($CHCl_3$) levels, correlating with high CO, acetylene (C_2H_2) and CH_3Cl, indicating that biomass burning is a small but significant source of these species.

Published in *Journal of Geophysical Research*, with J. Lelieveld, J.A. de Gouw, C. van der Veen, and H. Fischer as co-authors.

3.1 Introduction

Recently, extensive surveys on the abundance and importance of chlorocarbons for atmospheric chemistry have been published [*McCulloch et al.*, 1999*; Lobert et al.*, 1999; *Keene et al.*, 1999; *Khalil and Rasmussen*, 1999]. They highlight the importance of methyl chloride (chloromethane, CH_3Cl) as the most abundant halocarbon, estimated to be about 43% of the total reactive chlorine in the troposphere [*Khalil and Rasmussen*, 1999]. The known sources of CH_3Cl, as described by *Keene et al.* [1999], include about 48% from biomass burning, ~35% by oceans and ~8% by wood rotting fungi. Furthermore, emissions from urban/industrial activity (including coal burning) contribute about 9%. The main sink of CH_3Cl in the troposphere is the reaction with OH radicals (~86%), resulting in an average atmospheric lifetime of about 1.3 years [*Khalil*, 1999]. A minor but significant loss mechanism is transport to the stratosphere, where CH_3Cl is destroyed by photo-dissociation and reaction with OH [*Keene et al.*, 1999], from which the reactive chlorine contributes to ozone loss. The relative contribution of CH_3Cl to the total recent Cl flux to the stratosphere has been estimated at 15 – 25% [*Montzka et al.*, 1996]. This fractional contribution is likely to increase in the near future due to the decline of long-lived anthropogenic halocarbons in response to the Montreal Protocol. The composite budget for CH_3Cl by *Keene et al.* [1999], however, suggests a substantial underestimation of sources (1.32 Tg Cl yr^{-1}) as compared to modeled sinks (2.78 Tg Cl yr^{-1}), i.e. about 1.45 Tg Cl yr^{-1} (Tg = 10^{12} g). Three possible explanations may account for the imbalance. *Keene et al.* [1999] state that the relatively large uncertainties of the emissions from known sources allow the possibility that one or more emission fluxes have been significantly underestimated. Secondly, a considerable uncertainty in the temperature dependence of the rate constant of the CH_3Cl oxidation by OH (described by *DeMore et al.*, 1997) could contribute to the discrepancy. Thirdly, the emissions from higher plants, which are not taken into account due to the lack of field measurement, may represent a major unidentified source of CH_3Cl. According to *Khalil and Rasmussen* [1999], 85% of CH_3Cl from known sources is produced in the tropics and subtropics in the 30°S – 30°N latitude band.

Here we focus on biomass burning, which is estimated to be the largest global source of CH_3Cl and a significant source for dichloromethane (CH_2Cl_2). Biomass burning appears to be mainly human-induced, with savanna fires and the burning of biofuels as major contributors [*Lobert et al.*, 1999]. Present estimates indicate that the use of biofuels, such as fuelwood, charcoal, agricultural residues waste and dung, and open field burning of unusable crop residues, contributes more than half (~53%) to the CH_3Cl emissions (and about 38% of both the CH_2Cl_2 and trichloromethane (chloroform, $CHCl_3$) emissions) from biomass burning [*Lobert et al.,* 1999]. India and neighbouring countries have the comparatively largest consumption of biofuel, which contributes about 25% to the global biofuel emissions [*Olivier et al.*, 1996]. Biomass burning emissions in Southeast Asia are responsible for about a third of all CH_3Cl emissions from biomass burning of 0.64 Tg Cl yr^{-1}, as estimated by *Lobert et al.* [1999].

We present hydrocarbon and chlorocarbon measurements from air samples, with emphasis on CH_3Cl, collected over the tropical Indian Ocean in February/March 1999 during the Indian Ocean Experiment (INDOEX). The measurement area was affected by pollution

outflow from India and Southeast Asia, inhabited by about half the world's human population. The measurements encompass air samples both with a strong continental influence and from the pristine southern Indian Ocean atmosphere. Enhancement ratios relative to carbon monoxide for CH_3Cl and other chlorocarbons, notably CH_2Cl_2 and $CHCl_3$, are inferred from the measurements, which we compare to available emission factors for biomass burning from the literature. We will use the CH_3Cl enhancement ratio to estimate emissions from biomass burning in India and Asia. Finally, we discuss the uncertainties in presently estimated source contributions from biomass burning for CH_3Cl.

3.2 Field campaign and measurement techniques

3.2.1 The INDOEX campaign

The INDOEX field campaign was an international collaboration between institutes from the United States, Europe, India and the Maldives, involving various measurement platforms on land, sea and in the air. The main purpose of INDOEX was to characterize the pollutant outflow from India and Southeast Asia and to study the effect on atmospheric chemistry and solar radiation attenuation by aerosols. We present measurements performed on-board a Cessna Citation-II twinjet aircraft operated by the Delft University of Technology, The Netherlands. The aircraft operated from the international airport of Malé, the capital of the Maldives. A total of 23 flights was performed up to 12.5 km altitude between 7°S and 8°N over the Indian Ocean. A detailed description of the flights, measurement payload during INDOEX, as well as an overview of the results is given by *de Gouw et al.* [2001]. Here we only summarize the measurement techniques relevant for this paper. For an overview of the main results from the different measurement platforms operating during INDOEX, focusing on the chemical composition of the outflow from South and Southeast Asia, we refer to *Lelieveld et al.* [2001].

3.2.2 Measurements of hydrocarbons, methyl chloride and other chlorocarbons

Air samples were collected with an automated airborne sampling system in 2.5-L stainless steel electro-polished canisters for post-campaign analysis of hydrocarbons and chlorocarbons, including CH_3Cl. Pre-cleaned pure nitrogen-containing canisters were evacuated and flushed for about 5 minutes prior to pressurizing with ambient air to 2.5 bars overpressure by a MB-602 metal bellows pump. The collection of a boundary layer sample took about 5 seconds, while in the upper troposphere (at ambient pressures less than 0.2 bar) sampling up to 3 minutes was necessary. Between 20 and 45 days after sampling, the canisters were analyzed in the laboratory. The analysis was performed with a gas chromatograph (Varian star 3600 CX) equipped with a CP-SilicaPLOT column (0.53 mm I.D.; 60 m long)

and detection by Flame Ionization Detection (hydrocarbons and CH_3Cl) and Electron Capture Detection (chlorocarbons). CH_3Cl is detected by both the ECD and the FID for quantitative evaluation. No interference could be observed in both the FID and the ECD peak. We chose the FID quantitative results for CH_3Cl for its higher precision due to larger peak areas and better stability than the ECD output. The detection limit of the peak integration for CH_3Cl is about 10 pptv (FID). The detection limit for hydrocarbons is <3 pptv, for CH_2Cl_2 <5 pptv, and for the other chlorocarbons <0.1 pptv. Pre-concentration of a 1-L sample was done with a *Varian* Sample Pre-concentration Trap (SPT) at a freeze-out temperature of -170° C. The reproducibility of the SPT with standard gas was better than 2% (1σ). A commercial gravimetrically prepared standard gas mixture (*PRAXAIR*) was used as reference air, with an absolute accuracy of 3% for hydrocarbons and 2% for chlorocarbons, as indicated by the supplier. CH_3Cl showed excellent linearity (N = 20; r = 0.998 at the 99% confidence level) with the FID response over a concentration range of 50 to 650 pptv, yielding a uniform and stable response factor. A comparison of eight canister sample analyses, prior to the INDOEX campaign, was performed between the laboratory of *J. Rudolph* (Centre for Atmospheric Chemistry, York University, Toronto) and our laboratory. The comparison indicated an overestimation of our CH_3Cl results based on the *PRAXAIR* standard by a factor of 1.17 ± 0.07 (N = 8) relative to their results. Our quantification was based on a commercial chlorocarbon standard (*PRAXAIR*), whereas *J. Rudolph* used a standard mixture prepared by the American National Institute of Standards and Technology (NIST) for quantification. To check the absolute concentrations in our *PRAXAIR* standard, an additional comparison was arranged with *S. A. Montzka* from NOAA/CMDL, Boulder, Co (about 18 months after INDOEX). The analysis of our standard by *S.A. Montzka,* indicated a significantly lower amount of CH_3Cl (by a factor of 0.76 ± 0.04) than stated by the manufacturer, in accordance with the earlier comparison with *J. Rudolph*. Good agreement, within the uncertainty of the measurements, was obtained between the NOAA/CMDL and the *PRAXAIR* standard for the other chlorocarbons. The comparison of the standards with *S.A. Montzka* suggested a slight declining trend of the CH_3Cl concentration in our standard. Hence, we corrected our CH_3Cl results by a factor of 0.85 from the earlier comparison with *J. Rudolph*, resulting in an additional uncertainty of about 5% (total accuracy 7%).

The precision (1σ) of CH_3Cl and non-methane hydrocarbons (for concentrations > 5 pptv detected by FID) and chlorocarbons (for concentrations >1 pptv detected by ECD), determined as the average relative standard deviation of duplicate analyses of up to 9 different samples, was as follows: methyl chloride 1%, ethane (C_2H_6) 4%, acetylene (C_2H_2) 3%, propane (C_3H_{10}) 10%, n-butane (n-C_4H_{10}) 30%, isoprene (C_5H_8) ~50%, benzene (C_6H_6) 10%, toluene (C_7H_8) 14%, dichloromethane (CH_2Cl_2) 21%, trichloromethane ($CHCl_3$) 7%, 1,1,1-trichloroethane (methyl chloroform, CH_3CCl_3) 2%, and tetrachloroethylene (C_2Cl_4) 2%. The relatively low analytical precisions (deviation >15%) of some species are due to low ambient concentrations (in case of n-butane and isoprene) or a weak detector response (in case of CH_2Cl_2) resulting in a low signal-to-noise ratio (<3) and poor peak integration. To test the stability of the chloro- and hydrocarbons in the canisters, we performed a re-analysis on five samples up to 43 days after the first analysis (and up to 75 days after sampling). The average of the relative standard deviations of the means of the first and the second analyses (N = 5) was found to be ±3%, within the 1σ precision for all compounds except for benzene and $CHCl_3$. For the latter two compounds the mean of the

relative standard deviations were about ±8% within the (1σ) precision. Hence, our tests indicate no significant storage effect up to 75 days after sampling for the hydrocarbons and chlorocarbons described in this study.

3.2.3 Carbon monoxide measurements

Tunable diode laser absorption spectroscopy (TDLAS) was applied to measure the carbon monoxide (CO) mixing ratios in-situ during the flights at a frequency of 1 Hz [*Wienhold et al.*, 1998]. For the INDOEX data the calibration accuracy was 2.8% and the average precision 3.6% (1σ). The CO results from the Citation aircraft during INDOEX are further discussed by *Williams et al.* [2002] and *de Gouw et al.* [2001].

3.2.4 Acetonitrile measurements

Acetonitrile (CH_3CN) measurements, amongst many other compounds, were carried out with a Proton-Transfer-Reaction Mass-Spectrometer (PTR-MS) on-board the measurement aircraft [*de Gouw et al.*, 2001]. The technique is described in detail by *Lindinger et al.* [1998]. Measurements were performed on-line every 12 seconds and finally smoothed over 5 points resulting in a measurement frequency of 1 minute. CH_3CN was detected with a precision of ±30% and a calibration uncertainty better than ±20%. The results from the PTR-MS instrument during INDOEX are described by *de Gouw et al.* [2001].

3.3 Measurement results

3.3.1 Overview of results

Table 3.1 presents an overview of the average concentrations of CH_3Cl, selected hydrocarbons, chlorocarbons, CO and CH_3CN measured in the marine boundary layer and in the free troposphere during the INDOEX flights. Mixing ratios are given in parts per billion by volume (ppbv, 10^{-9} mol × mol^{-1}) for CO and parts per trillion by volume (pptv, 10^{-12} mol × mol^{-1}) for hydrocarbons, chlorocarbons and CH_3CN. We compare CH_3Cl results with carbon monoxide and acetylene, propane, n-butane and benzene, because they are all released from combustion processes involving either biomass or fossil fuels. We include the biogenically emitted isoprene, which has a very short lifetime (a few hours), as tracer for nearby natural emissions. C_2Cl_4 and CH_3CCl_3 are included as tracers for urban/anthropogenic pollution. Furthermore, we show boundary layer results of CH_2Cl_2 and $CHCl_3$, of which emission ratios relative to CO and CO_2 from biomass burning have been reported as well [*Rudolph et al.,* 1995].

Table 3.1: Average trace gas mixing ratios during INDOEX (1999).[a]

Species	INDOEX ~6.5°S Flight 11 *Indian Ocean* N = 3 < 0.5 km alt.	INDOEX 0°S – 8°N Flight 13 to 16 *Arabian Sea* N = 11 < 0.5 km alt.	INDOEX 0°S – 8°N Flight 1 to 10 *Bay of Bengal* N = 16 < 0.5 km alt.	INDOEX 8°S – 8°N All Flights *Indian Ocean* N = 71 1.2 –12.5 km alt.
CO, ppbv	47 (7)	131 (14)	206 (35)	114 (22)
CH_3Cl, pptv	542 (6)	666 (35)	757 (62)	639 (31)
CH_3CN, pptv	194 (65)	257 (70)	273 (71)	126 (62)
C_2H_6, pptv	195 (37)	467 (107)	817 (243)	542 (139)
C_2H_2, pptv	2 (3)	102 (44)	291 (173)	109 (51)
C_3H_8, pptv	6 (1)	36 (33)	50 (35)	48 (22)
n-C_4H_{10}, pptv	3 (1)	10 (8)	10 (7)	14 (11)
benzene, pptv	3 (2)	47 (18)	99 (40)	35 (17)
toluene, pptv	3 (1)	14 (19)	6 (2)	15 (12)
isoprene, pptv	21 (6)	29 (15)	15 (16)	10 (8)
C_2Cl_4, pptv	0.8 (0.02)	1.8 (0.4)	2.8 (0.4)	2.7 (0.7)
CH_3CCl_3, pptv	66 (0.1)	67 (2)	65 (3)	70 (3)
CH_2Cl_2, pptv	8 (0.5)	22 (5)	26 (5)	29 (12)
$CHCl_3$, pptv	3.3 (0.1)	6.6 (0.9)	7.9 (1.2)	9.4 (1.1)

[a]The CO and CH_3CN data are averages for the flight levels during which the canisters samples were collected. The source regions are given in italics. The 1σ standard deviation is indicated between parentheses. N denotes to the number of air samples.

In this study, we present CH_3CN data because it has been proposed as a distinct marker of biomass burning [*Lobert et al.*, 1991; *Holzinger et al.*, 1999]. Laboratory measurements of biomass burning emissions by *Holzinger et al.* [1999] showed a strong correlation between CO and CH_3CN (among many other organics) leading to the conclusion that biomass burning dominates the global budget of CH_3CN. The sub-division in Table 3.1 for the northern Indian Ocean marine boundary layer measurements indicates the different source areas as distinguished on the basis of back-trajectories provided by the Royal Netherlands Meteorological Institute (KNMI) [*de Gouw et al.,* 2001; *Verver et al.*, 2001]. The trajectories were calculated on the basis of archived 3D wind data from the European Center for Medium Range Weather Forecasts (ECMWF) model [*Stohl et al.*, 2001]. Figure 3.1 shows a compilation of 5-day back-trajectories representative for the marine boundary layer flight tracks. The marine boundary layer height over the Maldives area was generally between 0.5 and 1 km altitude. The trajectories end in the marine boundary layer at the ~150 m flight altitude of the Cessna Citation During the first part of the campaign, from February 14 to early March (flights 1 to 10), a steady northeasterly monsoon carried polluted air masses from northern India and the Bay of Bengal region. During the second part of the campaign (flights 13 to 16) from early to late March, the flow shifted toward a more northwesterly direction, carrying relatively cleaner air masses from the Arabian Sea to the measurement area (Figure 3.1). The trajectories from the Bay of Bengal region indicate travel times of the encountered air masses between about 2 and 5 days from potential source regions around the Bay of Bengal. In most cases, the ITCZ (Inter Tropical Convergence Zone) was too far south (between 5°S and 12°S) to be

reached by the Citation. Only on March 4 (flight 11; Figure 3.1), when the ITCZ was located at 1° – 3°S, the aircraft was able to cross the ITCZ and to reach pristine southern hemispheric air masses in the marine boundary layer at ~6.5°S. For an extensive survey of the meteorology during INDOEX we refer to *Verver et al.* [2001].

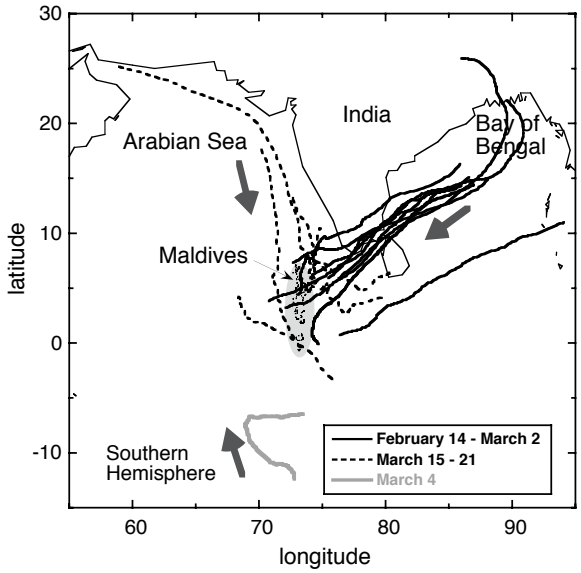

Figure 3.1: Composite of ECMWF 5-day back-trajectories for each boundary layer flight track over the Maldives area. During flights 1 to 10 (performed between February 14 to March 2; black lines) polluted air masses originating from the Bay of Bengal were encountered. On flight 11 (March 4; gray line) a boundary flight track was flown behind the ITCZ in pristine southern hemispheric air. Flights 13 to 16 (March 15 to 21; dotted lines) correspond to less polluted air masses coming from the Arabian Sea area. The fat arrows indicate the general flow directions.

3.3.2 Boundary layer results

The marine boundary layer measurements are, as explained before, subdivided into three regimes based on the meteorology during INDOEX. The most polluted conditions (i.e. highest CO) were encountered during the first part of the campaign (February to early March) when a steady northeasterly flow from the highly populated Bay of Bengal region dominated the measurement area near the Maldives. All tracers that characterize biomass combustion processes, including CH_3Cl (Table 3.1), were strongly enhanced. The flow from the Arabian Sea region carried cleaner air masses (lower CO) but still high CH_3Cl, originating from the less densely populated Middle East and the Arabian Peninsula. Cleanest conditions were encountered during a boundary layer track on March 11 at ~6.5°S, when our aircraft crossed the ITCZ at about 1°S.

As expected, the tracer for natural terrestrial emissions (isoprene) was low levels throughout the campaign. The lifetime of isoprene (by reaction with the OH radical) in the marine boundary was on the order of one hour (based on a reaction coefficient (K_{OH}) of 1.0 $\times 10^{-10}$ cm^3 molecule s^{-1} by *Atkinson* [1990], and a diurnal average OH concentration of 2.5 $\times 10^6$ molecules cm^{-3}, from *de Laat and Lelieveld* [2001]). Thus, within a day, high concentrations (~1 – 2 ppbv) from the continent would be depleted. The low, though non-negligible, background concentration may have originated from the ocean. A marine source of isoprene related to phytoplankton activity has been reported earlier by several investigators (e.g., *Bonsang et al.*, 1992*; Milne et al.*, 1995; *Broadgate et al.*, 1997).

The tracer C_2Cl_4 is an indicator of urban/industrial activity. This chlorocarbon has almost no natural sources and is used as an industrial solvent. Its atmospheric lifetime is about 150 days, mainly due to reaction with the OH radical [*Khalil*, 1999]. We measured rather low and homogeneously distributed concentrations of C_2Cl_4 over the northern Indian Ocean, which underscores the low level of urban/industrial emissions from South and Southeast Asia. CH_3CCl_3 measured at the PEM-West A campaign (Pacific Exploratory Mission) over the western Pacific, proved to be a good tracer for coastal East-Asian industrial activity [*Blake et al.*, 1996]. During INDOEX we found no significant difference in the CH_3CCl_3 concentration between polluted and pristine air masses. In fact, the average CH_3CCl_3 concentration of about 66 pptv in polluted air masses resembles closely the global tropospheric mean for 1999 of about 65 pptv [*Montzka et al.*, 1999], which emphasizes the minor contribution of urban/industrial activity. A recent laboratory study by *Rudolph et al.* [2000] indicated that the release of CH_3CCl_3 from biomass burning is of marginal importance, being even much smaller than previously assumed. Our results agree with this. CH_2Cl_2 and $CHCl_3$, on the other hand, were slightly enhanced in polluted air masses during INDOEX, correlating with high CH_3Cl, acetylene and CO concentrations (further discussed in Section 3.4.2). This strongly suggests that these compounds have biomass burning sources, in agreement with earlier findings by *Rudolph et al.* [1995].

3.3.3 Comparison with other measurements

To our knowledge, there are no other reports of extensive hydrocarbon and chlorocarbon measurements performed in the INDOEX region to compare with. Hence, we compare average results from INDOEX with results from the Pacific Exploratory Mission over the Western Pacific (PEM-West A), which took place in September and October 1991 in Southeast Asia [*Blake et al.*, 1996]. The PEM-West results were strongly influenced by outflow of highly polluted air masses from large urban centers in Eastern Asia, resulting in relatively high mean concentrations. In Table 3.2 the average concentrations from canisters samples collected below 2 km altitude from INDOEX and PEM-West A are shown. The PEM-West source regions in eastern Asia, which include East China, South Korea and Japan, are characterized by a higher level of economic and industrial development than the INDOEX region. We find the most prominent differences for propane, n-butane, CH_3CCl_3 and C_2Cl_4. Notably, these hydrocarbon species are expected to be more abundant in more developed urban/industrialized regions sampled during PEM-West A, for which fossil fuel use was a primary source. The INDOEX concentrations of these species were considerably

lower, whereas other combustion tracers like acetylene were fairly similar, as these gases are less specific, being emitted from both fossil and biofuel use. The relatively high CH_3CCl_3 concentrations measured during the PEM-West A campaign in 1991 correspond to the global average around 150 pptv at the time [*Montzka et al.*, 1999]. Since the beginning of 1990, its concentrations have declined to around 65 pptv in 1999, due to the Montreal Protocol for halocarbons [*Montzka et al.*, 2000].

Table 3.2: Comparison of the average INDOEX (February/March 1999) data, for altitudes <2 km, with the PEM-West A (September/October 1991) hydrocarbon results.[a]

Species	INDOEX 6.5°S – 8°N Indian Ocean N = 34 <2 km altitude	PEM-West A[b] 0.5°S – 59.5°N Western Pacific N = 421 <2 km altitude
CO, ppbv	173 (45)	n.a.
CH_3Cl, pptv	711 (65)	n.a.
CH_3CN, pptv	260 (71)	n.a.
C_2H_6, pptv	677 (248)	758 (414)
C_2H_2, pptv	207 (153)	172 (265)
C_3H_8, pptv	46 (33)	150 (318)
n-C_4H_{10}, pptv	10 (7)	70 (290)
benzene, pptv	73 (39)	53 (98)
toluene, pptv	9 (12)	49 (367)
isoprene, pptv	21 (16)	<3
C_2Cl_4, pptv	2.4 (0.6)	9 (21)
CH_3CCl_3, pptv	66 (3)	176 (75)
CH_2Cl_2, pptv	25 (6)	n.a.
$CHCl_3$,pptv	7.3 (1.2)	n.a.

[a]The standard deviation (1σ) is given between parentheses. The CO and CH_3CN data are averages for the flight levels during which the canisters samples were collected. N denotes to the number of air samples.
[b]From *Blake et al.* [1996].

We compare average boundary layer CH_3Cl mixing ratios measured during INDOEX with average observed CH_3Cl based on monthly means of January to April 1999 from selected NOAA/CMDL remote surface stations (Mauna Loa, Hawaii, USA (19°N); Samoa, USA (14°S); Cape Grim, Tasmania, Australia (40°S)), and a global mean for the same period (based on all seven NOAA/CMDL remote sampling locations; see *Montzka et al.* [1999]) provided by *S.A. Montzka (personal communication)* from NOAA/CMDL (Table 3.3). *Khalil et al.* [1999] report a global average atmospheric mixing ratio for CH_3Cl of about 540 pptv, slightly lower than the global mean of 553 pptv for January to April 1999 *S.A. Montzka, personal communication, 2000)*.

The latitudinal variation from the data provided by *Montzka (personal communication, 2000)* shows a positive gradient towards the tropics where the highest concentrations are measured, in agreement with results from *Khalil et al.* [1999]. Compared to the average concentration of 590 ± 20 pptv CH_3Cl, representative for the remote northern hemispheric

tropics, the average marine boundary layer concentration of 720 ± 69 pptv during INDOEX is significantly higher. In the relatively clean air south of the ITCZ (see Table 3.1), encountered on March 4, the lowest CH_3Cl concentration of 542 pptv was observed, similar to the southern hemispheric tropical average of *Montzka*.

Table 3.3: Comparison of INDOEX mean CH_3Cl mixing ratio (or concentration) in pptv with average observed CH_3Cl mixing ratios based on monthly means of January to April 1999 from selected NOAA/CMDL surface stations.[a]

		Northern Hemisphere	Southern Hemisphere	
Year 1999	Global	Tropical[1]	Tropical[2]	Temporate[3]
NOAA/CMDL	553 (3)	590 (20)	541 (13)	516 (4)
INDOEX		720 (69)	542 (6)	

[a]Surface stations are Mauna Loa[1] (19°N), Samoa[2] (14°S), Cape Grim[3] (40°S)). Data provided by S. A. Montzka, NOAA/CMDL, Boulder, CO, USA). The 1σ standard deviation of 4 monthly means (in parentheses) indicates the atmospheric variability.

3.3.4 Photochemical age of polluted air masses in the boundary layer

Back-trajectory analysis by the ECMWF-model [*Verver et al.,* 2001] indicated that the air masses from the Indian continent had traveled over the Bay of Bengal and the Indian Ocean for about 2 to 5 days to the measurement area over the Maldives. A further diagnostic of the (photochemical) age of air masses away from continental sources is provided by the NMHC composition and concentrations. Mixing ratios of NMHC such as ethane, acetylene, propane, n-butane, benzene and toluene, originating from combustion sources over the continent, can be used to mark the photochemical age of an air mass, because they have no significant oceanic sources, and their sink is mainly reaction with OH radicals. Estimated photochemical lifetimes of these species in the marine boundary layer during INDOEX are 18.6, 5.1, 4.2, 3.8, 2.1 days and 0.7 day for ethane, acetylene, propane, benzene, n-butane and toluene, respectively, based on reaction coefficients (K_{OH}) by *Atkinson et al.* [1992], an average boundary layer temperature of 298 K and a diurnal average OH concentration of 2.5×10^6 molecules cm^{-3}, according to *de Laat and Lelieveld* [2001]. Thus, significant mixing ratios above background level (generally >10 pptv) of short-lived compounds, like n-butane and toluene, can only be present in relatively fresh plumes (<2 days old), whereas longer-lived compounds like benzene, acetylene and propane can still be enhanced in aged plumes (<5 days). When applying this simple diagnostic to the mean results for the Bay of Bengal data, as presented in Table 3.1, we find that toluene and n-butane were both close to their background as found in aged air masses (Indian Ocean, ~6.5°S), while benzene was still significantly enhanced. This implies that the polluted air masses advected from the Bay of Bengal had a photochemical age between 2 and 4 days from continental sources.

3.3.5 Free tropospheric results

The mean results of 71 air samples, collected during INDOEX in the free troposphere between 1.2 and 12.5 km altitude over a latitude range of 6.5°S to 8°N, are presented in Table 3.1 (last column). Back-trajectory analysis did not clearly indicate dominant source areas, as was the case for the marine boundary layer air masses. Furthermore, the travel distances of the air masses were, as can be expected, much longer due to higher wind speeds in the free troposphere. As a result, air mass mixing and plume dilution is more efficient, so that the absolute concentrations and the variability (1σ standard deviation) are generally smaller in the free troposphere compared to the boundary layer. Nevertheless, compared to the pristine conditions encountered during the southern hemispheric flight track, average trace gas concentrations in the free troposphere, notably of CH_3Cl, were significantly enhanced, being comparable to the boundary layer conditions of the air masses from the Arabian Sea region (Table 3.1).

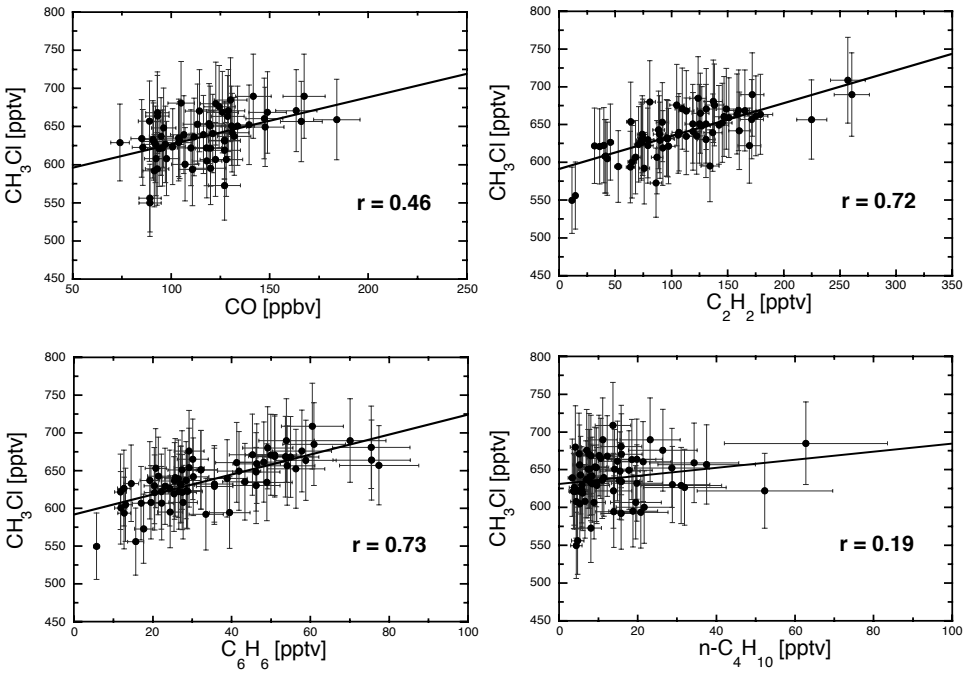

Figure 3.2: Correlation of CH_3Cl with CO, C_2H_2, C_6H_6, and n-C_4H_{10} in the free troposphere during INDOEX (data between 1.2 and 12.5 km altitude, r at the 95% confidence level). Error bars denote the measurement uncertainty (sum of the absolute accuracy and measurement precision), which is 6.4% for CO, 8% for CH_3Cl, 6% for C_2H_2, 13% for C_6H_6, and 33% for n-C_4H_{10}.

In general, it appears that the free troposphere was influenced by biomass burning emissions, either from distant source regions or local convection of polluted boundary layer air. This significance of biomass burning sources in the free troposphere is underscored by the correlation of CH_3Cl with the combustion tracers acetylene and benzene (r of 0.72 and 0.73 for N = 71, respectively, at a 99% confidence level), shown in Figure 3.2. The correlation with CO (Figure 3.2) is weaker (r = 0.46; 99% confidence level), indicating the influence of other combustion sources. The very poor correlation (r = 0.19; 99% confidence level) between CH_3Cl and n-butane (Figure 3.2) is due to the very short atmospheric lifetime of n-butane relative to CH_3Cl. As a result, most of the n-butane measurements are at background levels.

3.3.6 Vertical distributions

In Figure 3.3a and b we show vertical profiles from all canister data collected between about 6.5°S and 8°N for CH_3Cl, CH_3CCl_3 and the combustion tracers acetylene, propane and benzene, and the short-lived tracer n-butane. We included n-butane as an indicator of fresh continental pollution transported upwards by deep convection. We observed a large variability for all compounds in the boundary layer related to different sources areas, source strengths and ages of the air masses (Figure 3.3a). Furthermore, there appears to be a local maximum at about 1.5 km altitude for the combustion tracers acetylene, propane and n-butane, just above the marine boundary layer (<1 km altitude), which is less prominent for the other compounds. This might be related to a pronounced maximum, which was found between 1 and 3 km altitude in profiles of ozone and pollutants like CO, measured from various platforms over the Maldives area [*Lelieveld et al.*, 2001]. It is hypothesized by *Lelieveld et al.* [2001] that such a polluted layer is related to a sea breeze circulation at the Indian coast, which adds pollution from the deep continental boundary layer (~2 km altitude) to a residual layer above the marine boundary layer.

Figure 3.3b shows the altitude profiles of the same species as in Figure 3.3a in the free troposphere up to about 12.5 km altitude. As expected, the long-lived tracers CH_3Cl and CH_3CCl_3 show less variability in the free troposphere as compared to the short-lived hydrocarbons. This is in agreement with the concept, first explored for the global distribution of long-lived tracer species by *Junge* [1974], that the atmospheric variability of a species is inversely proportional to its atmospheric lifetime. Recently, *Jobson et al.* [1998], showed that an inverse variability-lifetime relationship applied for short-lived hydrocarbons on a regional scale as well. In addition, *Jobson et al.* [1999] reported inverse relationships between the measured variability and the OH lifetime for hydrocarbons and halocarbons for various tropospheric data sets.

Enhanced hydrocarbon mixing ratios and a high variability, most clearly seen in benzene and n-butane, were measured in air masses in the upper troposphere above 8 km. Here, outflow of pollutants from the boundary layer by convective clouds is expected [*de Gouw et al.*, 2001]. Hence, enhancements at higher altitudes, notably of species with relatively short chemical lifetimes such as benzene and n-butane (on the order of 10 and 5 days in the upper free troposphere, respectively), point to the influence of deep convection in the region and rapid long-range transport. The absence of enhanced CH_3Cl above 8 km

altitude indicates that source regions are dominated by fossil fuel emissions rather than by emissions from biofuel burning. Indeed, ten-day back-trajectories indicate that rapid long-range transport of pollutants, which originated from more industrialized distant source regions in southeastern Asia and China, could play a role as well. Additional indications of convective transport during INDOEX are discussed by *de Gouw et al.* [2001] and *Williams et al.* [2002].

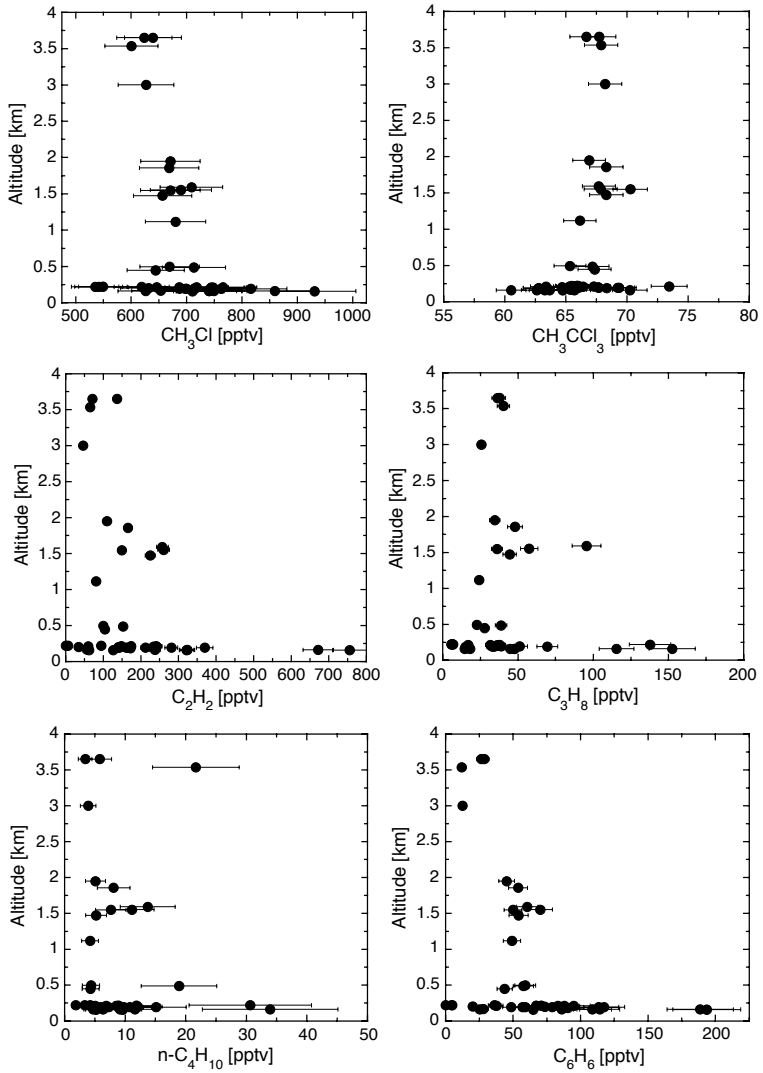

Figure 3.3a: Altitude profiles of CH_3Cl, CH_3CCl_3, C_2H_2, C_3H_8, n-C_4H_{10}, and C_6H_6 data from 150 m in the boundary layer up to about 3.5 km altitude in the free troposphere. The error bars denote the measurement uncertainty.

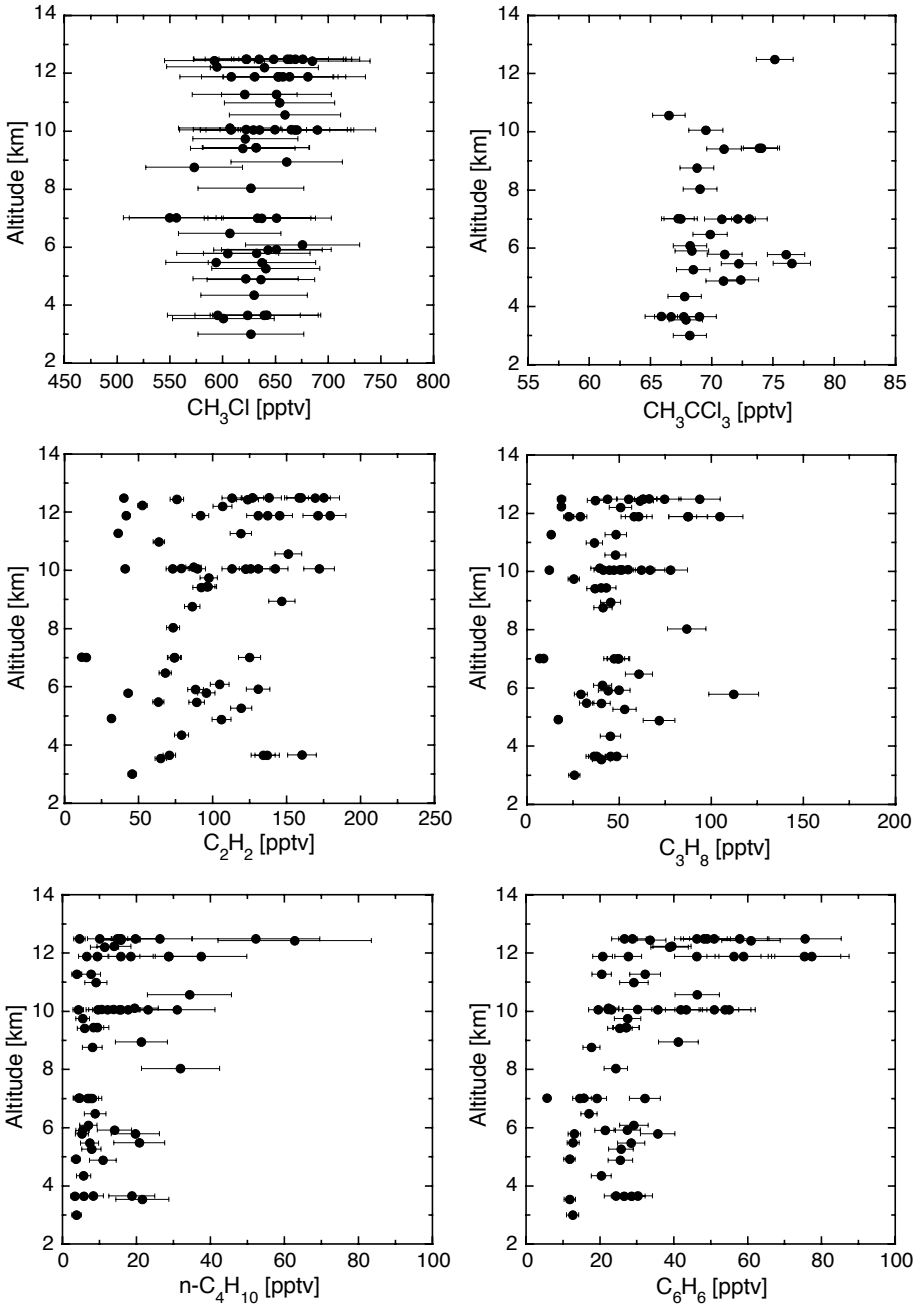

Figure 3.3b: Altitude profiles of CH_3Cl, CH_3CCl_3, C_2H_2, C_3H_8, n-C_4H_{10}, and C_6H_6 data from 3.5 to about 12.5 km altitude in the free troposphere. The error bars denote the measurement uncertainty.

3.4 Sources of CH_3Cl and other chlorocarbons

3.4.1 Sources of enhanced CH_3Cl

Reports in the literature of high CH_3Cl concentrations (up to ~1 ppbv), as observed during INDOEX, relate to measurements in biomass burning plumes [e.g., *Blake et al.*, 1996, 1999] or terrestrial sources in coastal areas, notably salt marshes [*H.-J. Li et al.*, 1999; *Yokouchi et al.*, 2000]. During the PEM-tropics A campaign [*Blake et al.*, 1999] over the remote South Pacific Ocean in 1996, for example, up to 700 pptv of CH_3Cl was measured in biomass burning plumes from South America. *H.-J. Li et al.* [1999] report CH_3Cl concentrations of 647 ± 52 at a remote coastal site (Okinawa, Japan) during August 1996. They suggest that the elevated CH_3Cl concentration (and the high variability), as compared to what is found over the remote ocean (e.g., see Table 3.3), might be due to large emissions from coastal areas (either from coastal waters or a nearby land source). *Yokouchi et al.* [2000] measured strongly enhanced CH_3Cl concentrations up to 1.5 ppbv at a remote subtropical coastal site, which they relate to a presently unknown land source, due to its strong correlation with terrestrial plant-related α-pinene. *Rhew et al.* [2000] show that CH_3Cl is released to the atmosphere from vegetation zones of coastal salt marshes in southern California. They do not present concentrations but their flux estimate of 0.17 Gg per year (range: 0.065 – 0.44 Gg) emphasizes the potential importance of this source.

Nevertheless, in polluted air masses affected by biomass burning, elevated CH_3Cl is always found together with high carbon monoxide and hydrocarbon concentrations. As a result of their common sources, hydrocarbons and CH_3Cl are generally well correlated with CO in biomass burning plumes [e.g., *Blake et al.*, 1996]. Enhanced continental boundary layer concentrations of CH_3Cl over Brazil and Southern Africa up to 1.3 ppbv were measured during the NASA TRACE-A project (Transport and Atmospheric Chemistry near the Equator-Atlantic) [*Blake et al.*, 1996], together with strongly enhanced hydrocarbons as well as CO from biomass fires in these regions. In the TRACE-A study correlation coefficients (r^2) between CO and CH_3Cl of ~0.9 (99% confidence level) were found (N = 25 over Brazil; N = 33 over Southern Africa).

In Figure 3.4 we present correlations between CH_3Cl (N = 16) and CO (N = 15; the CO measurement is missing for 1 canister), hydrocarbons (N = 16) and CH_3CN (N = 9; the acetonitrile measurement is not available for 7 canisters) for the marine boundary layer measurements during INDOEX. We show the correlation coefficients between CH_3Cl and the selected tracers only for the data from the most polluted Bay of Bengal region. We find that CH_3Cl is highly correlated with carbon monoxide, acetylene and benzene ($r > 0.9$ for N = 16; 95% confidence level), all important products of incomplete combustion of fossil and biofuels. A weaker and no correlation at all was found with n-butane and toluene, respectively, because they were mainly detected at background levels due to their short atmospheric lifetimes. Furthermore, an excellent correlation with acetonitrile of $r = 0.98$ (N = 9; 95% confidence level) was found, in spite of the lower number of measurements. Acetonitrile is a strong indicator of biomass burning activity.

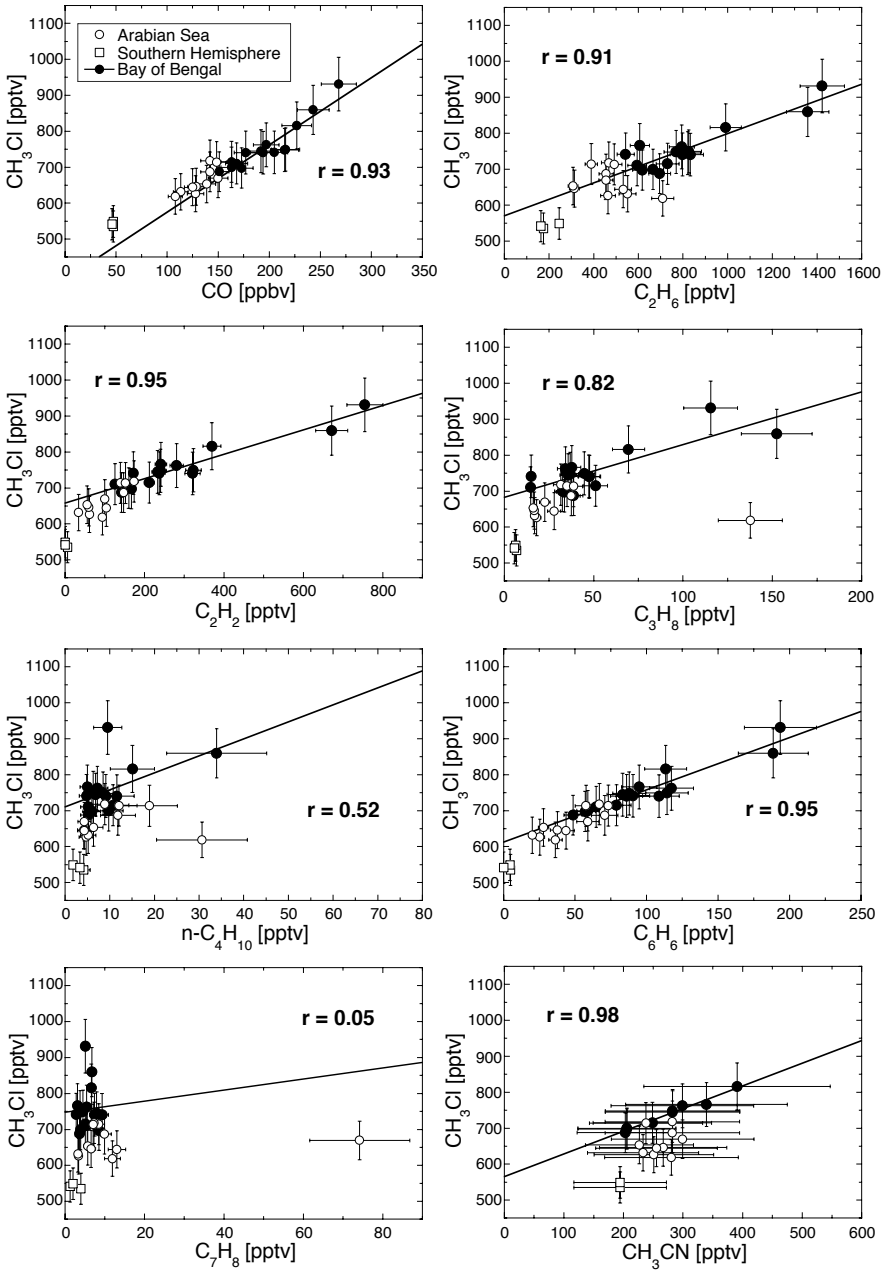

Figure 3.4: Correlations between CH_3Cl, carbon monoxide and other trace gases in the marine boundary layer during INDOEX. The CO data correspond to the in-situ CO measurement at the time of the air canister sampling. The linear fit and correlation coefficient r (95% confidence level) correspond to the Bay of Bengal data (most polluted case). Measurement uncertainty is indicated by error bars.

Here we focus on biomass burning emissions, notably from the use of biofuels, from India and neighbouring countries (includes Bangladesh, Sri Lanka, Myanmar, Nepal and Pakistan), which have the largest potential to have influenced our measurements. The domestic energy consumption pattern in Asia, and in particular in India, has been studied extensively, focusing on the domestic use of biofuels [*Ravindranath and Ramakrishna*, 1997; *Sinha et al.*, 1998; *Streets and Waldhoff*, 1999]. *Streets and Waldhoff* [1999] made a detailed emission database, RAINS-Asia (Regional Air Pollution Information and Simulation Model for Asia), which contains estimates of CO and CO_2 emissions from 23 countries in Asia (including India). They present an estimate of biofuel and fossil fuel use in Asia for 1990 in Tg C per year, indicating that biofuels comprise 28% of the total energy consumption. For India alone, *Streets and Waldhoff* [1999] estimate that 54% of all anthropogenic carbon emissions originates from the use of biofuels. In close agreement with the RAINS-Asia database, the EDGAR (Emission Database for Global Atmospheric Research) database estimates that about 60% of all the anthropogenic CO_2 emissions emitted in India and neighbouring countries is related to the use of biofuels [*Olivier et al.,* 1996]. The biofuel consumption in India is mainly residential in rural areas. *Ravindranath and Ramakrishna* [1997] report that about 93% of the Indian rural energy use depends on biofuels. The remaining 7% is made up of fossil fuels (e.g. kerosene, LPG). In urban areas the estimated fossil fuel component increases to about 56%, whereas the remaining 44% of biofuels is dominated by firewood [*Ravindranath and Ramakrishna*, 1997], in agreement with estimates by *Streets and Waldhoff* [1999]. They found for India and neighbouring countries that 59% of the used biofuel consists of firewood, the remaining part being divided between dung (17%) and agricultural waste (24%).

3.4.2 Sources of other chlorocarbons

Sources of CH_2Cl_2 are dominated by natural emissions from oceans and soils (together about 90%) [*Aucott et al.,* 1999], whereas sources of $CHCl_3$ are mainly industrial (70%) and oceanic (23%) [*McCulloch et al.,* 1999*; Khalil et al.,* 1999]. CH_3CCl_3 and C_2Cl_4 are almost entirely produced by industry (98% and 95%, respectively) [*Keene et al.,* 1999, *and references therein*]. In addition, *Rudolph et al.* [1995] showed that CH_2Cl_2, and to a much lesser extent $CHCl_3$ and CH_3CCl_3, might have small but significant emissions from biomass burning. No biomass burning emissions have been reported for C_2Cl_4, although this urban/industrial tracer might have a small biological source in the surface ocean, contributing <5% [*Keene et al.,* 1999, *and references therein*]. *Lobert et al.* [1999] used emission ratios relative to CO and CO_2 from *Rudolph et al.* [1995], to estimate that biomass burning contributes a significant portion of about 10% to the globally combined sources of CH_2Cl_2. For $CHCl_3$ and CH_3CCl_3, the emissions from biomass burning appear to play only a minor role, representing about 0.4% and 2%, respectively, of their global source strength. On a regional scale, however, the emission from biomass burning might play a relatively larger role.

To determine the significance of the above-mentioned emission sources for CH_2Cl_2 and $CHCl_3$ levels during INDOEX we investigated correlations with biomass burning tracers (CO, C_2H_2, CH_3Cl, and CH_3CN) and urban/industrial tracers (C_2Cl_4 and CH_3CCl_3) presen-

ted in Figure 3.5 and 3.6, respectively. We show correlation coefficients, r (N = 15 for CO, N = 16 for C_2H_2 and CH_3Cl and N = 9 for CH_3CN; 95% confidence level), for the Bay of Bengal measurements, where the highest level of pollution was encountered. CH_2Cl_2, and $CHCl_3$ show weak correlations (r ≈ 0.4) with increasing concentrations of CO, acetylene, as well as CH_3Cl, suggesting an influence by biomass burning sources beside the ocean surface as a diffuse large-scale source. There is a positive but very poor correlation between CH_2Cl_2 and CH_3CN (r ≈ 0.2; upper right panel in Figure 3.5), whereas the correlation between $CHCl_3$ and CH_3CN is comparable to the other biomass burning tracers for $CHCl_3$ (r ≈ 0.4; upper right panel in Figure 3.6). The latter corroborates the indication of biomass burning emissions as a source of $CHCl_3$ during INDOEX. No correlation of CH_2Cl_2, and $CHCl_3$ with CH_3CCl_3 (r ≈ 0) and a very poor correlation of both species with C_2Cl_4 (r = 0.1 to 0.2) is found for the Bay of Bengal measurements, suggesting no significant common sources originating from urban/industrial activities. Variable oceanic sources of CH_2Cl_2 and $CHCl_3$ are the most probable cause of the high variability in the data and the weak correlations with the biomass burning tracers in Figure 3.5 and 3.6. Nevertheless, our data seem to confirm that biomass burning emissions are a minor source of enhanced CH_2Cl_2 and $CHCl_3$ beside the oceans as major source.

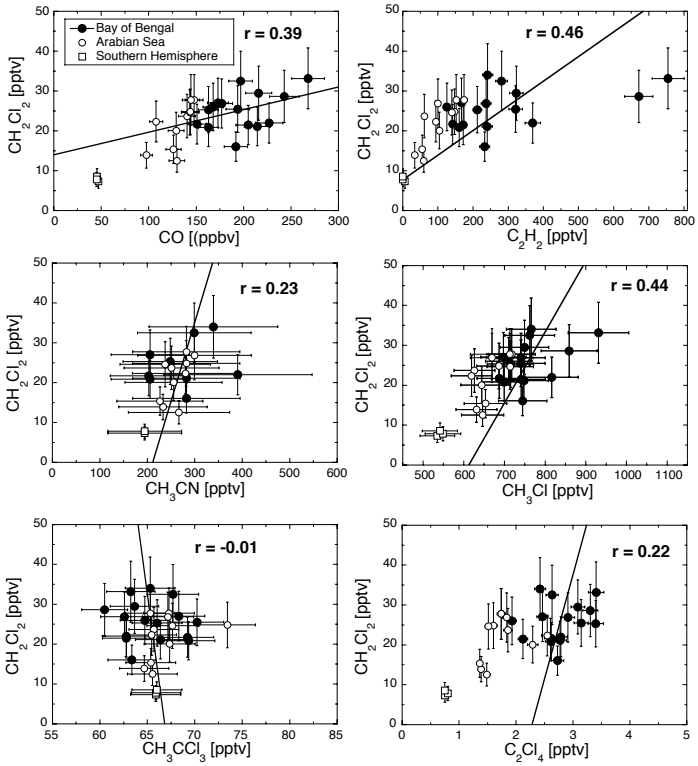

Figure 3.5: Correlations between CH_2Cl_2 and biomass burning tracers (CO, C_2H_2, CH_3CN, and CH_3Cl) and urban/industrial tracers (CH_3CCl_3 and C_2Cl_4) in the marine boundary layer during INDOEX. The linear fit and correlation coefficient r (95% confidence level) corresponds to polluted Bay of Bengal data. The error bars denote the measurement uncertainty.

In Figure 3.7 we show correlations between C_2Cl_4 and biomass burning tracers (CO, C_2H_2, CH_3Cl and CH_3CN). The positive correlations between C_2Cl_4 and CO, as well as C_2H_2 and CH_3Cl of r ≈ 0.5, 0.7 and 0.5 (Bay of Bengal measurements; 95% confidence level), respectively, together with the lack of correlation with CH_3CN (r ≈ 0), show that biomass burning and urban/industrial emissions are to some extent coincident. In Figure 3.8, finally, we present correlations of CH_3CCl_3 with CO, acetylene, CH_3CN, CH_3Cl, and C_2Cl_4 , which appear to be all negative for the Bay of Bengal measurements (r = -0.2 to -0.8; 95% confidence level), pointing to the absence of CH_3CCl_3 sources in the Bay of Bengal area.

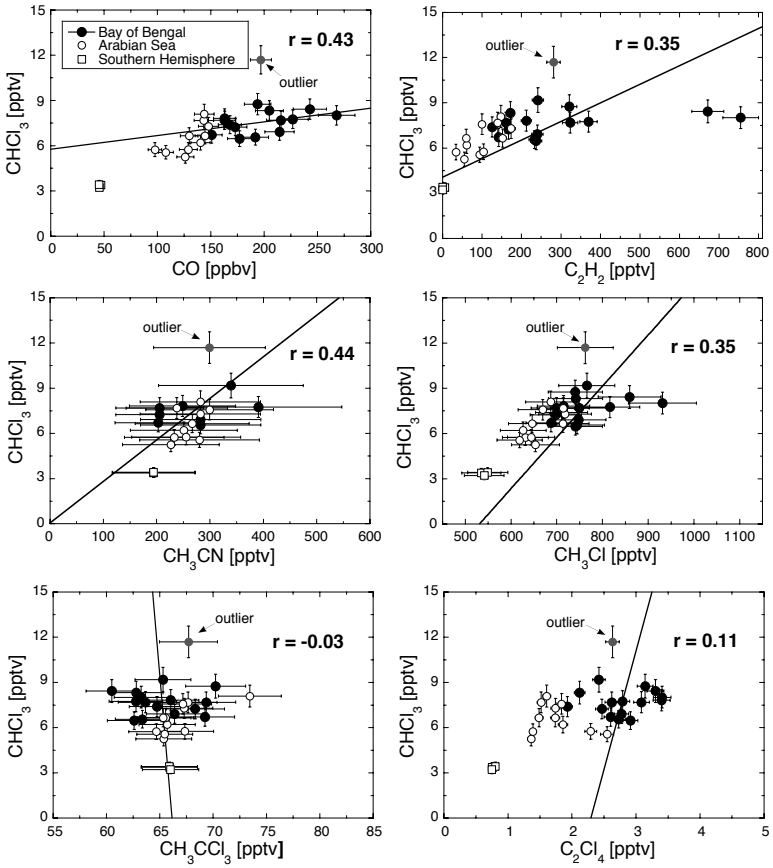

Figure 3.6: Correlations between $CHCl_3$ and biomass burning tracers (CO, C_2H_2, CH_3CN, and CH_3Cl) and urban/industrial tracers (CH_3CCl_3 and C_2Cl_4) in the marine boundary layer during INDOEX. The CO data relate to the in-situ measurement periods during the air canister sampling. The linear fit and correlation coefficient r (95% confidence level) correspond to the Bay of Bengal data. Note that the outlier in the $CHCl_3$ data is not included in the correlations and the linear fits. The error bars denote the measurement uncertainty.

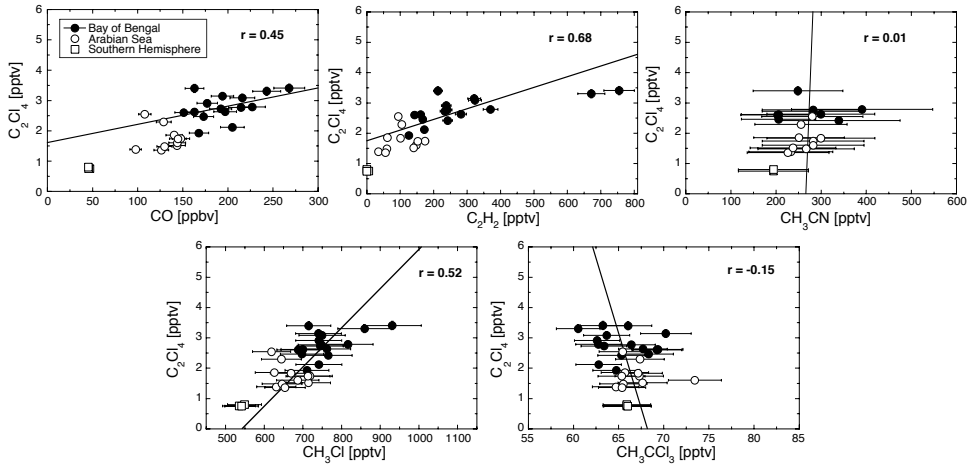

Figure 3.7: Correlations between C_2Cl_4 and biomass burning tracers (CO, C_2H_2, CH_3Cl, and CH_3CN), and CH_3CCl_3 in the marine boundary layer during INDOEX. The linear fit and correlation coefficient r (95% confidence level) correspond to the Bay of Bengal data. Error bars denote the measurement uncertainty.

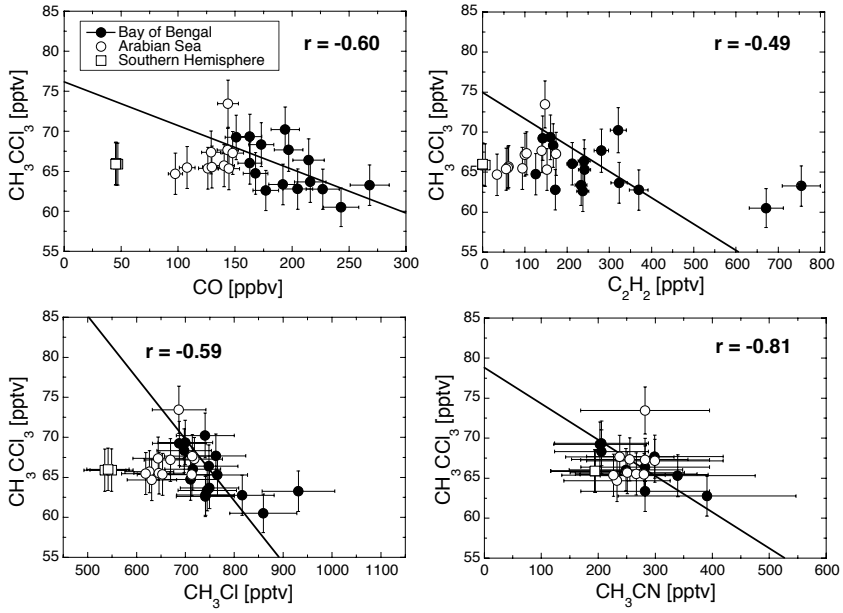

Figure 3.8: Correlations between CH_3CCl_3 and biomass burning tracers (CO, C_2H_2, CH_3CN, and CH_3Cl), and C_2Cl_4 in the marine boundary layer during INDOEX. The linear fit and correlation coefficient r (95% confidence level) correspond to polluted Bay of Bengal data. The error bars denote the measurement uncertainty.

3.5 Enhancement ratios for CH_3Cl and other chlorocarbons

3.5.1 Determination of enhancement ratios

We have shown that carbon monoxide, as the most important product of incomplete combustion, was highly elevated in polluted air masses originating from the Bay of Bengal area. A high correlation between carbon monoxide and other combustion related species, such as CH_3Cl, is an indication of their common sources and can be used to obtain a source specific enhancement or emission ratio. Enhancement ratios can be determined as the slope of the linear regression relating the molar mixing ratio of species X to the corresponding molar mixing ratio of the reference gas CO ($\Delta X/\Delta CO$). We obtained enhancement ratios from an orthogonal distance regression (ODR) analysis, a linear regression technique in which errors are allowed in both variables [*Press et al.*, 1992]. We used the most polluted Bay of Bengal measurements to obtain an enhancement ratio for CH_3Cl and selected chlorocarbons, assuming that these are representative of pollution from India and surrounding countries. Enhancement ratios for a number of non-methane hydrocarbons from the INDOEX marine boundary layer measurements are discussed in the paper of *de Gouw et al.* [2001].

Linear regression avoids possible errors due to the derived emission ratios by wrongly defined background concentrations. A limitation of the use of enhancement ratios is, however, imposed by the occurrence of variable background mixing ratios. The use of linear regression to determine emission ratios from field measurements therefore assumes that one relevant trace gas source is dominant, e.g. biomass burning. Furthermore, the effect of photochemical aging and dilution of an air mass has to be considered. The marine boundary layer during INDOEX was characterized by a stable northeasterly flow (winter monsoon) throughout the campaign, induced by strong subsidence over the Bay of Bengal region, that minimized vertical mixing. As a result a strong vertical gradient was observed in the mixing ratios of chemically active tracer species between the marine boundary layer and the free troposphere (see Figure 3.3a).

The ratio of species X versus CO will evolve as function of its removal rate from the atmosphere relative to that of CO. We have estimated that the polluted air masses from the Bay of Bengal during INDOEX had aged about 3 ± 1 days on average. However, the atmospheric lifetimes of the chlorocarbons are so large (>100 days; see *Khalil* [1999]), as compared to the travel time from the source regions, that their concentrations remain virtually unaffected by photochemical loss. For example, the chemical lifetime of CH_3Cl in the Indian ocean boundary layer is about 110 days (for a daily mean OH concentration of 2.5×10^6 molecules cm^{-3} in the marine boundary layer [*de Laat and Lelieveld*, 2001], and the reaction coefficient ($k_{[OH]}$) of 4.27×10^{-14} cm^3 $molecule^{-1}$ s^{-1} at 298 K by *Atkinson et al.* [1992]). Thus, within 3 ± 1 days travel time from the source, the CH_3Cl concentration decreases less than 1% by chemical loss. However, due to the relatively short chemical lifetime of CO in the tropical boundary layer of ~19 days ($k_{[OH]}$: 2.0×10^{-13} cm^3 $molecule^{-1}$ s^{-1} at 298 K by *Atkinson et al.* [1997]), the $\Delta CH_3Cl/\Delta CO$ ratio is expected to increase by 10 to 20% over the period considered. Hence, the above arguments suggest that photochemistry

was more important than vertical mixing in altering the concentrations, and thus the enhancement ratios during transport.

3.5.2 Enhancement ratio of CH_3Cl

The ODR method was applied to the measurements of the most polluted marine boundary air masses from the Bay of Bengal (Figure 3.4; upper left panel). This resulted in a molar enhancement ratio (slope) $\Delta CH_3Cl/\Delta CO$ of $1.98 \pm 0.24 \times 10^{-3}$ with a correlation coefficient of r = 0.93 (95% confidence level). We have argued that the mixing effects on chemically active trace gas concentrations in the marine boundary layer during INDOEX were probably small compared to chemical decay on a timescale of several days. Hence, taking only chemical destruction of CO by the OH-radical into account and assuming an average transport time of 3 days, we derive a $\Delta CH_3Cl/\Delta CO$ 'source' enhancement ratio of $1.74 \pm 0.21 \times 10^{-3}$ mol mol^{-1}.

We can compare the INDOEX $\Delta CH_3Cl/\Delta CO$ 'source' ratio to enhancement ratios of various wood and agricultural waste burning emissions reported in the literature. A ratio of $0.57 \pm 0.28 \times 10^{-3}$ mol mol^{-1} is the overall median enhancement ratio from various natural and anthropogenic wood and savanna burning sources used in the global emission inventory by *Lobert et al.* [1999]. It includes, for example, the mean enhancement ratios of $0.57 \pm 0.03 \times 10^{-3}$ mol mol^{-1} from African savanna burning and $0.85 \pm 0.06 \times 10^{-3}$ mol mol^{-1} from Brazilian forest fires derived from the 'Transport and Atmospheric Chemistry Near the Equator-Atlantic' aircraft expeditions (TRACE-A) by *Blake et al.* [1996]. Very few directly observed $\Delta CH_3Cl/\Delta CO$ ratios for agricultural waste burning are available in the literature and none for dung to our knowledge. A laboratory study by *Lobert et al.* [1991] of the emission of CH_3Cl from the burning of different types of grass, hay, straw, and one type of wood, resulted in a range of 0.18 to 4.4×10^{-3} mol mol^{-1} for $\Delta CH_3Cl/\Delta CO$ and a median of 1.6×10^{-3} mol mol^{-1}. *Rasmussen et al.* [1980] performed laboratory studies of the emissions from the burning of straw, cornstalk and dead oak leaves relative to CO_2. They inferred $\Delta CH_3Cl/\Delta CO_2$ ratios between 8.5 and 30×10^{-5} mol mol^{-1}. From this range and the mean ratio of CO/CO_2 of ~6.6% for this fuel category reported by *Lobert et al.* [1999], we can infer a $\Delta CH_3Cl/\Delta CO$ ratio between 1.3 and 4.5×10^{-3} mol mol^{-1}, which agrees very well with *Lobert et al.* [1991]. From the results of both laboratory studies we calculate a mean $\Delta CH_3Cl/\Delta CO$ ratio of $\sim 2.5 \pm 1.4 \times 10^{-3}$ mol mol^{-1}, representative of agricultural waste burning. Since cattle dung has a similar chlorine content as agricultural waste, as earlier mentioned, we expect a similar enhancement ratio for dung burning. Relatively high emission ratios for agricultural waste and dung are consistent with the high Cl contents of these fuels as compared to wood fuels [*Lobert et al*., 1999]. The Cl content measured in various biofuels varied between 650 (grapefruit leaves) and 9500 (hay) mg Cl kg^{-1} of dry fuel, with a median value of 4840 mg Cl kg^{-1}, close to the 4360 mg Cl kg^{-1} that has been found for Indian dung [*Lobert et al*., 1999, and references therein]. Tropical and subtropical wood, tree litter and leaves have a much lower Cl content of 50 to 1600 mg Cl kg^{-1}, and a median value of 530 mg Cl kg^{-1} of dry fuel [*Lobert et al*., 1999]. Note that these estimates are quite uncertain, as they are based on only a few measurements.

The burning efficiency, or the phase of a fire, is also a significant factor for the release

of CH_3Cl. In the smoldering phase, during which many reduced compounds are released, the CH_3Cl emission can be a factor of three larger than during the flaming phase [*Lobert et al.*, 1999]. *Lobert et al.* [1991] and *Rudolph et al.* [1995] showed that CH_3Cl was better correlated with CO than with CO_2 because CO is primarily a product of smoldering combustion as well. Since biomass combustion in India predominantly involves smoldering fires in ovens or furnaces [*Ravindranath and Ramakrishna*, 1997], a relatively high CH_3Cl emission can be expected.

We infer that the $\Delta CH_3Cl/\Delta CO$ ratio for the polluted INDOEX marine boundary layer of $1.74 \pm 0.21 \times 10^{-3}$ mol mol^{-1} lies in between the high derived mean emission ratio for agricultural waste (and dung) of $2.5 \pm 1.4 \times 10^{-3}$ mol mol^{-1} and the low mean emission factor for various wood fuels of $0.57 \pm 0.28 \times 10^{-3}$ mol mol^{-1}, pointing to a mixture of various biomass burning sources. It appears that the enhanced $\Delta CH_3Cl/\Delta CO$ ratio of CH_3Cl measured in polluted air masses from the Bay of Bengal relates to the extensive use of biofuels in the region, with emphasis on the low burning efficiency of residential fires and the high fraction of chlorine rich fuels like agricultural waste and dung.

3.5.3 Enhancement ratios for other chlorocarbons

We calculate weak correlations ($r \approx 0.4$; 95% confidence level) between both CH_2Cl_2 and $CHCl_3$ and CO as well as with C_2H_2 and CH_3Cl in polluted air masses originating from the Bay of Bengal area, suggesting some influence from biomass burning sources (Figure 3.5 and 3.6). Negative correlations with CO, C_2H_2, CH_3CN and CH_3Cl, were found for CH_3CCl_3 ($r \approx -0.6$ to -0.8; 95% confidence level). Enhancement ratios for CH_2Cl_2, $CHCl_3$ and CH_3CCl_3 relative to CO were determined as the slope of orthogonal distance regression for the Bay of Bengal measurements (N = 15) and compared with results from the FOS/DECAFE 91 (Fire Of Savannas/Dynamique Et Chemie de l'Atmosphère en Forêt Equatorial) experiment, which was conducted during February 1991 in Equatorial Africa (Table 3.4). In this experiment about 20 air samples were collected in plumes of savanna fires to derive enhancement ratios (in their study referred to as emission ratios) of halocarbon species versus CO (and CO_2). Contrary to the FOS/DECAFE 91 results, the INDOEX enhancement ratios relate, most probably, to a mixture of emissions from biofuel burning with different fuel and burning characteristics, as well as other unidentified potential sources (e.g., oceanic or industrial). Hence, this allows only a qualitative comparison. The negative correlation between CH_3CCl_3 and CO (and other tracers) indicates that biomass burning was not a significant source. As mentioned before, a recent laboratory study of CH_3CCl_3 emissions from wood burning by *Rudolph et al.* [2000] emphasized the marginal importance of biomass burning as a global source (the enhancement factor is given in Table 3.4). We derive enhancement ratios for CH_2Cl_2 and $CHCl_3$, which are roughly two to ten times higher, respectively, than the savanna fire estimates (taking the effect of photochemical aging (~3 days) on the CO concentration into account). Since biomass burning is a relatively small source, we cannot rule out that other (notably industrial) sources are responsible for the discrepancy. The high uncertainty in both emission estimates (~30%) and the weaker correlation of the INDOEX data contributes to the difference as well. Nevertheless, our results suggest a contribution of biomass burning to sources of CH_2Cl_2

and $CHCl_3$ in the INDOEX measurement area. The uncertainty of the calculated enhancement ratios is, however, too large to reasonably estimate biomass burning emissions.

Table 3.4: Enhancement ratios of chlorocarbons relative to CO ($\Delta X/\Delta CO$).[a]

	$\Delta X/\Delta CO \times 10^{-5}$, mol mol^{-1}				
Species	FOS/DECAFE 1991 savanna fires[a]	r	Laboratory Study wood burning[b]	INDOEX Bay of Bengal	r
CH_2Cl_2	2.5 (0.6)	0.78	NA	4.4 (4.7)	0.39
$CHCl_3$	0.07 (0.02)	0.87	NA	0.9 (0.5)	0.43
CH_3CCl_3	0.72 (0.45)	0.64	0.127 (0.026)	-5.3 (2.1)	-0.59

[a]Ratios from the INDOEX polluted boundary layer were compared to results from the FOS/DECAFE 91 campaign [*Rudolph et al.*, 1995] and a laboratory study by *Rudolph et al.* [2000]. Standard deviation (1σ) of enhancement ratios in parentheses. The regression coefficient is given by r (95% confidence level). Note that the outlier in the INDOEX $CHCl_3$ measurements has not been included in the regression analysis.

[b]*Rudolph et al.* [1995]; [c]*Rudolph et al.* [2000].

3.6 CH_3Cl biofuel burning emission estimate

3.6.1 Approach

To estimate CH_3Cl emissions (in 10^9 g per year or Gg Cl yr^{-1}) from biomass burning, notably from India and Southeast Asia, we apply the $\Delta CH_3Cl/\Delta CO$ 'source' enhancement ratio (ER) of 1.74×10^{-3} mol mol^{-1} from the INDOEX measurements. The amount of emitted CH_3Cl in Gg Cl yr^{-1}, as a function of the CO emissions from biomass burning of the source region of interest, is then described by:

$$Cl_{CH3Cl} = (C_{CO\text{-}biofuel} / 12) \text{ x ER x } 35.5 \qquad (3.1)$$

where Cl_{CH3Cl} is the amount of Cl emitted as CH_3Cl in Gg yr^{-1}; $C_{CO\text{-}biofuel}$ / 12 is the amount of C emitted as CO from biofuel consumption in Gg yr^{-1} divided by the molar mass of C (g), ER x 35.5 is the enhancement ratio for CH_3Cl over CO in mol mol^{-1} multiplied by the molar mass of Cl (g). This method is referred to as the 'CO-method' similar to *Lobert et al.* [1999]. Clearly, Cl estimates based on the CO-method are directly proportional to the enhancement ratio for CH_3Cl over CO. *Lobert et al.* [1999] used a $\Delta CH_3Cl/\Delta CO$ of 0.57×10^{-3} mol mol^{-1} for global biofuel emission estimates. Thus the higher $\Delta CH_3Cl/\Delta CO$ enhancement ratio of 1.74×10^{-3} mol mol^{-1} from INDOEX implies that emissions from biofuel consumption in India and Southeast Asia could have been underestimated by a factor of three based on the CO-method alone.

Besides the CO-method, *Lobert et al.* [1999] apply a second method to estimate CH_3Cl emissions based on the Cl-content of biofuels and the estimated release of Cl as CH_3Cl

during the burning process. This method, referred to as the 'Cl-method', describes the release of CH_3Cl in Gg Cl yr^{-1} as follows:

$$Cl_{CH3Cl} = (C_{biofuel} / 0.45) \times Cl_{biofuel} \times F_{Cl} \times F_{Cl\text{-}CH3Cl} \quad (3.2)$$

where Cl_{CH3Cl} is the emitted mass of chlorine from CH_3Cl in Gg $Cl^{yr\text{-}1}$; ($C_{biofuel}$ / 0.45) is the total dry mass of burned biofuel (wood fuel, crop residues and dung) in Tg yr^{-1}, assuming that all biomass contains 45% of carbon; $Cl_{biofuel}$ is the biofuel chlorine content in g per kg dry fuel; F_{Cl} is the fraction of total fuel Cl being emitted, estimated at 72 ± 22% [*Lobert et al.,* 1999]; $F_{Cl\text{-}CH3Cl}$ is the fraction of Cl emitted as CH_3Cl, estimated at 12.8 ± 13.9% [*Lobert et al.,* 1991; *Andreae et al.*, 1996]. The $Cl_{biofuel}$ used by *Lobert et al.* [1999] for wood fuel and agricultural waste (and dung) is 0.205 g Cl and 4.84 g Cl per kg dry fuel, respectively. These values comprise the weighted means for these fuel categories from an overview of chlorine content of biomass fuels by *Lobert et al.* [1999]. In our estimates we applied the biofuel use partitioning from *Streets and Waldhoff* [1999] for India+ (includes Bangladesh, Sri Lanka, Myanmar, Nepal, Pakistan) of 41% agricultural waste and dung, and 59% wood fuel, and for Southeast Asia (includes India+, S. Korea, Indonesia, Malaysia, Philippines, Thailand) of 49% agricultural waste and dung and 51% woodfuel.

Lobert et al. [1999] argue that the Cl-method is based on the best input data with respect to fuel variability, however, neglecting burning efficiency, whereas the CO-method results in estimates with the lowest variability, being less dependent on burning efficiency. As a result, their best estimate for biofuel burning emission of CH_3Cl (in Gg Cl yr^{-1}) is based on the average of the CO- and the Cl-method. For their estimates *Lobert et al.* [1999] use a global carbon emission inventory valid for the year 1990 from *J.A Logan* and *R. Yevich* (unpublished manuscript, 1998), which specifies biomass burning emissions on a 1° latitude by 1° longitude grid. According to this inventory, carbon emissions from agricultural waste and dung burning, and woodfuel burning are 323 Tg C yr^{-1} and 876 Tg C yr^{-1}, respectively. We apply the EDGAR database [*Olivier et al.*, 1996], because it provides detailed carbon emissions estimates from biofuel use in Asia on a country and regional basis. The EDGAR-database, developed partly in support of the Global Emission Inventory Activity (GEIA), contains detailed CO_2, CO and CH_4 emission inventories for the year 1990. The biofuel use has been divided between residential and industrial use, and is separated into different fuel categories (includes wood, crop residues and dung). The emission estimates for Asia are in close agreement with the RAINS-Asia database [*Streets and Waldhoff*, 1999]. The uncertainty in the EDGAR global carbon emissions from biofuel use is estimated to be ±100% [*Olivier et al.*, 1996]. We note that global carbon emissions from biofuel burning from EDGAR of 1599 Tg C yr^{-1} appear to be about 33% higher than the emission estimates used by *Lobert et al.* [1999]. Such considerable discrepancies between emission inventories, which are within the uncertainty of these databases, might explain part of the missing sources of CH_3Cl described by *Keene et al.* [1999].

3.6.2 Emission estimates

The global CH_3Cl emission estimate by *Lobert et al.* [1999] for biofuel burning (sum of all fuel categories) results is 112 Gg Cl yr^{-1} with the CO-method and 357 Gg Cl yr^{-1} by the Cl-method. The mean of both methods is 234 Gg Cl yr^{-1} (with a 1σ standard deviation of 122 Gg Cl yr^{-1}), which amounts to about 37% of all biomass burning sources in the emission inventory of *Lobert et al.* [1999]. All CH_3Cl biomass burning emissions (including a large fraction from biofuel burning) for Southeast Asia were estimated at 219 Gg Cl yr^{-1} by *Lobert et al.* [1999], which is about one-third of the global CH_3Cl emission from biomass burning. They estimated that their calculated fluxes are reliable to within a factor of 2 to 3. The INDOEX enhancement factor for CH_3Cl of 1.74×10^{-3} mol mol^{-1} enables revision of the emission estimates of CH_3Cl (in Gg Cl yr^{-1}) from biofuel burning, notably of the India region and Southeast Asia. We estimated the emission of CH_3Cl from biofuel use from India+ and Southeast Asia on basis of the EDGAR database and the INDOEX CH_3Cl enhancement ratio. We derive CH_3Cl emissions of 103 Gg Cl yr^{-1} for India+ and 144 Gg Cl yr^{-1} for Southeast Asia with the CO-method. By means of the Cl-method (equation 3.2), we derive CH_3Cl emissions of 153 Gg Cl yr^{-1} for India+ and 259 Gg Cl yr^{-1} for Southeast Asia. The combined error in these estimates (apart from the uncertainty in the carbon emissions from the EDGAR database) is of the order of 60%. Table 3.5 gives an overview of emission estimates in Gg Cl per year from biofuel burning from the CO- and the Cl-method for India+ and Southeast Asia, as well as the mean values for both methods. Interestingly, the estimates on the basis of the INDOEX enhancement ratio are much closer to the results from the Cl-method than the CO-method estimate by *Lobert et al.* [1999]. Furthermore, taking the uncertainty of the mean estimates in Table 3.5 into account, there appears to be reasonable agreement between the mean estimate based on CH_3Cl enhancement ratio from *Lobert et al.* [1999] and the one from this work. We infer that our mean emission estimates are 30-35% higher than estimates with the $\Delta CH_3Cl/\Delta CO$ enhancement ratio from *Lobert et al.* [1999] (based on the EDGAR carbon emissions). Applying the enhanced INDOEX ER to the global biofuel burning emission estimate (CO-method) from *Lobert et al.* [1999], the global CH_3Cl emission of 112 Gg Cl yr^{-1} increases by a factor of 3.05 to 342 Gg Cl yr^{-1}. Thus, the mean with the 357 Gg Cl yr^{-1} from the Cl-method estimate from *Lobert et al.* [1999] (which remains unchanged) becomes 350 Gg Cl yr^{-1} (with a 1σ standard deviation of 8 Gg Cl yr^{-1}), which corresponds to a mean increase of 116 Gg Cl yr^{-1} (range 0 – 247 Gg) or +50% globally.

Although enhancement ratios can be determined with reasonable accuracy (<20%), global biofuel CO_2 and CO emission estimates suffer from considerable uncertainties, as indicated earlier by significant differences between various emission inventories. For example, the annual global carbon (CO and CO_2) emissions from biofuel burning applied by *Lobert et al.* [1999] of 1199 Tg C per year, is 400 Tg C yr^{-1} lower then the EDGAR (Emission Database for Global Atmospheric Research) database estimate by *Olivier et al.* [1996] (1599 Tg C yr^{-1}). Applying the EDGAR annual global carbon emissions in the Cl emission estimate by *Lobert et al.* [1999] leads to a mean CH_3Cl emission of 300 Gg Cl yr^{-1}. Thus, an increase of 66 Gg Cl yr^{-1}, as compared to the global estimate by *Lobert et al.* [1999] (234 Gg Cl yr^{-1}) can arise from the higher carbon emissions estimate alone. Combining the global carbon emission estimates from EDGAR with the INDOEX $\Delta CH_3Cl/\Delta CO$

factor, results in a global mean of 435 Gg Cl yr^{-1} (with a 1σ standard deviation of 33 Gg Cl yr^{-1}) from biofuel consumption. Up to now, about 1.45 Tg of Cl from CH_3Cl emissions is "missing" due to underestimated sources, uncertainties in emission ratios, and uncertainties in the chlorine content of fuels [*Keene et al.*, 1999]. Our global estimate might account for about 200 Gg Cl or ~14% of the "missing" sources suggested by *Keene et al.* [1999]. We speculate that other biomass burning sources, notably the burning of crop residues in fields (~214 Tg C yr^{-1} according to *Lobert et al.*, [1999]), of which sparse or no measurements are reported in the literature, could be underestimated as well from applying a too low $\Delta CH_3Cl/\Delta CO$ emission ratio.

Table 3.5: Emission estimate of CH_3Cl in Gg Cl per year from biofuel consumption in India+ and Southeast Asia.

Source region	EDGAR-database Tg C-CO	Tg C	CO-method *Lobert*-ER	*INDOEX*-ER	Cl-method[b]	Mean Cl- and CO-method *Lobert*-ER	*INDOEX*-ER
India+	20	356	34	103	153	94 (60)	128 (25)
S-E Asia	28	510	47	144	259	153 (106)	202 (58)

[a]Emission estimates are in Gg Cl per year from biofuel consumption in India+ (includes Bangladesh, Sri Lanka, Myanmar, Nepal, Pakistan) and Southeast Asia (includes India+, S-Korea, Indonesia, Malaysia, Philippines, Thailand) on the basis of carbon emissions estimates from the EDGAR-database for the year 1990, the $\Delta CH_3Cl/\Delta CO$ for biofuels from *Lobert et al.* [1999] of $0.57 \pm 0.28 \times 10^{-3}$ mol mol^{-1} (*Lobert*-ER), and the $\Delta CH_3Cl/\Delta CO$ from this work of $1.74 \pm 0.21 \times 10^{-3}$ mol mol^{-1} (*INDOEX*-ER). The standard deviation (1σ) of the mean of the Cl- and CO-method is given in parentheses.

[b]We adopted 4.84 g Cl kg^{-1} dry fuel for agricultural waste and dung and 0.205 g C/kg dry fuel for wood from *Lobert et al.* [1999]. Furthermore, for the Cl-method we applied the biofuel partitioning from *Streets and Waldhoff* [1999] for India+ and Southeast Asia (India+: 41% agricultural waste and dung, and 59% woodfuel; S-E Asia: 49% agricultural waste and dung, and 51% woodfuel).

3.7 Conclusions

We present measurements of CH_3Cl and selected hydrocarbons and chlorocarbons from analyses of canister samples collected on-board an aircraft during the INDOEX campaign over the Indian Ocean in February / March 1999. We measured strongly enhanced CH_3Cl and related combustion tracers (CO, hydrocarbons and CH_3CN) in polluted air masses originating from India and Southeast Asia. We attribute the enhanced CH_3Cl levels to extensive biofuel use, notably the burning of agricultural waste and dung with a comparatively high chlorine content. We infer a high emission ratio relative to CO ($\Delta CH_3Cl/\Delta CO$) of $1.74 \pm 0.21 \times 10^{-3}$ mol mol^{-1}. The recent emission inventory by *Lobert et al.* [1999] applied a mean value of 0.57×10^{-3} mol mol^{-1} to estimate global CH_3Cl emissions from biofuel use. On the basis of our measurements we suggest that the contribution to CH_3Cl emissions from the use of biofuels may previously have been underestimated by 30-35% for India and Southeast Asia. According to *Keene et al.* [1999], the combined emissions of CH_3Cl from known sources account only for half the modeled sinks. By extrapolating the INDOEX $\Delta CH_3Cl/\Delta CO$ enhancement ratio to a global scale, our higher emission estimate might account for about 14% of the "missing" source. In accord with earlier findings by *Rudolph et*

al. [1995] we infer small biomass burning sources for CH_2Cl_2 and $CHCl_3$. Future work should, in particular, provide improved estimates of the chlorine content of biofuels and the release of CH_3Cl and other chlorocarbons as a function of burning efficiency.

Acknowledgements

We gratefully acknowledge the excellent cooperation with the Citation team of Delft University of Technology and the meteorological support of the KNMI. We especially thank S.A. Montzka of NOAA/CMDL, for helpful discussions, providing halocarbon data and for testing our calibration standard. The collaboration with J. Rudolph from York University, Toronto, was part of the STREAM 1998 project supported by the European commission. This project was supported by N.W.O in the Netherlands.

4 The impact of monsoon outflow from India and Southeast Asia in the upper troposphere over the eastern Mediterranean

Abstract. A major objective of the Mediterranean INtensive Oxidant Study (MINOS) was to investigate long-range transport of pollutants (notably ozone precursor species). Here we present trace gas measurements from the DLR (German Aerospace Organization) Falcon aircraft in the eastern Mediterranean troposphere. Ten-day backward trajectories and a coupled chemistry-climate model (ECHAM4) were used to study the nature and origin of pollution observed in the upper troposphere between 6 and 13 km altitude. We focus on a large pollution plume encountered over the eastern Mediterranean between August 1 and 12 originating in South Asia (India and Southeast Asia), referred to as the Asian plume, associated with the Asian Summer Monsoon. Vertical as well as longitudinal gradients of methane, carbon monoxide, hydrocarbons including acetone, methanol, and acetonitrile, halocarbons, ozone and total reactive nitrogen (NO_y) are presented, showing the chemical impact of the Asian plume compared to westerly air masses containing pollution from North America. The Asian plume is characterized by enhanced concentrations of biomass burning tracers (acetylene, methyl chloride, acetonitrile), notably from biofuel use. Concentrations of the new automobile cooling agent HFC-134a were significantly lower in the Asian plume than in air masses from North America. Relatively high levels of ozone precursors (CO, hydrocarbons) were found in both air masses, whereas lower ozone concentrations in the Asian plume suggest NO_x-limited conditions. Consistently, ECHAM4 model simulations indicate that the expected future increase of NO_x emissions in Asia enhances the photochemical ozone production in the Asian plume. The size and location of the Asian plume near the tropopause provides an important potential for pollution transport into the lowermost stratosphere. We present observations indicative of Asian pollution transport into the lower stratosphere.

Published in *Atmospheric Chemistry and Physics Discussions*, with J. Lelieveld, G.J. Roelofs, J. Williams, H. Fischer, M. de Reus, J.A. de Gouw, C. Warneke, R. Holzinger, H. Schlager, T. Klüpfel M. Bolder, C. van der Veen, and M. Lawrence as co-authors.

4.1 Introduction

Observations and model work have indicated that the summertime Mediterranean stands out as one of the most polluted regions on earth in terms of photochemical ozone formation and aerosol loading [*Kouvarakis et al.*, 2000; *Lelieveld and Dentener*, 2000]. The MINOS project (Mediterranean Intensive Oxidant Study) was initiated to improve our understanding of the transport processes, chemical mechanisms and main pollution sources that determine the chemical composition in the eastern Mediterranean troposphere. As a result, an intensive field campaign was carried out from Crete during August 2001 involving a ground station (Finokalia; 35.19°N, 25.40°E) and two aircraft to perform measurements of a wide range of trace gases and aerosols. An overview of major findings of MINOS is presented by *Lelieveld et al.* [2002].

A major objective of MINOS was to examine the role of long-range transport of pollutants into the region, notably to observe outflow from the southern Asian Summer Monsoon (ASM hereafter) over the eastern Mediterranean. The Asian plume, which also influences the Indian Ocean troposphere as found during the 1999 Indian Ocean Experiment (INDOEX) [*Lelieveld et al.*, 2001], contains high concentrations of ozone precursors (e.g., carbon monoxide (CO), non-methane hydrocarbons (NMHC)), partly oxidized hydrocarbons (POH, e.g., acetone (CH_3COCH_3), methanol (CH_3OH))) and chlorocarbons (notably methyl chloride (CH_3Cl)) [*Scheeren et al.*, 2002], as well as aerosols from fossil fuel and biomass burning emissions from the densely populated South Asian region. The less soluble species can be effectively transported to the upper troposphere by deep convection in the ASM. High altitude easterlies can carry Asian pollution across northern Africa and the Mediterranean. Indeed, back-trajectories [*Traub et al.*, 2003] and model simulations [*Lawrence et al.*, 2003; *Roelofs et al.*, 2003] indicate that the eastern Mediterranean upper troposphere (> 9 km altitude) was dominated by a southeasterly flow originating over India and Southeast Asia during the first half of August. During the second half of August the easterly flow weakened, after which a westerly flow dominated the upper troposphere, advecting air masses from the Atlantic region and North America to the MINOS region. Furthermore, the middle to upper tropospheric westerlies appeared to be regularly affected by downward transport of ozone-rich air from stratospheric origin [*Roelofs et al.*, 2003; *Heland et al.*, 2003].

Here we report on trace gas measurements performed with a German Falcon jet aircraft, which operated from Heraklion airport (35°N, 25°E). A total of 14 flights was conducted from the boundary layer up to 13 km, mainly over the Aegean Sea. In this study, we focus on the eastern Mediterranean upper troposphere between 6 and 13 km altitude. The measurement techniques are described in Section 4.2. We discuss the dynamics of the eastern Mediterranean troposphere during MINOS in Section 4.3. In Section 4.4, we show tropospheric distributions of C_2 – C_7 NMHC, halocarbons (including new anthropogenic halocarbons HFC-134a (CH_2FCF_3), HCFC-141b (CH_3CCl_2F), and HCFC-142b (CH_3CClF_2)), CO, CO_2, CH_4, O_3 organic species (acetone, methanol and acetonitrile (CH_3CN)) and NO_x ($NO + NO_2$) and NO_y (sum of reactive oxidized nitrogen; mainly $NO+NO_2+NO_3+N_2O_5+HNO_4+HNO_3+RONO_2$+peroxy acetyl nitrate (PAN)). We examine the upper tropospheric chemistry in the Asian plume and compare this with westerly air masses

originating over the Atlantic and North American region and with results from INDOEX. Furthermore, observations of Asian pollution transport into the lower stratosphere are presented in Section 4.5.

In addition, we use a coupled tropospheric chemistry-climate model (ECHAM4; see *Roelofs et al.*, 2003) to analyze contributions of the different origins or source regions of ozone, CO, and NMHC in the upper troposphere during MINOS presented in Section 5.6. Finally, the possible impact of future Asian emissions of NMHC, CO and NOx on tropospheric ozone is discussed.

4.2 Measurements techniques

First we summarize the measurements techniques employed and report the uncertainty and precision of the data presented. The in-situ measurements and air sample collection were performed on-board the German Falcon twin-jet research aircraft (operated by the German Aerospace Center (DLR)), using forward facing inlets on top of the aircraft fuselage.

The Max-Planck Institute for Chemistry (MPI-C) provided the Tunable Diode Laser Spectrometry (TDLAS) instrument to measure CO, CO_2 and CH_4 with a 1 s time resolution, at 1σ precision of 1.6 ppmv (μmol mol^{-1}), 1.5 ppbv (nmol mol^{-1}), and 16.5 ppbv, respectively and an absolute accuracy of ±1% for all species [*Wienhold et al.*, 1998].

The DLR performed the measurements of NO, NO_y (total oxidized nitrogen species) as well as O_3, which are described in detail by *Heland et al.* [2003]. Ozone was detected by means of UV absorption using a modified *Thermo Environmental 49* monitor from the DLR at a time resolution of 4 s. Accuracy and 1σ precision are ~1 ppbv and ±5%, respectively. NO is measured with a well characterized *ECO Physics CLD 790 SR* chemiluminescence detector (CLD), NO_y is measured with a second CLD in combination with a gold converter at 300°C with CO (0.2%) as the reduction agent [*Ziereis et al.*, 1999]. Both NO and NO_y were measured at a 1 Hz time resolution. The detection limits of the instruments are 5 pptv for NO, and 15 pptv for NO_y. The nominal accuracies of the NO and NO_y measurements are 5% and 15%, respectively.

The measurements of acetone, methanol and acetonitrile reported here were carried out using a Proton-Transfer-Reaction Mass-Spectrometer (PTR-MS) from NOAA Aeronomy Laboratory (Boulder, Colorado) with a 12 seconds time resolution. A precision of ±30% and a calibration uncertainty better than ±20% were achieved. Peroxy acetyl nitrate (PAN) was detected with an additional PTR-MS operated by the MPI-C at and an uncertainty of ~50%. For details about the PTR-MS technique we refer to *Lindinger et al.* [1998] and *de Gouw et al.* [2003].

Non-methane hydrocarbons and halocarbons were detected in whole air samples collected in 2.4 L electropolished pre-cleaned stainless steel canisters equipped with *Swagelok Nupro SS4H* valves. An automated airborne sampling system suitable for filling 12 canisters per flight, resulted in a time resolution of about 1 air sample per 15 minutes of flight [*Scheeren et al.*, 2002]. A total of 103 canisters were filled on flight 2 to 11 and 13 (no canisters were filled on flight 1 (August 1) due to a system malfunctioning, and on flight 12 and 14 (August 22) because of a limited amount of canisters). To limit storage artifacts, the

air samples were analyzed within a few weeks after collection. The analysis was performed at the IMAU laboratory using a gas chromatograph (GC; *Varian star 3600 CX*) equipped with a *CP-Sil 5 CB* pre-column (*WCOT* Fused Silica, 0.53 mm I.D.; 10 m long) in series with a *CP-SilicaPLOT* column (*PLOT* Fused Silica, 0.53 mm I.D.; 60 m long) and detection by Flame Ionization Detection (hydrocarbons and CH_3Cl) and Electron Capture Detection (halocarbons). We note that we used the FID instead of the ECD for quantitative evaluation of CH_3Cl to improve the precision. Pre-concentration of a 1 L sample was done with a *Varian* Sample Pre-concentration Trap (SPT) at a freeze-out temperature of -170° C at a flow rate of 33 ml min^{-1} regulated by a mass flow controller. The reproducibility of the SPT with standard gas is better than 2% (1σ). Before entering the SPT, water was removed from the sample stream by passing it through a *Nafion* drier tube mounted inside a countercurrent flow of purified dry nitrogen. Here we show results for C_2 – C_5 hydrocarbons, benzene and toluene, and halocarbons CH_3Cl, dichloromethane (CH_2Cl_2), trichloromethane (chloroform, $CHCl_3$), tetrachloroethylene (C_2Cl_4), CFC-12 (CF_2Cl_2), CFC-11 ($CFCl_3$), HFC-134a (CH_2FCF_3), HCFC-141b (CH_3CCl_2F), and HCFC-142b (CH_3CClF_2). The detection limit for hydrocarbons is <3 pptv (pmol mol^{-1}), for CH_3Cl (on the FID) and CH_2Cl_2 <10 pptv, and for the other halocarbons <0.1 pptv. Calibration was performed on a routine basis, using commercial gravimetrically prepared standard gas mixtures of hydrocarbons and halocarbons in nitrogen gas (*PRAXAIR*) as reference air with an accuracy of <3% for hydrocarbons and <2% for halocarbons. The halocarbons standard mixture has been additionally calibrated against primary standards at the Netherlands Metrology Institute (NMI). The halocarbons HFC-134a, HCFC-141b and HCFC-142b were detected and calibrated on the basis of reference samples provided by *S. A. Montzka* of NOAA, CMDL (Boulder, CO, USA) resulting in an accuracy < 5%. The overall precision was <10% for the NMHC and <3% for the remaining halocarbons except for CH_2Cl_2 (<15%) due to its poor detector response.

4.3 Free tropospheric meteorology

We used 10-day back trajectories calculated by the Royal Netherlands Meteorological Institute (KNMI) to study long-range transport routes and the origin of the encountered air masses. The trajectory model uses analyzed (6-hour averaged) 3-D wind fields from the European Centre for Medium-range Weather Forecast (ECMWF) [*Scheele et al.*, 1996; *Stohl et al.*, 2001]. Back trajectories were computed for each time a canister sample was taken, resulting in a set of trajectories that indicate the major transport pathways into the region. Here, we focus on the middle to upper troposphere between 6 to 13 km altitude dominated by long-range transport. For an outline of transport pathways and chemical characteristics of air masses encountered in the entire troposphere including the boundary layer we refer to *Lelieveld et al.* [2002] and *Traub et al.* [2003].

An overview of 10-day back trajectories for air masses encountered above 6 km altitude between August 3 and 22 (flight 2 to 11 and 13) is presented in Figure 4.1. Shown are trajectories as a function of latitude and longitude (upper panel) and as a function of pressure and longitude (lower panel).

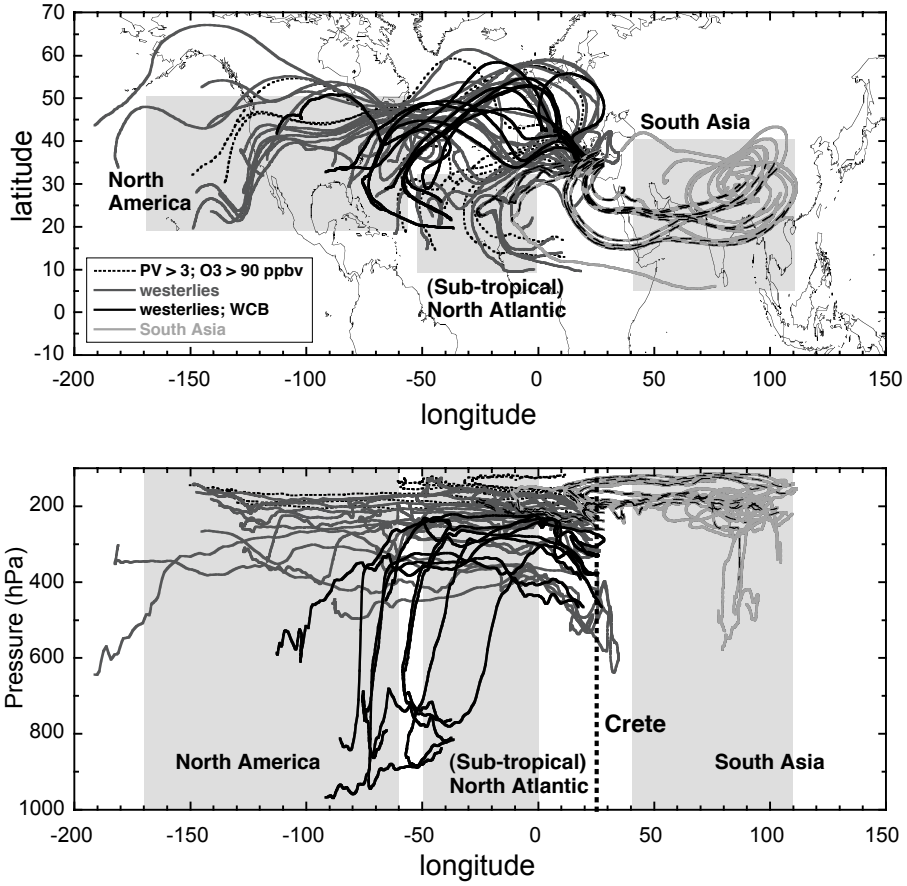

Figure 4.1: Results from a 10-day backward trajectory analysis based on ECMWF wind fields. The trajectories were computed for the times and locations of air samples collected during August 2 and 22 (1 to 2 trajectories per flight level of ~15 minutes). The shaded areas denote the air mass origins, being North America, the (subtropical) North Atlantic and South Asia. Light gray trajectories relate to South Asia (dashed lines denote 5 days backward), in dark gray westerly trajectories are shown ending between 8 and 12 km altitude, in solid black trajectories relate to WCB transport (ending between 6 and 9 km). Dashed black trajectories indicate air masses, which have been subject to stratosphere-troposphere exchange based on their PV-history.

Between 6 and 9 km we occasionally found polluted air (solid black trajectories) originating below 700 hPa over the eastern United States and the eastern Atlantic region (roughly between 60° and 90°W), 5 to 10 days prior to the flight. These polluted layers (discussed in Section 4.4.1) appear to be the results of fast upward motion associated with warm conveyor belt (WCB) transport ahead of a cold front [*Stohl and Trickl*, 1999]. In dark gray are tropospheric air masses encountered between 8 and 12 km altitude, which were

dominated by westerlies from North America and the North Atlantic region up to about 9 km. Above 9 km altitude a southeasterly flow prevailed during the first two weeks of August originating in South Asia (India and Southeast Asia), which is referred to as the Asian plume, shown as light gray trajectories (superimposed dashed lines denote 5 days back in time).

During July and August the South Asian region (India, Pakistan, and the Bay of Bengal area) is subject to the Asian summer monsoon (ASM). Satellite images (GOES-5 visible and infrared channel; http://www.eumetsat.de/en/dps/archive/historic.html) show a strong monsoonal activity through the presence of large clusters of convective clouds over India and the Bay of Bengal 10 – 15 days prior to the easterly plume in the Mediterranean upper troposphere between July 1 and 12, 2001. The ASM is associated with one of the largest upper tropospheric anti-cyclones on earth present from May to September. It has been the subject of intense study for over 150 years [*Hastenrath*, 1991; *Hsu et al.*, 1999]. The ASM is triggered in May. The Tibetan plateau starts to heat up after winter and an upper tropospheric anti-cyclone is formed through upward motion of warm air over the Central Asian mountain range. The warming causes a reversal of the meridional temperature gradient towards the Indian Ocean region, which redirects the low-level northeasterly winds into a southwesterly direction and the upper tropospheric subtropical westerly jet into an easterly direction [*Hsu et al.*, 1999]. Deep convection associated with the ASM can carry polluted Asian boundary layer air into the upper tropospheric anti-cyclonic circulation. Thus, pollution from South Asia is transported in the upper troposphere over Africa and the Mediterranean along with the easterly tropical jet (Figure 4.1; light gray trajectories), in conjunction with an upper tropospheric anticyclone over the Arabian Peninsula. During the second half of August 2001, the position of the Arabian anticyclone shifted to the southeast, reducing the influence of the Asian plume over the eastern Mediterranean.

Model work indicates that stratosphere-to-troposphere-exchange (STE) associated with the passing of cold fronts over the North Atlantic may contribute about 30% of the ozone in the westerlies [*Roelofs et al.*, 2003]. Air mass trajectories associated with STE are shown in blue, where we assume that a potential vorticity value that exceeds 3.0 potential vorticity (PV) units (1 PV-unit = 10^{-6} K m^2 kg^{-1} s^{-1}) anywhere along the 10-day trajectory in combination with ozone concentrations larger than 90 ppbv indicates a STE event.

An additional potential source of pollution in the Mediterranean free troposphere is convection of polluted air boundary layer air over continental areas to the free troposphere, associated with synoptic disturbances or with thunderstorms. An event of fresh pollution lifted up to an altitude of 6 km, associated with thunderstorm activity over eastern Turkey was encountered on August 3 (flight 2) and will be discussed in more detail in Section 4.4.1. A unique example of deep convective injection of polluted air into the tropopause region has been observed on August 22 and is described in detail by *Fischer et al.* [2002]. Here, sharp increases of tropospheric pollutants (e.g., CO, acetone, methanol and acetonitrile) were detected during ascent into the lower stratosphere above the anvil of a large thunderstorm system. Apart from these examples, the impact of deep convective events over the Mediterranean during MINOS in the upper troposphere appears to be rather small compared to the long-range transport of pollution into the region. This is caused by prevailing large-scale subsidence in the descending branch of the Hadley circulation, which lies directly over the region and the relative stability of the free troposphere induced by the UT anti-cyclone [*Roelofs et al.*, 2003].

4.3.1 Air mass classification

Air masses have been classified according to their geographical location 7 – 10 days back in time deduced from the 10-day backward trajectories presented in Figure 4.1. Air masses originating between 50°W to 170°W and 20°N to 50°N were classified as North American; those with an origin between 0°W to 50°W and 10°N to 30°N as (sub-tropical) North Atlantic, and air masses coming from 40°E to 110°E and 5°N to 40°N were classified as South Asian. A stratospheric origin was determined by a PV > 3 along the trajectory in combination with an ozone concentration exceeding 90 ppbv.

A general point of concern is the accuracy of computed trajectories, which decreases with time and increasing geographical scales [*Scheele et al.*, 1995; *Stohl*, 1998]. For instance, *Stohl* [1998] estimated position errors up to 20% of the travel distance. In this study we focus on, however, large-scale motions in the middle to upper troposphere as well as large-scale lifting events associated with the ASM and the WCB in order to distinguish between easterly or westerly air mass origin. In addition, we find good agreement with another more detailed trajectory analysis of the MINOS flights by *Traub et al.* [2003], who computed 5-day backward trajectories at a one minute time resolution along the flight track.

Based on the number of selected trajectories (55) for air masses between 6 and 13 km altitude in Figure 4.1, we could classify 38% of the air masses as North American, 14% as North Atlantic, 24% as South Asian, and 14% as stratospheric. The remaining 9% were associated with other source regions. Hence, we can distinguish two major source regions, i.e., the South Asian and the North American / North Atlantic region with possible pollution transport towards the eastern Mediterranean upper troposphere. In the following sections we will focus on the comparison of the chemical characteristics of the Asian plume and the westerly air masses of North American and North Atlantic origin.

4.4 Chemical characteristics of the free troposphere

4.4.1 Vertical distribution of trace gases

We present altitude profiles of a number of gaseous trace species measured between August 3 and 22 over the eastern Mediterranean from the boundary layer to about 13 km altitude in Figure 4.2. All data points, except for NMHC and halocarbons from the canister analysis, correspond to the mean of ~5 minutes in-situ measurements coinciding with the filling of a canister (1 – 2 per flight level of ~15 minutes), while the error bars reflect the measured variability (1σ standard deviation). Different markers denote the air mass origin above 6 km altitude based on 10-day backward trajectories (Section 4.3). Air masses from South Asia are depicted in solid black squares, open squares relate to the North Atlantic region, crossed open squares show the air masses originating over North America, dark gray dots correspond to air masses in the WCB over the eastern North Atlantic region (see

Figure 4.1, lower panel) and open triangles relate to pollution from local deep convection (explained in more detail later). Air masses below ~6 km are depicted in gray. They have not been classified with respect to their origin, but back-trajectory analysis by *Traub et al.* [2003] shows that European emissions play an important role. For a detailed chemical characterization of boundary layer pollution from European sources during MINOS we refer to *Gros et al.* [2003]. Gray squares in the upper troposphere relate to air masses, which have been influenced by stratosphere-troposphere exchange. Table 4.1 gives an overview of mean concentrations (and 1σ standard deviation) in the upper troposphere (≥ 6 km) of the data presented in Figure 4.1 for air masses originating in the North American/North Atlantic region and the South Asian region. Detailed aerosol properties in the troposphere during MINOS are addressed by *Minikin et al.* [2003] and are therefore not included here. We note that aerosol number concentrations were not particularly enhanced in the upper troposphere, although relatively high number concentrations of freshly produced Ultrafine Condensation Nuclei (UCN; between 5 and 14 nm particle diameter) of 1000 to 4000 particle cm^{-3} (stp) were encountered in the Asian plume and occasionally in the North American plume.

Figure 4.2 shows that the lower atmosphere in the eastern Mediterranean region contained the highest concentrations of CO, NMHC and oxidized organic species associated with pollutant emissions from Europe. CO_2, however, shows somewhat lower concentrations in the boundary layer than aloft, which is related to enhanced uptake by the vegetation during summer [*Strahan et al.*, 1998]. Although large-scale subsidence prevails during the Mediterranean summer, enhanced concentrations of reactive pollutant tracer species such as PAN, acetone, methanol, acetylene, propane and benzene were detected in the lower free troposphere up to ~6 km altitude. Convective transport is the most probable mechanism for mixing of polluted boundary layer air to the free troposphere, partly associated with land-sea breezes and orographic effects [*Millan et al.*, 1997]. A pronounced layer of relatively fresh pollution was encountered on August 3 (flight 2) at an altitude of 6 km (depicted as open triangles in Figure 4.2). This pollution plume was most likely related to outflow from a band of convective clouds and associated thunderstorm activity, which occurred over western Turkey and the Black Sea upwind of the flight track 1 – 2 days prior to the flight. Figure 4.3 shows an AVHRR thermal infrared image (NOAA 16 satellite) of this convective system close to the flight track were the pollution was observed. In addition, this polluted layer has been reproduced in model simulations by *Lawrence et al.* [2003] and *Good et al.* [2003], pointing to a well-mixed plume of a few days old of regional origin.

Above ~6 km altitude, long-range transport of pollution from outside Europe to the region appears to determine the vertical tracer concentration gradients. Between 6 and 9 km westerlies carry pollution from the North American continent to the region, mainly associated with the warm conveyor belt in synoptic disturbances [e.g., *Cooper et al.*, 2001]. As such, moist air containing pollution from the North American east coast can reach Europe in 3 to 5 days as shown by *Stohl and Trickl* [1999]. Air masses associated with North American pollution (dark gray dots) contained relatively high benzene concentrations, probably related to traffic emissions, as well as high concentrations of the air conditioning agent HCFC-134a (discussed further in Section 4.4.2.4).

Table 4.1: Means and 1σ standard deviation of trace gas concentrations observed in the upper troposphere (6 – 13 km altitude) for different air mass origins based on 10-day backward trajectory analysis. Air masses with a recent history of stratosphere-to-troposphere exchange were excluded from the data set. The regions of origin are 0°W – 170°W by 20°N – 50°N for North America/North Atlantic and 40°E – 110°E by 5°N – 40°N for South Asia.

Species	North America/ North Atlantic	South Asia
O_3 ppbv	73 (18)	57 (8)
CO ppbv	74 (12)	102 (4)
CO_2 ppmv	368 (3)	362 (2)
CH_4 ppbv	1819 (26)	1882 (21)
NO ppbv	0.1 (0.08)	0.1 (0.05)
NOy ppbv	0.75 (0.34)	0.59 (0.14)
PAN pptv	278 (144)	328 (71)
H_2O–vapor g/kg	0.23 (0.27)	0.05 (0.04)
CH_3OH pptv	610 (308)	1006 (199)
CH_3CN pptv	126 (12)	168 (32)
CH_3COCH_3 pptv	957 (331)	1093 (106)
C_2H_6 pptv	319 (72)	448 (57)
C_2H_2 pptv	44 (36)	186 (44)
C_3H_8 pptv	54 (39)	58 (13)
n-C_4H_{10} pptv	12 (11)	8 (2)
n-C_5H_{12} pptv	6 (8)	2 (1)
C_6H_6 pptv	11 (19)	14 (5)
C_7H_8 pptv	3 (3)	1 (1)
C_2-C_7 ppbC	1.15 (0.48)	1.65 (0.26)
CH_3Cl pptv	576 (19)	675 (22)
CH_2Cl_2 pptv	20 (6)	23 (3)
$CHCl_3$ pptv	5.4 (1.4)	7.6 (1.0)
C_2Cl_4 pptv	1.8 (1.3)	1.0 (0.3)
CFC-12 pptv	561 (12)	551 (5)
CFC-11 pptv	263 (8)	270 (3)
HFC-134a pptv	25.0 (3.4)	19.0 (2.2)
HCFC-142b pptv	13.6 (1.7)	13.0 (1.7)
HCFC-141b pptv	14.0 (4.7)	13.5 (2.4)

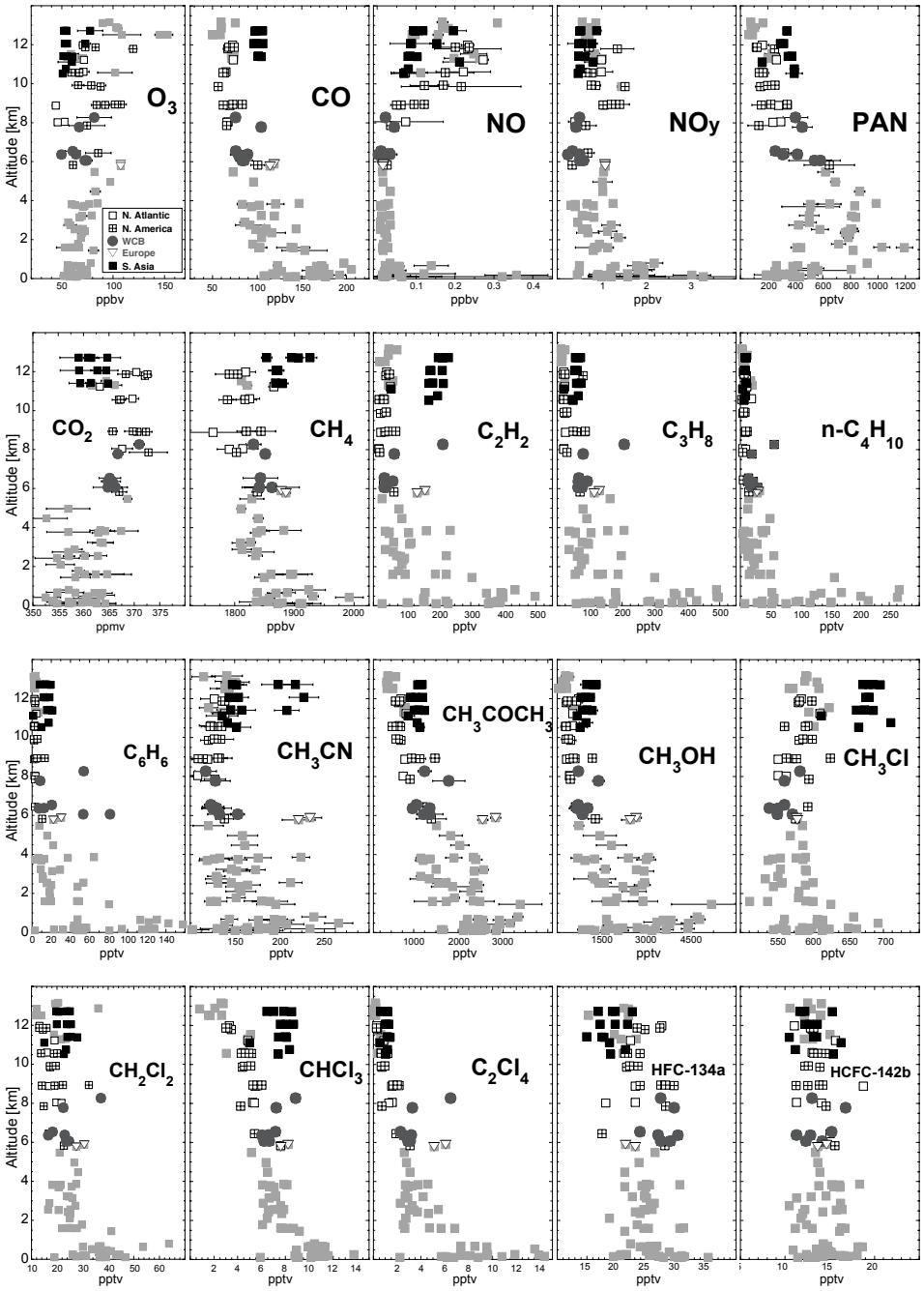

Figure 4.2: Altitude profiles of gases measured between August 3 and 22 over the eastern Mediterranean. The data points (other than NMHC) correspond to the mean of ~5 minutes in-situ measurements coinciding with the collection of an air samples, while the error bars reflect the variability (1σ standard deviation). Different markers denote the air mass origin (crossed squares: N. America, open squares: N. Atlantic, solid black squares: S. Asia, gray dots: WCB transport from eastern N. America, open triangles: southern European pollution from deep convection).

Figure 4.3: Satellite image (NOAA 16 AVHRR thermal IR channel) taken on August 2, 2001, at 1:11 UTC, showing a thick cloud band over northern Turkey and the black sea. The thick line resembles the flight track at 6 km altitude, whereas the gray arrows denote the general flow direction at that altitude.

An example of rapid uplifting of polluted air advected from the North American east coast is depicted by the back-trajectory in Figure 4.4 (see also the black trajectories in Figure 4.1). The WCB is visible in the cloud band along the North American east coast taken from a GOES 8 infrared satellite image (courtesy of METEOFRANCE) on August 15, 2001, at 12:00 UTC. The trajectory relates to a strongly polluted air mass encountered on August 19, 2001, at about 8 km altitude containing high NMHC (notably benzene and propane), halocarbons as well as high ozone (~80 ppbv) most likely resulting from photochemical production. Higher in the upper troposphere at 10 – 13 km the South Asian plume, denoted by the solid black squares in Figure 4.2, is associated with a strong signature of biomass burning, i.e. enhanced concentrations of CO, acetylene, benzene, acetone, acetonitrile, methyl chloride, and chloroform. This relates to the extensive use of biofuels in Asia, consistent with INDOEX measurements over the Indian Ocean [e.g., *Lelieveld et al.*, 2001; *de Gouw et al.*, 2001; *Scheeren et al.*, 2002).

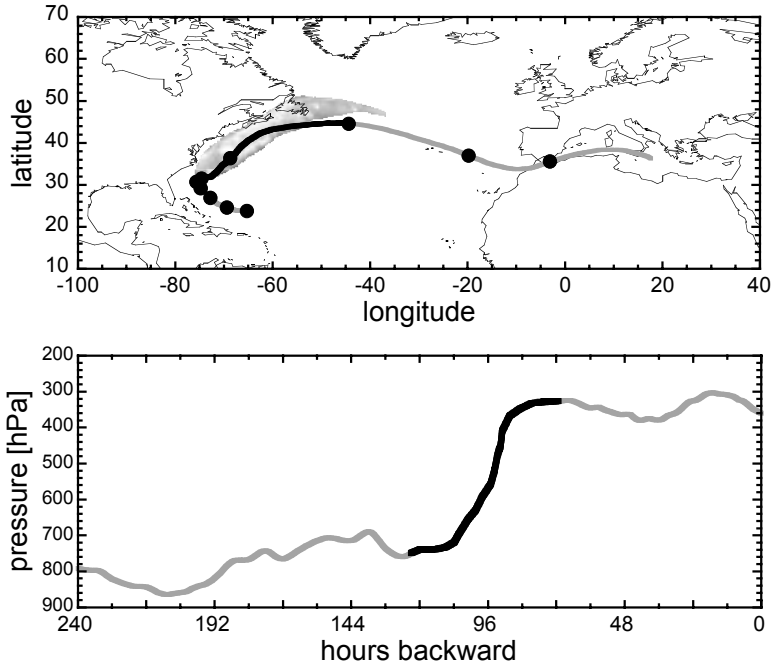

Figure 4.4: Backward trajectory showing rapid uplifting of boundary layer air along the North American east coast 4 to 5 days prior to the flight on August 19, 2001. The superimposed cloud band along the North American east coast was taken from an infrared satellite image (GOES 8) on August 15, 2001, at 12:00 UTC associated with the WCB.

4.4.2 Longitudinal tracer gradients in the upper troposphere

Complementary to the vertical gradients in Figure 4.2, Figure 4.5 shows observed upper tropospheric concentrations of several trace species (between 6 and 13 km) as a function of longitude of origin. The latter is deduced from the 10-day back-trajectory analysis. For this we applied the geographical end-point of the 10-day backward trajectories, which appeared to be representative of the travel distance and position of an air parcel between 7 to 10 days back in time. In addition, 7 to 10 days agree well with the travel times of pollution from the major source regions to Mediterranean as indicated by the trajectories. We note that the latitudinal variability of the air mass origins varied between 20°N and 50°N for the westerlies and between 5°N and 40°N for the easterlies. An analysis of latitudinal gradients showed no significant relationships and is therefore not shown here.

We applied a least squares linear fit on the data to illustrate the significance of the gradient (when present). Air masses with a recent stratospheric input (gray squares) were excluded from the linear fit (PV > 3.0 along the 10-days back trajectory in combination with

observed ozone exceeding 90 ppbv), because we are interested in the tropospheric origin of the species. Air masses that could be related to pollution lifted-up from the North American east coast (WCB) and advected across the Atlantic to Europe (based on the solid black trajectories in Figure 4.1) are marked as crossed open squares.

4.4.2.1 O_3, CO, NOy and NMHC

The longitudinal gradients and mean values (Table 4.1) show that O_3, NO and NO_y concentrations were generally lower in the Asian plume than in the westerly air masses, while PAR (C_2 – C_5 alkanes or paraffin's) and CO were similar or higher. This points to NO_x-limited conditions for photochemical O_3 production in the Asian plume and therefore a suppressed OH regeneration by NO [*Lelieveld et al.*, 2001]. The ratio of anthropogenic NO_x emissions to the total CO and hydrocarbon emissions is estimated to be smaller for Asia than for Europe and North America [*Olivier et al.*, 1996], which is associated with less efficient combustion processes. In addition, the lifetime of NO_x in the tropical boundary layer is very short (< 1 day) due to efficient reaction to HNO_3 and subsequent removal through wet and dry deposition [*Lelieveld and Dentener*, 2000]. The lower NO_y in the Asian plume may be partly related to the efficient removal of HNO_3 in deep convection in the ASM.

Furthermore, the role of lightning produced NO_x, which provides a fresh source of NO_x in the free troposphere, where the lifetime of NO_x is longer (up to about a 1 week), is still poorly understood. In particular over the North Atlantic the lightning fraction of NO_x in the westerlies might be relatively large [*Jeker et al.*, 2000]. Relatively high CO and PAR in the westerlies originated from the North American east coast and are associated with WCB transport (crossed open squares). The influence of stratosphere-to-troposphere transport, shown as gray squares in Figure 4.5, is absent in the Asian plume but increases significantly towards more westerly air mass origins. In these air parcels ozone is significantly enhanced, while concentrations of CO, higher hydrocarbon and oxidized organic tracer species are lower. This strongly influences the observed longitudinal trend of CO and O_3. The longitudinal gradients of O_3, CO, NO_y and NMHC are further investigated in Section 4.5 using the ECHAM4 general circulation model.

4.4.2.2 Methanol and acetone

Both methanol and acetone depict a negative east-west trend as function of longitude. The main terrestrial sources of atmospheric methanol are plant emissions, and to a lesser extent emissions from plant decay, industrial production and biomass burning, making it an abundant organic species in the background atmosphere [*Galbally and Kirstine*, 2002]. The chemical lifetime of methanol in the free troposphere based on reaction with OH is of the order of 2 weeks [*Singh et al.*, 1995], suggesting that the mean age of the plumes we encountered is shorter than that. The release of methanol from biomass burning is typically associated with oxygen deficient smoldering fires, e.g. in the domestic and small industrial use of biomass fuel in Asia [*Scheeren et al.*, 2002], resulting in an enhancement in the Asian plume.

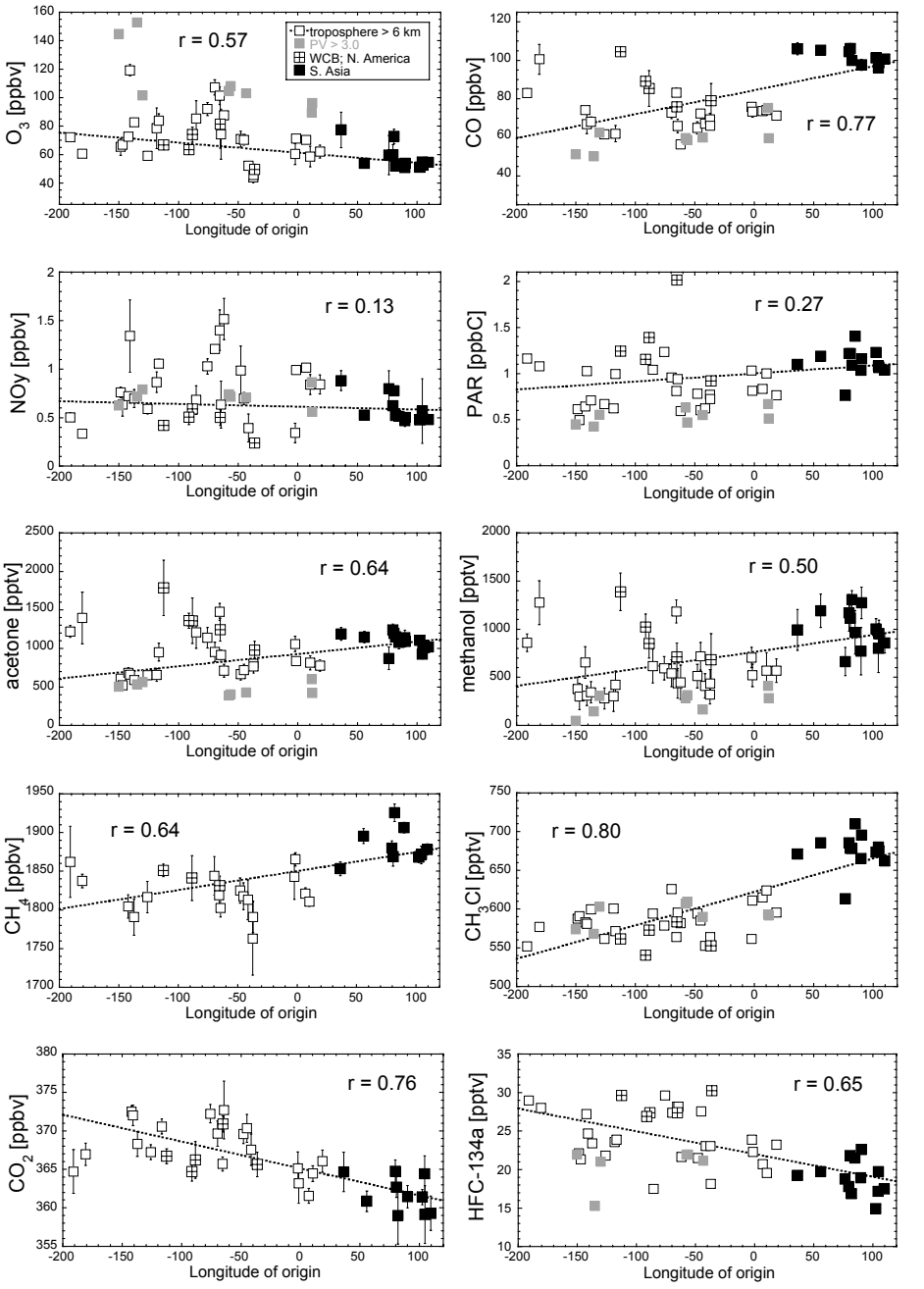

Figure 4.5: Longitudinal gradients of selected gaseous tracer species in the upper troposphere (between 6 and 13 km altitude). The longitude of origin for each data point is deduced from 10-day backward trajectory analysis. The data points (other than C_2 – C_5 alkanes or paraffin's (PAR)) correspond to the mean of ~5 minutes in-situ measurements coinciding with the collection of air samples. The error bars denote the measured variability of the selected data (1σ standard deviation). Different markers relate to specific air mass characteristics (gray squares: stratospheric, crossed open squares: WCB transport from eastern North America, black squares: Southern Asian).

Similar to methanol, acetone has large natural sources (vegetation and oceans), is emitted by biomass burning but it is also formed in the atmosphere by hydrocarbon oxidation [*Singh et al.*, 1995; *Jacob et al.*, 2002]. The chemical lifetime of acetone in the free troposphere as determined by photolysis and reaction with OH is of the order of 10 – 15 days, which is close to the chemical age of the upper tropospheric plumes. Nevertheless, the acetone concentration in the Asian and North American plumes of about 1 ppbv significantly exceeded the ~0.5 ppbv representative of the background upper troposphere [*Jacob et al.*, 2002]. Acetone and methanol correlated well ($r \geq 0.7$) with CO and total $C_2 - C_7$ NMHC in the upper troposphere, shown in Figure 4.6, suggesting that primary combustion sources and in-situ photochemical production explain the general enhancement above background levels. *Holzinger et al.* [2003] analyzed the biomass burning influence on acetone, methanol, CO and PAN over the eastern Mediterranean during MINOS. They found strong indications of secondary photochemical production of acetone and methanol, in agreement with our analyses. Relatively high concentrations of ~2.5 ppbv of acetone and methanol in the free troposphere have been observed in fresh pollution on August 2 at 6 km altitude, most probably related to convection over northern Turkey (Figure 4.3), described in Section 4.4.1.

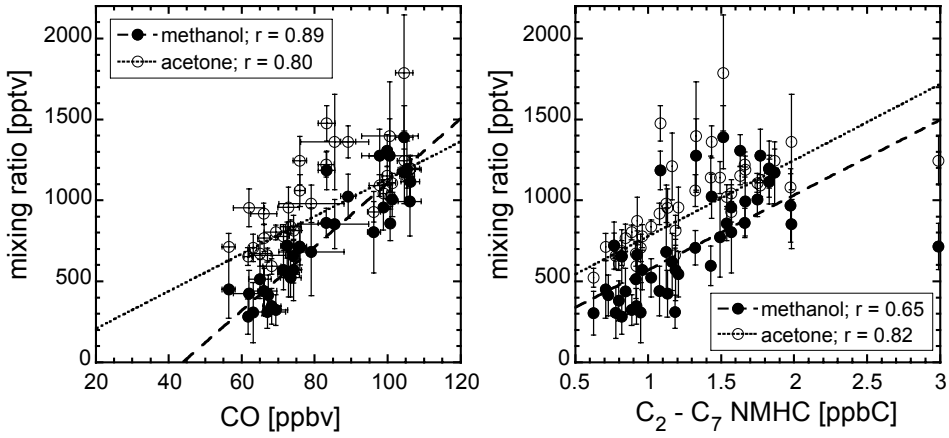

Figure 4.6: Correlation of methanol and acetone with CO and $C_2 - C_7$ NMHC in the free troposphere (> 6 km) during MINOS (r at the 95% significance level). The error bars show the 1σ standard deviation of the data points.

4.4.2.3 CH_4 and CH_3Cl

Both CH_4 and CH_3Cl are enhanced in the Asian plume, resulting in a negative longitudinal east-west gradient. Methane may be enhanced in the northern mid-latitude boundary layer (relative to a mid-latitude Northern Hemispheric background of ~1800 ppbv from AGAGE, *Prinn et al.*, 2000) from the production and use of natural gas (see Figure 4.2), while enhancements in tropical air masses most likely relate to emissions from rice paddies and natural wetlands [*Houweling et al.*, 2000]. Methyl chloride has strong terrestrial (vegetation

and soils) and oceanic sources [*Yokouchi et al.*, 2001; *Lee-Taylor et al.*, 2001] contributing to the global background of ~550 pptv. An additional large source in South Asia is biofuel burning [*Scheeren et al.*, 2002], leading to the large enhancement observed in the Asian plume. During the northern mid-latitude summer emissions from natural forest fires at mid-latitudes could also play a role, as can be deduced from the average concentration of 576 ± 19 pptv, which is somewhat higher than the CH_3Cl background.

4.4.2.4 HFC-134a, HCFC-141b and HCFC-142b

The relatively new fluorocarbon HFC-134a (in use since 1990) shows a consistently lower concentration in the Asian plume (19 ± 2 pptv) compared to westerly air masses (25 ± 3). Highest concentrations were detected in the European boundary layer (27 ± 5) and in air masses associated with WCB transport from the North American east coast (29 ± 1). At present, HFC-134a is mainly used as cooling agent in automobile air-conditioning systems as a replacement of CFC-11 [*AFEAS*, 2002]. Mobile air conditioning is considered as one of the major sources of fluorocarbons with annual leakage rates up to 10% per year [*EIA*, 2002]. Emissions of HFC-134a are concentrated in the US and Europe with vehicle numbers of about 200 million each in the year 2000, whereas the number of registered vehicles in India and China is presently of the order of ~20 million [*WRI*, 2002]. It is estimated that presently ~35% of European and ~90% of all American motor vehicles are equipped with air-conditioning. The HFC-134a chemical lifetime of ~14 years [*Kanakidou et al.*, 1995] has caused an accumulation of HFC-134a to its present background level of ~20 pptv. HFC-134a can serve as a tracer for western pollution, so that enhanced concentrations suggest North American or European pollution. The chlorofluorocarbons HCFC-142b and HCFC-141b, not shown in Figure 4.5, are mainly used as industrial solvents and for long-life applications as a blowing agent for closed-cell foams (in use since 1981 and 1990, respectively [*AFEAS*, 2002]). Emissions of HCFC-141b and HCFC-142b to the atmosphere are therefore smaller than of HFC-134a and not so wide-spread, while their chemical lifetimes are similar (~10 and ~20 years, respectively [*Kanakidou et al.*, 1995]), explaining their lower atmospheric variability (see Table 4.1).

4.4.2.5 CO_2

The longitudinal gradient of CO_2 shows a strong positive tendency from east to west. Model and measurement based studies have shown that the seasonality of CO_2 at the surface has a larger amplitude in the extra-tropics than in the tropics [*Strahan et al.*, 1998; *Matsueda et al.*, 2002]. Therefore, during summer CO_2 concentrations are lower at high latitudes. In the upper troposphere, however, the CO_2 seasonal cycle is less pronounced and has approximately the same amplitude and phase in both the extra-tropics and the tropics [*Strahan et al.*, 1998]. This would not lead to the observed longitudinal CO_2 gradient, which points to pollution sources in the westerlies. Upper tropospheric CO_2 concentrations have been correlated with concurrent HFC-134a, CH_4, CH_3Cl and CH_3CN to investigate possible sources, presented in Figure 4.7. We find a significant positive correlation between CO_2 and HFC-134a (at the 95% significance level), a tracer for pollution from North American

continent, and a negative correlation between CO_2 and CH_4, and the biomass burnings tracers CH_3Cl and CH_3CN. Our measurements thus indicate that pollution originating from the North American east coast is enriched in CO_2, most likely from fossil fuel burning.

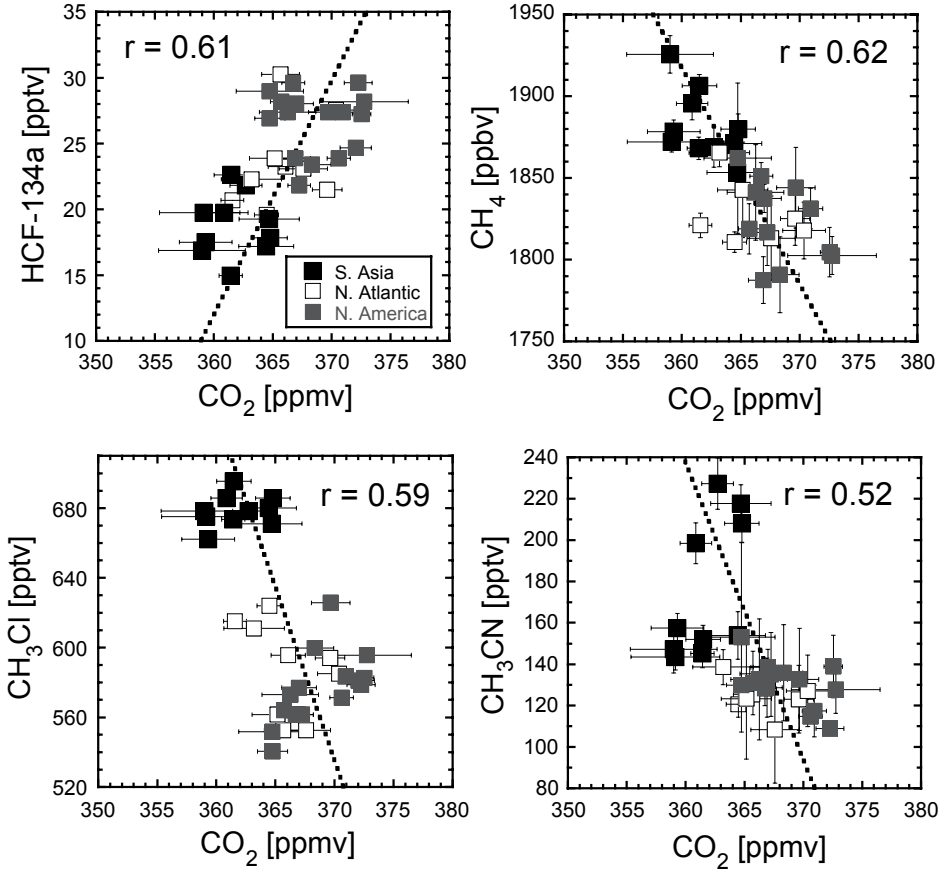

Figure 4.7: Correlation of HCF-134a (North American pollution tracer), CH_4 (tropical air mass tracer), CH_3Cl and CH_3CN (biomass burning tracers) with CO_2 (r at the 95% significance level) in the upper troposphere (> 6 km). Black squares relate to a South Asian origin, open squares to the (sub-tropical) northern Atlantic, and gray squares to North America. The error bars denote the measured variability of the data points (1σ standard deviation).

4.4.3 Chemical age of the Asian plume

The age of the Asian pollution detected in the upper troposphere refers to the travel time of pollutant species away from their sources. We estimate the air mass age from the enhan-

cement or emission ratio (ER) of biomass burning species with different photochemical lifetimes relative to CO that will change as function of travel time. The ER of species X can be determined as the slope of a linear regression fit ($\Delta X/\Delta CO$). We focus on typical biomass burning species methyl chloride, acetonitrile, acetylene and benzene that are chemically removed by the OH radical only. We compared ER's from MINOS measurements (ER_t) in the Asian plume with ER's from INDOEX 1999 measurements obtained over the Indian Ocean reported by *de Gouw et al.* [2001] and *Scheeren et al.* [2002], which we consider as source ER's (ER_0). The INDOEX ER_0 are typical for pollution from the Indian continent, which is considered as one of the main source regions for the Asian plume pollution, dominated by emissions from the industrial and residential use of biofuels. The MINOS ER's (ER_t) were taken as the slope from a linear regression fit performed on the hydrocarbon to CO relationship in the Asian plume, depicted in Figure 4.8. Depending on the reactivity of the species relative to CO, the source ratio ER_0 changes as a function of transport time or chemical age Δt and the mean OH radical concentration. The relationship between the ER_0 and the ER_t can be described by:

$$ER_0 = ER_t / e^{(k_{CO} - k_S)[OH]\Delta t} \tag{4.1}$$

where k_{CO} and k_S are the OH reaction rate coefficients for CO and emission species S taken from *Atkinson et al.* [1997], respectively, (OH) is the diurnal mean OH radical concentration in molecules cm^{-3}. The chemical age Δt can be determined from equation 4.1.

We assumed mean temperature and pressure conditions of 235 K and 225 hPa measured in the Asian plume and a daily mean OH concentration of $1.0 \pm 0.2 \times 10^6$ molecules cm^{-3} taken from the ECHAM4 general circulation model (described in more detail in Section 5) for 6 to 12 km altitude. Using equation 4.1, we derived a best match of the MINOS ER, apart from acetylene, with the INDOEX ER_0 values at a Δt of about 13 days presented in Table 4.2. The low acetylene ER from INDOEX might be related to additional breakdown away from combustion sources in the Asian boundary layer prior to deep convection into the upper troposphere. A better agreement is found with the mean biomass burning ER of 8 ± 4 pptv $ppbv^{-1}$ for acetylene found in fresh biomass burning emissions from various studies reported by *Veldt and Berdowski* [1995].

Based on the back trajectory analysis (shown in Figure 4.1), the transport times from South Asia towards the Mediterranean are 5 – 10 days in the upper troposphere. *Traub et al.* (2003) present 20-day forward trajectories with starting points in two West Indian cities (Madras, 80.76°E / 13.85°N; Patna, 85.72° E/ 26.01°N) for July, 2001, indicating travel times of 2 - 5 days for deep convection from the boundary layer to the upper troposphere over India. Hence, combining these back and forward trajectories, we can deduce travel times from the Asian boundary layer to the Mediterranean upper troposphere ranging from 7 to 15 days. In spite uncertainties involved in estimating the chemical age [*Jobson et al.*, 1998], the chemical age of the encountered pollution in the Asian plume seems to be quite realistic and in agreement with trajectory analysis.

Table 4.2: Comparison between biomass burning Emission Ratios (ER) relative to CO from INDOEX (ER_0) with ER's derived for the MINOS Asian plume (ER_t). Standard deviation (1σ) of ER between parentheses. A best match is achieved when assuming a photochemical age of the Asian plume of ~13 days (at mean temperature and pressure of 235 K and 225 hPa measured in the Asian plume and a diurnal mean OH concentration of ~1×10^6 molecules cm^{-3} estimated by the ECHAM model for 6 – 12 km altitude).

Emission species	ER_0 pptv $ppbv^{-1}$	MINOS ER_t pptv $ppbv^{-1}$	MINOS ER_t at -5 days	-10 days	-13 days
CH_3CN[a]	1.1(0.4)	1.5 (0.3)	1.44	1.36	1.31
CH_3Cl[b]	1.98 (0.24)	2.32 (0.28)	2.17	2.05	1.98
C_2H_2[a]	3.3 (0.2)	5.1(0.3)	5.9	6.8	7.4
C_6H_6[a]	0.95 (0.05)	0.32 (0.08)	0.48	0.72	0.92

[a] *de Gouw et al.* [2001]

[b] *Scheeren et al.* [2002]

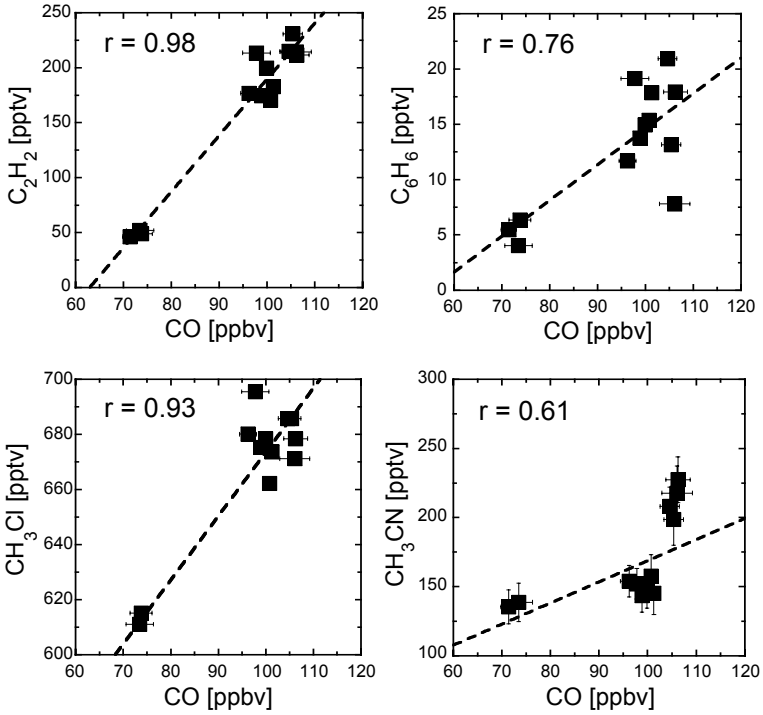

Figure 4.8: Correlations of selected biomass burning tracers with CO in the South Asian plume. Linear regression (r at the 95% confidence level) provided biomass burning Emission Ratios (ER) relative to CO. Error bars denote the measured variability (1σ standard deviation).

4.5 Asian pollution observed in the lowermost stratosphere

Besides the global impact of the ASM dynamics, model studies indicate an important potential for pollution transport into the lower stratosphere (Chen, 1995; Dethof et al., 2000). Deep convection in the ITCZ (InterTropical Convergence Zone) over South Asia adds pollution to the upper tropospheric anti-cyclonic circulation. The associated upward motion pushes the subtropical tropopause to ~16 km altitude over a relatively large region [*Roelofs et al.*, 2003]. The subtropical tropopause slopes down to about 11 km towards higher latitudes, providing favorable conditions for isentropic cross-tropopause transport. The potential impact of the Asian plume for pollution transport into the lower stratosphere is large because of its high pollution level, large-scale and its persistent presence between June and September.

The tropopause over the MINOS measurement area was generally located above the maximum flight altitude of the Falcon aircraft of ~13 km. Fortunately, on August 16 and 17, a trough located north of Crete lowered the tropopause to about 10 - 11 km altitude providing an opportunity to sample the upper tropopause/lower stratosphere over the region. Hence, on August 16 (flight 8) the aircraft first crossed the tropopause at about 10.5 km altitude measuring ozone values of ~100 ppbv. It then climbed to about 12.5 km and traversed the trough again observing ozone values >150 ppbv. Six air samples were collected in the trough and the air mass origin was analyzed with 10-day backward trajectories depicted in Figure 4.9. It shows that air masses with a westerly component (green) converged with air masses with an easterly component (orange), coming from the (shaded) region affected by the Asian plume (northern Africa and the tropical North Atlantic). Measurements in the trough of CO, O_3, NMHC, CH_3Cl, acetone and methanol, along with PV from the ECMWF analysis are presented in Table 4.3. We found enhanced concentrations of CO, NMHC, CH_3Cl and methanol in air masses with an easterly component, that closely resemble the chemical characteristics of the Asian plume in presented in Table 4.1 and Figure 4.2. These results provide first indications that troposphere-to-stratosphere exchange of Asian pollution affects the lowermost stratosphere over the Mediterranean. Clearly, dedicated measurements and model work are needed to quantitatively asses TSE of Asian pollution associated with the ASM.

Table 4.3: Indications of Asian pollution observed in the upper tropopause/lower stratosphere region (PV > 3.0) on August 16, 2002 over the eastern Mediterranean at an altitude of 10.5 – 12.8 km. Shown are mean values and 1σ standard deviation.

Air mass origin	PV PV-units	O_3 ppbv	CO ppbv	NMHC ppbC	CH_3Cl pptv	Acetone pptv	Methanol pptv
Westerly	3.8 (0.2)	149 (6)	51 (1)	0.54 (0.02)	571 (4)	522 (65)	100 (128)
Easterly	3.2 (0.6)	103 (5)	60 (1)	0.71 (0.07)	600 (10)	412 (61)	263 (126)

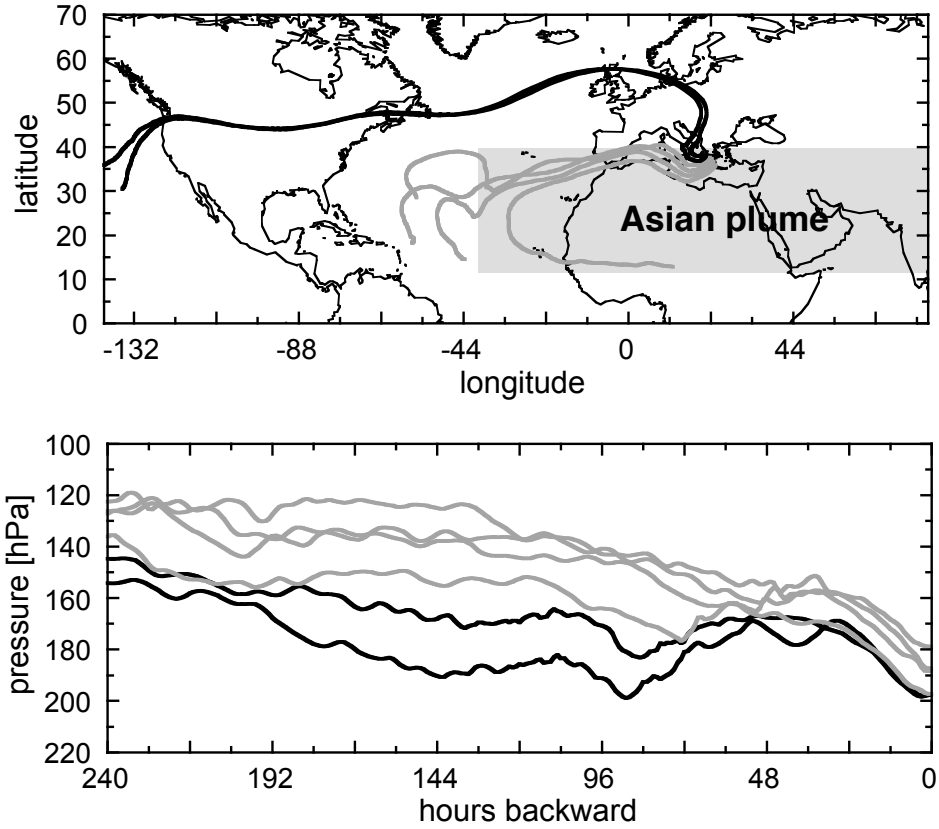

Figure 4.9: Ten-day backward trajectories for air masses sampled in the tropopause/lower stratosphere region during August 16 (flight 8) over the eastern Mediterranean. The shaded area denotes the geographical range, where the Asian plume affects atmospheric chemistry during August 2001 based on model simulations.

4.6 Model simulations of the upper troposhere

We used the ECHAM4 general circulation model (European Centre Hamburg Model version 4) to simulate observed gradients of CO, O_3, NOy and total carbon from the sum of C_2-C_5 alkanes (PAR) to help us better understand the characteristics of the upper troposphere during MINOS. The model has a T63 horizontal resolution of approximately 1.9° × 1.9°, a time step of 15 minutes, and has 19 vertical levels up to 10 hPa (the troposphere between 5 and 14 km consists of 6 model layers). The model has been initiated from January 2001 and uses analyzed ECMWF winds fields similar to the trajectory analysis. For

more details about the model we refer to *Roelofs and Lelieveld* [2000].

4.6.1 Simulated longitudinal gradients of O_3, CO, NO_y and NMHC

Figure 4.10 shows the qualitative agreement between simulated and observed longitudinal gradients of CO, O_3, NO_y and C_2 – C_5 alkanes (parafines; PAR). For clarity, a weighted fit through the model output is shown, leaving out the individual data points. In addition, the mean model and measurement results for westerly air masses (North American and North Atlantic) and the Asian plume as well as the mean model to measurement ratio are presented in Table 4.4. The mean model to measurement ratio represents an attempt to compare model and measurements in a more quantitative way. Measured and modeled mean NO concentrations (not shown in Figure 4.10) are also included in Table 4.4.

Looking at CO and O_3 gradients, it appears that the general agreement between modeled and measured values in the upper troposphere is quite good, which is reflected in a mean model/measurements ratio close to 1. A closer look shows that enhanced CO associated with WCB uplifting of North American pollution (purple dots) is not well reproduced by the model. Hydrocarbons (C_2 – C_5 alkanes) are reasonably well simulated in the Asian plume (mean model/measurement ratio of 1.3) but underestimated by factor of 2.4 in the westerly air masses. Here the stratospheric influence appears to be overestimated while the contribution of North American pollution, including CO, is underestimated. The ECHAM4 model tends to overestimate the role of downward tracer transport, notably of stratospheric ozone across the tropopause [*Roelofs et al.*, 2003]. In addition, the relatively coarse vertical resolution of the model allows more efficient mixing between shallow layers of pollution than might be realistic. For example, the WCB transports fresh North American pollution plumes to an altitude of 6 to 9 km across the Atlantic, which were typically encountered as distinct layers of a few hundreds of meters thick. As a result, modeled hydrocarbons (PAR) and CO can be underestimated, while the stratospheric influence is overestimated at the expense of photochemically produced ozone. Indeed, for the selected WCB data points the model/measurement ratio for O_3 and PAR is 1.2 and 0.2, respectively.

NO_y is reasonably well simulated in the Asian plume, but misses most of the enhanced NO_y concentrations observed in the westerlies. NO is underestimated by a factor of 3 in the Asian plume and by a factor of 1.8 in the westerlies (Table 4.4). The observed enhanced tropospheric NO_y (and NO_x) values are most probably related to lightning produced NO_x over the Atlantic, not well represented in the model. Recent observations of NO_x in the tropopause region over the United States and the Northern Atlantic have shown that in-situ lightning production is as important as convective transport from the polluted boundary layer for the NO_x budget during summer [*Jeker et al.*, 2000; *Brunner et al.*, 2001].

In summary, the Asian plume chemistry is reasonably well simulated by the model, whereas in the westerlies the influence of stratosphere-to-troposphere exchange tends to be overestimated, while the influence of North American pollution is underestimated.

Table 4.4: Comparison between measurements (MINOS) and model simulations (ECHAM) for O_3, CO, C_2 – C_5 alkanes (PAR), NO and NOy species. Mean concentrations (and 1σ standard deviation) and the ECHAM/MINOS ratios R are shown for the Asian plume and westerly air masses > 6 km altitude (North American and North Atlantic air masses).

	O_3 ppbv	CO ppbv	PAR ppbC	NO pptv	NOy ppbv
MINOS Asian plume	57 (8)	102 (4)	1.12 (0.15)	0.11 (0.05)	0.59 (0.14)
ECHAM Asian plume	51 (3)	111 (6)	1.41 (0.17)	0.03 (0.01)	0.47 (0.03)
MINOS westerlies	73 (18)	74 (12)	0.91 (0.32)	0.11 (0.08)	0.76 (0.34)
ECHAM westerlies	76 (17)	73 (7)	0.34 (0.14)	0.04 (0.02)	0.49 (0.06)
R-Asia	0.90 (0.14)	1.11 (0.09)	1.27 (0.17)	0.31 (0.08)	0.83 (0.20)
R-westerlies	1.10 (0.34)	1.01 (0.18)	0.42 (0.24)	0.57 (0.44)	0.79 (0.44)

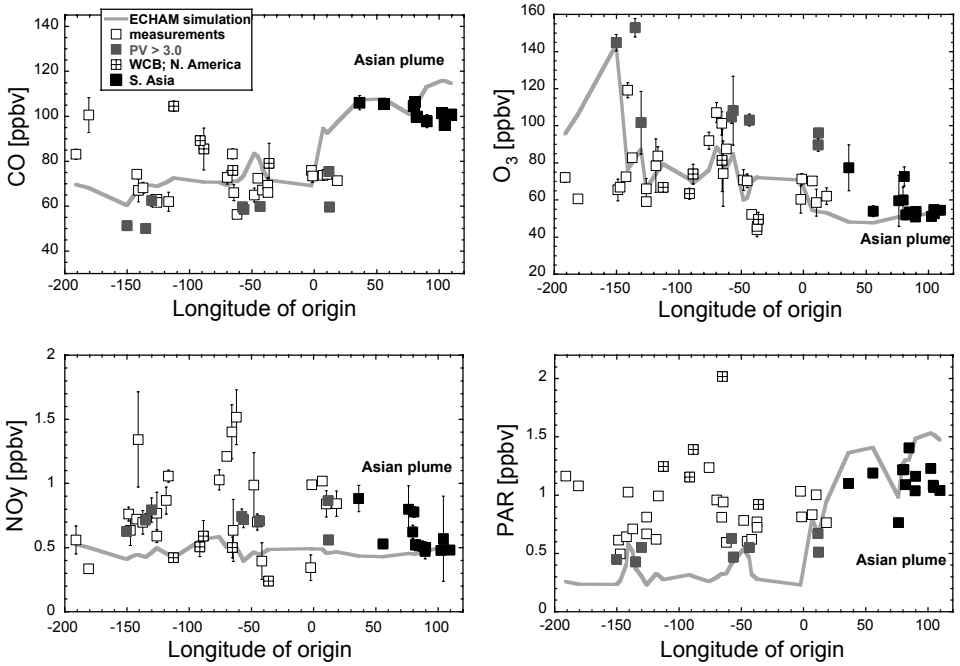

Figure 4.10: Comparison between simulated and observed longitudinal gradients of CO, O_3, NO_y and C_2 – C_5 alkanes (paraffin's; PAR). The model output is shown by the solid line (weighted fit through the model output). The error bars on the measurement points of CO, O_3 and NO_y depict the measured variability (1σ standard deviation).

4.6.2 Simulated source contributions to O_3 and CO

In *Roelofs et al.* [2003] ECHAM4 is used to investigate contributions to upper tropospheric (6 – 13 km altitude) concentrations of O_3 from different source regions, being eastern and western Europe, Africa, India, South Asia, North America, lightning and the stratosphere. Here we extend the analysis to CO. The simulated source contributions are shown as function of longitude of origin derived from the ECMWF 10-day back trajectory analysis in Figure 4.11. Older air masses that could not be attributed to one of the source regions are defined as "background", which also contributes up about 25% to the tropospheric ozone column. We focus specifically on the contributions of South Asia (India and Southeast Asia) to O_3 and CO in the Asian plume. About 10 to 16 ppbv or 20 – 30% of total O_3 and 28 to 44 ppbv or 30 - 40% of CO in the Asian plume can be attributed to recent emissions from South Asia. The second largest contributor to ozone in the Asian plume appears to be lightning NO_x associated with the ASM, contributing 6 to 11 ppbv (10 – 20%) to total O_3 in the plume. In the westerlies, the simulated ozone concentration variability appears to be associated with downward mixing of stratospheric air. The NMHC concentration in the westerlies is underestimated by the model (see Table 4.4). As mentioned earlier, the simulated stratospheric contribution may be overestimated thereby artificially reducing the photochemical ozone production in polluted air masses from the North American continent.

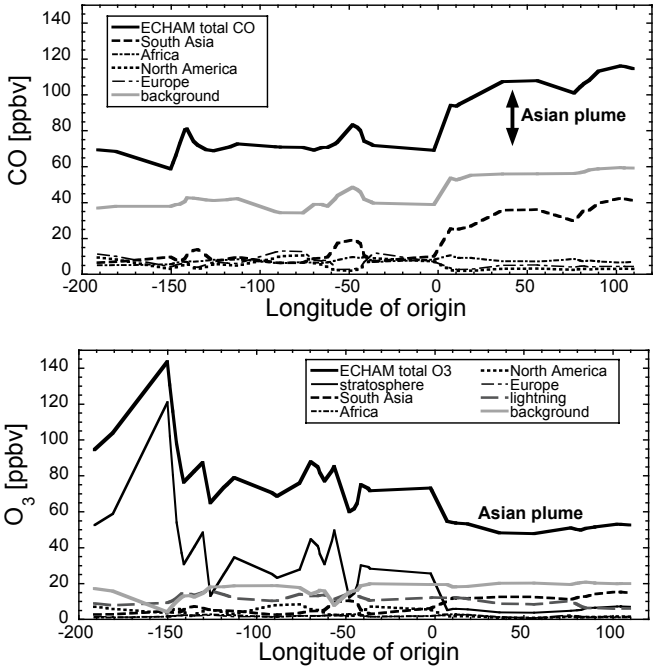

Figure 4.11: Simulated source contributions to CO and O_3 as function of longitude of origin (deduced from 10-day backward analysis) computed for the times and locations of air samples collected during August 2 and 22 in the upper troposphere (> 6 km). Shown is a weighted fit through the model data.

4.6.3 Impact of increasing Asian NO_x emissions on tropospheric ozone

South Asia (notably India and China) is the fastest growing region in the world in terms of population and economic development. This may have a significant impact on a hemispheric scale on the atmospheric levels of ozone and ozone precursors [*Lelieveld et al.*, 2001; *Lelieveld and Dentener*, 2000; *Hauglustaine and Brasseur*, 2001]. A relatively large increase is expected for Asian NO_x emissions in the next 25 years, due to the expected strong increase of fossil fuel use replacing biofuels (wood, dung and agricultural waste). Fossil fuel combustion generally produces lower CO and unburned hydrocarbon emissions than smoldering biofuel burning, but is more strongly NO_x-producing because of higher temperature and pressure conditions. Assuming the IPCC IS92a growth emission scenario for a future (2025) atmospheric chemistry simulation with the ECHAM4 model, it was found that O_3 in the Asian plume increases with ~7 ppbv, which is ~14% of the present concentration. We note that this increase is only ≤ 1 ppbv larger than in a future model run in which only NO_x emissions are assumed to increase, illustrating again the NO_x-limited conditions for photochemical ozone production in the Asian plume. Consistently, the correlation between observed ozone and total $C_2 - C_7$ NMHC concentrations is insignificant in the Asian plume, whereas in the westerly plume a hydrocarbon-limited regime appears to dominate, as can be seen in Figure 4.12.

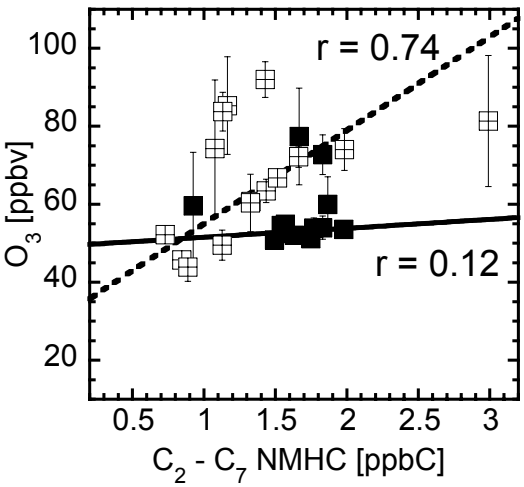

Figure 4.12: Correlation between observed O_3 and NMHC in the Asian plume (black squares) and westerly plume (crossed squares).

Our results agree with the model study of *Stevenson et al.* [2002], who simulated an ozone increase around 20% in the Asian plume over the Mediterranean for ozone precursor emissions representative of 2030. Tropospheric ozone is an effective greenhouse gas

accounting currently for ~0.4 W m^{-2} of the global mean radiative forcing of climate which is about 25% of the forcing by CO_2 [*Lelieveld and Dentener*, 2000]. This is relatively small compared to the radiative forcing due to the backscatter of solar radiation caused by anthropogenic aerosols over the eastern Mediterranean resulting in a cooling of about 6.6 W m^{-2} at the top of the atmosphere [*Lelieveld et al.*, 2002; *Markovic et al.*, 2002]. While the radiative forcing of tropospheric ozone is likely to increase in the future, the aerosol radiative effect might decrease as result of the implementation of cleaner combustion and fuel technologies and emission reduction measures in Europe. On the other hand, higher ozone levels in the future Asian plume affect the tropospheric ozone budget over Northern Africa and the (sub-)tropical Atlantic as well, contributing to the oxidizing capacity of the atmosphere over these regions.

4.7 Summary and conclusions

Deep convection associated with the Asian summer monsoon followed by long-range transport carries Asian pollution towards the eastern Mediterranean and northern Africa. Model studies indicate that this Asian plume is a yearly recurrent phenomenon over the Mediterranean. We present observations of trace species during MINOS in August 2001, showing that the Asian plume has a large impact on the chemical composition of the upper troposphere over the eastern Mediterranean. Enhanced levels of CO, and hydrocarbons were found to be comparable to or higher than those found in westerly air masses, containing pollution from the North American continent. The Asian plume shows a signature of biomass burning (notably from the use of biofuels) by enhanced concentrations of CO, acetylene, benzene, acetonitrile, methyl chloride and chloroform, in agreement with observations from the 1999 INDOEX campaign in outflow from India. The mean photochemical age of the encountered Asian pollution is estimated to be about 2 weeks, based on the comparison of emission ratios relative to CO from MINOS with ER's derived from INDOEX results, consistent with trajectory analysis. Acetone levels in the Asian plume are of the same magnitude as those observed in the westerlies, exceeding upper tropospheric background levels. On the other hand, methanol levels are higher in the Asian plume, probably related to emissions from Asian biofuel use. The new automobile air conditioning agent HFC-134a was significantly enhanced above background values in air masses originating from North America, serving as a tracer for western pollution. The extensive fossil fuel use in North America is associated with relatively large CO_2 concentrations in the westerlies, correlating with enhanced HFC-134a.

In spite of high pollution levels in the Asian plume, ozone concentrations are still relatively low (~55 ppbv) and show no clear relationship with higher hydrocarbons. This suggests a NO_x-limited photochemical ozone production regime. Model simulations, carried out with a tropospheric chemistry-climate model, indicate that the expected increase of Asian emissions in the next few decades may enhance photochemically produced ozone in the Asian plume by about 14%.

The influence of recent stratosphere-to-troposphere exchange is absent in the Asian plume but appears to have affected the chemical composition of air masses from westerly

origin. STE causes a significant enhancement of ozone concentrations while CO, and hydrocarbon concentrations are decreased. The Asian plume, on the other hand, represents a large reservoir of pollutants near the tropopause. Observations in the lowermost stratosphere over the Aegean Sea suggest that troposphere-to-stratosphere transport of Asian pollution may have occurred during MINOS.

Acknowledgements

We gratefully acknowledge the excellent cooperation with the DLR Falcon team. We thank Rinus Scheele from the KNMI for computing the 10-day back trajectories. We are grateful to S.A. Montzka of NOAA/CMDL for providing halocarbon reference measurements.

5 Measurements of reactive chlorocarbons over the Surinam tropical rainforest: indications for strong biogenic emissions

Abstract. Contrary to the understanding of the emissions and chemical behavior of halocarbons from anthropogenic sources (e.g. CFCs and HCFCs), the biogeochemistry of naturally emitted halocarbons is still poorly understood. We present measurements of chloromethane (methyl chloride, CH_3Cl), trichloromethane (chloroform, $CHCl_3$), dichloromethane (CH_2Cl_2), and tetrachloroethylene (C_2Cl_4) from air samples taken over the Surinam rainforest during the 1998 LBA/CLAIRE campaign. The samples were collected in stainless steel canisters on-board a Cessna Citation jet aircraft and analyzed in the laboratory using a gas chromatograph equipped with FID and ECD. The chlorocarbons we studied have atmospheric lifetimes of ~1 year or less, and appear to have significant emissions from natural sources including oceans, soils and vegetations, as well as biomass burning. These sources are primarily concentrated in the tropics (30°N – 30°S). We detected an increase with decreasing latitude of methyl chloride, chloroform, and tetrachloroethylene mixing ratios, in pristine air masses advected from the Atlantic Ocean toward the central Amazon. In the absence of significant biomass burning sources, we attribute this increase to biogenic emissions from the Surinam rainforest. From our measurements, we deduce fluxes from the Surinam rainforest of 7.6 ± 1.8 μg CH_3Cl m^{-2} h^{-1}, 1.11 ± 0.08 μg $CHCl_3$ m^{-2} h^{-1}, and 0.36 ± 0.07 μg C_2Cl_4 m^{-2} h^{-1}. Extrapolated to a global scale, our emission estimates suggest a large potential source of 2 Tg CH_3Cl yr^{-1} from tropical forests, which could account for the net budget discrepancy (underestimation of sources), as indicated previously. In addition, our estimates suggest a potential emission of 57 ± 17 Gg C_2Cl_4 yr^{-1} from tropical forest soils, equal to half of the currently missing C_2Cl_4 sources. We hypothesize that the extensive deforestation over the last two decades relates to the observed global downward trend of atmospheric methyl chloride.

Submitted to *Atmospheric Chemistry and Physics* with, J. Lelieveld, J. Williams, H. Fischer, and C. Warneke as co-authors.

5.1 Introduction

The magnitude of natural sources in the global budgets of reactive organic chlorine species such as chloromethane (methyl chloride, CH_3Cl), dichloromethane (CH_2Cl_2), trichloromethane (chloroform, $CHCl_3$), and tetrachloroethylene (C_2Cl_4) is still poorly constrained [*Khalil et al.*, 1999; *Keene et al.*, 1999]. These reactive organic chlorine species have an atmospheric lifetime from reaction with OH radicals of about 1.3 years for CH_3Cl, 0.5 years for $CHCl_3$, 0.4 years for CH_2Cl_2 and 0.3 years for C_2Cl_4 [*Khalil*, 1999]. About 60% of the total emissions of reactive organic chlorocarbons (including chlorinated ethanes and ethenes) appear to be natural and concentrated in the tropics [*Khalil*, 1999; *Keene et al.*, 1999]. Although the atmospheric budget of reactive chlorocarbons (dominated by CH_3Cl) represents only about 15% of the total standing chlorine concentration, these compounds constitute the dominant source of reactive chlorine in the troposphere and lower stratosphere. An understanding of their present budget allows us to assess their role in atmospheric chemistry in the past, in the absence of anthropogenic chlorine sources, and in the future after anthropogenic chlorine has decreased significantly.

The most prominent organic chlorine species is CH_3Cl with a present mean background concentration of ~550 pptv (pptv = 10^{-12} mol mol^{-1}) in the extra-tropics and ~600 pptv in the tropics [*Lee-Taylor et al.*, 2001; *Scheeren et al.*, 2002; 2003]. At present about 17% of chlorine catalyzed ozone destruction can be attributed to CH_3Cl [*Harper*, 2000]. CH_3Cl is removed from the atmosphere mainly by reaction with the OH radical (3.43 Tg), and to a lesser extend by soil uptake (0.26 Tg) and loss to the stratosphere (0.28 Tg) [*Keene et al.*, 1999]. To date only about half of the estimated global sink of about 3.97 Tg CH_3Cl per year has been accounted for by emissions from the oceans and biomass burning within a fair degree of uncertainty [*Keene et al.*, 1999]. Several studies have pointed to higher plants as potential major source of CH_3Cl [*Lobert et al.*, 1999; *Khalil et al.*, 1999; *Harper*, 2000, *Yokouchi et al.*, 2000]. The emission of CH_3Cl from higher plants (potato tubers) was first reported by *Varns* [1982], and later in a more extensive laboratory study by *Saini et al.* [1995] (involving herbaceous species and halophytes). Recent observations by *Yokouchi et al.* [2002], supported by a model study by *Lee-Taylor et al.* [2001], point to large fluxes of CH_3Cl from tropical vegetation. *Lee-Taylor et al.* [2001] deduced that the source-sink discrepancy cannot be explained by an overestimated sink from the uncertainty in the OH-radical + CH_3Cl reaction coefficient or to underestimated known sources. They show that observed mixing ratios and latitudinal distributions are best reproduced in their model by addition of a large tropical terrestrial CH_3Cl source of the order of 2.3 Gg yr^{-1}.

Besides the search for new CH_3Cl sources, there has been a considerable effort to identify and quantify natural sources of other reactive chlorocarbons such as $CHCl_3$, CH_2Cl_2 and C_2Cl_4 to decrease the considerable uncertainties in their global budgets. There have been reports of emission fluxes of $CHCl_3$ and CH_3Cl from peat land [*Dimmer et al.*, 2001], CH_3Cl fluxes from wetlands [*Varner et al.*, 1999] and coastal salt marshes [*Rhew et al.*, 2000; *Bill et al.*, 2002], and CH_3Cl emissions from coastal waters [*Li et al.*, 1999], and emissions $CHCl_3$ from biomass burning [*Rudolph et al.*, 1995; *Scheeren et al.*, 2002]. Moreover, there have been extensive studies on $CHCl_3$ fluxes from forest soils related to bio-degradation processes involving fungi [*Watling and Harper*, 1998; *Hoekstra et al.*, 1998;

2001; *Haselmann et al.*, 2000a, 2000b]. In addition to industrial emissions as a major source of CH_2Cl_2 and C_2Cl_4, there have been indications of small but significant natural emissions of these species from biomass burning [*Rudolph et al.*, 1995; *Scheeren et al.*, 2002], as well as from the oceans [*Keene et al.*, 1999; and references therein]. *Hoekstra et al.* [2001] observed a small soil flux of C_2Cl_4 in Douglas fir forest. To our knowledge there have been no reports of biogenic land-based emissions of CH_2Cl_2.

For a comprehensive review of formation and degradation processes of organohalogens in terrestrial environments, we refer to a recent special issue of 26 papers in *Chemosphere* [2003] and a recent paper by *Hamilton et al.* [2003] with emphasis on CH_3Cl. *Hamilton et al.* [2003] present important evidence that abiotic conversion of Cl^- to CH_3Cl occurs readily in decaying plant material, with the plant component pectin acting as methyl donor. They conclude that this mechanism may explain a significant part of the CH_3Cl emissions previously observed from a variety of plant sources and terrestrial ecosystems (e.g. tropical plants, salt marshes and peatlands).

This paper presents measurements of reactive chlorocarbons from air samples collected over the rainforest of Surinam, South America, as part of the Large-scale Biosphere-atmosphere experiment in Amazonia – Co-operative LBA Airborne Regional Experiment (LBA/CLAIRE) in March 1998. The air samples were collected during 10 measurement flights conducted from Zanderij airport in Surinam (5.4°N – 55.2°W) using a Cessna Citation II aircraft operated by the Delft University of Technology. The flights covered an area roughly between 2°N – 7°N and 53°N – 59°W at altitudes ranging from 50 to 12500 m. The measurement payload provided in-situ observations of ozone (O_3), carbon monoxide (CO), carbon dioxide (CO_2), methane (CH_4), organic tracer species (notably, acetone (CH_3COCH_3), isoprene, and acetonitrile (CH_3CN)), and aerosols. In total, 80 air samples were collected for laboratory analyses on non-methane hydrocarbons (NMHC) and chlorocarbons. Detailed analyses of the trace gas distributions of acetone, isoprene, CO and CO_2 during LBA/CLAIRE have been reported by *Pöschl et al.* [2001], *Warneke et al.* [2001], and *Williams et al.* [2001b], respectively. Part of the NMHC results has been included in a study on the variability-lifetime relationship of organic trace gases by *Williams et al.* [2001a], and in a study focusing on a high altitude biomass burning plume by *Andreae et al.* [2001]. Here, we focus on measurements of the chlorocarbons CH_3Cl, CH_2Cl_2, $CHCl_3$, and C_2Cl_4, which have been analyzed in concurrence with measurements of NMHC, CO, and acetonitrile over the Surinam rainforest.

Apart from the coastal region were the majority of the population of about 400.000 people resides, Surinam is covered by pristine Amazonian rainforest. Hence, our chlorocarbons measurements provide new information on the role of tropical rainforest ecosystems as natural source of chlorocarbons to the atmosphere. The measurements are used to estimate fluxes of chlorocarbons from the Surinam tropical rainforest, and to estimate global annual mean emission fluxes from tropical rainforest ecosystems. Finally, we discuss the relationship between observed decreasing trends in atmospheric CH_3Cl and global tropical forest cover over the last two decades.

5.2 Measurement techniques

The measurement techniques employed in this study have all been described in detail elsewhere. Here, we briefly summarize the methods, their precision and accuracy.

CO was measured by an airborne Tunable Diode Laser Spectrometer (TDLAS) developed and operated by the Max Planck Institute in Mainz, Germany [*Wienhold et al.*, 1998; *Williams et al.*, 2001b). CO was detected at 1 Hz with an accuracy of ±3% and precision of ±2%.

Acetone and acetonitrile were detected by an airborne Proton-Transfer-Reaction Mass-Spectrometer (PTR-MS), which was developed operated by Innsbruck University [*Lindinger et al.*, 1998; *Crutzen et al.*, 2000]. About 10 masses (including acetone and acetonitrile) could be identified at a time resolution of 10 s. For a detailed interpretation of mass scans obtained over the Surinam rainforest we refer to *Williams et al.* [2001c]. The detection limit was 0.4 ppbv for acetone and 0.2 ppbv for acetonitrile. The measurement accuracy was better than ±30%, while the precision was typically ±20% for acetone and ±30% for acetonitrile.

A total of 80 whole air samples were collected in stainless steel canisters between 0.1 to 12.5 km altitude, for subsequent laboratory analysis of hydrocarbons and chlorocarbons by a Gas Chromatograph equipped with a Flame Ionization and Electron Capture Detector (GC-FID/ECD). For technical details of the GC-method we refer to *Williams et al.* [2001a] and *Scheeren et al.* [2002]. The accuracy based on commercial gravimetrically prepared standard mixtures (*PRAXAIR*) was ±3% for hydrocarbons and ±2% for chlorocarbons. The precision for hydrocarbons > 15 pptv used in this study was 11% for acetylene (C_2H_2), 5% for propane (C_3H_8), 7% for n-butane (n-C_4H_{10}), 6% for benzene (C_6H_6). The precision for chlorocarbons was 4% for CH_3Cl, 11% for CH_2Cl_2, 5% for $CHCl_3$, and 7% for C_2Cl_4.

5.3 Meteorology

During the short dry season from February to April, Surinam lies in the northern meteorological hemisphere with the Inter Tropical Convergence Zone (ITCZ) located at a few degrees south. The (short) dry season is generally characterized by low precipitation due to strong subsidence over the region suppressing deep convective activity. March 1998 was a particularly dry month due to the “El Niño” phenomenon. Northeasterly trade winds carry pristine air masses from the Atlantic Ocean land over the tropical rainforest towards the ITCZ, allowing primary organic emissions and their oxidation products to accumulate.

During the day, a dry convective boundary layer is formed, coupling the rainforest canopy to the atmosphere above through turbulent mixing. This layer is referred to as the mixing layer, where emissions from the rainforest build-up. In contrast to the marine conditions, the boundary layer over land has a distinct diurnal cycle driven by solar heating during the day and surface radiative cooling during the night. During night, the daytime mixing layer is decoupled from the surface by a strong temperature inversion. After dawn, the shallow nocturnal mixing layer starts to grow via turbulent mixing, reaching a maximum depth around 1500 m in the afternoon during the dry season [*Martin et al.*, 1988]. A shallow

convective cloud layer forms above the mixing layer in the course of the day. The convective clouds transport air between the mixing layer and the convective cloud layer. The shallow convective cloud tops generally coincide with the top of the trade wind inversion, which acts as a barrier to mass transport out of the boundary layer to the free troposphere [*Martin et al.*, 1988; *Zimmerman et al.*, 1988].

The typical evolution of the mixed layer height over the Amazon tropical rainforest during the dry season is shown in Figure 5.1. The diurnal pattern has been composed from observed temperature inversions in potential temperature profiles from the 1985 Amazon Boundary Layer Experiment (ABLE 2A) [*Martin et al.*, 1988] and from profiles obtained from ascent and descent with the Citation aircraft during LBA/CLAIRE [*Krejci et al.*, 2003]. It was found that the depth of the mixing layer during LBA/CLAIRE reached an altitude between 1300 to 1700 m at midday (depicted as a gray band in Figure 1) in good agreement with the ABLE 2A observations.

Deep convection in the ITCZ brings boundary layer (BL) air masses into the middle and upper troposphere, where they can be caught in a southerly return flow. Indeed, outflow from the ITCZ has been clearly observed in the middle troposphere on March 19, 21 and 29, which will be discussed in the next section, and on March 26, which has been described in detail by *Andreae et al.* [2001].

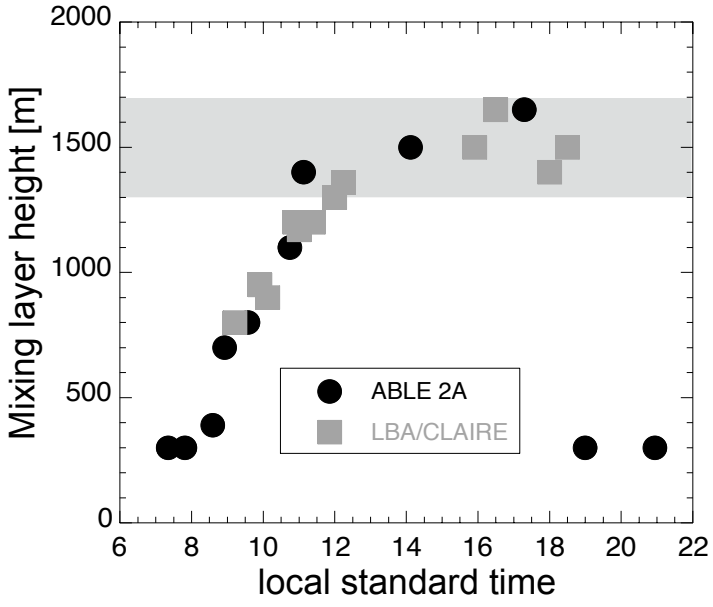

Figure 5.1: Typical mixing layer heights over the Amazon rainforest during the dry season based on observed (potential) temperature inversions. The black dots are based on balloon and rawinsonde profiles made during the ABLE 2A campaign (July 1985, Manaus region, Central Amazonia). The gray squares refer to temperature profiles obtained during March 1998 over the Surinam rainforest from ascents and descents with the Citation. The gray band denotes the range of mixing layer heights corresponding with the Surinam boundary layer measurements.

The mean observed north-south wind component for all flights, expressed as the cosine of the wind angle multiplied by the observed wind speed is shown in Figure 5.2 (running mean over 1278 points; negative values indicate southerly winds). Northeasterly trade winds prevailed up to about 2.5 km altitude. Southerly winds were generally observed in the free troposphere (FT) between 2.5 and 4 km, 5.5 and 8 km, and between 8 and 12 km relating to ITCZ outflow. For more details about the meteorology during LBA/CLAIRE we refer to *Williams et al.* [2001b] and *Krejci et al.* [2003].

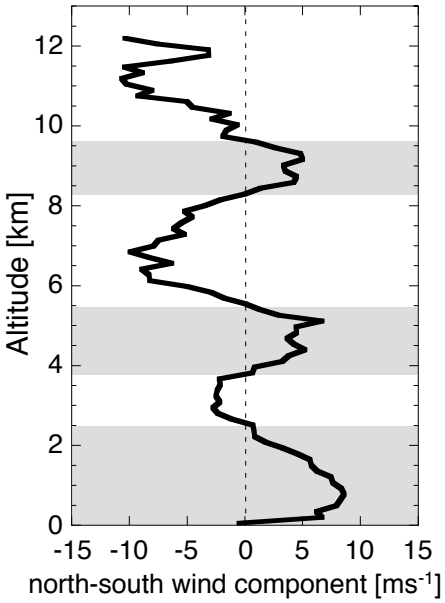

Figure 5.2: Mean vertical wind profile showing the north-south wind component as cos(WA) × WS in m s^{-1}. Gray areas denote northerly winds.

5.4 Results

5.4.1 Vertical distributions

Before we focus on the boundary layer measurements, we present a general overview of the vertical distributions of chlorocarbons and selected combustion tracers measured simultaneously during March 1998. As such, we show vertical concentration profiles (in pptv) of the reactive chlorocarbons CH_3Cl, CH_2Cl_2, $CHCl_3$, and C_2Cl_4 as detected in all canister samples (80) collected during March 1998 in Figure 5.3a. In Figure 5.3b, profiles of the combustion tracers CO and CH_3CN from in-situ measurements, as well as the hydrocarbons acetylene, propane and benzene from the canisters are shown. The CO and CH_3CN data are averaged time series corresponding with the duration of the canister

sampling (~1 – 3 minutes). Error bars in Figure 5.3 denote the measurement uncertainty, which is larger than the 1σ standard deviation of the mean for CO and CH_3CN. Enhanced CO and hydrocarbons (notably acetylene and propane), in combination with enhanced concentrations of the biomass burning tracer CH_3CN [*Lobert et al.*, 1990; *Holzinger et al.*, 1999], point to the influence of biomass burning emissions. Elevated concentrations of benzene from fossil fuel use and of C_2Cl_4 from industrial use (a degreasing agent used notably in dry cleaning) are related to urban/industrial pollution. The flights in which the highest tracer concentrations have been observed in the FT between 8 and 12 km altitude are depicted by different markers in Figure 5.3: black dots for flight 4 (March 19), gray dots for flight 5 (March 21), dark gray diamonds for flight 8 (March 26), and crossed squares for flight 10 (March 29). In addition to the vertical profiles, an overview of average and median mixing ratios of all air samples collected below 2 km in the mixing layer, between 2 – 7 km in the lower free troposphere (LT), and above 7 km in the middle free troposphere (MT) is presented in Table 5.1.

Table 5.1: Overview of the mean ± 1σ standard deviation and median (between parenthesis) trace gas concentrations in the mixing layer (ML), the lower free troposphere (LT), and the middle free troposphere (MT). The number of canister samples is denoted by N.

Species	ML-mean (median) < 2 km alt. N = 42		LT-mean (median) 3 – 7 km alt. N = 12		MT-mean (median) 7 – 12 km alt. N = 26	
CO ppbv	131 ± 11	(134)	119 ± 12	(117)	125 ± 29	(120)
CH_3CN pptv	192 ± 83	(183)	201 ± 65	(207)	143 ± 68	(133)
C_2H_6 pptv	837 ± 193	(769)	630 ± 87	(610)	778 ± 346	(658)
C_2H_2 pptv	86 ± 31	(78)	95 ± 44	(97)	120 ± 72	(111)
C_3H_8 pptv	92 ± 31	(81)	64 ± 23	(60)	89 ± 59	(66)
n-C_4H_{10} pptv	15 ± 5	(15)	18 ± 11	(17)	19 ± 10	(19)
C_6H_6 pptv	30 ± 17	(26)	24 ± 9	(27)	57 ± 50	(41)
CH_3Cl pptv	624 ± 36	(628)	640 ± 31	(630)	635 ± 51	(636)
CH_2Cl_2 pptv	26.0 ± 2.9	(26.2)	16.4 ± 0.3	(16.4)	16.3 ± 4.4	(17.5)
$CHCl_3$ pptv	9.2 ± 2.3	(9.0)	6.6 ± 1.7	(6.5)	6.9 ± 3.5	(6.3)
C_2Cl_4 pptv	3.8 ± 1.3	(3.5)	4.3 ± 2.5	(3.9)	4.4 ± 3.0	(3.2)

Figure 5.3 and the results in Table 5.1 demonstrate that besides the boundary layer, the highest mixing ratios (except for CH_2Cl_2 and $CHCl_3$) have been observed above 7 km in the MT, whereas the LT shows a minimum. Moreover, the results in Table 5.1 show that in the case of C_2H_2 and C_6H_6 the MT was significantly more polluted than the lower atmosphere, emphasizing the minor role of local pollution sources. This MT maximum in hydrocarbons, notably of benzene with a relatively short photochemical lifetime of a week or less, points to rapid uplifting of polluted air masses into the MT. The vertical wind profile in Figure 5.2 indicates that the MT airflow was predominantly southerly, originating over the region

where the ITCZ was active. Hence, the most likely transport mechanism is deep convection and subsequent outflow of boundary layer air into the MT associated with the ITCZ. Meteorological evidence of ITCZ outflow encountered in the MT is provided by 10-day backward trajectory analysis presented in Figure 5.4. The back-trajectories, calculated by the Royal Netherlands Meteorological Institute (KNMI), are based on 6-hour averaged 3-D wind field from the European Centre for Medium-range Weather Forecast (ECMWF) [*Stohl et al.*, 2001]. Every 2 minutes along the flight track a back-trajectory was computed.

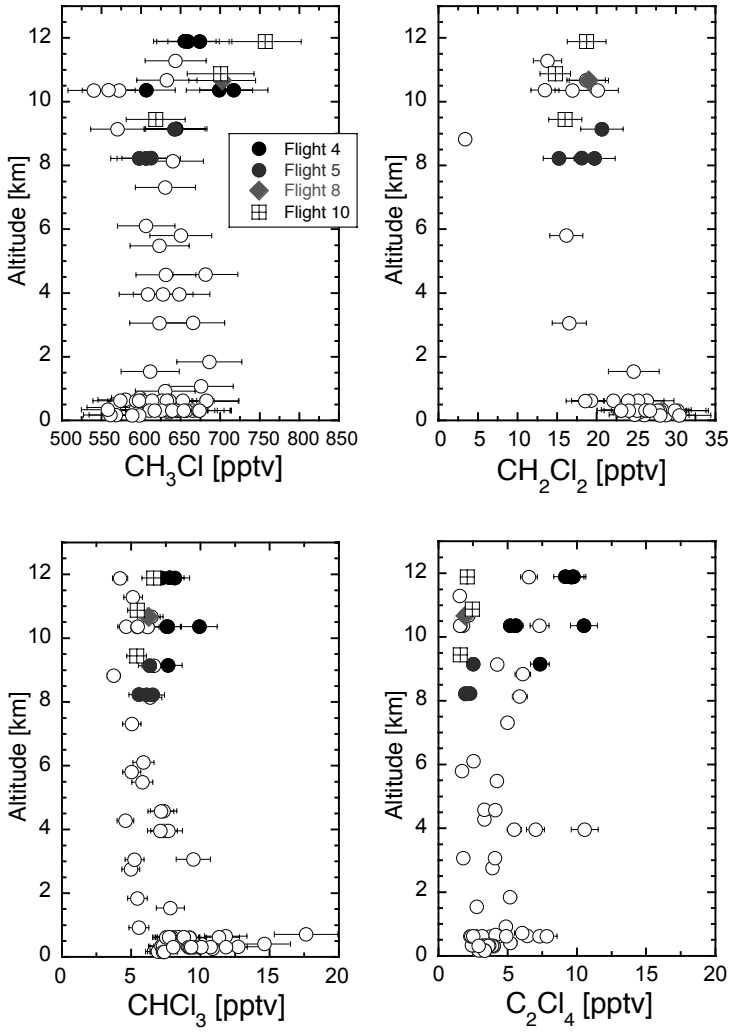

Figure 5.3a: Vertical profiles of selected chlorocarbons. Error bars denote the measurement uncertainty. The different markers between 8 and 12 km altitude refer to the flights, where outflow from the ITCZ has been observed.

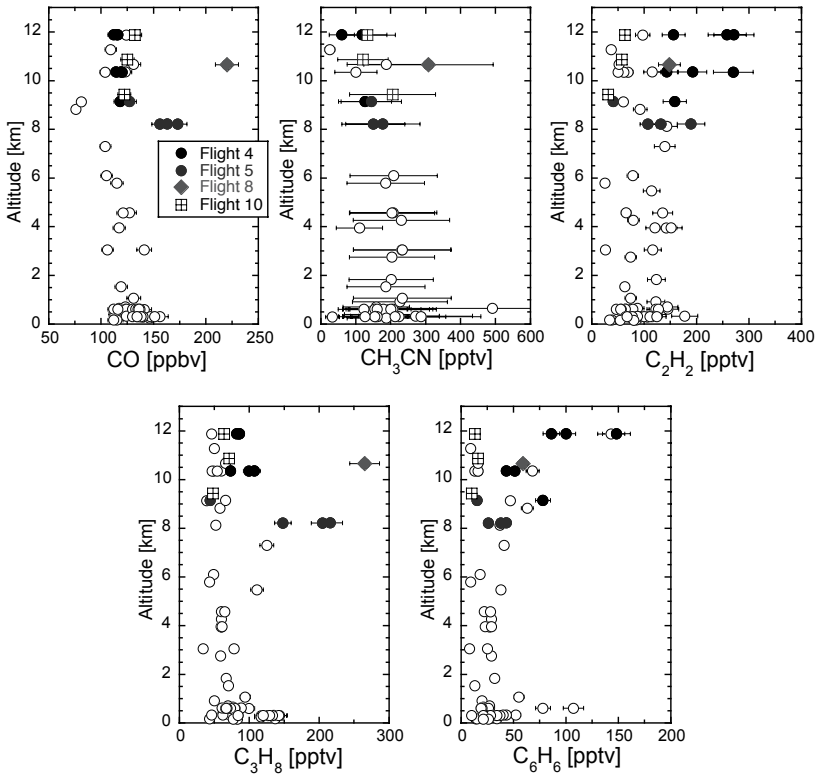

Figure 5.3b: Vertical profiles of selected combustion tracers. Error bars denote the measurement uncertainty. The different markers between 8 and 12 km altitude refer to the flights, where outflow from the ITCZ has been observed.

Figure 5.4 shows a selection of back-trajectories along the MT flight tracks, where the highest tracer concentrations have been observed. In black we show back-trajectories starting on March 19 (flight 4) between altitudes of 10 – 12 km, in gray trajectories starting on March 21 (flight 5) between 8 – 9 km are shown, and the dashed black lines represent trajectories starting on March 29 (flight 10) between 9 – 12 km. The ITCZ, denoted by the gray band in Figure 5.4, was located at about 5°S of the Guyana's based on GOES satellite visible and infrared images of March 1998 (http://www.satmos.meteo.fr). The back-trajectories analysis depicted in Figure 5.4 clearly reveals the occurrence of rapid upward transport of lower tropospheric and boundary layer air into the upper troposphere (8 – 12 km altitude) over central to northwestern Brazil in the ITCZ region, 3 to 9 days prior to the flights.

The enhancements of C_2Cl_4, C_2H_2 and C_6H_6 on March 19 (flight 4) as well as high CO, C_2H_2 and C_3H_8 encountered in the MT on March 21 (flight 5) suggest a strong influence of anthropogenic pollution, which appears to originate over the populated northwestern coastal region of Brazil (Figure 5.4, black and gray trajectories). The peak at about 11 km altitude observed on March 26 (flight 8), notably of CO, CH_3CN and CH_3Cl is a strong

signature of biomass burning. This event was related to large savanna/forest fires that took place near the Brazil/Venezuela border and is described in detail by *Andreae et al.* [2001]. Finally, on March 29 (flight 10) high CH_3Cl mixing ratios (> 700 pptv) have been observed at an altitude of 11 – 12 km in the absence of enhanced combustion tracers (e.g., C_2H_2, CH_3CN) pointing to a strong natural source. Here, the back-trajectory analysis suggests an air mass origin over the pristine rainforest of central Amazonia. In the next section, we focus on chlorocarbon gradients in the mixing layer as observed over the pristine Surinam rainforest.

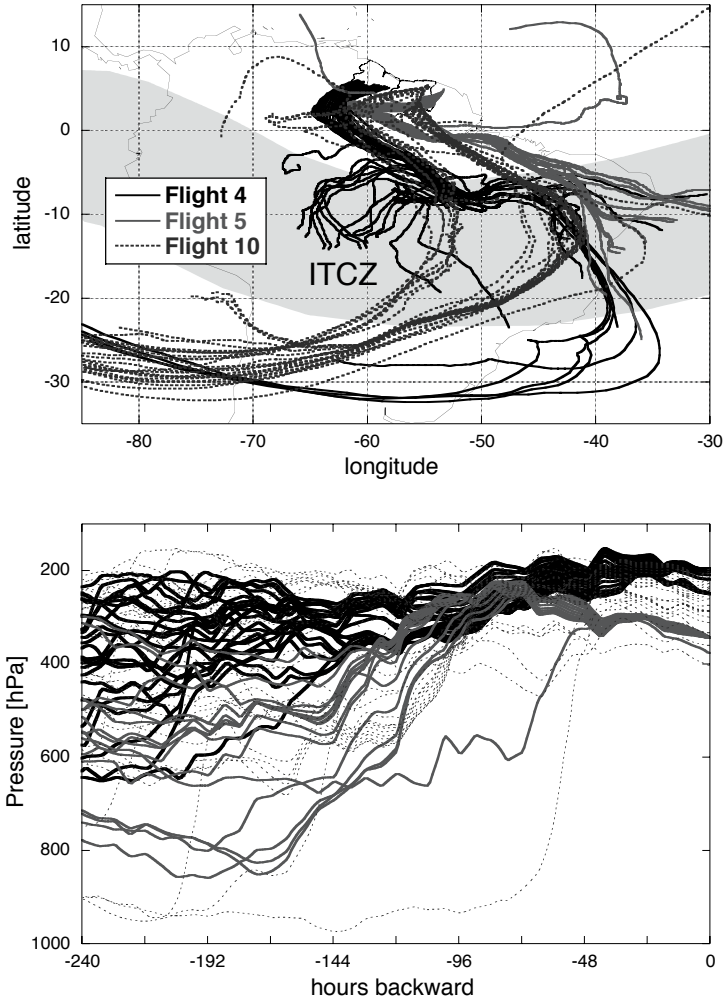

Figure 5.4: Overview of 10-day back-trajectories based on ECMWF wind fields starting in the MT along the flight track of flight 4 (March 19), flight 5 (March 21) and flight 10 (March 29). The top plate (trajectories as a function of latitude and longitude) shows a predominant southwesterly air mass origin. The bottom plate (trajectories as a function of pressure and time) shows several events of fast upward transport associated with the ITCZ.

5.4.2 Accumulation of chlorocarbons in the mixing layer

Yokouchi et al. [2002] showed that tropical plants emit significant amounts of CH_3Cl, while others have reported forest soil emissions of $CHCl_3$ [e.g., *Watling and Harper*, 1998] and possibly that of C_2Cl_4 [*Hoekstra et al.*, 2001]. Here, we investigate the latitudinal gradients of chlorocarbons in the mixing layer over the Surinam tropical rainforest to assess the biogenic sources. To do so, we investigated the relationship between observed chlorocarbons mixing ratios and the time the encountered air masses spend in the mixing layer over the Surinam rainforest while moving into a southeasterly direction, referred to as the Forest Contact Time (FCT). The FCT, defined as the time (in hours) an air parcel spends in the mixing layer starting from the coast the coast (6˚N) towards the Brazilian border (2˚N), was determined as following:

$$FCT = \Delta L / \cos(WA) \times WS / 3600 \quad (5.1)$$

where ΔL is the latitudinal distance from the coast (m); cos(WA) is the cosine of the mean wind angle (WA) taken from the aircraft measurement along the boundary layer flight track; WS is the mean wind speed in the boundary layer from the aircraft measurement (m s^{-1}). The average wind angle and wind speed of all boundary layer flight legs was 45° ± 13°N and 10 ± 3 m s^{-1}.

A significant linear relationship between the trace gas concentrations and the FCT of the encountered air masses can point to biogenic sources. Hence, the slope of a linear regression analysis, $\Delta C/\Delta FCT$, can be used to estimate fluxes. First, however, the mixing layer data set was screened for possible influences of local pollution sources such as biomass burning or of anthropogenic origin. CH_3Cl and to a lesser extend $CHCl_3$ are emitted from biomass burning [*Lobert et al.*, 1999], while CH_2Cl_2 and C_2Cl_4 have urban-industrial sources [*Keene et al.*, 1999]. Therefore, air samples affected by emissions from biomass burning, anthropogenic combustion processes, or urban/industrial activities were excluded since they can contain enhanced chlorocarbon concentrations. We note that apart from some isolated small biomass burning events encountered on March 15 and 26, there were no indications of widespread fire activity in Surinam during course of the campaign [*Williams et al.*, 2001b]. Nevertheless, we decided to reject an air sample when the C_2H_2 and C_6H_6 and/or CH_3CN mixing ratios exceeded twice their “background” value, as detected over the ocean of ~50, ~30 and ~150 pptv and/or CO exceeded 140 ppbv, based on a study by *Williams et al.* [2001b]. In addition, we selected only daytime observations after 10:00 local time to avoid effects from the break-up of the nocturnal boundary layer in the early morning. Emissions from the rainforest (or other ground sources) accumulate in the shallow nocturnal boundary layer [*Zimmerman et al.*, 1988]. During dawn the nocturnal BL breaks up, which can cause a temporarily peak in the concentrations of the accumulated species.

After applying the selection criteria to exclude other potential sources than biogenic, a total of 27 air samples in the mixing layer over the Surinam rainforest remained. The selected air samples were collected between 10:30 and 17:30 local time at altitudes

between 96 and 1070 m. The geographical distribution of the air samples collected in the Surinam mixing layer is depicted in Figure 5.5. It shows that the data represent an area spanning ~500 kilometers of pristine tropical rainforest from the Atlantic coast to the Brazilian border.

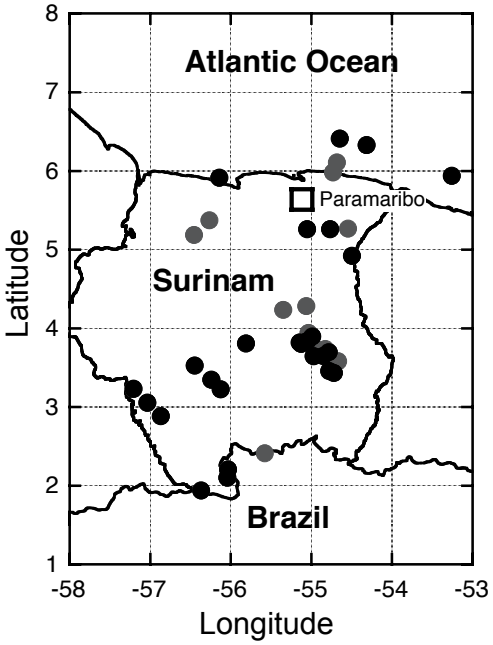

Figure 5.5: Geographical distribution of the air samples (dots) collected in the Surinam boundary layer. The black dots are the samples selected for the flux analysis. The square denotes the location of Paramaribo, the capital of Surinam.

In Figure 5.6 the concentrations of combustion species (Figure 5.6a) and chlorocarbons (Figure 5.6b) from the selected air samples are shown as a function of FCT. The correlation coefficient r (at the 95% confidence level) indicates the significance of the linear relationship. Figure 5.6a shows that the combustion tracers C_2H_2, C_6H_6 and CH_3CN have no significant relationship with the FCT, clearly demonstrating that biomass burning or other non-biogenic sources were negligible. CO, on the other hand, shows a significant positive trend with increasing FCT. An important source of CO over the tropical rainforest, apart from biomass burning, is the oxidation of isoprene and terpenes emitted by vegetation [*Zimmerman et al.*, 1988]. According to *Williams et al.* [2001b] isoprene oxidation resulted in a net increase of 29 pptv CO km^{-1} over the Surinam rainforest during March 1998. Our selection of CO data shows a similar increase of ~23 ± 3 pptv km^{-1}, close to the result of *Williams et al.* [2001b]. Thus, we can attribute the CO increase as a function of FCT to the oxidation of biogenic hydrocarbons, in particular isoprene.

In Figure 5.6b we show that there is a significant linear relation ($r > 0.5$ at the 95% confidence limit) between the atmospheric concentration of CH_3Cl and $CHCl_3$ and the FCT.

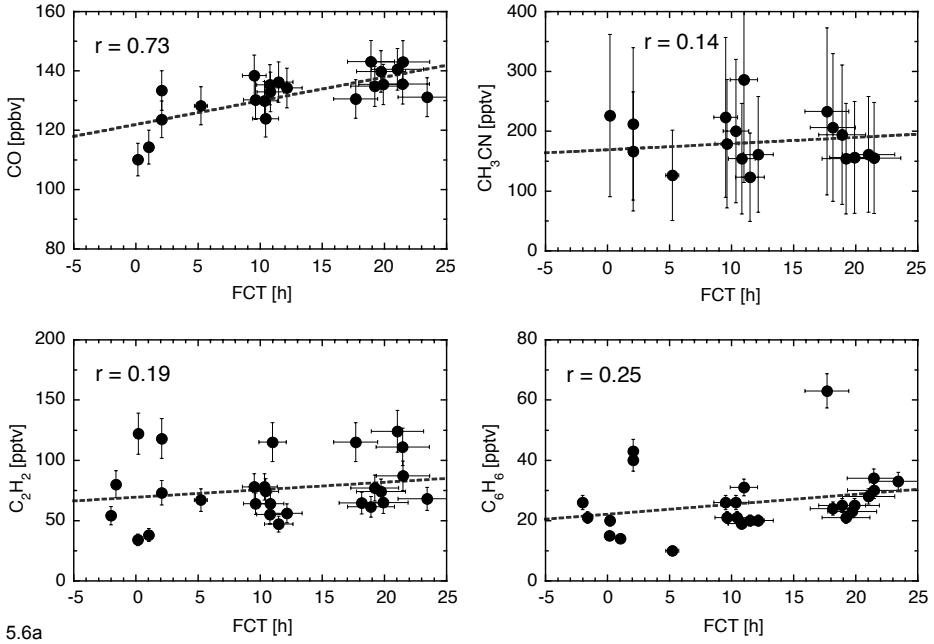

5.6a

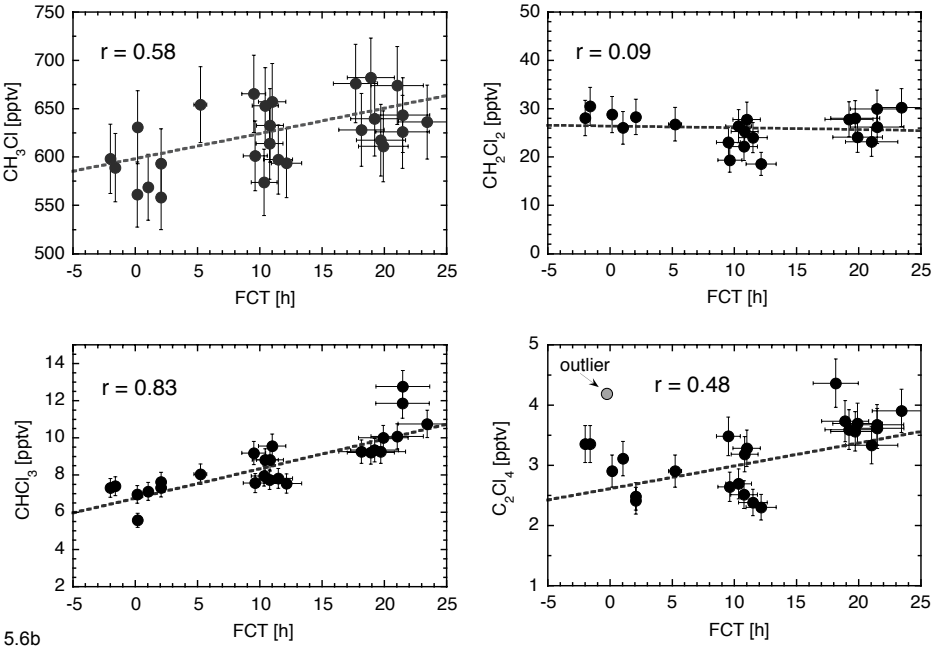

5.6b

Figure 5.6a & 5.6b: The concentration of combustion species (5.6a) and halocarbons (5.6b) as a function of the air mass Forest Contact Time (FCT) in hours (h) in the mixing layer over the Surinam rainforest. Error bars denote the uncertainty.

When we exclude an outlier in the C_2Cl_4 data we find a small but significant increase of C_2Cl_4 over the Surinam rainforest as well. There are no indications of an emission flux of CH_2Cl_2. In the absence of significant biomass burning or urban/industrial sources, we attribute the positive gradients of CH_3Cl, $CHCl_3$, C_2Cl_4 to biogenic emissions from the tropical rainforest ecosystem. Note that we use the term "ecosystem" because it is difficult to differentiate between the various biogenic sources, such as direct emissions from vegetation or microbiological activity in the forest soil. However, based on present knowledge the enhancement of CH_3Cl is most likely related to emissions from tropical vegetation [e.g., *Yokouchi et al.*, 2002], whereas the $CHCl_3$ and C_2Cl_4 emissions are predominantly related to the biological decay of organic material in the forest soil [e.g., *Hoekstra et al.*, 2001].

To determine the slope, $\Delta C/\Delta FCT$, of the relationship between the chlorocarbon mixing ratio and the FCT, a least-squares linear regression analysis was performed allowing precision errors in both the x- and the y-variable (linear fit in Figure 5.6b). The estimated error in the FCT was ~10%, while precision errors of 4% for CH_3Cl, 5% for $CHCl_3$ and 7% for C_2Cl_4 were applied. This linear regression technique, described by *Press et al.* [1992] is referred to as an orthogonal distance regression (ODR) analysis. The results and uncertainties of the ODR analysis are summarized in Table 5.2. The relative uncertainties in the $\Delta C/\Delta FCT$ are 23% for CH_3Cl, 7% for $CHCl_3$ and 16% for C_2Cl_4. In the next section, we use the $\Delta C/\Delta FCT$ values to estimate chlorocarbon fluxes from the tropical rainforest.

Table 5.2: Emission factors of chlorocarbons as a function of the FCT, $\Delta C/\Delta FCT$ in nmol h^{-1}. The number of measurements is denoted by N. The correlation coefficient, r, is given at the 95% confidence limit.

Species	$\Delta C/\Delta FCT$	N	r
CH_3Cl	2.62 ± 0.61	27	0.58
$CHCl_3$	0.161 ± 0.011	26	0.83
C_2Cl_4	0.038 ± 0.006	24	0.48

5.5 Chlorocarbon emission fluxes from the tropical rainforest

5.5.1 Flux calculation method

The flux, F, in g m^{-2} h^{-1} of a chlorocarbon out of the rainforest at the top of the mixing layer was estimated using the linear regression slope, $\Delta C/\Delta FCT$ in nmol h^{-1}, of the chlorocarbons in the following equation:

$$F = \Delta C/\Delta FCT \times L_{ml} \times (p \times M/R \times T) \quad (5.2)$$

where L_{ml} is the mean mixing layer height (m); p is the mean air pressure; M is the molecular weight of the chlorocarbon (g); R = 0.08314 is the gas constant (hPa m^3 K^{-1}); T is the mean air temperature (K) in the mixing layer. This simple flux estimate can be applied assuming a well mixed mixing layer of a constant height, a negligible loss out of the mixing layer over the course of a day, and assuming a homogeneous flux out of the forest canopy.

5.5.2 Fluxes of CH_3Cl, $CHCl_3$, and C_2Cl_4

The evolution of the mixing layer height during a typical day in March 1998 over the Surinam rainforest was shown in Figure 5.1. The data selection used to calculate the $\Delta C/\Delta FCT$ corresponds to a local time between 10:30 – 17:30 hours. Based on typical diurnal mixing layer heights observed over the Amazon rainforest (Figure 5.1), we assume a mean mixing height of ~1.5 (±0.2) km, corresponding to the times of the selected observations. Applying a mean BL-height of 1.5 km, a mean temperature of 298 K, a mean pressure of 950 hPa, and the calculated $\Delta C/\Delta FCT$ values (Table 5.2) in equation (5.2), we derive fluxes in μg m^{-2} h^{-1} of 7.6 ± 1.8 for CH_3Cl, 1.11 ± 0.08 for $CHCl_3$ and of 0.36 ± 0.07 for C_2Cl_4.

The accuracy of the flux estimate is dependent on the uncertainty in the $\Delta C/\Delta FCT$ emission factors, the variability in the mixing layer height, and the assumption of a homogeneous well mixed mixing layer with minimum losses at the top. Errors induced by inhomogeneous conditions in the mixing layer are incorporated in the uncertainty of the calculated $\Delta C/\Delta FCT$ values (Section 5.4.2). The uncertainties in the emission factors and mixing layer height add up to ~35% for CH_3Cl, ~20% for $CHCl_3$, and to ~30% for C_2Cl_4. To get a first indication of possible losses at the top of the mixing layer due to turbulent and convective mixing, we used a single column model version of the ECHAM4 chemistry-climate model [*Ganzeveld et al.*, 2002]. The model was run with meteorological conditions representative for the Surinam dry season and a homogeneous CH_3Cl canopy flux. Running the model without convective mixing (no shallow cumulus layer), it appeared that losses due to turbulent fluxes at the top of the mixing layer are negligible. However, when convective mixing was included in the model, losses at the top of the mixing layer could become as large as 25% in the afternoon. This estimate provides a first indication that losses are likely to be smaller than 25% over the course of a day. Clearly, a more detailed sensitivity analysis, which is beyond the scope of this study, would be necessary to quantify the role of convective mixing more accurately. Hence, compensating for losses at the top of the mixing layer would increase our flux estimates. Thus, our estimates can be considered as lower limits.

The flux estimates are summarized in Table 5.3, and can be compared to flux estimates for forest sites from other studies. We find a remarkably good agreement, in light of the uncertainties, with other flux estimates of CH_3Cl, notably with that of *Yokouchi et al.* [2002] for tropical vegetation. For $CHCl_3$ our estimate lies at the low-end of other flux estimates ranging from 0.1 to 53 μg m^{-2} h^{-1}. Our flux estimate of C_2Cl_4 is, to our knowledge, the first estimate of emissions from tropical vegetation. It is more than an order of magnitude higher than the median value of 0.022 μg m^{-2} h^{-1} observed above Dutch Douglas fir forest soil by *Hoeksta et al.* [2001]. In agreement with our finding, there have been no

reports, to our knowledge, of biogenic land-based emissions of CH_2Cl_2.

Table 5.3: Overview of mean flux estimates in μg m^{-2} h^{-1} for CH_3Cl and $CHCl_3$ from forest sources. Uncertainty (1σ standard deviation) or range is given between parentheses.

Species	Flux	Forest source	Reference
CH_3Cl	3.9 (2.1)	Irish conifer forest soil	*Dimmer et al.* [2001]
	5.4 (3.8–8)	Glasshouse tropical forest	*Yokouchi et al.* [2002]
	7.6 (1.8)	Surinam rainforest	*This work*
	53 (12)	Tropical coastal land (Okinawa island)	*Li et al.* [1999]; *Yokouchi et al.* [2000]
$CHCl_3$	0.033 (0.003–0.2)	Danish spruce forest soil	*Haselmann et al.* [2000a]
	0.11 (0.05–0.12)	Dutch fir forest soil	*Hoekstra et al.* [2001]
	0.34 (0.97–0.77)	Wood chips covered soil	*Hoekstra et al.* [2001]
	1.11 (0.08)	Surinam rainforest	*This work*
	8.6 (8.2)	Irish conifer forest soil	*Dimmer et al.* [2001]
C_2Cl_4	0.022 (0.008–0.04)	Dutch fir forest soil	*Hoekstra et al.* [2001]
	0.36 (0.067)	Surinam rainforest	*This work*

5.5.3 Global chlorocarbon emission fluxes from tropical forest

We applied the chlorocarbon flux estimates for the Surinam rainforest to obtain a global annual emission estimate from tropical rainforest. According to *Yokouchi et al.* [2002], we can assume a constant emission flux of CH_3Cl from tropical vegetation independent of the time of day. This also implies a low seasonal variability when evergreen tropical plants are a major tropospheric source. Indeed, the observed seasonal cycle amplitude decreases with altitude and is less than 5% (of the yearly mean) in the tropical regions for CH_3Cl [*Khalil and Rasmussen*, 1999]. It appears to be largely driven by the variability in the OH radical concentration and the enhanced biomass burning occurring during the dry seasons in the tropics. Therefore, for the estimates of annual emissions from tropical rainforest we assumed a seasonally independent flux.

Another factor of to be considered is the role of soil salinity (or the availability of chlorine to biogenic chlorocarbon metabolism). There are indications that a high soil salinity (Cl^- content) enhances biosynthesis and subsequent emissions of CH_3Cl from fungi and higher plants [*Harper*, 2000]. In addition, model simulations by *Lee-Taylor et al.* [2001] suggest that tropical coastal and near-coast CH_3Cl emissions may be more important than those further inland, dependent on the deposition of sea salt containing aerosol. Although not apparent in our Surinam rainforest gradients, this implies that the estimated fluxes for the

Surinam rainforest may be enhanced relative to fluxes from the rainforest deeper into the Amazon. During the LBA-CLAIRE 1998 campaign, *Formenti et al.* [2002] observed advection of Saharan dust at two sites in Surinam (Zanderij airport, 55.47°N, 55.12°W, and Sipaliwini, 2.12°N – 56.06°W) and a site in Brazil (Albina, 1.55°S, 59.24°W), at more than 800 km inland. They found that the wet and dry deposition of Saharan dust to the rainforest ecosystem is an important source of sea salt elements (Na, Cl, S), beside crustal dust elements (e.g. Al, Si, Ca, Fe). It was shown that maritime air significantly contributed to the concentrations of Cl in aerosol samples collected at Balbina. The results of *Formenti et al.* [2001] corroborate earlier work by *Artaxo et al.* [1995] and *Williams and Fisher* [1997], concluding that the transport of sea salt aerosol, embedded in dust plumes transported at low altitudes, is responsible for excess Cl soil concentrations observed deep into the Amazon basin. Hence, we assume that soil salinity is not a limiting factor for global biogenic chlorocarbon production.

To obtain annual fluxes in Gg yr^{-1} of CH_3Cl, $CHCl_3$ and C_2Cl_4 from tropical rainforests we used the following equation:

$$\text{Annual flux} = \text{Surinam flux} \times \text{Emission period} \times \text{Forest cover area} \quad (5.3)$$

where the “Surinam flux” is the flux estimate obtained for the Surinam rainforest (in $\mu g\ m^{-2}\ h^{-1}$); the “Emission period” is the amount of emission hours per year (365×24 hrs for the evergreen tropical forest); the “Forest cover area” estimates were adopted from the latest FAO Forest Resource Assessment 2000 report [*FAO*, 2001] being 8.158×10^{12} m^2 for the Amazon region, 2.704×10^{12} m^2 of Asian tropical forest and 7.258×10^{12} m^2 for the remaining tropical forest (mainly Africa).

About half of the Asian tropical forest is lowland tropical forest, which is different from Asian highland tropical forest in terms of vegetation composition [*Yokouchi et al.*, 2002]. Asian lowland tropical forest constitutes for about a third of certain types of ferns and tropical plants from the Dipterocarpaceae family, which can emit considerable amounts of CH_3Cl [*Yokouchi et al.*, 2002]. They performed a study on CH_3Cl emissions from a wide range of Asian tropical plants in a glasshouse from which they estimated a CH_3Cl flux from Dipterocarpaceae in southeast Asian lowland tropical forest of 0.91 Tg yr^{-1} based on 1997 FAO forest cover estimates. Using the latest FAO 2000 tropical forest cover estimates [*FAO*, 2001], this flux estimate becomes 0.88 Tg yr^{-1}. When we apply the Surinam emission factor to estimate a yearly flux of CH_3Cl from the remaining fraction of Asian (highland) tropical forest this yields an additional flux 0.09 Tg yr^{-1}.

Summing up, we find a total global emission of 2 Tg CH_3Cl per year from (sub)tropical vegetation, which is more than sufficient (within the uncertainty of the estimates) to account for the total of missing sources and to close the global tropospheric budget. Our estimates are in good agreement with the model study by *Lee-Taylor et al.* [2001], who found that observed mixing ratios are best reproduced by addition of a large tropical terrestrial source of ~2.3 Tg, which includes 0.18 Gg yr^{-1} redistributed from Asian biomass burning emissions. Interestingly, the latter is in conflict with new estimates of biomass burning emissions of CH_3Cl from the use of biofuels in Southeast Asia by *Scheeren et al.* [2002]. They find that CH_3Cl emissions from the use of biofuels could be underestimated by 30 – 35% (~0.28 Gg yr^{-1}) for India and Southeast Asia based on measurements performed over the Indian Ocean during the INDOEX 1999 experiment. These conflicting estimates illustrate the level

of uncertainty still present in quantifying the major CH_3Cl sources.

Our estimates of annual fluxes of $CHCl_3$ from global tropical forest of 175 ± 35 Gg yr^{-1} (based on the Surinam emission flux) and a flux from temperate forest of ~5 Gg yr^{-1} (based on a forest soil flux of 0.033 μg m^{-2} h^{-1} from *Haselmann et al.* [2000a] and temperate forest cover of 1.881×10^{13} m^2 from *FAO* [2001]) combine to 180±35 Gg yr^{-1}. This number compares well to the ~200 Gg yr^{-1} from (forest) soil emissions estimated by *Khalil et al.* [1999], which are mainly concentrated in the tropics. Extrapolating the Surinam rainforest C_2Cl_4 flux onto a global scale, we can estimate a total flux from tropical forests of 57 ± 17 Gg yr^{-1}. This flux could account for almost half of the amount of missing C_2Cl_4 sources (~128 Gg yr^{-1}) in the global budget by *Keene et al.* [1999].

5.5.4 Global emission budgets of CH_3Cl, $CHCl_3$, and C_2Cl_4

In Table 5.4 we summarize our flux estimates for tropical rainforests and include emission flux estimates from the literature of the oceans, biomass burning, industrial sources and other newly identified biogenic sources. As such, an overview is given of the global annual source budgets of CH_3Cl, $CHCl_3$, and C_2Cl_4 in Tg yr^{-1}. *Wiedman et al.* [1994] was able to model the global distribution of C_2Cl_4 consistently without biogenic input. However, the uncertainty in the global budget remains to be large [*Keene et al.*, 1999] and allows for the inclusion of newly identified natural sources. In addition to Table 5.4, the composition of global source budgets of CH_3Cl, $CHCl_3$, and C_2Cl_4 is illustrated in pie-plots in Figure 5.7. CH_2Cl_2 is not included here because it has no terrestrial biogenic sources. Note that an annual emission flux of 128 Gg CH_3Cl yr^{-1} from fungal (soil) activity [*Lee-Taylor et al.*, 2001] has not been included, because we consider this to be incorporated in the fluxes from tropical forest ecosystems. We adopted annual global net flux estimates from the oceans of 477 Gg CH_3Cl yr^{-1} from *Lee-Taylor et al.* [2001], and 359 Gg $CHCl_3$ yr^{-1} and 19 Gg C_2Cl_4 yr^{-1} from *Khalil et al.* [1999]. A small flux of 3.6 Gg C_2Cl_4 yr^{-1} and 5.4 Gg $CHCl_3$ yr^{-1} was estimated for the global temperate forest [*FAO*, 2001] using the mean C_2Cl_4 forest soil flux measured by *Hoekstra et al.* [2001] and the mean $CHCl_3$ forest soil flux from *Haselmann et al.* [2000a], respectively.

Recently identified biogenic global source fluxes, included in Table 5.4, are 170 (65 – 440) Gg CH_3Cl yr^{-1} from coastal salt marshes [*Rhew et al.*, 2000], 24 Gg $CHCl_3$ yr^{-1} and 35 Gg CH_3Cl yr^{-1} from peat land and freshwater wetland ecosystems [*Dimmer et al.*, 2001], a global conifer forest floor source of 85 (39 – 131) Gg CH_3Cl yr^{-1}, and a global flux of 5.8 Gg CH_3Cl yr^{-1} from rice paddies. We assumed global biomass burning emissions of 909 Gg CH_3Cl yr^{-1} and 2 Gg $CHCl_3$ yr^{-1} according to *Lobert et al.* [1999], and an additional biomass burning source of 118 Gg CH_3Cl yr^{-1} from Asian biofuel use from *Scheeren et al.* [2002]. Global annual emissions of ~10 Gg CH_3Cl, 62 ± 25 Gg $CHCl_3$, and 366 ± 20 Gg C_2Cl_4 from industrial activities, 107 ± 10 Gg CH_3Cl and ~1.9 Gg C_2Cl_4 from fossil fuel combustion, and 45 ± 33 Gg CH_3Cl from waste incineration for the year 1990 were taken from *McCulloch et al.* [1999a,b] and *Aucott et al.* [1999]. We note that these emissions were estimated for the year 1990. *McCulloch et al.* [1999b] showed that the production and emission of industrial chlorocarbons is directly proportional to the economic activity. Industrial emissions for the

year 2000, although not yet available, are probably somewhat higher than in 1990 due to the increased world economy over that decade.

We find a total annual CH_3Cl source flux of about 4 Tg, which is in excellent agreement with the annual global sink of 3.97 Tg by *Keene et al.* [1999]. The annual source fluxes of 0.64 Tg $CHCl_3$ and 0.45 Tg C_2Cl_4 agree reasonably well (within the uncertainty) with their estimated annual global total sinks of 0.46 Tg and 0.51 Tg from *Keene et al.* [1999]. The overestimation of the global annual source of 0.17 Tg $CHCl_3$ (+29%) is most likely mainly due to the highly uncertain ocean source estimate from *Khalil et al.* [1999]. Although the missing source of 0.13 Tg C_2Cl_4 yr^{-1}, reported by *Keene et al.* [1999], can be reduced by half by our flux estimate from global forests, the budget of C_2Cl_4 remains to be unbalanced by -60 Gg.

Table 5.4: Global source and sink budgets of CH_3Cl, $CHCl_3$, and C_2Cl_4 in the troposphere in Tg yr^{-1}.

Sources	CH_3Cl	$CHCl_3$	C_2Cl_4	Reference
Amazon forest	0.544	0.079	0.026	*This work*
Asian lowland forest	0.882			*Yokouchi et al.* [2002]
		0.013	0.004	*This work*
High Asian tropical forest	0.090	0.013	0.004	*This work*
Other tropical forest	0.484	0.070	0.023	*This work*
Temperate forest soil		0.0054		after *Haselmann et al.* [2000a]
			0.0036	after *Hoekstra et al.* [2001]
Conifer forest soil	0.085			*Dimmer et al.* [2001]
Oceans	0.477			*Lee-Taylor et al.* [2001]
		0.36	0.019	*Khalil et al.* [1999]
Coastal salt marches	0.17			*Rhew et al.* [2000]
Wetlands (incl. Peatbog)	0.035	0.024		*Dimmer et al.* [2001]
Rice paddies	0.006			*Redeker et al.* [2000]
Biomass burning	0.909	0.002		*Lobert et al.* [1999]
Asian biofuel emissions	0.118			after *Scheeren et al.* [2002]
Industry	0.010	0.069	0.366	*McCulloch et al.* [1999]
Waste incineration	0.045			*McCulloch et al.* [1999]
Fossil fuel combustion	0.107		0.0019	*McCulloch et al.* [1999]
All sources	3.96	0.63	0.45	
All sinks	3.97	0.46	0.51	*Keene et al.* [1999]
Sources - Sinks	-0.01	0.17	-0.06	

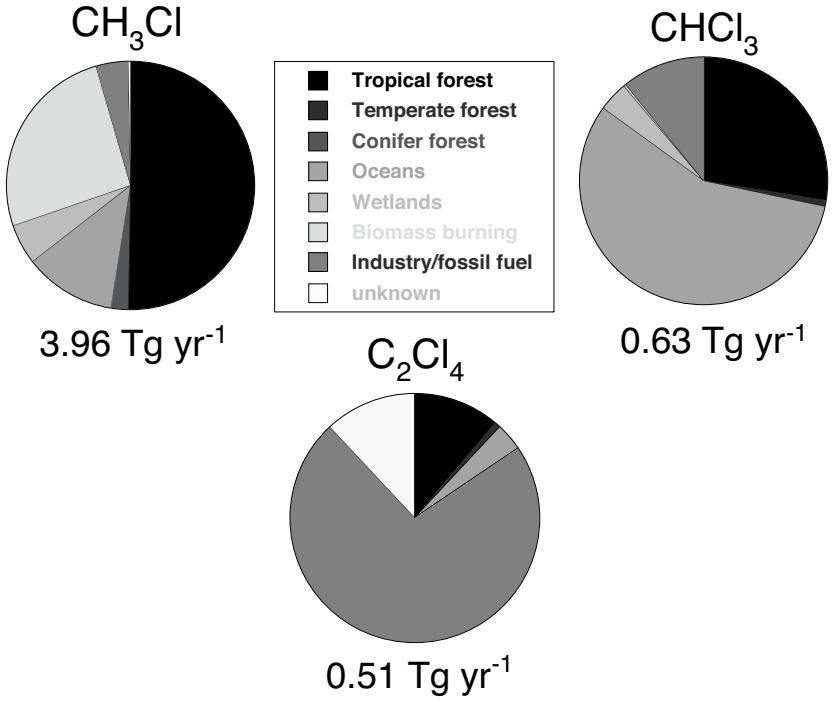

Figure 5.7: Pie plots showing the composition of global source budgets of CH_3Cl, $CHCl_3$ and C_2Cl_4, according to present knowledge.

5.6 Decreasing trends in atmospheric CH_3Cl

In the literature, there exist two long-term CH_3Cl datasets from polar firn samples [*Butler et al.*, 1999; *Kaspers et al.*, 2003] and one from atmospheric measurements [*Khalil and Rasmussen*, 1999]. *Khalil and Rasmussen* [1999] present a record of CH_3Cl measurements from 1981 to 1997 from various background sites around the world. A compilation of these measurements suggests a weak decreasing trend of methyl chloride of the order of a few pptv per year over the last two decades. A similar trend was deduced from recent firn air analyses by *Kaspers et al.* [2003], who found a decrease of 1.2 ± 0.6 pptv CH_3Cl per year (-0.2 ± 0.1% per year) between 1980 and 2000. In contrast, the measurements from *Butler et al.* [1999] suggest an increase of 5-10% in atmospheric CH_3Cl over the past century. Although we cannot explain this inconsistency, the majority of evidence suggests that CH_3Cl decreased over the last 20 years. *Khalil and Rasmussen* [1999] explained the global trend from a possible decrease of the OH-radical over the last 20 years reported by *Krol et al.* [1998] and later by *Prinn et al.* [2001]. Recent work by *Krol et al.* [2003] has indicated however, that the previously reported negative OH trend in the 1990s seems to be unlikely and appears to be related to underestimated sources of methyl chloroform

(1,1,1-trichloroethane) in global models. Methyl chloroform is used in global models to estimate the OH-radical budget since it has only anthropogenic sources and its main removal is by reaction with OH. Hence, in the absence of an OH trend, it appears that one or more sources of CH_3Cl have become smaller over the last two decades.

The main CH_3Cl sources are biomass burning, the oceans and tropical vegetation (see previous section). In a recent study on interannual and seasonal variability of biomass burning by *Duncan et al.* [2003], no apparent trend in biomass burning emissions over the last two decades was reported. When we perform a linear regression analysis on the global CO biomass burning emissions of CO (in Tg C yr^{-1}) as a function of time (in years), we can deduce a weak positive trend of the order of 0.6% per year (r = 0.55 at the 95% confidence limit) between 1980 and 1997. Clearly, a biomass burning emission trend, if any, is most likely not related to a decrease in CH_3Cl. In addition, there are no studies, to our knowledge, indicative of any long-term trend in oceanic emissions. There is, however, significant evidence that the oceans have warmed up over the last 40 years due to the increase of greenhouse gases in the atmosphere [*Barnett et al.*, 2001; *Levitus et al.*, 2001]. This suggests that the release of CH_3Cl from the oceans could have increased over that period. Although significant for the earth climate system, the global mean sea-surface temperature rise was less than 1 °C over the last century [*Levitus et al.*, 2001]. Therefore, we consider the temperature effect on oceanic CH_3Cl emissions over the last 20 years to be negligible.

Based on this and other work [*Lee-Taylor et al.*, 2001; *Yokouchi et al.*, 2002] we find that the largest source of CH_3Cl is emissions from tropical vegetation. The latest estimates of global forest area cover by the FAO [*FAO*, 2001] show that the amount of tropical forest has decreased from 210.4×10^7 ha in 1980 to 179.1×10^7 ha in the year 2000 (corrected for replanted forest area), which equals a decrease of -0.74% per year. The trends of CH_3Cl, biomass burning and tropical forest cover are presented in Figure 5.8. The extrapolated CH_3Cl trend between 1980 and the year 2000 is –1.4 pptv yr^{-1} or –0.2% yr^{-1} (r = 0.67). Hence, we propose that the strong decrease of tropical forest cover from anthropogenic activities over the last two decades could explain the observed weak decrease in global mean methyl chloride.

In order to test the relationship between CH_3Cl and tropical forest cover more quantitatively, we assume that the yearly global mean atmospheric CH_3Cl concentration $[CH_3Cl]_t$ (of the year t) is composed of the relative fractions (in pptv) of the major sources:

$$[CH_3Cl]_{t0} = ((1\text{-}n_a\,\Delta t)\,(S_a / \Sigma S) + 1\text{-}n_b\,\Delta t\,(S_b / \Sigma S) + ...) \times [CH_3Cl]_{t1} \qquad (5.4)$$

where $(1\text{-}n_a\Delta t)$ is the relative annual trend "n" of source "a" over a period Δt denoting the number of years between the year t_0 (1980) and t_1 (2000); $(S_a / \Sigma S)$ is the fraction of source "a" relative to the sum of all sources ΣS.

We assume that global emissions from oceans, wetlands as well as the relatively small contribution from industrial emissions of CH_3Cl remained constant over the last two decades. For the reference year 2000 we can calculate a $[CH_3Cl]_{2000}$ of 581 ± 8 pptv based on the trend shown in Figure 7. Applying a linear trend back in time of –0.6% per yr for the biomass burning fraction and of +0.74% per yr for the fraction of tropical forests, we can then calculate a $[CH_3Cl]_{1980}$ of 606 pptv (Table 5.5). This value compares very well with the $[CH_3Cl]_{1980}$ of 608 ± 7 pptv based on the observed trend and shows more quantitatively that the clearing of tropical forest can explain the observed decrease of the global mean CH_3Cl

concentration. Clearly, our hypothesis implies that the atmospheric CH_3Cl concentration could have varied strongly in the geological past as a function of climate variability and global forest cover.

Table 5.5: Contribution of different source fractions in pptv, f(source), to the global mean CH_3Cl concentration in the year 2000 (reference) and the year 1980.

Year	f(forests)	f(biomass burning)	f(oceans&others)	[CH_3Cl]
2000	293	151	137	581
1980	336	133	137	606

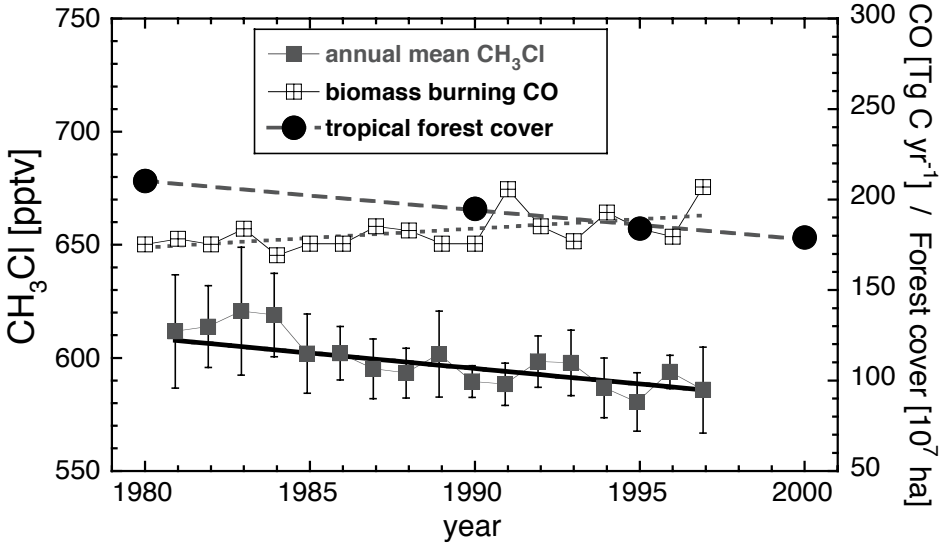

Figure 5.8: Global trends of atmospheric CH_3Cl, tropical rainforest area cover, and biomass burning emissions between the year 1980 and 2000. The error bar in CH_3Cl denotes the 1σ standard deviation of the mean.

5.7 Summary and conclusions

We have presented measurements of reactive chlorocarbons CH_3Cl, CH_2Cl_2, $CHCl_3$ and C_2Cl_4 in the boundary layer and free troposphere over Surinam during March 1998. The horizontal and vertical distributions have been analyzed with the help of concurrent

measurements of CO, CH_3CN, and non-methane hydrocarbons, as well as with 10-day back-trajectories. The vertical profiles show enhanced concentrations in the boundary layer and in the free troposphere (between 8 – 12 km). We find that the free troposphere at 8 – 12 km altitude was strongly affected by deep convective outflow associated with the ITCZ, which was located a few degrees south of Surinam. Polluted air masses containing enhanced chlorocarbons appear to originate over the populated northwestern part of Brazil. High CH_3Cl concentrations correlating with relatively low CO, CH_3CN and C_2 – C_6 NMHCs seem to come from the Central Amazonia pointing to biogenic sources.

We found a significant positive gradient of the CH_3Cl, $CHCl_3$ and C_2Cl_4 concentration in the mixing layer between the Surinam coast and the Brazilian border at 6°S. No correlation of CH_2Cl_2 with latitude was found. These gradients point to significant biogenic sources and corroborate the findings of *Yokouchi et al.* [2002]. The change of chlorocarbon concentration as a function of air mass residence time over the rainforest was used to calculate an emission factor in pptv h^{-1}. For this we used a selection of the data, representing air masses not affected by local biomass burning emissions or urban/industrial pollution. With these emission factors we could calculate fluxes of 7.6 ± 2.7 μg CH_3Cl m^{-2} h^{-1}, 1.11 ± 0.22 μg $CHCl_3$ m^{-2} h^{-1}, and 0.36 ± 0.067 μg C_2Cl_4 m^{-2} h^{-1}, representative for the Surinam tropical rainforest ecosystem. Hence, these fluxes encompass emissions from microbiological soil processes, fungal decomposition of wood, as well as direct emission from plants. Extrapolating these fluxes onto a continental scale and using the FAO 2000 tropical forest cover estimates [*FAO*, 2001], we can estimate annual emission fluxes from the Amazon tropical rainforest of 0.544 Tg CH_3Cl yr^{-1}, 0.079 Tg $CHCl_3$ yr^{-1}, and 0.026 Tg C_2Cl_4 yr^{-1}. The total emission flux estimates from tropical rainforests in South-America, Asia and Africa applying the Surinam flux value and the flux value from *Yokouchi et al.* [2002] for Asian highland tropical forest add up to 2 Tg CH_3Cl yr^{-1}. This value compares well with the model estimate of 2.3 Tg yr^{-1} by *Lee-Taylor et al.* [2001] and can account for the remaining missing sources in the CH_3Cl budget. Our estimate of an annual flux of ~57 Gg C_2Cl_4 yr^{-1} from global forest ecosystems can account for half of the previously missing sources in the budget by *Keene et al.* [1999].

The important role of tropical vegetation in the global budget of CH_3Cl indicates that changes in tropical forest cover could affect the atmospheric concentration. Indeed, we show that there are strong indications that the reduction of tropical forest area over the past 20 years can largely explain the downward trend in atmospheric CH_3Cl observed by *Khalil and Rasmussen* [1999] and *Kaspers et al.* [2003].

Acknowledgements

We gratefully acknowledge the excellent cooperation with the whole Citation team and the staff of the Surinam Meteorological Service. We thank Peter van Velthoven from the KNMI for providing the 10-day back-trajectories. We are grateful to Laurens Ganzeveld of the MPI for Chemistry (Mainz, Germany) for model simulations with the single column model version of ECHAM4.

6 General conclusions and future perspectives

The general aim of this thesis was to improve our understanding of the sources, distributions and chemical role of reactive NMHC and chlorocarbons in the troposphere and lower stratosphere. In Chapters 2 – 4 we have presented and analyzed a unique data set of selected C_2 – C_7 NMHC and chlorocarbons derived from six aircraft measurement campaigns conducted between 1995 and 2001. The measurement locations include tropical, midlatitude and polar regions between the equator to about 70ºN, covering different seasons and pollution levels in the troposphere and lower stratosphere. The reactive NMHC and chlorocarbon data have been analyzed along with a wide range concurrent measurements, which includes O_3, CO, NO, NO_y, CO_2, CH_4, acetone, methanol, acetonitrile, HCF-134a, HCFC-141b, and HCFC-142b and long-lived tracers N_2O, CFC-11, CFC-12. These additional measurements have provided important additional information about the air mass origin, pollution sources, and chemical age of the encountered air.

Here, we highlight the most important conclusions and new insights from the Chapters 2 – 4. We do this on the basis of the scientific objectives defined in Chapter 1.

Availability of hydrocarbon measurements in the UT and LS

This thesis presents a large and unique data set of high quality NMHC and chlorocarbon measurements. Thus, this work augments the sparse availability of NMHC and chlorocarbons measurements in the free troposphere and lower stratosphere, in particular in the tropics. The data are available to the Atmospheric Chemistry and Physics research community through the work presented in this thesis and on CD-rom (on request).

Seasonality of NMHC and acetone levels the lowermost stratosphere

In **Chapter 2**, data of selected C_2 – C_6 NMHC and acetone are presented, which were collected during November/December 1995 (late fall), March 1997 (late winter) and July 1998 (summer) as part of STREAM in the extratropical upper troposphere and lowermost stratosphere. We found a strong seasonal variability in the abundance of reactive organic species in the extratropical lowermost stratosphere. Concentrations of NMHC and acetone were enhanced up to potential temperatures of 370 K during summer, while during winter, enhanced concentrations extended up to the 340 K isentrope. These findings are in agreement with seasonal variations in mixing layer depth determined by *Hoor et al.* [2002], based on correlations between CO and O_3. Model results [*Chen*, 1995; *Dethof et al.*, 2000], show enhanced isentropic transport above the ~340 K isentrope during summer relative to winter, which is driven by the Asian and Mexican monsoon circulations. Indeed, we found increasing methyl chloride concentrations at higher isentropic levels (360 – 370 K) in the lowermost stratosphere during summer, which pointed to a recent (sub-)tropical origin.

The observed NMHC + acetone concentrations in the mixing layer equaled during summer and fall (2.3 ± 1.7 ppbC and 2.2 ± 0.5 ppbC, respectively) and were more than a factor of two higher than during winter (0.9 ± 0.3 ppbC). A surprisingly good agreement was found between mean results of STREAM (March 1997 and July 1998) and the February/March 1994 PEM West B campaign and the October/November 1997 SONEX campaign, in spite of the differences in location and time.

The NMHC and acetone measurements from STREAM contribute to our understanding of the ozone chemistry and the dynamics of the lowermost stratosphere and provide input for numerical models. Moreover, this work gives new insight in the seasonality of isentropic cross-tropopause exchange, associated with frontal dynamics at the polar and sub-tropical jet streams.

Role of summertime acetone levels on OH in the lowermost stratosphere

In **Chapter 2,** we show that the amount of acetone equaled the sum of NMHC (in ppbC) making it the dominant reactive organic tracer species in the lowermost stratosphere after ethane. The relatively large acetone concentrations (around 1 ppbv) in the lowermost stratosphere, especially during summer, are the result of enhanced isentropic transport at the sub-tropical tropopause. They emphasize the dominance of terrestrial vegetation and of oceanic sources in the upper tropospheric acetone budget as suggested by *Jacob et al.* [2002]. Acetone photolysis can be an important source of HO_x radicals in the upper troposphere and lower stratosphere. We used a photo-chemical box model to indicate that the observed acetone levels of 0.5 to 1 ppbv can explain 30 to 50% of the enhanced OH concentrations in the extratropical summertime lowermost stratosphere up to at least θ = 360 K.

Troposphere-to-stratosphere mixing timescales

In **Chapter 2,** we present and demonstrate a simple method based on a modified mass balance calculation, to estimate the photochemical age of a tropospheric air parcel in the stratospheric mixing layer. This gives us an indication of timescales of (isentropic) troposphere-to-stratosphere mixing, indicating the transit time between the mixing event and the encounter with the measurement aircraft. The method uses the decay of the reactive organic species acetylene and propane in the mixing layer, with photochemical lifetimes of a few weeks during summer. The concentration of these species in the lowermost stratosphere is determined by the upper tropospheric “source-concentration”, the mixing intensity, and the photochemical lifetime of these species in the stratosphere. From a number of troposphere-to-stratosphere mixing events, with acetylene and propane concentrations of 25 – 80 pptv (well above their detection limit), we calculated mixing timescales of 3 to 14 days. These results corroborate the studies of *Dethof et al.* [2000] and *Hoor et al.* [2002], demonstrating that the summertime midlatitude lowermost stratosphere is subject to intense and frequent mixing with tropospheric air.

The role of Asian biomass burning in global budgets of reactive chlorocarbons

In **Chapter 3,** we focus on pollution outflow from Southeast Asia observed over the Indian Ocean during the 1999 INDOEX campaign. We present observations of strongly enhanced CH_3Cl and related combustion tracers (CO, hydrocarbons and CH_3CN), which we relate to extensive biofuel use, notably the burning of agricultural waste and dung in India and Southeast Asia. We deduced a relatively high emission ratio relative to CO of $1.74 \pm 0.21 \times 10^{-3}$ mol mol^{-1}, compared to a mean value of 0.57×10^{-3} mol mol^{-1} used for biofuel emissions in a recent comprehensive global emission inventory by *Lobert et al.* [1999]. Hence, we point out that the contribution to CH_3Cl emissions from the use of biofuels might previously have been underestimated by 30-35% for India and Southeast Asia. According to *Keene et al.* [1999], the combined emissions of CH_3Cl from the reasonably well quantified sources (oceans and biomass burning), account only for half the modeled sinks (~ 4×10^{12} g yr^{-1}). The other half remains to be accurately identified (further discussed in Chapter 5). The possible underestimation of biomass burning emissions cannot account for the "missing" source. By extrapolating the INDOEX $\Delta CH_3Cl/\Delta CO$ emission ratio to a global scale, we can justify about 14% of the missing CH_3Cl source.

In accord with earlier findings by *Rudolph et al.* [1995], we infer small biomass burning sources for CH_2Cl_2 and $CHCl_3$ as well. Indications for biomass burning emissions of methyl chloroform (CH_3CCl_3), as proposed by *Rudolph et al.* [1995], were however not found. The results in Chapter 3 improve our insight in the important role of tropical biomass burning emissions in global budgets of reactive chlorocarbons. In **Chapter 5**, we investigate tropical biogenic emissions, which can account for a major fraction of the missing CH_3Cl source.

The role of tropical biogenic emissions in global budgets of reactive chlorocarbons

The role of tropical emissions on the global budgets of the reactive chlorocarbons CH_3Cl, CH_2Cl_2, $CHCl_3$, and C_2Cl_4 is further explored in **Chapter 5**. Here, we present measurements of NMHC and chlorocarbons in the boundary layer and free troposphere over Surinam during March 1998. We find that the free troposphere above 8 km altitude was strongly affected by deep convective outflow associated with the ITCZ, located a few degrees south of Surinam. We found a significant positive gradient of the CH_3Cl, $CHCl_3$, and C_2Cl_4 concentration in the mixing layer between the Surinam coast and the Brazilian border at 6°S, in the absence of significant pollution sources. These gradients point to significant biogenic sources and corroborate the findings of *Yokouchi et al.* [2002] on CH_3Cl emissions from tropical vegetation. No correlation of CH_2Cl_2 with latitude was found.

The change of chlorocarbon concentration as a function of air mass residence time over the rainforest was used to calculate an emission factor in pptv h^{-1}, representative for the Surinam tropical rainforest ecosystem (sum of emissions from microbiological soil processes, fungal decomposition of wood, as well as direct emission from plants). Extrapolated to a global scale, our emission estimates suggest a large potential source of ~2×10^{12} g CH_3Cl yr^{-1} from tropical forests, which could account for the net budget discrepancy (underestimation of sources). In addition, we estimated a potential emission of ~57×10^9 g

C_2Cl_4 yr^{-1} from tropical forest soils, which equals half of the currently missing C_2Cl_4 sources.

Finally, we show that there are strong indications that the reduction of tropical forest area over the past 20 years could largely explain the downward trend in atmospheric CH_3Cl observed by *Khalil and Rasmussen* [1999] and *Kaspers et al.* [2003].

The impact of Asian pollution on tropospheric chemistry on a hemispheric scale

In **Chapter 4,** we present observations of trace species during MINOS in August 2001, which show that the Asian plume has a large impact on the chemical composition of the upper troposphere over the eastern Mediterranean. Deep convection associated with the ITCZ (Asian summer monsoon) followed by long-range transport carries Asian pollution towards the eastern Mediterranean and northern Africa. As a result, enhanced levels of CO, and hydrocarbons were found to be comparable to or higher than those found in westerly air masses, containing pollution from the North American continent. In agreement with observations from the 1999 INDOEX campaign, we found that the Asian plume shows a clear signature of biomass burning (notably from the use of biofuels) by enhanced concentrations of CO, C_2H_2, C_6H_6, acetonitrile, and the chlorocarbons CH_3Cl and $CHCl_3$. Acetone levels in the Asian plume were of the same magnitude as those observed in the westerlies, exceeding upper tropospheric background levels. Methanol levels were higher in the Asian plume, which we related to Asian biofuel burning emissions. The mean photochemical age of the Asian pollution was estimated to be about 2 weeks, consistent with trajectory analysis.

We show that the new automobile air conditioning agent HFC-134a can serve as a tracer for western pollution. From this, we conclude that the correlation between relatively high CO_2 and HFC-134a concentrations in the westerlies, relates to extensive fossil fuel use in North America.

In spite of high pollution levels in the Asian plume, we observed that ozone concentrations are still relatively low (~55 ppbv). They show no clear relationship with higher hydrocarbons, which suggests a NO_x-limited photochemical ozone production regime. This might change in the future. We investigated chemical impact from the projected increase of Asian NMHC, CO and NO_x emissions in the next 25 years, due to the expected strong increase of fossil fuel use (replacing biofuels), with a tropospheric chemistry-climate model. The model simulations we carried out indicate that the expected increase of Asian emissions in the next few decades may enhance photochemically produced ozone in the Asian plume by about 14%. Considering the size of the Asian plume, this may have a significant impact on the ozone contribution to radiative forcing in the Northern Hemisphere.

We point out that the size and location of the Asian plume near the tropopause provides an important potential for pollution transport into the lowermost stratosphere (as described in Chapter 2). We present observations which provide first indications of Asian pollution transport into the lower stratosphere. Clearly, we need more research to investigate this further.

The main achievements of this work can be summarized as following:

- We have presented a unique and comprehensive data set of NMHC and chlorocarbon

trace gases.
- We improved our understanding of the role reactive NMHC and acetone in the lower stratosphere, notably on the OH budget.
- We provided new insight in the mixing timescales of isentropic mixing.
- The understanding of the role of tropical sources in the global budget of reactive chlorocarbons has been greatly improved.
- The important impact of Asian pollution redistributed by the ITCZ on a hemispheric scale is described and analyzed.

Recommendations for future research

Based on the work presented in this thesis we give some recommendations for future research.

In Chapter 2 we present a simple method to use NMHC mixing ratios to estimate mixing timescales of isentropic troposphere to stratosphere transport. Obviously, our analysis of mixing timescales during the 1998 summer is hampered by the low number of encountered mixing events, which is due to the limited canister sample frequency. By increasing the number of NMHC measurements in future campaigns, a better representation of the background reservoir conditions could be achieved. At the same time, a larger number of TSE-events will be encountered allowing a more quantitative analysis.

To improve our knowledge on the role of biomass burning as a source of reactive chlorocarbons, future work could focus on to improve estimates of the chlorine content of biofuels, for example in laboratory studies, and to investigate the release of chlorocarbons as a function of burning efficiency.

With respect to the MINOS measurements presented in Chapter 4, future research should focus of the role of Asian pollution transport to the lower stratosphere associated with the monsoon circulation. Our measurements provide only a first, but important indication of the potential role of this mechanism in stratosphere troposphere exchange.

The LBA/CLAIRE measurements have proven that Surinam is an excellent location to study trace gas exchange of between pristine tropical rainforest and the atmosphere, free of significant anthropogenic influence. Our flux estimates suffer, nevertheless, from considerable uncertainties related to limitations in time and space. Hence, more organic trace gas flux measurements over the Surinam tropical rainforest, on a regular basis, would greatly improve our knowledge on, notably, seasonal variations and would provide valuable input for chemistry-transport models. In addition, a next step in the analysis of biogenic fluxes from the Surinam rainforest would be the use of a dedicated chemical-transport model, which includes a more realistic representation of the boundary layer meteorology. A first step in this direction, applying a single column model version of the ECHAM4 chemistry and climate model, looks promising.

We have shown the important role of tropical vegetation in the global budget of CH_3Cl and indicated that changes in tropical forest cover could affect the atmospheric concentration. Hence, it would be interesting to do a model study on the role of possibly high atmospheric CH_3Cl concentrations in the past from higher tropical biogenic emissions.

Appendix: Air sampling and analysis system

Air sampling method

Air samples have been collected with an automated airborne canister air sampling system developed and build at Wageningen and Utrecht University by Ing. M. Bolder. The latest version can contain 12 stainless steel canisters of 2.4 L. The canisters have been manufactured by and purchased from the Max-Planck-Institute for Chemistry in Mainz. The sampling system uses 1/4" and 1/2" stainless steel tubing and connectors (*Swagelok*). The in- and outlets of the canisters and tubing are regulated by computer controlled stainless steel pneumatic valves (*Swagelok Nupro SS4H*). A 0.5 L pressurized cylinder with synthetic air is carried along to establish the pressure for the pneumatic valves. The pictures below (Figure A1, A2) show the demountable section of the sampling system, which can contain up to 12 canisters.

Figure A1: Demountable canister unit, suitable for twelve 2.4 L canisters

Figure A2: Detail of the tubing and *Swagelok* couplings.

A manually controlled switch starts the sequence for the collection of an air sample. A *MB-602* stainless steel bellows pump (Figure A3) is employed to subsequently evacuate and flush canister and tubing for 4 minutes prior to the collection of an air sample to a preset overpressure of typically 2 - 3 bar. Depending on atmospheric pressure, filling takes ~10 s at 0 - 1 km altitude and up to 240 seconds at ~12 km to obtain a sufficient amount of air. After the flight, the canisters are replaced and send back to the laboratory for analysis.

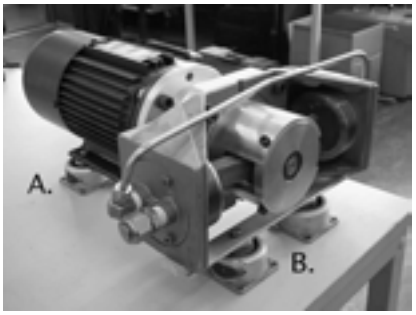

Figure A3: Metal bellows pump (A: pump; B: pump head with bellows).

In the following scheme the flushing, evacuation and filling of a canister is shown:

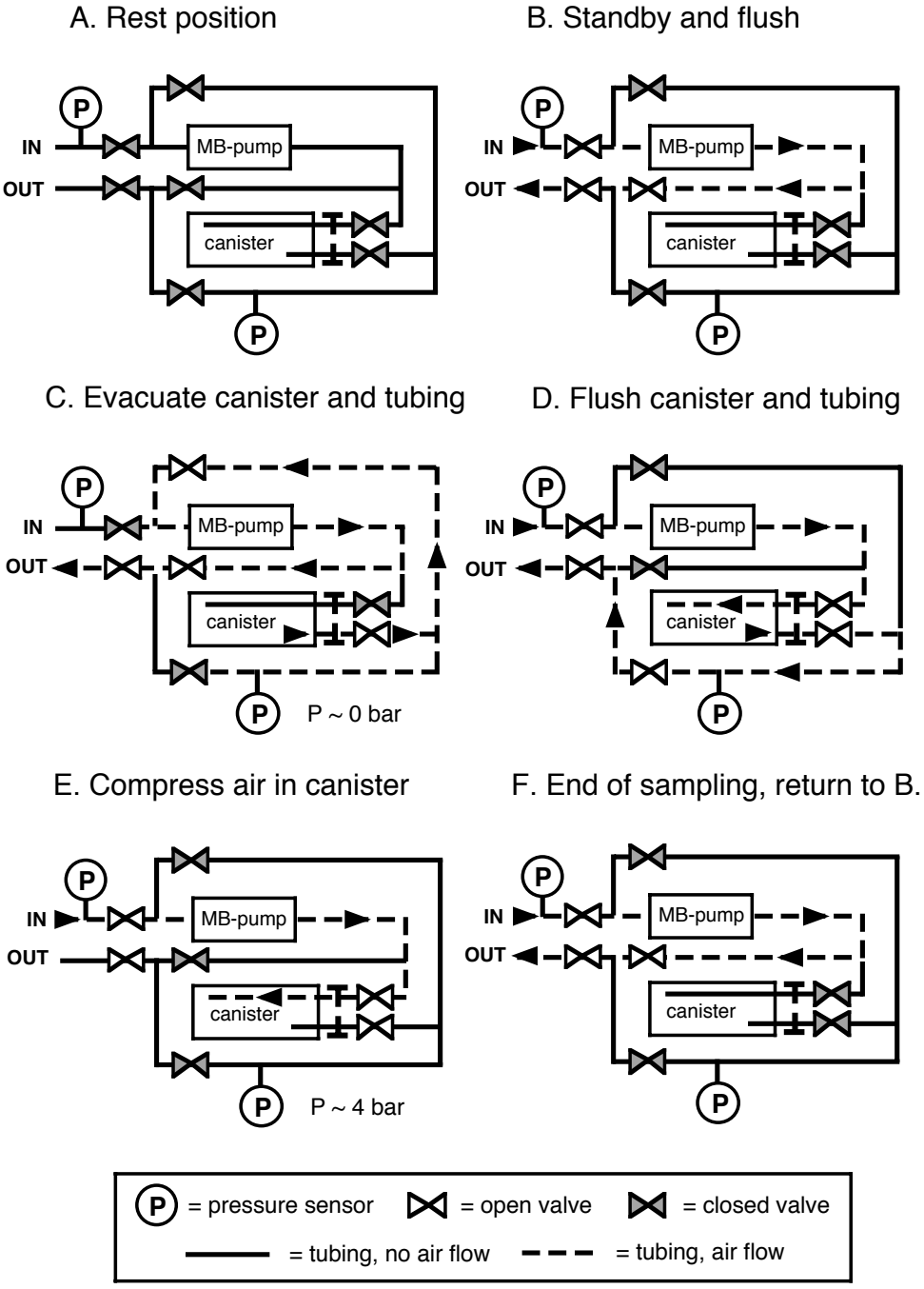

In the next panel, we show the canister and inlet pressure as a function of time for the collection of an air sample in the boundary layer, the middle (4 km), and the upper troposphere (12 km). The filling time stops automatically when the preset overpressure is reached (here 3.2 bar) or after 240 s (preset maximum filling time).

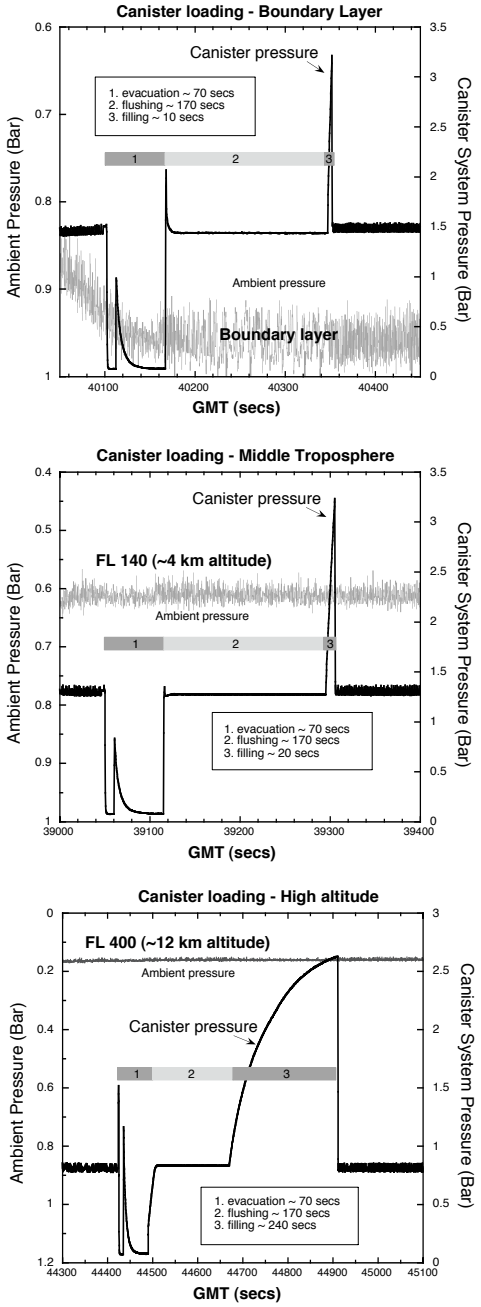

Gas Chromatograpghy (GC) analysis systems

Here we show schematics of the different GC-systems and the sample handling applied. Finally, we give some typical examples of chromatograms for the GC-FID and GC-ECD system from an air sample of the MINOS 2001 campaign.

Abbreviations used in the panels:

SPT Sample Pre-concentration Trap (VARIAN) filled with glass beads
MFC Mass Flow Controller
8PV 8-Port Valve
6PV 6-Port Valve
PLOT Porous Layer Open Tubular column
LN_2 Liquid Nitrogen (-196 ˚C)
LArLiquid Argon (-186 ˚C)
FID: Flame Ionisation Detector (separated compounds → hydrogen/air-flame → ionisation → current → amplification)
ECD: Electron Capture Detector (separated compounds →radioactive source (^{63}Ni) → β-radiation → ionisation of carrier gas → background current→ electronegative compounds take up electrons → change of current → amplification)

STREAM 1995 - 1997 (Wageningen University)

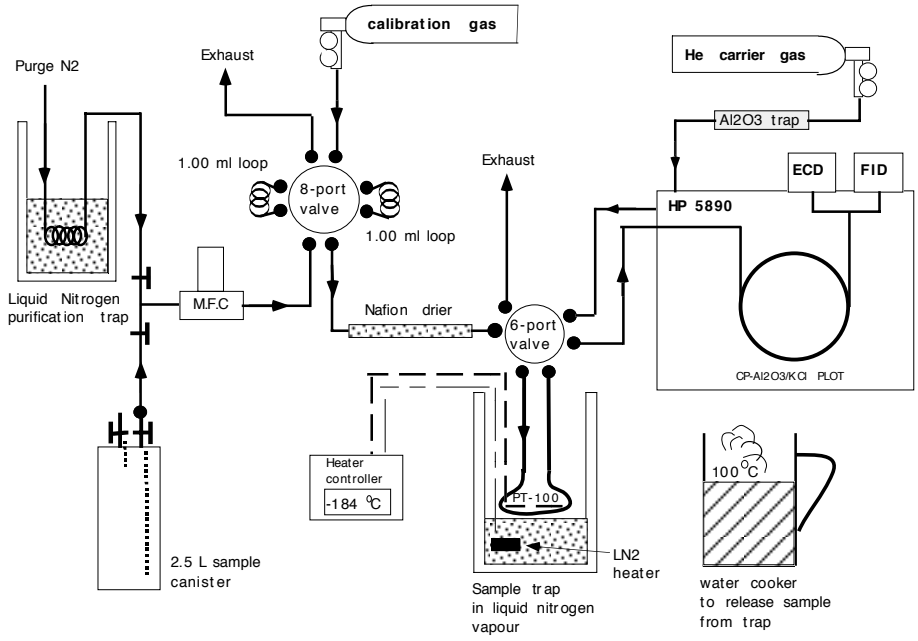

LBA-CLAIRE 1998 (Wageningen University)

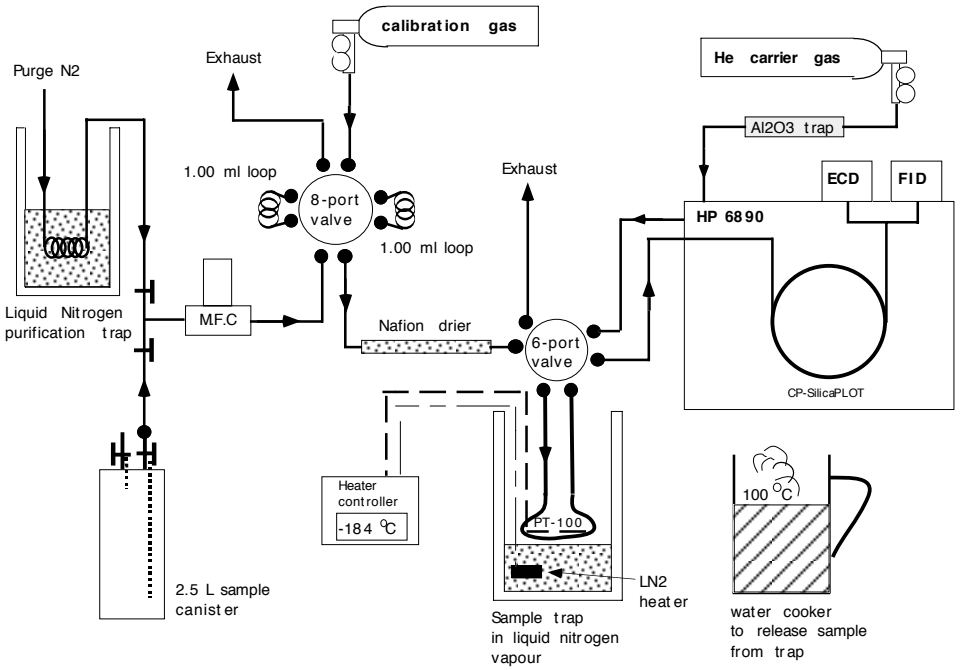

Sample handling system at the Department of Air Quality, Wageningen University:

1. 6PV in inject position, sample trap (10 cm stainless steel tube filled with glass beads) is positioned just above the LN_2 and cooled to -180˚C (controlled by a PT-100 temperature sensor). The sample flow is conditioned for two minutes at 33.3 ml/min with a MFC.
2. 6PV in load-position. The sample flow is led over the sample trap for exactly 30 minutes. A *Nafion* drier tube (selective molecular sieve) is applied to remove water vapor from the sample stream (water diffuses through the *Nafion* tube into a dry N_2 counter flow). At 33.3 ml/min 1 liter of air is sampled and pre-concentrated.
3. 6PV in inject-position, the sample trap is quickly removed and the sample trap is heated with boiling water for 1 minute, releasing the trapped organic compounds onto the column. The GC temperature program is started.

Temperature program GC-column during STREAM / LBA-CLAIRE 1995 – 1998 (Wageningen University):

35˚C (4 min) 6˚/min
210˚C (12 min)

For the GC-system at York University, we show the four stages of the sampling handling being 1. system conditioning; 2. sample pre-concentration; 3. cryofocusing prior to injection; 4. sample injection.

STREAM 1998 (York University, Toronto)

1. conditioning

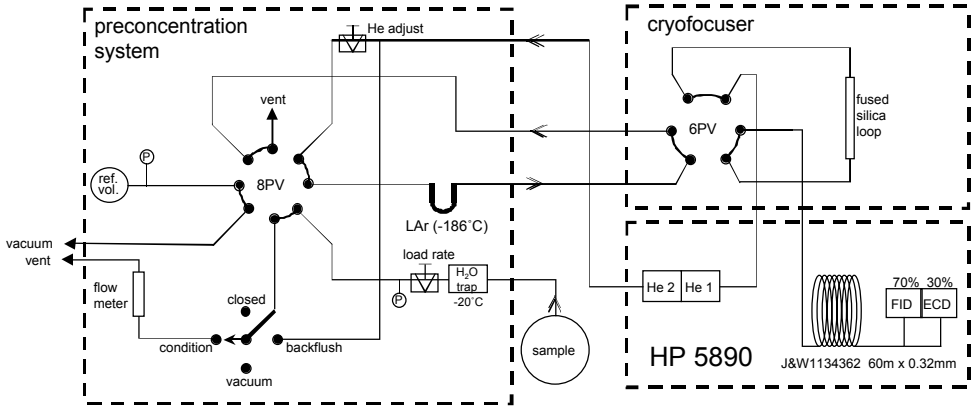

STREAM 1998 (York University, Toronto)

2. preconcentrating

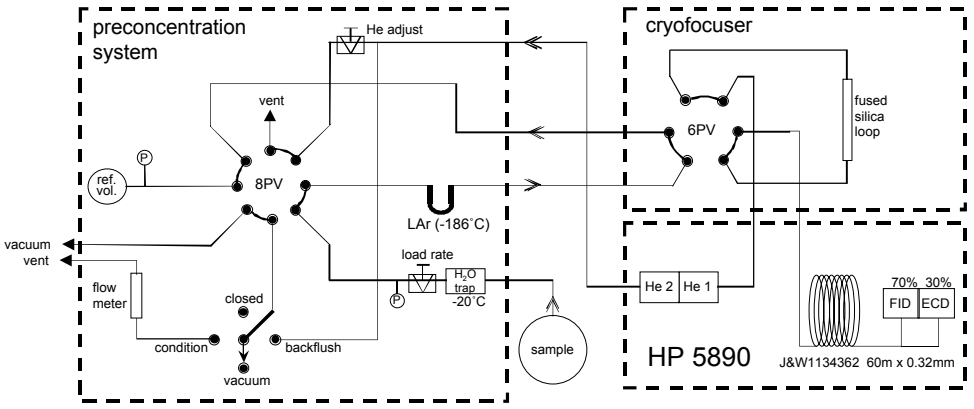

STREAM 1998 (York University, Toronto)

3. cryofocusing

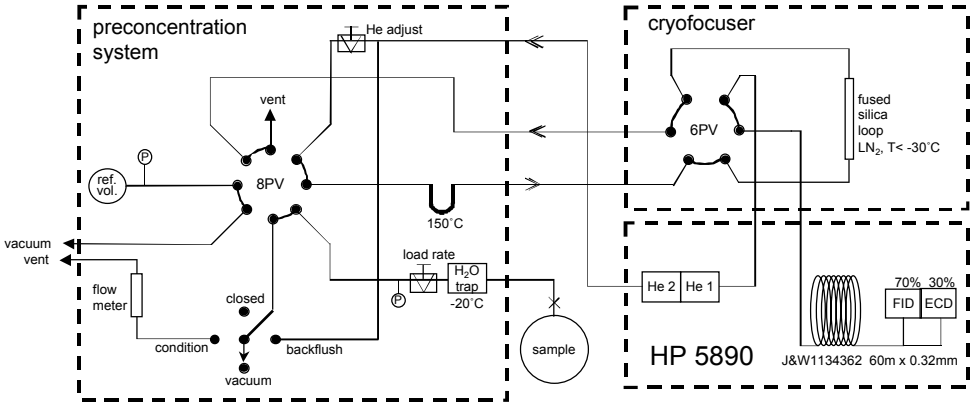

STREAM 1998 (York University, Toronto)

4. injection

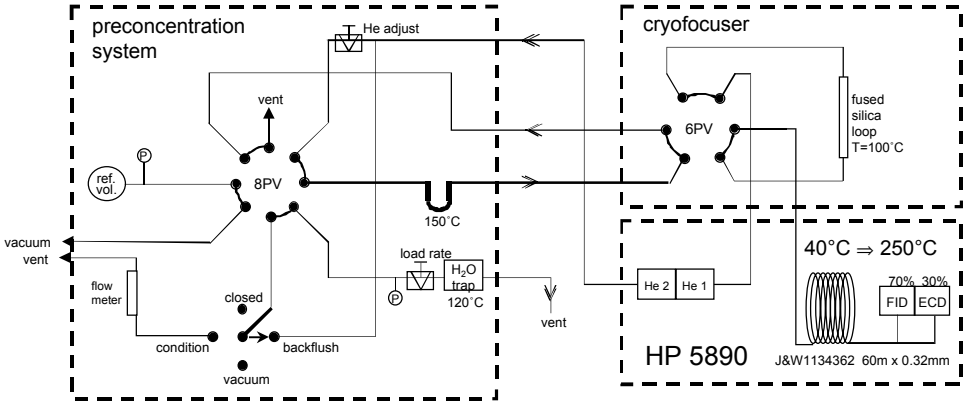

Sampling handling at the Centre for Atmospheric Chemistry, York University, Toronto:

1. 8PV in inject position, 6PV in inject position, 3-way selection valve in condition position. The sample flow is led through a flow meter for 3 minutes. The needle valve

is used to adjust the sample flow. In the mean time, the reference volume is evacuated. The pre-concentration loop is cooled in LAr, and the H_2O-trap is cooled to -20˚C using dry ice (solid CO_2)

2. 8PV in load position, 6PV in inject position, 3-way valve in vacuum position. The sample air is led over the pre-concentration loop to the reference volume and the pressure difference is a measure for the total amount of sampled air.
3. 8PV in inject position, 6PV in load position, 3-way valve in vacuum position. The fused silica loop is cooled using LN_2. When the temperature goes below -30˚C, the LAr from the pre-concentration loop is replaced by a heating element. A He-flow transports the organic compounds to the fused silica cryoloop in the cryofocuser.
4. 8PV in inject position, 6PV in inject position, 3-way valve in backflush position. The cryofocused sample is injected onto the GC-column. The GC temperature program starts. The coolant is removed from the H_2O-trap and it is heated to 120 ˚C. The water is then removed by a He-backflush through the sample inlet.

Temperature program GC-column during STREAM 1998 (York University, Toronto):

40˚C (2 min) 4˚/min
100˚C 3˚/min
250˚C (20 min)

INDOEX 1999 (Utrecht University)

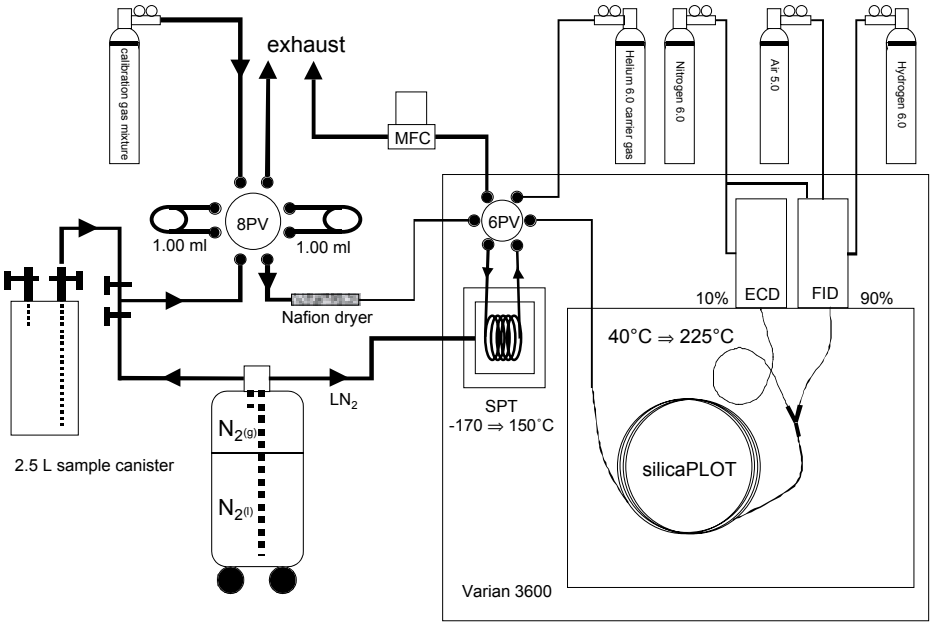

MINOS 2001 (Utrecht University)

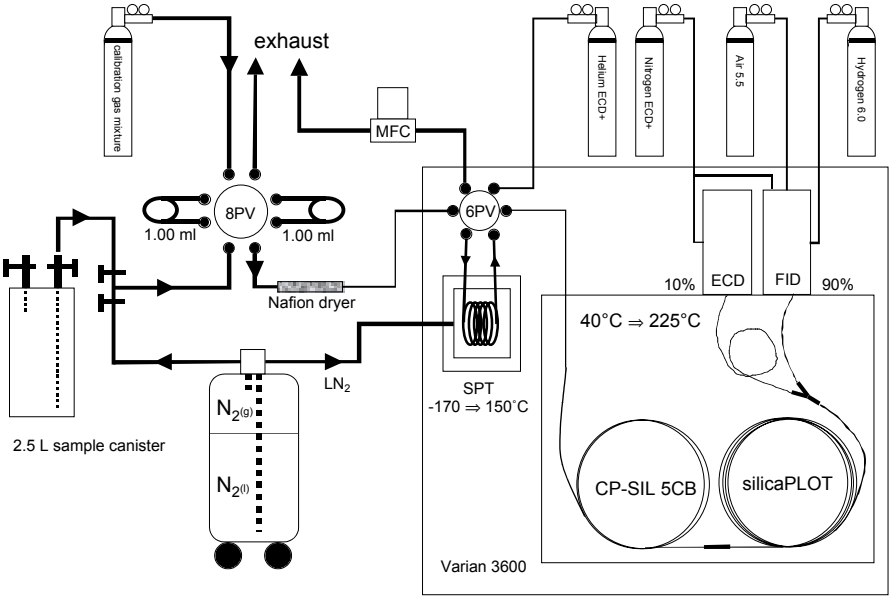

Sample handling at the Institute for Marine and Atmospheric research Utrecht, Utrecht University:

1. 6PV in inject position, SPT is cooled to -170˚C. The sample flow is conditioned for two minutes at 33.3 ml/min.
2. 6PV in load position. The sample flow is led over the SPT for exactly 30 minutes. A *Nafion* drier tube (selective molecular sieve) is applied to remove water vapor from the sample stream. At 33.3 ml/min (MFC) 1 liter of air is sampled.
3. 6PV in inject position, SPT is kept -170 ˚C for 4 minutes, to avoid a switching peak in the detector signals.
4. 6PV in inject position, SPT is quickly heated to 150˚C (it takes less than 30 seconds to reach 150˚C), releasing the organic compounds onto the GC-column. The GC temperature program starts.

Temperature program GC-column during INDOEX 1999 (A.) and MINOS 2001 (B.) (IMAU):

A. 40˚C (5 min) 6.5˚/min
   225˚C (11 min)

B. 40˚C (5 min) 5.0˚/min
   90˚C 8.0˚/min
   225˚C (10 min)

GC chromatograms

Below we give some typical examples of chromatograms for the GC-FID and GC-ECD. Shown here is a 1.00 L air sample taken during the second flight of the MINOS campaign (August 3, 2001) at an altitude of about 160 m above sea level. In addition, we show blank test of cleaned and pure nitrogen filled canisters.

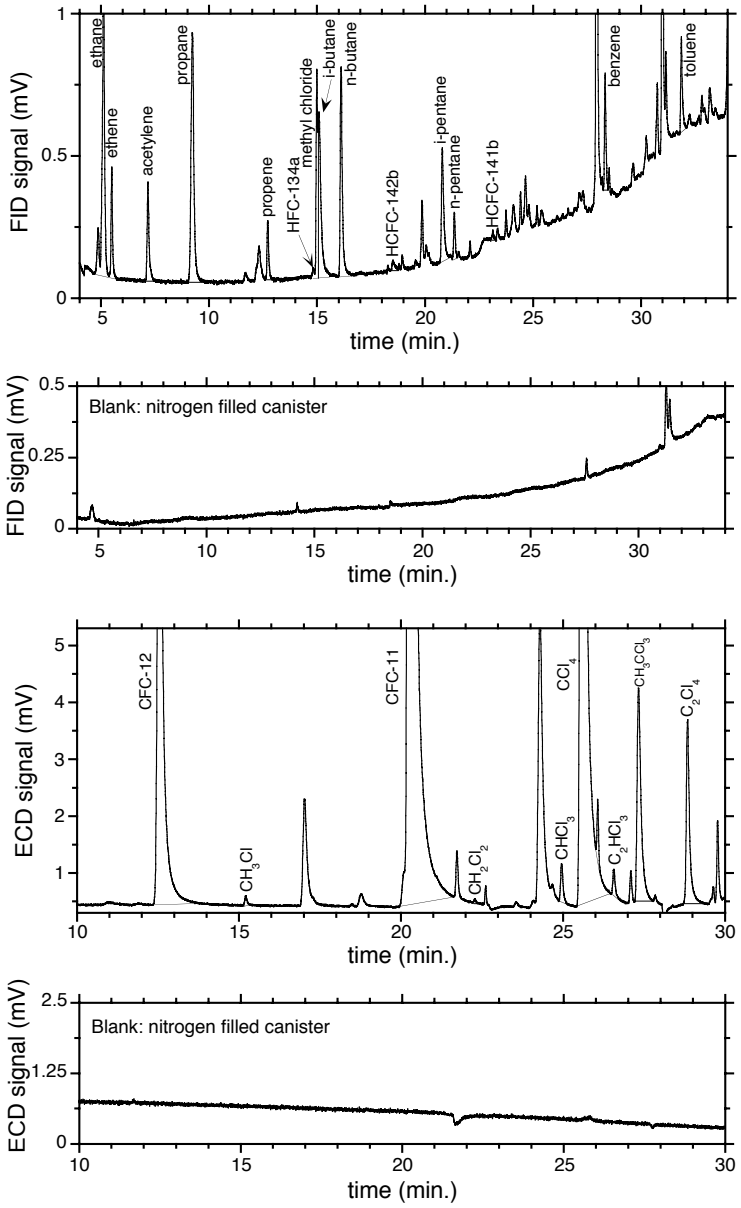

Detection limit of the GC-system

Here we show an example of the detection limit of i-pentane and n-pentane on the GC-FID. The chromatogram is from a 1.00 L air sample taken during the second flight of the MINOS campaign (August 3, 2001) at an altitude of about 12 km above sea level. We note that the accuracy at these low concentrations is very poor. The peaks at a retention time of 21 min. and 21.6 min. belong to unidentified species.

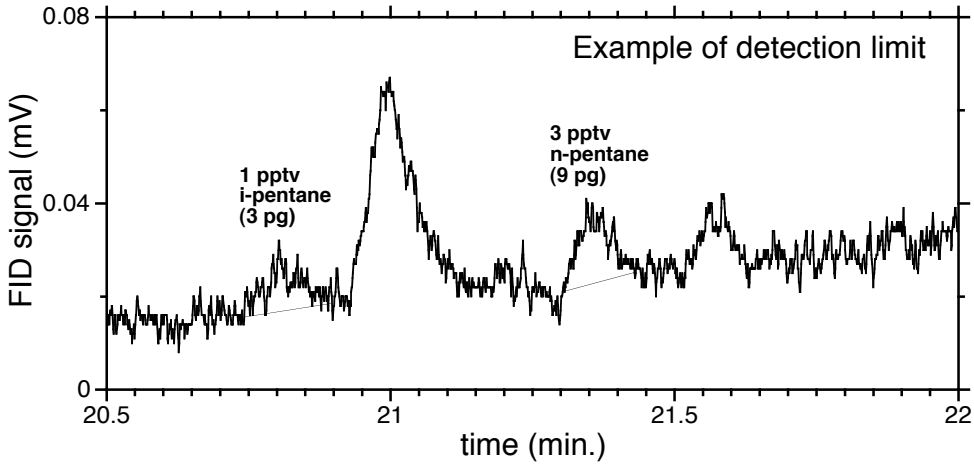

Bibliography

Alternative Fluorocarbons Environmental Acceptability Study (AFEAS), Production and Sales of Fluorocarbons, on http://www.afeas.org/production_and_sales.html, Arlington, VA, USA, 2002.

Andreae, M. O., Artaxo, P., Fischer, H., Freitas, S. R., Grégoire, Hansel, A., Hoor, P., Kormann, R., Krejci, R., Lange, L., Lelieveld, J., Lindinger, W., Longo, K., Peters, W., de Reus, M., Scheeren, B., Silva Dias, M. A. F., Ström, J., van Velthoven, P. F. J., and Williams, J., Transport of biomass burning smoke to the upper troposphere by deep convection in the equatorial region, *J. Geophys. Lett.*, *28*, 951–954, 2001.

Andreae, M.O., et al., Methyl halide emissions from savanna fires in southern Africa*, J. Geophys. Res*., *101*, 23603–23613, 1996.

Andrews, A. E., Boring, K. A., Daube, B. C., Wofsy, S. C., Loewenstein, M., Jost, H., Podolske, J. R., Webster, C. R., Herman, R. L., Scott, D. C., Flesch, G. J., Moyer, E. J., Elkins, J. W., Dutton, G. S., Hurst, D. F., Moore, F. L., Ray, E. A., Romashkin, P. A., and Strahan, S. E., Mean ages of stratospheric air derived from in situ observations of CO_2, CH_4, and N_2O, *J. Geophys. Res.*, *106*, 32295–32314, 2001.

Appenzeller, C., Holton, J. R., and Rosenhof, K. H., Seasonal variation of mass transport across the tropopause, *J. Geophys. Res.*, *101*, 15071–15078, 1996.

Arnold, F., Burger, V., Droste-Fanke, B., Grimm, F., Krieger, A., Schneider, J., and Stilp, T., Acetone in the upper troposphere and lower stratosphere: Impact on trace gases and aerosols, *Geophys. Res. Lett.*, *24*, 3017–3020, 1997.

Artaxo, P., and Hansson, H. -C., Size distribution of biogenic aerosol particles from the Amazon Basin, *Atmos. Environ.*, *29*, 393–402, 1995.

Atkinson, R. A., Gas-phase tropospheric chemistry of organic compounds: a review, *Atmos. Environ.*, *24*, 1–41, 1990.

Atkinson, R. A., Baulch, D. L., Cox, R. A., Hampson-Jr., R. F., Kerr, J. A., and Troe, J., Evaluated kinetic and photochemical data for atmospheric chemistry - Supplement IV, *J. Phys. Chem. Ref. Data, 21*(6), 1125, 1992.

Atkinson, R. A., Baulch, D. L., Cox, R. A., Hampson-Jr., R. F., Kerr, J. A., Rossi, M. J., and Troe, J., Evaluated kinetic, photochemical data and heterogeneous data for atmospheric chemistry - Supplement V, *J. Phys. Chem. Ref. Data*, *21*(3), 521, 1997.

Atkinson, R., Baulch, D. L., Cox, R. A., Crowley, J. N., Hampson-Jr, R. F., Kerr, J. A., Rossi, M. J., and Troe, J., Summary of evaluated kinetic and photochemical data for atmospheric chemistry, *Web Version December 2002*., IUPAC Subcommittee on Gas Kinetic data Evaluation for Atmospheric Chemistry, on http://www.iupac-kinetic.ch.cam.ac.uk/, 2002.

Aucott, M. L., Graedel, T. E., Kleiman, G., McCulloch, A., Midgley, P., and Li, Y.-F., Anthropogenic emissions of trichloromethane (chloroform) and chlorodifluoromethane (HCFC-22): Reactive Chlorine Emissions Inventory, *J. Geophys. Res., 104*, 8405–8415, 1999.

Ballschmiter, K., Pattern and sources of naturally produced organohalogens in the marine environment: biogenic formation of organohalogens, *Chemosphere*, *52*, 313–314,2003. Bamber, D. J., Healey, P. G. W., Jones, B. M. R., Penkett, S. A., and Vaughan, G., Vertical profiles of tropospheric gases: Chemical consequences of stratospheric intrusions, *Atmos. Environm.*, *18*, 1759–1766, 1984.

Barnett, T. P., Pierce, D. W., Schnur, R., Detection of anthropogenic climate change in the world's oceans, *Science*, *292*, 270–274, 2001.

Bill, M., Rhew, R. C., Weiss, R. F., Goldstein, A. H., Carbon isotope ratios of methyl bromide and methyl chloride emitted from a coastal salt marsh, *Geophys. Res. Lett.*, *29*, doi:10.1029/2001GL012946, 2002.

Blake, N. J., Blake, D. R., Sive, B. C., Chen, T.-Y., Rowland, F. S., Collins-Jr., J. E., Sache, G. W. and Anderson, B. E., Biomass burning emissions and vertical distribution of atmospheric methyl halides and other reduced carbon gases in the South Atlantic region, *J. Geophys. Res.*, *101*, 24151–24164, 1996.

Blake, N. J., Blake, D. R., Wingenter, O. W., Sive, B. C., McKenzie, L. M., Lopez, J. P., Simpson, I. J., Fuelberg, H. E., Sache, G. W., Anderson, B. E., Gregory, G. L., Carroll, M. A., Albercook, G. M., and Sherwood-Rowland, F., Influence of southern hemispheric biomass burning on mid-tropospheric distributions of non-methane hydrocarbons and selected halocarbons over the remote South Pacific, *J. Geophys. Res.*, *104*, 16213–16232, 1999.

Boering, K. A., Daube, B. C., Wofsy, S. C., Loewenstein, M., Podolske, J. R., and Keim, E. R., Tracer-tracer relationships and lower stratospheric dynamics: CO_2 and N_2O correlations during SPADE, *Geophys. Res. Lett.*, *21*, 2567–2570, 1994.

Boering, K. A., Wofsy, S. C., Daube, B. C., Schneider, H. R., Lowenstein, M., Podolske, J. R., and Conway, T. J., Stratospheric mean ages and transport rates from observations of carbon dioxide and nitrous oxide, *Science*, *274*, 1340–1343, 1996.

Bonsang, B., Polle, C., and Lambert, G., Evidence for marine production of isoprene, *Geophys. Res. Lett., 19*, 1129–1132, 1992.

Bregman, A., Arnold, F., Bürger, V., Fischer, H., Lelieveld, J., Scheeren, B. A., Schneider, J., Siegmund, P. C., Ström, J., Waibel A., and Wauben, W. M. F., In-situ trace gas and particle measurements in the summer lower stratosphere during STREAM II: implications for O_3 production, *J. Atmos. Chem.*, *26*, 275–310, 1997.

Bregman, A., Lelieveld, J., van den Broek, M., Siegmund, P., Fischer, H., and Bujok, O., The N_2O and O_3 relationship in the lowermost stratosphere: a diagnostic for mixing processes as represented by a three-dimensional chemistry-transport model, *J. Geophys. Res., 105*, 17279–17290, 2000.

Brewer, A. W., Evidence for a world circulation provided by measurements of helium and water vapor in the stratosphere, *Quart. J. Roy. Meteorol. Soc., 75*, 351–363, 1949.

Broadgate, W. J., Liss, P. S., and Penkett, S. A., Seasonal emissions of isoprene and other reactive gases from the ocean, *Geophys. Res. Lett., 24*, 2675–2678, 1997.

Brühl, C., Pöschl, U., Crutzen, P. J., and Steil, B., Acetone and PAN in the upper troposphere: impact on ozone production from aircraft emissions, *Atmos. Environ.*, *34*, 3931–3938, 2000.

Brune, W. H., Faloona, I. C., Tan, D., Weinheimer, A. J., Campos, T., Rodley, B. A., Vay, S. A., Collins, J. E., Sachse, G. W., Jaeglé, L., and Jacob, D. J., Airborne in-situ OH and

HO_2 observations in the cloud-free troposphere and lower stratosphere during SUCCESS, *Geophys. Res. Lett.*, *25*, 1701–1704, 1998.

Brunner, D., Staehelin, J., Jeker, D., Wernli, H., and Schumann, U., Nitrogen oxides and ozone in the tropopause region of the Northern Hemisphere: Measurements from commercial aircraft in 1995 / 1996 and 1997, *J. Geophys. Res.*, *106*, 27673–27699, 2001.

Bujok, O., Tan, V., Klein, E., Nopper, R., Bauer, R., Engel, A., Gerhards, M.-T., Afchine, A., McKenna, D. S., Schmidt, U., Wienhold, F. G., Fischer, H., GHOST – A novel airborne gas chromatograph for in situ measurements of long-lived tracers in the lower stratosphere: method and applications*, J. Atmos. Chem.*, *39,* 37–64, 2001.

Butler, J. H., Battle, M., Bender, M. L., Montzka, S. A., Clarke, A. D., Saltzman, E. S., Sucher, C. M., Severinghaus, J. P., and Elkins, J. W., A record of atmospheric halocarbons during the twentieth century from polar firn air, *Nature*, *399*, 749–755, 1999.

Chemosphere: Special Issue on Naturally Produced Organohalogens, *Chemosphere*, *52*, 287–537, 2003.

Chen, P., Isentropic cross-tropopause mass exchange in the extratropics, *J. Geophys. Res., 100*, 16661–16673, 1995.

Cooper, O. R., Moody, J. L., Parrish, D. D., Trainer, M., Ryerson, T. B., Holloway, J. S., Hübler, G., Fehsenfeld, F. C., Oltmans, S. J., and Evans, M. J., Trace gas signatures of the airstreams within North Atlantic cyclones: Case studies from the North Atlantic Regional Experiment (NARE '97) aircraft intensive, *J. Geophys. Res.*, *106*, 5437–5456, 2001.

Crutzen, P. J., and Arnold, F., Nitric acid cloud formation in the cold Antarctic stratosphere: a major cause for the springtime "ozone hole", *Nature*, *324*, 651–655, 1986.

Crutzen, P. J., Williams, J., Pöschl, U., Hoor, P., Fischer, H., Warneke, C., Holzinger, R., Hansel, A., Lindinger, W., Scheeren, B., and Lelieveld, J., High spatial and temporal resolution measurements of primary organics and their oxidation products over the tropical forests of Surinam, *Atmos. Environ.*, *34*, 1161–1165, 2000.

Danielsen, E. F., Stratospheric-troposphere exchange based upon radioactivity, ozone and potential vorticity, *J. Atmos. Sci.*, *25*, 501–518, 1968.

Danielsen, E. F., In situ evidence of rapid, vertical, irreversible transport of lower tropospheric air into the lower tropical stratosphere by convective cloud turrets and by large-scale upwelling in tropical cyclones, *J. Geophys. Res.*, *98*, 8665–8681, 1993.

de Gouw, J. A., Lelieveld, J., Scheeren, H. A., Bolder, M., van der Veen, C., Warneke, C., Williams, J., Crutzen, P. J., Fischer, H., Lange, L., and Wong, S., Overview of the measurements onboard the Citation aircraft during the Intensive Field Phase of INDOEX*, J. Geophys. Res.*, *106*, 28453–28467, 2001.

de Laat, J., and Lelieveld, J., Source analysis of carbon monoxide pollution during INDOEX, *J. Geophys. Res., 106*, 28469–28496, 2001.

DeMore, W. B., *et al.*, Chemical kinetics and photochemical data for use in stratospheric modeling, in *Evaluation 12, NASA JPL Rep.*, Jet Propul. Lab. Pasadena, Calif., *97*-4, 1997.

Dessler, A. E., Hintsa, E. J., Weinstock, E. M., Anderson, J. G., and Chan, K. R., Mechanism controlling the water vapor in the lower stratosphere: "A tale of two stratospheres", *J. Geophys. Res.*, *100*, 23167-23172, 1995.

Dethof, A., O'Neill, A., and Slingo, J., Quantification of the isentropic mass transport across the dynamical tropopause, *J. Geophys. Res.*, *105*, 12279–12293, 2000.

Dickerson, R., Huffman, G., Luke, W., Nunnermacker, L., Pickering, K., Leslie, A., Lindsey, C., Slinn, W., Kelly, T., Daum, P., Delany, A., Greenberg, J., Zimmermann, P., Boatman, J., Ray, J., and Stedman, H., Thunderstorms: an important mechanism in the transport of air pollutants, *Science*, *231*, 460–464, 1987

Dimmer, C. H., Simmonds, P. G., Nickless, G., Bassford, M. R., Biogenic fluxes of halomethanes from Irish peatland ecosystems, *Atmos. Environ.*, *35*, 321–330, 2001.

Dobson, G. M. B., Origin and distribution of polyatomic molecules in the atmosphere, *Proc. R. Soc. London*, *Ser. A*, *236*, 187–193, 1956.

Duncan, B. N., martin, R. V., Staudt, A. C., Yevich, R., and Logan, J. A., Interannual and seasonal variability of biomass burning emissions constrained by satellite observations, *J. Geophys. Res.*, *108*, doi:10.1029/2002JD002378, 2003.

Energy Information Administration (EIA), Emissions of Greenhouse gases in the United States 1997 – Halocarbons and Other Gases, on http://www.eia.doe.gov/oiaf/1605/gg98rpt/halocarbons.html, Washington, DC, USA.

Farman, J. C., Gardiner, B. G., and Shanklin, J. D., Large losses of total ozone in Antarctica reveal seasonal ClO_x/NO_x interaction, *Nature*, *315*, 207–210, 1985.

Fischer , H., Wienhold, F. G., Hoor, P., Bujok, O., Schiller, C., Siegmund, P., Ambaum, M., Scheeren, H. A., and Lelieveld, J., Tracer correlations in the northern high latitude lowermost stratosphere: Influence of cross-tropopause mass exchange, *Geophys. Res. Lett.*, *27*, 97–100, 2000.

Fischer, H., Brunner, D., Harris, G., Hoor, P., Lelieveld, J., Mckenna, D., Rudolph, J., Scheeren, H. A., Siegmund, P., Wernli, J., Williams, J., and Wong, S., Synoptic tracer gradients in the upper troposphere over central Canada during the STREAM 1998 summer campaign, *J. Geophys. Res.*, 107, doi:10.1029/2000JD000312, 2002.

Fischer, H., de Reus, M., de Gouw, J., Warneke, C., Schlager, H., and Minikin, A., Deep convective injection of boundary layer air into the lowermost stratosphere at midlatitudes, *Atmos. Chem. Phys. Discuss.*, *2*, 2003–2019, 2002.

Fischer, H., Kormann, R., de Reus, M., Lawrence, M., Brühl, C., von Kuhlmann, R., Warneke, C., de Gouw, J. Holzinger, R., Williams, J., and Lelieveld, J., Formaldehyde over the Eastern Mediterranean during MINOS: Comparison of Airborne In-situ Measurements with 3D-Model Results, *Atmos. Chem. Phys. Discuss., 2*, 2003–2019, 2002.

Flocke, F., Herman, R. L., Salawitch, R. J., Atlas, E., Webster, C. R., Schauffler, S. M., Lueb, R. A., May, R. D., Moyer, E. J., Rosenlof, K. H., Scott, D. C., Blake, D. R., and Bui, T. P., An examination of chemistry and transport processes in the tropical lower stratosphere using observations of long-lived and short-lived compounds obtained during STRAT and POLARIS, *J. Geophys. Res.*, *104*, 26625–26642, 1999.

Food and Agricultural Organization of the UN (FAO), Forest Resources Assessment 2000, on http://www.fao.org/forestry/fo/fra/index.jsp, Rome, Italy, 2001.

Formenti, P., Andreae, M. O., Lange, L., Roberts, G., Cafmeyer, J., Rajta, I., Meanhaut, W., Holben, B. N., Artaxo, P., and Lelieveld, J., Saharan dust in Brazil and Suriname during the Large-scale Biosphere-atmosphere experiment in Amazonia (LBA) - Cooperative LBA Airborne Regional Experiment (CLAIRE) in March 1998, *J. Geophys. Res.*, *106*, 14919–14934, 2001.

Frank, H., Scholl, H., Renschen, D., Rether, B., Laouedj, A., Norokorpi, Y., Haloacetic acids, phytotoxic secondary air pollutants, *Environ. Sci. Pollut. Res.*, *1*, 4–14, 1994.

Ganzeveld, L. N., Lelieveld J, Dentener FJ, Krol MC, Roelofs GJ et al., Atmosphere-biosphere trace gas exchanges simulated with a single-column model, *J. Geophys. Res.*, *107*, doi:10.1029/2001JD000684, 2002.

Galballi, I.E., and Kirstine, W., The production of methanol by flowering plants and the global cycle of methanol, *J. Atmos. Chem.*, *3*, 195–229, 2002.

Good, P., Giannakopoulos, C., O'Connor, F.M., Arnold, S. R., de Reus M., and Schlager H., Constraining tropospheric mixing timescales using airborne observations and numerical models, *Atmos. Chem. Phys. Discuss.*, *3*, 1213–1245, 2003.

Gribble, G. W., The diversity of naturally produced organohalogens, *Chemosphere*, *52*, 289–297, 2003.

Gros, V., Williams, J., Krol, M., Berresheim, H., Salisbury, G., Hofmann, R., and Lelieveld, J., Investigating source origins and photochemical processing of the VOCs during the MINOS-2001 campaign, *Atmos. Chem. Phys. Discuss.*, *3*, 1893–1923, 2003.

Guenther, A., Hewitt, C. N., Erickson, D., Fall, R., Geron, C., Graedel, T., Harley, P., Klinger, L., Lerdau, M., McKay, W. A., Pierce, T., Scholes, B., Steinbrecher, R., Tallamraju, R., Taylor, J., and Zimmerman, P., A global model of natural volatile organic compound emissions, *J. Geophys. Res.*, *100*, 8873–8892, 1995.

Haagen-Smit, A. J., and M. M. Fox, Ozone formation in photochemical oxidation of organic substances, *Ind. Eng. Chem., 48*, 1484, 1956.

Haagen-Smit, A. J., and M. M. Fox, Photochemical ozone formation with hydrocarbons and automobile exhaust, *J. Air Poll. Contr. Assoc. 4*, 105–109, 1954.

Hamilton, J. T. G., McRoberts, W. C., Keppler, F., Kalin, R. M., Harper, D. B., Chloride methylation by plant pectin: an efficient environmentally significant process, *Science*, *301*, 206–209, 2003.

Harper, D. B., The global chloromethane cycle: biosynthesis, biodegradation and metabolic role, *Nat. Prod. Rep.*, *17*, 337–348, 2000.

Haselmann, K. F., Ketola, R. A., Laturnus, F., Lauritsen, F. R., Grøn, C., Occurrence and formation of chloroform at Danish forest sites, *Atmos. Environ.*, *34*, 187–193, 2000a.

Haselmann, K. F., Laturnus, F., Svensmark, B., Grøn, C.: Formation of chloroform in spruce forest soil – results from laboratory incubation studies, *Chemosphere*, *41*, 1769–1774, 2000b.

Hastenrath, S., Climate dynamics of the tropics, *Atmospheric Sciences Library*, *8*, Kluwer Acadamic Publishers, Dordrecht, the Netherlands, 1991.

Hauglustaine, D. A., and Brasseur, G. P., Evolution of tropospheric ozone under anthropogenic activities and associated radiative forcing of climate, *J. Geophys. Res.*, *106*, 32337–32360, 2001.

Heland, J., Ziereis, H. Schlager, H., Hauser, C., Stock, P., Roiger, A., de Reus, M., Traub, M., and Roelofs, G. -J., Aircraft observations of trace gas correlations during MINOS 2001 - case studies on the origin of air masses, *Atmos. Chem. Phys. Discuss*, *3*, 1991–2026, 2003.

Hintsa E. J., Boering, K. A., Weinstock, E. M., Anderson, J. G., Gary, B. L., Pfister, L., Daube, B. C., Wofsy, S. C., Loewenstein, M., Podolske, J. R., Margitan, J. J., and Bui, T. P., Troposphere-to-stratosphere transport in the lowermost stratosphere from mea-

surements of H_2O, CO_2, N_2O and O_3, *J. Geophys. Res.*, *25*, 2655—2658, 1998.

Hoekstra , E. J., Lassen, P., Van Leeuwen, J. G. E., De Leer, E. W. B., Carlsen, L., Formation of organic chlorine compounds of low molecular weight in the chloroperoxidase-mediated reaction between chloride and humic material, in *Naturally-Produced Organohalogens*, edited by Grimvall, A., De Leer, E. W. B., *Kluwer Academic Publishers*, Dordrecht, pp.149–158, 1995.

Hoekstra, E. J., Duyzer, J. H., de Leer, E. W. B., Brinkman, U. A. Th., Chloroform – concentration gradients in soil air and atmospheric air, and emission fluxes from soil, *Atmos. Environ.*, *35*, 61–70, 2001.

Hoekstra, E. J., Verhagen, F. J. M., Field, J. A., de Leer, E. W. B., Brinkman, U. A. Th., Natural production of chloroform by fungi, *Phytochem.*, *49*, 91–97, 1998.

Hoerling, M. P., Schaack, T. K., and Lenzen, A. J., A global analysis of stratosphere-troposphere exchange during northern winter, *Month. Wea. Rev.*, *121*, 162–172, 1993.

Holton, J. R., Haynes, P. H., McIntyre, M. E., Douglass, A. R., Rood, R. B., and Pfister, L., Stratosphere-troposphere exchange, *Rev. Geophys.*, *33*, 403-–439, 1995.

Holzinger, R., Klüpfel, T., Salisbury, G., Williams, J., de Reus, M., Fischer, H., Traub, M., Crutzen, P. J., Lelieveld, J.: Assessing the biomass burning contribution to the tropospheric burden of CO, acetone, methanol and PAN over the eastern Mediterranean, submitted to *Atmos. Chem. Phys. Discuss*, 2003.

Holzinger, R., Warneke, C., Hansel, A., Jordan, A., and Lindinger, W., Biomass burning as a source of formaldehyde, acetaldehyde, methanol, acetonitrile, and hydrogen cyanide, *Geophys. Res. Lett., 26*, 1161–1164, 1999.

Hoor, P., Fischer, H., Lange, L., Lelieveld, J., and Brunner, D., Seasonal variation of a mixing layer in the tropopause region as identified by the CO-O_3 correlation from in-situ measurements, *J. Geophys. Res.*, *107*, doi:10.1029/2000JD000289, 2002.

Hoor, P., Fischer, H., Wong, S., Engel, A., and Wetter, T., Intercomparison of airborne N_2O measurements using tunable diode laser absorption spectroscopy and in situ gas chromatography, *SPIE Proceedings*, *vol. 3658*, 109–1115, 1999.

Hoskins, B. J., Towards a PV-θ view of the general circulation, *Tellus*, *Ser. AB*, *43*, 27–35, 1991.

Houweling, S., Kaminski, T., Dentener, F., Lelieveld, J., Heimann, M., Inverse modeling of methane sources and sinks using the adjoint of a global transport model, *J. Geophys. Res.*, *104*, 26137–26160, 1999.

Houweling, S., Dentener, F., Lelieveld, J., Walter, B, and Dlugokencky, E., The modeling of tropospheric methane: How well can point measurements be reproduced by a global model?, *J. Geophys. Res.*, *105*, 8981–9002, 2000.

Hsu, H., Terng, C., and Chen, C., Evolution of Large-Scale Circulation and Heating during the first transition of Asian summer monsoon, *J. Climate*, *12*, 793–810, 1999.

Hutchinson, S. A., Biological activity of volatile fungal metabolites, *Transactions of the British Mycological Society*, *57*, 185–200, 1971.

IPPC-TAR, Atmospheric Chemistry and Greenhouse gases, in Climate Change 2001: Contribution of Working group I to the Third assessment report in the *Intergovernmental Panel on Climate Change*, edited by *J. Houghton et al.*, p. 881, *Cambridge University press*, Cambridge and New York, NY, USA, 2001.

Jacob, D. J., Field, B. D., Jin, E. M., Bey, I., Li, Q., Logan, J. A., and Yantosca, R. M.,

Atmospheric budget of acetone, *J. Geophys. Res.*, *107*, doi:10.1029/201JD000694, 2002.

Jeker, D. P., Pfister, L., Thompson, A. M., Brunner, D., Boccipio, D. J., Pickering, K. E., Wernli, H., Kondo, Y., and Staehelin, J., Measurements of nitrogen oxides at the tropopause: Attribution to convection and correlation with lightning, *J. Geophys. Res.*, *105*, 3679–3700, 2000.

Jobson, B. T., Parrish, D. D., Goldan, P., Kuster, W., Fehsenfeld, F. C., Blake, D. R., Blake, N. J., and Niki, H., Spatial and temporal variability of non-methane hydrocarbon mixing ratios and their relation to photochemical lifetime, *J. Geophys. Res.*, *1 0 3*, 13557–13567, 1998.

Jobson, B. T., S. A. McKeen, D. D. Parrish, F. C. Fehsenfeld, D. R. Blake, A. H. Goldstein, S. M. Schauffler, and J. W. Elkins, Trace gas mixing variability versus lifetime in the troposphere and stratosphere: Observations, *J. Geophys. Res.*, *104*, 16090–16113, 1999.

Junge, C. E., Global ozone budget and exchange between stratosphere and troposphere, *Tellus*, *14*, 363–377, 1962.

Junge, C.E., Residence time and variability of tropospheric trace gases, *Tellus, 16*, 477–488, 1974.

Kanakidou, M., Dentener, F. J., and Crutzen, P. J., A global three-dimensional study of the fate of HCFCs and HFC-134a in the troposphere, *J. Geophys. Res.*, *100*, 18781–18880, 1995.

Kaspers, K. A., van de Wal, R. S. W., de Gouw, J. A., Hofstede, C. M., van den Broeke, M. R., van der Veen, C., Neubert, R., Meijer, H. A. J., Brenninkmeijer, M. A. K., Karlöf, L., and Winther, J. –G., Analyses of firn gas samples from Dronning Maud Land, Antarctica. Part 1: Study of non-methane hydrocarbons and methyl chloride, submitted to *J. Geophys. Res.*, 2003.

Keene, W. C., Khalil, M. A. K., Erickson, D. J., McCulloch, A., Greadel, T. E., Lobert, J. M., Aucott, M. L., Gong, S. –L., Harper, D. B., Kleinman, G., Midley, P., Moore, R. A., Seuzaret, C., Sturges, W. T., Benkovitz, C. M., Koropalov, V., Barrie, L. A., and Li, Y. -F., Composite global emissions of reactive chlorine from anthropogenic and natural sources: The Reactive Chlorine Emissions Inventory, *J. Geophys. Res.*, *104*, 8429–8440, 1999.

Keppler, F., Eiden, R., Niedan, V., Pracht, J., Schöler, H. F., Halocarbons produced by natural oxidation processes during degradation of organic matter, *Nature*, *403*, 298–301, 2000.

Khalil, M. A. K., Reactive halogen compounds in the atmosphere, in *The Handbook of Environmental Chemistry Vol. 4 Part E*, edited by P. Fabian and O.N. Singh, *Springer-Verlag*, Berlin Heidelberg, 1999.

Khalil, M. A. K., and Rasmussen, R. A., Atmospheric methyl chloride, *Atmos. Environ.*, *33*, 1305–1321, 1999.

Khalil, M. A. K., Moore, R. M., Harper, D. B., Lobert, J. M., Erickson, D. J., Koropalov, V., Sturges, W. T., and Keene, W. C.: Natural emissions of chlorine-containing gases: Reactive Chlorine Emissions Inventory, J. Geophys. Res., 104, 8333–8346, 1999.

Koropalov, W.T. Sturges, and W.C. Keene, Natural emissions of chlorine-containing gases: Reactive Chlorine Emissions Inventory, *J. Geophys. Res., 104*, 8333 – 8346, 1999.

Kouvarakis, K., Tsigaridis, K., Kanakidou, M., and Mihalopoulos, N., Temporal variations of surface regional background ozone over Crete island in the southeast Mediterranean, *J. Geophys. Res.*, *105*, 4399–4407, 2000.

Krejci, R., Ström, J., de reus, M., Williams, J., and Andreae, M. O., Spatial and temporal distribution of the atmospheric aerosols in the lowermost troposphere over the Amazonian rainforest, *Ph.D. thesis - Chapter 2*, Stockholm University, Stockholm, Sweden, 2002.

Kritz, M. A., Rosner, S. W., Danielsen, E. F., and Selkirk, H. B., Air-mass origins and troposphere-to-stratosphere exchange associated with mid-latitude cyclogenesis and tropopause folding inferred from ^{7}Be measurements, *J. Geophys. Res.*, *96*, 17405–17414, 1991.

Krol, M., van Leeuwen, P. J., Lelieveld, J., Global OH trend inferred from methylchloroform measurements, *J. Geophys. Res.*, *103*, 10697–10712, 1998.

Krol, M. C., Lelieveld, J., Oram, D. E., Sturrock, G. A., Penkett, S. A., Brenninkmeijer, C. A. M., Gros, V., Williams, J., and Scheeren, H. A., Continuing emissions of methyl chloroform from Europe, *Nature*, 421, 131–135, 2003.

Lacis , A. A., Weubbles, D. J., and Logan, J. A., Radiative forcing of climate by changes in the vertical distribution of ozone, *J. Geophys. Res.*, *95*, 9971–9981, 1990.

Lal, S., Naja, M., and Subbaraya, B. H., Seasonal variations in surface ozone production and its precursors over an urban site in India, *Atmos. Environ.*, *34*, 27183–2724, 2000.

Lange, L., Aircraft-borne trace gas measurements during the STREAM 98 campaign, *Ph.D. thesis*, pp. 71–93, Utrecht University, Utrecht, the Netherlands, 2001.

Lawrence, M. G., Rasch, P. J., von Kuhlmann, R., Williams, J., Fischer, H., de Reus, M., Lelieveld, J., Crutzen, P. J., Huntrieser, H., Heland, J., Stohl, A., Forster, C., Schultz, M., Stier, P., and Dickerson, R., Chemical weather forecasting as a tool for field campaign planning: Predictions and observations of large-scale features during INDOEX, MINOS, and CONTRACE, *Atmos. Chem. Phys.*, *3*, 267–289, 2003.

Lee-Taylor, J. M., Brasseur, G. P., and Yokouchi, Y., A preliminary three-dimensional global model study of atmospheric methyl chloride distributions, *J. Geophys. Res.*, *106*, 34221–34233, 2001.

Lelieveld, J., Bregman, B., Arnold, F., Bürger, V., Crutzen, P. J., Fischer, H., Waibel, A., Siegmund, P., and van Velthoven, P. F. J., Chemical perturbation of the lowermost stratosphere through exchange with the tropopause, *Geophys. Res. Lett., 24,* 603-606, 1997.

Lelieveld, J., Bregman, B., Scheeren, H. A., Ström, J., Carslaw, K. S., Fischer, H., Siegmund, P. C., and Arnold, F., Chlorine activation and ozone destruction in the northern lowermost stratosphere, *J. Geophys. Res.*, *104*, 8201–8214, 1999.

Lelieveld, J., and Dentener, F. J., What controls tropospheric ozone?, *J. Geophys. Res.*, *105*, 3531–3551, 2000.

Lelieveld, J., Crutzen, P.J., Ramanathan, V., Andreae, M.O., Brenninkmeijer, C.A.M., Campos, T., Cass, G.R., Dickerson, R.R., Fischer, H., de Gouw, J. A., Hansel, A., Jefferson, A., Kley, D., de Laat, A. T. J., Lal, S., Lawrence, M. G., Lobert, J. M., Mayol-Bracero, O., Mitra, A. P., Novakov, T., Oltmans, S. J., Prather, K. A., Reiner, T., Rodhe, H., Scheeren, H. A., Sikka, D., and Williams, J.: The Indian Ocean Experiment: widespread air pollution from South and South-East Asia, Science, 291, 1031–1036,

2001.

Lelieveld, J., Berresheim, H., Bormann, S., Crutzen, P. J., Dentener, F. J., Fischer, H., Feichter, J., Flatau, P. J., Heland, J., Holzinger, R., Kormann, R., Lawrence, M. G., Levin, Z., Markowicz, K. M., Mihalopoulos, N., Minikin, A., Ramanathan, V., de Reus, M., Roelofs, G. -J., Scheeren, H. A., Scaire, J., Schlager, H., Schultz, M., Siegmund, P., Steil, B., Stephanou, E. G., Stier, P., Traub, M., Warneke, C., Williams, J., Ziereis, H., Global air pollution crossroads over the Mediterranean, *Science*, 298, 794–799, 2002.

Levitus, S., Antonov, J. I., Wang, J., Delworth, T. L., Dixon, K. W., Broccoli, A. J., Anthropogenic warming of the earth's climate system, *Science*, *292*, 267–270, 2001.

Levy, H., II, Normal atmosphere: Large radical and formaldehyde concentrations predicted, *Science*, *173*, 141–143, 1971.

Li, H. -J., Yokouchi, Y., Akimoto, H., Measurements of methyl halides in the marine atmosphere, *Atmos. Environ.*, *33*, 1881–1887, 1999.

Lindinger, W., Hansel, A., and Jordan, A., On-line monitoring of volatile organic compounds at pptv level by means of Proton-Tranfer-Reaction Mass Spectrometry (PTR-MS) - Medical applications, food control, and environmental research, *Int. J. Mass Spectrom. Ion Processes, 173*, 191–241, 1998.

Lobert, J. M., Scharffe, D. H., Hao, W. M., Crutzen, P. J., Importance of biomass burning in the atmospheric budgets of nitrogen-containing gases, *Nature*, *346*, 552–554, 1990.

Lobert, J. M., Scharffe, D. H., Hao, W. M., Kuhlbusch, T. A., Seuwen, R., Warneck, P., and Crutzen, P. J., Experimental evaluation of biomass burning emissions: Nitrogen and carbon containing compounds, in *Global Biomass Burning: Atmospheric Climatic and Biospheric Implications*, edited by J.S. Levine, pp. 289–304, *MIT Press*, Cambridge, Mass., 1991.

Lobert, J. M., Keene, W. C., Logan, J. A., and Yevich, R., Global chlorine emissions from biomass burning: Reactive Chlorine Emissions Inventory, *J. Geophys. Res.*, *104*, 8373–8389, 1999.

Markowicz, K. M., Flatau, P. J., Ramana, M. V., Crutzen, P. J., and Ramanathan, V., Absorbing Mediterranean aerosols lead to a large reduction in the solar radiation at the surface, *Geophys. Res. Lett.*, *29*(20), doi:10.1029/2002GL015767, 2002.

Martin, C. L., Fitzjarrald, D., Garstang, M., Oliveira, A. P., Greco, S., and Browell, E., Structure and growth of the mixing layer over the Amazonian rainforest, *J. Geophys. Res.*, *93*, 1361–1375, 1988.

Matsueda, H., Inoue, H. Y., Ishii, M., Aircraft observation of carbon at 8-13 km altitude over the western Pacific from 1993 to 1999, *Tellus*, *54B*, 1–21, 2002.

McCulloch, A., Aucott, M. L., Benkovitz, C. M., Graedel, T. E., Kleiman, G. K., Midgley, P. M., and Li, Y. -F., Global emissions of hydrogen chloride and chloromethane from coal combustion, incineration and industrial activities: Reactive Chlorine Emission Inventory, *J. Geophys. Res.*, *104*, 8391–8403, 1999a.

McCulloch, A., Aucott, M. L., Graedel, T. E., Kleiman, G. K., Midgley, P. M., and Li, Y. -F., Industrial emissions of trichloroethene, tetrachloroethene, and dichloroethane: Reactive Chlorine Emission Inventory, *J. Geophys. Res.*, *104*, 8417–8428, 1999b.

McCulloch, A., Aucott, M. L., Benkovitz, C. M., Graedel, T. E., Kleiman, G., Midgley, P. M., and Li, Y.-F., Global emissions of hydrogen chloride and chloromethane from coal

combustion, incineration and industrial activities: Reactive Chlorine Emissions Inventory, *J. Geophys. Res., 104*, 8391–8403, 1999.

Merrill, J. T., and Moody, J. L., Synoptic meteorology and transport during the North Atlantic Regional Experiment (NARE) intensive: Overview, *J. Geophys. Res.*, *101*, 29201–29211, 1996.

Millan, M. M., Salvador, R., Mantilla, E., Kallos, G., Photo-oxidant dynamics in the Mediterranean basin in summer: Results from European research projects, *J. Geophys. Res.*, *102*, 8811–8823, 1997.

Milne, P. J., Riemer, D. D., Zika, R. G., and Brand, L. E., Measurement of vertical distribution of isoprene in surface seawater and its emission from several phytoplankton monocultures, *Mar. Chem., 48*, 237–244, 1995.

Minikin, A., Mihalopolous, N., Economou, C., Sciare, J., Schneider, J., Levin, Z., Teller, A., Ganor, E., Stein, C., Berresheim, H., de Reus, M., Rasch, P., Chourdakis, G., and Papayannis, A., Tropospheric vertical profiles of aerosol properties in the eastern Mediterranean region in summer 2001 (MINOS campaign), submitted to *Atmos. Chem. Phys. Discuss.*, 2003.

Molina, M. J., and Rowland, F. S., Stratospheric sink for chlorofluoromethanes: chlorine atom-catalyzed destruction of ozone, *Nature*, *249*, 810–812, 1974.

Montzka, S. A., Butler, J. M., Myers, R. C., Thompson, T. M., Swanson, T. H., Clarke, A. D., Lock, L. T., and Elkins, J. W., Decline in tropospheric abundance of halogen from halocarbons: implication for stratospheric ozone depletion, *Science, 272*, 1318–1322, 1996.

Montzka, S. A., Butler, J. M., Elkins, J. W., Thompson, T. M., Clarke, A. D., and Lock, L. T., Present and future trends in the atmospheric burden of ozone depleting halogens, *Nature, 398*, 690–694, 1999.

Montzka, S. A., Spivakovsky, C. M., Butler, J. H., Elkins, J. W., Lock, L. T., and Mondeel, D. J., New observational constrains for atmospheric hydroxyl on global hemispheric scales, *Science, 288*, 500–503, 2000.

NOAA/CMDL, National Oceanic and Atmospheric Administration /Climate Monitoring and Diagnostics Laboratory, data dissemination via http://www.cmdl.noaa.gov/, 2003.

Olivier, J.G.J, A.F. Bouwman, C.W.M. van der Maas, J.J.M. Berdowski, C. Veldt, J.P.J. Bloos, A.J.H. Visschendijk, P.Y.J. Zandveld and J.L. Haverlag*,* Description of EDGAR version 2.0, *Report 771060 002*, Rijksintituut Voor Volksgezondheid en Milieu (RIVM), Bilthoven, The Netherlands, 1996.

Pöschl, U., Williams, J., Hoor, P., Fischer, H., Crutzen, P. J., Warneke, C., Holzinger, R., Hansel, A., Jordan, A., Lindinger, W., Scheeren, H. A., Peters, W., and Lelieveld, J., High acetone concentrations throughout the 0–12 km altitude range over the tropical rainforest in Surinam, *J. Atmos. Chem.*, *38*, 115–132, 2001.

Poulida, O., Dickerson, R., and Heymsfield, A., Stratosphere-troposphere exchange in a midlatitude mesoscale convective complex, *J. Geophys. Res.*, *101*, 6823–-6836, 1996.

Press, W. H., Teukolsky, S. A., Vetterling, W. T., and Flannery, B. P., Numerical Recipes in FORTRAN, 2nd ed., 963 pp., *Cambridge Univer. Press*, New York, 1992.

Prinn, R. G. Weiss, R. F., Fraser, P. J., Simmonds, P. G., Cunnold, D. M., Alya, F. N., O'Doherty, S., Salameh, P., Miller, B. R., Huang, J., Wang, R. H. J., Harley, D. E.,

Harth, C., Steele, L. P., Sturrock, G., Midley, P. M., McCulloch, A., A history of chemically and radiatively important gases in air deduced from ALE/GAGE/AGAGE, *J. Geophys. Res.*, *105*, 17751–17792, 2000.

Prinn, R. G., Huang, J., Weiss, R. F., Cunnold, D. M., Fraser, P. J., Simmonds, P. G., McCulloch, A., Harth, C., Salameh, P., O'Doherty, S., Wang, R. H. J., Porter, L., Miller B. R., Evidence for substantial variations of atmospheric hydroxyl radicals in the past two decades, *Science*, *292*, 1882–1888, 2001.

Rasmussen, R. A., Rasmussen, L. E., Khalil, M. A. K., and Dalluge, R. W., Concentration distribution of methyl chloride in the atmosphere, *J. Geophys. Res., 85,* 7350–7356, 1980.

Ravindranath, N.H., and Ramakrishna, J., Energy options for cooking in India, *Energy Policy, 25*, 63–75, 1997.

Ray, E. A., Moore, F. L., Elkins, J. W., Dutton, G. S., Fahey, D. W., Vömel, H., Oltmans, S. J., and Rosenlof, K. H., Transport into the Northern Hemisphere lowermost stratosphere revealed by in situ tracer measurements, *J. Geophys. Res.*, *104*, 26565–26580, 1999.

Redeker, R. C., Wang, N.-Y., Low, J. C., McMillian, M., Tyler, S. C., and Cicerone, R. J., Emissions of methyl halides and methane from rice paddies, *Science*, *290*, 966–969, 2000.

Rhew, R. C., Miller, B. J., and Weiss, R. F., Natural methyl bromide and methyl chloride emissions from coastal salt marshes, *Nature*, *403*, 292–295, 2000.

Roelofs, G. -J., Lelieveld, J., Tropospheric ozone simulation with a global chemistry-climate model: Influence of higher hydrocarbon chemistry, *J. Geophys. Res.*, *105*, 22697–227112, 2000.

Roelofs, G.-J., Scheeren, H. A., Kentarchos, T., and Lelieveld, J., Distribution and origin of ozone in the eastern Mediterranean free troposphere, *Atmos. Chem. Phys. Discuss.*, *3*, 1247–1272, 2003.

Rood, R. B., Douglass, A. R., Cerniglia, M. C., Read, W. G., Synoptic-scale mass exchange from the troposphere to the stratosphere, *J. Geophys. Res.*, *102*, 23467–23485, 1997.

Rudolph, J., Ehhalt, D. H., and Tönnissen, A., Vertical profiles of ethane and propane in the stratosphere, *J. Geophys. Res.*, *86*, 7267–7272, 1981.

Rudolph J., Khedim, A., Koppmann, R., and Bonsang, B.: Field study of the emissions of methyl chloride and other halocarbons from biomass burning in Western Africa, *J. Atmos. Chem.*, *22*, 67–80, 1995.

Rudolph, J., von Czapiewski, K., and Koppmann, R., Emissions of methyl chloroform (CH_3CCl_3) from biomass burning and the tropospheric methyl chloroform budget, *Geophys. Ress. Lett., 27*, 1887–1890, 2000.

Rudolph, J., Measurement of Nonmethane hydrocarbons in the atmosphere, in *Volatile organic compounds in the Troposphere*, edited by R. Koppmann, and D. H. Ehhalt, Proceedings of the Workshop on Volatile Organic Compounds in the Troposphere, Juelich (Germany) October 27-31, 1997, *Schriftenreihe des Forschungszentrum Jülich*, *16*, 11–35, 1999.

Saini, H. S., Attieh, J. M., and Hanson, A. D., Biosynthesis of halomethanes and methanethiol by higher plants via a novel methyltransferase reaction, *Plant, Cell and*

Environment, *18*, 1075–1033, 1995.

Scheele, M. P., Siegmund, P. C., and van Velthoven, P. F. J., Sensitivity of trajectories to data resolution and its dependence on the starting point: In or outside a tropopause fold, *Meteorol. Appl.*, *3*, 267–273, 1996.

Scheeren, H. A., Lelieveld, J., de Gouw, J. A., van der Veen, C., and Fischer, H.: Methyl chloride and other chlorocarbons in polluted air during INDOEX, *J. Geophys. Res.*, *107*, doi:10.1029/2001JD001121, 2002.

Scheeren, H. A., Lelieveld, J., Roelofs, G. J., Williams, J., Fischer, H., de Reus, M., de Gouw, J. A. , Warneke, C., Holzinger, R., Schlager, H., Klüpfel, T., Bolder, M., van der Veen, C., and Lawrence, M., The impact of monsoon outflow from India and Southeast Asia in the upper troposphere over the eastern Mediterranean, *Atmos. Chem. Phys. Discuss.*, *3*, 2285–2330, 2003.

Scheeren, H. A., Lelieveld, J., Williams, J., Fischer, H., and Warneke, C., Measurements of reactive chlorocarbons over the Surinam tropical rainforest: indications for strong biogenic emissions, submitted to *Atmos. Chem. Phys. Discuss.*, 2003.

Seo, K. –H., and Bowman, K. P., A climatology of cross-tropopause exchange, *J. Geophys. Res.*, *106*, 28159–28172, 2001.

Singh, H. B., Kanakidou, M., Crutzen, P. J., and Jacob, D. J., High concentrations and photochemical fate of oxygenated hydrocarbons in the global troposphere, *Nature*, *378*, 50–54, 1995.

Singh, H. B., Chen, Y., Gregory, G. L., Sachse, G. W., Talbot, R., Blake, D. R., Kondo, Y., Bradshaw, J. D., Heikes, B., and Thornton, D., Trace chemical measurements from the northern midlatitude lowermost stratosphere in early spring: Distributions, correlations, and fate, *Geophys. Res. Lett.*, *24*, 127–130, 1997.

Singh, H., Chen, Y., Tabazadeh, A., Fukui, Y., Bey, I., Yantosca, R., Jacob, D., Arnold, F., Wohlfrom, K., Atlas, E., Flocke, F., Blake, D., Blake, N., Heikes, B., Snow, J., Talbot, R., Grogory, G., Sache, G., Vay, S., and Kondo, Y., Distribution and fate of selected oxygenated organic species in the troposphere and lower stratosphere over the Atlantic, *J. Geophys. Res.*, *105*, 3795–3805, 2000.

Sinha, C. S., Sinha, S., and Joshi, V., Energy use in the rural areas of India: setting up a rural energy data base, *Biomass and Bioenergy, 14*, 489–503, 1998.

Solomon, S., Garcia, R. R., Rowland, F. S., and Weubbles, D. J., On the depletion of Antarctic ozone, *Nature*, *321*, 755–758, 1986.

Spreng, S., and Arnold, F., Balloon-borne mass spectrometer measurements of HNO_3 and HCN in the winter Arctic stratosphere – Evidence for HNO_3 processing by aerosols, *Geophys. Res. Lett.*, *21*, 1251–1254, 1994.

Sprenger, M., and Wernli, H., A northern hemispheric climatology of cross-tropopause exchange for the ERA15 time period (1979-1993), submitted to *J. Geophys. Res.,* 2002.

Stevenson, D., Johnson, C., Collins, B., and Derwent, D., Projected changes in global tropospheric ozone to 2030, poster at the *International Global Atmospheric Chemistry (IGAC) conference*, Crete, Greece, 2002.

Stohl, A., Computation, accuracy and applications of trajectories – A review and bibliography, *Atmos. Environ.*, *32*, 947–996, 1998.

Stohl, A., and Trickl, T., A textbook example of long-range transport: Simultaneous

observations of ozone maxima of stratospheric and North American origin in the free troposphere over Europe, *J. Geophys. Res.*, *104*, 30445–30462, 1999.

Stohl A., Haimberger, L., Scheele, M. P., Wernli, H., An intercomparison of results from three trajectory models, *Meteorol. Appl.*, *8*, 127–135, 2001.

Strahan, S. E., Douglas, A. R., Nielsen, J. E., and Boering, K. A., The CO_2 seasonal cycle as a tracer of transport, *J. Geophys. Res.*, *103*, 13729–13741, 1998.

Streets, D. G., and Waldhoff, S. T., Greenhouse-gas emissions from biofuel combustion in Asia*, Energy, 24*, 841–855, 1999.

Traub, M., Fischer, H., de Reus, M., Kormann, R., Heland, J., Ziereis, H., Schlager, H., Holzinger, R., Williams, J., Warneke, C., de Gouw, J., and Lelieveld, J., Chemical characteristics assigned to trajectory clusters during the MINOS campaign, *Atmos. Chem. Phys.*, *3*, 459–468, 2003.

Urhahn, T., Ballschmiter, K., Chemistry of the biosynthesis of halogenated methanes, C_1-organohalogens as pre-industrial chemical stressors in the environment, *Chemosphere*, *37*, 1017–1032, 1998.

Van Aardenne, Dentener, F. J., Olivier, J. G. J., Klein Goldewijk, C. G. M., and Lelieveld, J., A 1º × 1º resolution data set of historical anthropogenic trace gas emissions for the period 1890 – 1990, *Global Biogeochemical Cycles*, *15*, 909–928, 2001.

Varner, R. K., Crill, P. M., and Talbot, R. W., Wetlands: a potentially significant source of atmospheric methyl bromide and methyl chloride, *Geophys. Res. Lett.*, *26*, 2433–2436, 1999.

Varns, J. L., The release of methyl chloride from potato tubers, American Potato Journal, 59, 593–604, 1982.

Vaughan, G., and C. Timmins, Transport of near-tropopause air into the lower midlatitude stratosphere, *Q. J. R. Meteorol. Soc.*, *124*, 1559–1578, 1998.

Veldt, C., and Berdowski, J. J. M., GEAI-note on the combustion of biomass fuels (emission factors for CO, CH_4 and NMVOC), *TNO Rep. R94/218*, Institute of Environmental Science, Netherlands Organization for Applied Scientific Research, Delft, The Netherlands, 1995.

Verver, G., Zachariasse, M., Sikka, D., and Stossmeister, G., Overview of the meteorological conditions and atmospheric transport processes during the INDOEX IFP 1999, *J. Geophys. Res., 106*, 28399–38414, 2001.

Volk, C. M., Elkins, J. W., Fahey, D. W., Dutton, G. S., Gilligan, J. M., Loewenstein, M., Podolske, J. R., Chan, K. R., and Gunson, M. R., On the evaluation of source gas lifetimes from stratospheric observations*, J. Geophys. Res.*, *102*, 25543–25564, 1997.

Warneke, C., Holzinger, R., Hansel, A., Jordan, A., Lindinger, W., Williams, J., Pöschl, U., Hoor, P., Fischer, H., Crutzen, P. J., Scheeren, H. A., Lelieveld, J., Isoprene and its oxidation products methyl vinyl ketone, methacrolein and isoprene peroxides measured online over the tropical rainforest of Surinam in March 1998, *J. Atmos. Chem.*, *38*, 167–185, 2002.

Watling, R., and Harper, D. B., Chloromethane production by wood-rotting fungi and an estimate of the global flux to the atmosphere, *Mycol. Res.*, *102*, 769–787, 1998.

Wernli, H., M. Bourqui, A Lagrangian “1-year climatology” of (deep) cross-tropopause exchange in the extratropical Northern Hemisphere, *J. Geophys. Res.*, *107*, doi:10.1029/2001JD000812, 2002.

Wiedmann, T. O., Güthner, B., Class, T., Ballschmiter, K., Global distribution of tetrachloroethene in the troposphere, measurements and modeling, *Environ. Sci. Techn.*, *28*, 2321–2329, 1994.

Wienhold, F. G., Fischer, H., Hoor, P., Wagner, V., Königstedt, R., Harris, G. W., Anders, J., Grisar, R., Knothe, M. Riedel, W. J., Lübken, F. -J., and Schilling, T.: TRISTAR – a tracer in-situ TDLAS for atmospheric research, *Appl. Phys. B*, 67, 411–417, 1998.

Williams, M. R., and Fisher, T. R., Chemical composition and deposition of rain in the Cetral Amazon, Brazil, *Atmos. Environ.*, *31*, 207–217, 1997.

Williams, J., Fischer, H., Wong, S., Crutzen, P. J., Scheele, R., and Lelieveld, J., Near equatorial CO and O_3 profiles over the Indian Ocean during the winter monsoon: High O_3 levels in the middle troposphere and of interhemispheric exchange, *J. Geophys. Res., 107*, doi:10.1029/2001JD001126, 2002.

Williams, J., Fischer, H., Harris, G. W., Crutzen, P. J., Hoor, P., Hansel, A., Holzinger, R., Warneke, C., Lindinger, W., Scheeren, B., and Lelieveld, J., Variability-lifetime relationship for organic trace gases: A novel aid to compound identification and estimation of HO concentrations, *J. Geophys. Res.*, *105*, 20473–20486, 2001a.

Williams, J., Fischer, H., Hoor, P., Pöschl, U., Crutzen, P. J., Andreae, M. O., and Lelieveld, J., The influence of the tropical rainforest on atmospheric CO and CO_2 as measured by aircraft over Surinam, South America, *Chemosphere – Global Change Science*, *3*, 157–170, 2001b.

Williams, J, Pöschl, U., Crutzen, P. J., Hansel, A., Holzinger, R., Warneke, C., Lindinger, W., Lelieveld, J., An atmospheric chemistry interpretation of mass scans obtained from a Proton Transfer Mass Spectrometer flown over the Tropical Rainforest of Surinam, *J. Atmos. Chem.*, *38*, 133–166, 2001c.

Wohlfrom, K.-H., Hauler, T., Arnold, F., Singh, H., Acetone in the free troposphere and lower stratosphere: Aircraft-based CIMS and GC measurements over the North Atlantic and first comparison, *Geophys. Res. Lett.*, *26*, 2849–2852, 1999.

World Resources Institute (WRI), Global Motor Vehicle Fleet, on http://www.wri.org/wr-98-99/autos2.htm, Washington D.C, USA, 2002.

Yokouchi, Y., Noijiri, Y., Barrie, L. A., Toom-Suantry, D., Machida, T., Inuzaka, Y., Akimoto, H., Li, H. -J., Fujinuma, Y., and Aoki, S.: A strong source of methyl chloride to the atmosphere from tropical coastal land, *Nature*, *403*, 295–298, 2000.

Yokouchi, Y., Ikeda, M., Inuzuka, Y., and Yukawa, T., Strong emission of methyl chloride from tropical plants, *Nature*, *412*, 163–165, 2002.

Zahn, A., Constraints on 2-way transport across the Arctic tropopause based on O_3 stratospheric tracer (SF_6) ages, and water vapor isotope (D, T) tracers, *J. Atmos. Chem.*, *39*, 303–325, 2001.

Ziereis, H., Schlager, H., Schulte, P., Köhler, I., Marquardt, R., and Feigl, C., In situ measurements of the NOx distribution and variability over the eastern North Atlantic, *J, Geophys. Res.*, *104*, 16021–16032, 1999.

Zimmerman, P. R., Greenberg, J. P., and Westberg, C. E., Measurements of atmospheric hydrocarbons and biogenic emission fluxes in the Amazon boundary layer, *J. Geophys. Res.*, *93*, 1407–1416, 1988.

Summary

This thesis focuses on measurements of chemical reactive C_2 – C_7 non-methane hydrocarbons (NMHC) and C_1 – C_2 chlorocarbons with atmospheric lifetimes of a few hours up to about a year. The group of reactive chlorocarbons includes the most abundant atmospheric species with large natural sources, which are chloromethane (CH_3Cl), dichloromethane (CH_2Cl_2), and trichloromethane ($CHCl_3$), and tetrachloroethylene (C_2Cl_4) with mainly anthropogenic sources. NMHC and chlorocarbons are present at relatively low quantities in our atmosphere (10^{-12} – 10^{-9} mol mol^{-1} of air). Nevertheless, they play a key role in atmospheric photochemistry. For example, the oxidation of NMHC plays a dominant role in the formation of ozone in the troposphere, while the photolysis of chlorocarbons contributes to enhanced ozone depletion in the stratosphere. In spite of their important role, however, their global source and sinks budgets are still not completely understood.

The overall aim of this thesis is to improve our understanding of the sources, distribution, and chemical role of reactive NMHC and chlorocarbons in the troposphere and lower stratosphere. To meet this aim, a comprehensive data set of selected C_2 – C_7 NMHC and chlorocarbons has been analyzed, derived from six aircraft measurement campaigns with two different jet aircrafts conducted between 1995 and 2001. The measurement locations include tropical, midlatitude and polar regions between the equator to about 70ºN, covering different seasons and pollution levels in the troposphere and lower stratosphere. Of special interest in this research are the tropical regions because they are becoming increasingly important in terms of global anthropogenic pollution and climate change. In addition, natural emissions of hydrocarbons (notably isoprene and terpenes from plants) and reactive chlorocarbons appear to be concentrated in the tropics, where the largest uncertainties exist with respect to source type and source strength.

Whenever available, the reactive NMHC and chlorocarbon data have been analyzed with the help of concurrent measurements, which includes ozone (O_3), carbon monoxide (CO), nitrogen oxide (NO), total reactive oxidized nitrogen (NO_y), nitrous oxide (N_2O), carbon dioxide (CO_2), methane (CH_4), acetone (CH_3COCH_3), methanol (CH_3OH), acetonitrile (CH_3CN), the chlorofluorocarbons CFC-11 (CCl_3F) and CFC-12 (CCl_2F_2), the hydrofluorocarbon HFC-134a (CH_2FCF_3), and the hydrochlorofluorocarbons HCFC-141b (CH_3CCl_2F) and HCFC-142b (CH_3CClF_2). These additional measurements provide important information about the air mass origin, pollution sources, and chemical age of the encountered air masses. For example, CH_3CN is a well established tracer for biomass burning emissions. We note that the measured C_2 – C_7 NMHC and long-lived chlorocarbons (e.g. CFCs) are mainly used as source tracers and indicators of the photochemical age of an air mass. Uncertainties in the global budgets of these species are considerably smaller than those of reactive chlorocarbons and are therefore not a major objective of this study.

The specific scientific objectives of this study can be summarized as follows:

1. To augment the sparse availability of NMHC and chlorocarbons measurements in the free troposphere and lower stratosphere, in particular in the tropics.

2. To investigate the role of cross-tropopause isentropic transport on the reactive C_2 – C_6 NMHC and acetone budget of the extra-tropical lowermost stratosphere at different seasons.
3. In relation to objective 2: To assess the impact of observed acetone concentrations on the OH radical concentration in the lowermost stratosphere.
4. To improve our understanding of cross-tropopause mixing timescales.
5. To improve our insight in the global source budgets of the reactive chlorocarbon CH_3Cl, CH_2Cl_2, $CHCl_3$, and C_2Cl_4, in particular in the role of tropical emissions.
6. To investigate the role of tropical deep convection in the vertical transport and redistribution of Asian pollution over the Northern Hemisphere and the impact of Asian air pollution on tropospheric chemistry.

The first research objective is addressed by presenting the NMHC and chlorocarbon measurements in this thesis and by making these data available to the atmospheric chemistry research community.

In Chapter 2 of this thesis the research objectives 2 – 4 are addressed. We present measurements of C_2 – C_6 NMHC from canister air samples, which have been obtained in the extratropical upper troposphere and lower stratosphere during the fall (November/December 1995), winter (March 1997) and summer seasons (July 1998) as part of the different Stratosphere Troposphere Experiments by Aircraft Measurements (STREAM) campaigns. The STREAM project focused on the region of the upper troposphere and lowermost stratosphere and investigated dynamical exchange processes associated with synoptic disturbances (e.g. frontal activity) that affect ozone chemistry. The measurement flights were carried out with the Dutch Cessna Citation jet aircraft (operated by the Delft University of Technology) from Amsterdam (the Netherlands) during fall, from Kiruna (Sweden) during winter, and from Timmins (Ontario, Canada) during summer. The NMHC measurements presented here, have been evaluated along with concurrent in situ measurements of acetone, CO, O_3, N_2O, and CFC-12. We found that the vertical distributions of NMHC and acetone as a function of ozone and potential temperature in the lowermost stratosphere show a strong seasonality. The observed NMHC + acetone concentrations in the lowermost stratospheric mixing layer equaled during summer and fall (2.3 ± 1.7 mol^{-9} mol^{-1} C (ppbC) and 2.2 ± 0.5 ppbC, respectively) and were more than a factor of two higher than during winter (0.9 ± 0.3 ppbC).

Enhanced concentrations of NMHC + acetone were found during July up to potential temperatures of Θ = 370 K, whereas during March this is limited to Θ = 340 K, in agreement with stronger isentropic cross-tropopause transport during summer. Model studies indicate that intensified mixing at the sub-tropical tropopause during summer is driven by the Asian and Mexican monsoon circulations. We observed increasing methyl chloride (CH_3Cl) concentrations with altitude during July. Because CH_3Cl shows a global trend of increasing concentrations towards lower latitudes, the enhanced CH_3Cl points to intensified mixing at the (sub-)tropical tropopause in agreement with model studies.

The relatively large acetone concentrations observed in the lowermost stratosphere (up to ~1 ppbv) as compared to NMHC, especially during summer, emphasize the dominance of terrestrial vegetation and of oceanic sources in the upper tropospheric acetone budget. Acetone photolysis can be an important source of OH and HO_2 radicals in the upper troposphere and lower stratosphere. Box model calculations indicate that the observed

acetone levels of 0.5 to 1 ppbv can explain 30 to 50% of the enhanced OH concentrations in the summertime lowermost stratosphere.

Using mass balance calculations, we show that a significant tropospheric fraction (≤30%) could be identified up to Θ = 370 K in the summertime lowermost stratosphere. During winter, however, the tropospheric fraction approached zero already at about Θ = 350 K. Again, this points to intensified cross-tropopause transport during mixing

Based on a modified mass balance calculation, we present and demonstrate a simple method to estimate the photochemical age of a tropospheric air parcel in the stratospheric mixing layer. The method uses the decay of reactive organic species propane and acetylene in the mixing layer, with photochemical lifetimes of a few weeks during summer. The concentration of these species in the lowermost stratosphere is determined by the upper tropospheric "source-concentration", the mixing intensity, and the photochemical lifetime of these species in the stratosphere (depending on the OH concentration). The method gives us an indication of timescales of (isentropic) troposphere-to-stratosphere mixing, indicating the transit time between the mixing event and the encounter with the measurement aircraft. From a number of selected troposphere-to-stratosphere mixing events, with acetylene and propane concentrations of 25 – 80 pptv (well above their detection limit of ~5 pptv), we calculated mixing timescales of 3 to 14 days. These results corroborate earlier studies, demonstrating that the summertime midlatitude lowermost stratosphere is subject to intense and frequent mixing with tropospheric air.

Chapter 3 of this thesis concentrates on pollution outflow from India and Southeast Asia observed during the 1999 Indian Ocean Experiment (INDOEX) campaign (research objective 5). We present measurements of C_2 – C_6 NMHC and selected chlorocarbons from air samples collected with the Dutch Cessna Citation jet aircraft operating from the Maldives over the northern Indian Ocean during February and March 1999. In general, the INDOEX study aimed at improving our understanding of the large and increasing role of Asian emissions in global atmospheric chemistry and air quality.

In this thesis, we focus on the sources of enhanced levels of reactive chlorocarbons with special emphasis on the most abundant natural chlorocarbon CH_3Cl, with oceans and biomass burning as major established sources. Estimates of global emissions still suffer from large uncertainties, mostly for the tropics. This is partly due to a lack of measurements. We found strongly enhanced CH_3Cl and related combustion tracers (CO, hydrocarbons and CH_3CN) over the Indian Ocean We relate this to extensive biofuel use, notably the burning of agricultural waste and dung in India and Southeast Asia, with emphasis on the low burning efficiency of residential and small-industrial fires and the high chlorine content of these fuels compared to wood. As a consequence, we deduce a relatively high emission ratio relative to CO ($\Delta CH_3Cl/\Delta CO$) of $1.74 \pm 0.21 \times 10^{-3}$ mol mol^{-1}, compared to a mean value of 0.57×10^{-3} mol mol^{-1} used for biofuel emissions in a recent comprehensive global emission inventory. Hence, we point out that the contribution to CH_3Cl emissions from the use of biofuels might previously have been underestimated by 30-35% for India and Southeast Asia.

The combined estimated emissions of CH_3Cl from oceans and all biomass burning sources (including natural) account only for half the modeled sinks (~ 4×10^{12} g yr^{-1}). The other half remains to be accurately quantified (this is further addressed in Chapter 5). By extrapolating the INDOEX $\Delta CH_3Cl/\Delta CO$ emission ratio to a global scale, we can justify about 14% of the missing CH_3Cl source. In addition to CH_3Cl, we infer small biomass

burning sources for CH_2Cl_2 and $CHCl_3$ as well. Indications for biomass burning emissions of methyl chloroform (CH_3CCl_3) are not found. The results in Chapter 3 improve our insight on the important role of tropical biomass burning emissions in global budgets of reactive chlorocarbons.

In Chapter 4 of this thesis, we present a variety of trace gas measurements obtained with the DLR Falcon jet aircraft (German Aerospace Organization) operating from Crete over the eastern Mediterranean during the August 2001 Mediterranean Intensive Oxidant Study (MINOS) campaign. The eastern Mediterranean region is one of the most polluted regions in the world in terms of photochemical ozone formation and aerosol loading. The objective of the MINOS project was to improve our understanding of the transport processes, chemical mechanisms, and main pollution sources that determine the chemical composition in the Mediterranean troposphere.

We use ten-day backward trajectories and a coupled chemistry-climate model (ECHAM4) to study the air mass origin and chemistry of the upper troposphere between 6 and 13 km altitude. This part of the troposphere is dominated by long-range transport processes. We focus on a large pollution plume encountered over the eastern Mediterranean between August 1 and 12, originating in South Asia (India and Southeast Asia), referred to as the Asian plume, associated with deep convection and long-range transport in the Asian Summer Monsoon (research objective 6). Vertical as well as longitudinal gradients of NMHC, halocarbons, O_3, NO_y, CH_4, CO, CO_2, acetone, CH_3OH, and CH_3CN are presented, showing the chemical impact of the Asian plume compared to westerly air masses, containing pollution from North America. In agreement with observations from the 1999 INDOEX campaign, we find that the Asian plume shows a clear signature of biomass burning (notably from the use of biofuels) by enhanced concentrations of CO, C_2H_2, C_6H_6, CH_3CN, and the chlorocarbons CH_3Cl and $CHCl_3$. Acetone levels in the Asian plume were of the same magnitude as those observed in the westerlies, exceeding upper tropospheric background levels. CH_3OH levels were higher in the Asian plume, which we related to Asian biofuel burning emissions. The mean photochemical age of the Asian pollution was estimated to be about 2 weeks, consistent with trajectory analysis. Concentrations of the new automobile cooling agent HFC-134a were significantly lower in the Asian plume than in air masses from North America, making it a suitable tracer for western pollution. In addition, we found a significant positive correlation between CO_2 and HFC-134a concentrations in the westerlies, which we relate to extensive fossil fuel use in North America.

In spite of high levels of ozone precursors (CO, hydrocarbons) in the Asian plume, we observed that ozone concentrations are still relatively low (~55 ppbv). Ozone show no clear relationship with higher hydrocarbons, which suggests a NO_x-limited photochemical ozone production regime. This might change in the future. ECHAM4 model simulations indicate that the expected increase of NO_x emissions in Asia in the next 25 years (due to the expected strong increase of fossil fuel use) could enhance the photochemical ozone production in the Asian plume by about 14%. Considering the size of the Asian plume, this may have a significant impact on the ozone contribution to radiative forcing in the Northern Hemisphere (presently, the radiative forcing by O_3 is about 25% of the forcing of CO_2).

Finally, we point out that the size and location of the Asian plume near the tropopause provides an important potential for pollution transport into the lowermost stratosphere (as described in Chapter 2). Indeed, we present observations which provide first indications of Asian pollution transport into the lower stratosphere. Clearly, more research is needed

here.

The role of tropical emissions on the global budgets of the reactive chlorocarbons CH_3Cl, CH_2Cl_2, $CHCl_3$, and C_2Cl_4 is further explored in Chapter 5 of this thesis. The magnitude of natural sources in the global budgets of these species is still poorly constrained. Here, we present measurements of NMHC and chlorocarbons from air samples collected in the boundary layer and free troposphere over Surinam during March 1998 (in the short dry season). The air samples were obtained on-board the Dutch Cessna Citation jet aircraft during the March 1998 Large-scale Biosphere-atmosphere experiment in Amazonia – Cooperative LBA Airborne Regional Experiment (LBA/CLAIRE) campaign. The NMHC and chlorocarbons measurements have been analyzed with the help of concurrent measurements of CO, acetone and CH_3CN (as a tracer of biomass burning).

A main objective of LBA/CLAIRE was to improve our knowledge on the exchange of trace gases and aerosols between the pristine tropical rainforest and the atmosphere important for atmospheric chemistry in the tropics. We find that the free troposphere above 8 km altitude was strongly affected by deep convective outflow associated with the Inter Tropical Convergence Zone (the ITCZ cloud-band form the South American monsoon), located a few degrees south of Surinam. More importantly, we find a significant positive gradient of the CH_3Cl, $CHCl_3$, and C_2Cl_4 concentration in the 1500 m thick mixing layer between the Surinam coast and the Brazilian border at 6°S, in the absence of significant pollution sources. These gradients point to important biogenic sources, which corroborate recent reports on CH_3Cl emissions from tropical plants. No correlation of CH_2Cl_2 with latitude was found.

The change of chlorocarbon concentration as a function of air mass residence time over the rainforest has been used to calculate an emission factor in pptv h^{-1}, representative for the Surinam tropical rainforest ecosystem (sum of emissions from microbiological soil processes, fungal decomposition of wood, as well as direct emission from plants). Hence, we deduce fluxes from the Surinam rainforest of 7.6 ± 1.8 μg CH_3Cl m^{-2} h^{-1}, 1.11 ± 0.08 μg $CHCl_3$ m^{-2} h^{-1}, and 0.36 ± 0.07 μg C_2Cl_4 m^{-2} h^{-1}. Extrapolated to a global scale, our emission estimates suggest a large potential source of ~2 Tg CH_3Cl yr^{-1} from tropical forests, which could account for the net budget discrepancy (underestimation of sources), as indicated previously (see Chapter 3). Hence, our measurement emphasize that tropical forests are the most important source of organic chlorine to the atmosphere. In addition, our estimates suggest a potential emission of 57 ± 17 Gg C_2Cl_4 yr^{-1} from tropical forest soils, equal to half of the currently missing C_2Cl_4 sources. Finally, we show that there are strong indications that the reduction of tropical forest area over the past 20 years could largely explain the observed downward trend in atmospheric CH_3Cl.

Summarizing, this thesis presents a unique and comprehensive data set of NMHC and chlorocarbon trace gases. The data augment the sparse availability of NMHC and chlorocarbons measurements in the free troposphere and lower stratosphere, in particular in the tropics. The NMHC and acetone measurements from STREAM contribute to our understanding of the role of reactive organic trace species in the lower stratosphere, notably on the OH budget. Additionally, new insights in the mixing timescales and importance of quasi-horizontal (isentropic) cross-tropopause transport are obtained. The impact of Asian pollution redistributed by the ITCZ on a hemispheric scale in the free troposphere, has been described and analyzed. Finally, our understanding of the role of tropical sources in the global budget of reactive chlorocarbons has been greatly improved.

Samenvatting

Dit proefschrift concentreert zich op metingen van chemisch reactieve C_2 – C_7 koolwaterstoffen (KW) en C_1 – C_2 chloorkoolwaterstoffen (Cl-KW) met een atmosferische levensduur variërend van een paar uur tot ongeveer een jaar. De groep van reactieve chloorkoolwaterstoffen omvat een aantal van de meest voorkomende organische chloorverbindingen in de atmosfeer met belangrijke natuurlijke bronnen (bijvoorbeeld oceanen), waaronder chloormethaan (CH_3Cl), dichloormethaan (CH_2Cl_2) en trichloormethaan of chloroform ($CHCl_3$), alsmede tetrachlooretheen (C_2Cl_4), dat voornamelijk industriële bronnen heeft. KW en Cl-KW komen in relatief lage concentraties voor in onze atmosfeer (10^{-12} – 10^{-9} mol mol^{-1} lucht) en vallen daarmee onder de groep van zogenaamde sporengassen. Toch spelen ze een zeer belangrijke rol in de chemie van de atmosfeer. De oxidatie van KW bijvoorbeeld, speelt een dominante rol in de fotochemische vorming van ozon in de troposfeer, terwijl de fotolyse van Cl-KW als bron van Cl-radicalen in de stratosfeer bijdraagt aan versterkte ozonafbraak. Ondanks de belangrijke rol van deze componenten in de atmosferische chemie is de kwantitatieve kennis over de voornaamste mondiale bronnen en verwijderingprocessen nog relatief gering.

Het belangrijkste doel van dit proefschrift is het verbeteren van ons begrip van de bronnen, distributieprocessen en chemische rol van reactieve KW en Cl-KW in de tropopsfeer en lagere stratosfeer. Om dit doel te bereiken is een uitgebreide dataset van geselecteerde C_2 – C_7 KW en Cl-KW geanalyseerd, die verkregen is uit zes verschillende vliegtuigmeetcampagnes uitgevoerd tussen 1995 en 2001. De meetlocaties bevinden zich in tropische, gematigde en polaire gebieden gelegen tussen de evenaar en 70ºN, waarbij gemeten is onder verschillende seizoenscondities en vervuilingsgraden in de troposfeer en lagere stratosfeer. Om verschillende redenen nemen de tropen in dit proefschrift een bijzondere plaats in. De tropen worden steeds belangrijker in termen van mondiale luchtvervuiling en de daarbij te verwachten klimaatsverandering. Daarnaast blijkt dat natuurlijke emissies van KW (met name in de vorm van isopreen en terpenen uit planten) en Cl-KW zich concentreren in de tropen, waar tevens de grootste onzekerheden bestaan met betrekking tot brontype en bronsterkte.

Daar waar mogelijk zijn de data van de reactieve KW en Cl-KW geanalyseerd aan de hand van gelijktijdige metingen van andere sporengassen, waaronder ozon (O_3), koolstofmonoxide (CO), stikstofmonoxide (NO), totaal reactief geoxideerd stikstof (NO_y), distikstofoxide (N_2O), koolstofdioxide (CO_2), methaan (CH_4), aceton (CH_3COCH_3), methanol (CH_3OH), acetonitril (CH_3CN), de chloorfluorkoolwaterstoffen CFK-11 (CCl_3F) en CFK-12 (CCl_2F_2), de hydrofluorkoolwaterstof HFK-134a (CH_2FCF_3), en de hydrochloorfluorkoolwaterstoffen HCFK-141b (CH_3CCl_2F) and HCFK-142b (CH_3CClF_2). Deze additionele metingen geven belangrijke extra informatie over de herkomst van de luchtmassa's, de vervuilingsbronnen, en de chemische levensduur van de onderzochte lucht (vanaf de emissiebron). Zo is CH_3CN een belangrijke indicator voor emissies van biomassa verbranding. De metingen van C_2 – C_7 KW en de langlevende Cl-KW (b.v. CFK's) zijn voornamelijk gebruikt als indicatoren voor de (antropogene) herkomst en de chemische levensduur van de luchtmassa's. Omdat de onzekerheden in de mondiale budgetten van deze componenten aanzienlijk kleiner zijn dan die voor de groep van reactieve Cl-KW, wordt hieraan in dit

proefschrift geen verdere aandacht aan besteed.

We kunnen de specifieke onderzoeksdoelen die in dit proefschrift aan bod komen als volgt omschrijven:

1. Het vergroten van de beschikbaarheid van KW- en Cl-KW metingen in de vrije troposfeer en lagere stratosfeer.
2. Het onderzoeken van de rol van horizontaal troposfeer-naar-stratosfeer-transport op de budgetten van reactieve KW en Cl-KW in de lagere stratosfeer onder verschillende seizoenscondities.
3. In samenhang met punt 2: Het onderzoeken van de invloed van waargenomen acetonconcentraties op de concentratie van het OH-radicaal (de belangrijkste oxidant in de atmosfeer) in de lagere stratosfeer.
4. Het verbeteren van ons begrip van de tijdschalen van horizontaal troposfeer-naar-stratosfeer-transport.
5. Het vergroten van onze kennis van de mondiale budgetten van de reactieve Cl-KW CH_3Cl, CH_2Cl_2, $CHCl_3$ en C_2Cl_4, met nadruk op de rol van tropische emissiebronnen.
6. Onderzoek naar de rol van tropische diepe convectie in het verticaal transport en de herverdeling van Aziatische luchtvervuiling over het Noordelijk Halfrond en de invloed daarvan op de chemie van de troposfeer.

De eerste onderzoeksdoelstelling wordt bereikt door het presenteren van de KW en Cl-KW metingen in dit proefschrift en het beschikbaar maken van de data aan de atmosferisch chemische onderzoeksgemeenschap.

In Hoofdstuk 2 van dit proefschrift wordt aandacht besteed aan de onderzoeksdoelen 2 – 4. Er worden metingen gepresenteerd van C_2 – C_6 KW uit luchtmonsters, die zijn verzameld in roestvrijstalen monsterflessen (canisters) in de hogere troposfeer en lagere stratosfeer gedurende de herfst (november/december 1995), de winter (maart 1997) en de zomer (juli 1998), als onderdeel van de verschillende “Stratosphere Troposphere Experiments by Aircraft Measurements” (STREAM) campagnes. De STREAM campagnes waren gericht op het overgangsgebied tussen de troposfeer en de lagere stratosfeer (de onderste 6 km van de stratosfeer), de uitwisseling tussen beide regimes en de effecten van die uitwisselingsprocessen op de locale chemie. De vluchten zijn uitgevoerd met het Nederlandse Cessna Citation laboratoriumstraalvliegtuig (onder beheer van de Technische Universiteit Delft) vanuit Schiphol Amsterdam tijdens de herfst, vanuit Kiruna (noord Zweden) tijdens de winter en vanuit Timmins (Ontario, Canada) tijdens het zomerseizoen. De gepresenteerde metingen zijn geanalyseerd aan de hand van gelijktijdige metingen die gedaan zijn van aceton, CO, O_3, N_2O en CFK-12.

Er is gevonden dat de verticale verdeling van KW en aceton, als functie van de ozonconcentratie en potentiële temperatuur (Θ), een sterke seizoensafhankelijkheid te zien geeft. (De potentiële temperatuur is de temperatuur van de lucht als die onder adiabatische condities naar 1000 mbar wordt gebracht. In de stratosfeer neemt de Θ sterk toe met de hoogte). De waargenomen KW + aceton-concentraties in de stratosferische menglaag (de laag boven de tropopauze (de grens tussen de troposfeer en de stratosfeer) waar de invloed van de troposfeer het sterkst is) waren van dezelfde ordegrootte tijdens zomer en herfst (respectievelijk 2.3 $\pm$ 1.7 mol^{-9} mol^{-1} C (ppbC) en 2.2 $\pm$ 0.5 ppbC) en meer dan een factor twee hoger dan tijdens de winter periode (0.9 $\pm$ 0.3 ppbC).

Verhoogde concentraties van KW + aceton zijn gedurende juli veel dieper in de stratosfeer waargenomen dan tijdens maart (tot potentiële temperaturen van Θ = 370 K in juli en tot Θ = 340 K in maart). Dit is in overeenstemming met de hypothese dat er meer uitwisseling van de troposfeer naar de lagere stratosfeer plaatsvindt in de zomer dan in de winter. Uit modelstudies blijkt dat deze uitwisseling in de zomer met name sterker is aan de subtropische tropopauze, samenhangend met de Aziatische en Mexicaanse moessoncirculaties. Bewijs hiervoor wordt geleverd door verhoogde CH_3Cl-concentraties, die gedurende juli hoog in de stratosfeer zijn waargenomen. CH_3Cl vertoont namelijk een sterke positieve concentratiegradiënt in de troposfeer in de richting van de evenaar, omdat de grootste bronnen zich in de tropen bevinden.

De relatief hoge acetonconcentraties in vergelijking tot de KW die zijn waargenomen in de lagere stratosfeer (tot ~1 ppbv), met name tijdens de zomer, onderstrepen het belang van natuurlijke acetonbronnen (vegetatie en oceanen) in het acetonbudget van de hogere troposfeer. De fotolyse van aceton kan een belangrijke bron zijn van OH- en HO_2-radicalen (de belangrijkste oxidanten in de atmosfeer) in de hogere troposfeer en lagere stratosfeer. Berekeningen met een chemisch 1D “box-model” geven aan dat de waargenomen aceton niveau’s van 0.5 tot 1 ppbv tussen de 30% en 50% van de OH radicaal concentraties tijdens de zomer in de lagere stratosfeer kunnen verklaren.

Op basis van massa-evenwichtsberekeningen aan de hand van stabiele sporengasprofielen kunnen we aantonen dat een significante troposferische fractie (≤ 30%) (lucht met een troposferische signatuur) tot diep in de lagere stratosfeer kan worden waargenomen (tot Θ = 370 K) in tegenstelling tot de wintersituatie, waar de lucht gemiddeld een veel oudere signatuur heeft. Dit geeft wederom aan dat er gedurende de zomer meer troposfeer-naar-stratosfeer-transport plaatsvindt.

Er wordt een eenvoudige methode gedemonstreerd om de fotochemische leeftijd te schatten van een troposferisch luchtpakketje, dat recentelijk in de stratosfeer is ingemengd. De methode maakt gebruik van de oxidatieve afbraak van de reactieve KW propaan en acetyleen in de lagere stratosfeer, met een fotochemische levensduur van enkele weken tijdens de zomer. De concentratie van deze stoffen in de lagere stratosfeer wordt bepaald door de bronconcentratie in de hogere troposfeer, de mate van menging en fotochemische levensduur van deze stoffen in de stratosfeer (afhankelijk van de OH-concentratie). De methode geeft een indicatie van de tijdschalen van troposfeer-naar-stratosfeer-uitwisseling, door een schatting te maken van de tijd tussen het moment van menging en de waarneming met het meetvliegtuig. Op basis van een aantal waargenomen verhoogde acetyleen- en propaanconcentraties in de lagere stratosfeer tussen de 25 – 80 pptv (ruim boven hun detectielimiet van ~5 pptv), zijn leeftijden bepaald van 3 tot 14 dagen voor gemengde lucht in de lagere stratosfeer. Deze bevindingen bevestigen de resultaten van eerdere studies en tonen aan dat de lagere stratosfeer gedurende de zomer onderhevig is aan frequente en intensieve menging met troposferische lucht (in tegenstelling tot de winter).

Hoofdstuk 3 van dit proefschrift concentreert zich op de uitstroom van vervuilde lucht uit India en Zuidoost Azië die tijdens de 1999 “Indian Ocean Experiment” (INDOEX) campagne is waargenomen boven de Indische Oceaan (onderzoeksdoel 5). Er worden metingen gepresenteerd van C_2 – C_6 KW en geselecteerde Cl-KW uit canister-luchtmonsters, die met de Nederlandse Cessna Citation zijn verzameld boven de noordelijke Indische Oceaan gedurende februari en maart 1999 opererend vanuit de Malediven. Het hoofddoel van de INDOEX campagne betrof het verbeteren van de kennis van de belangrijke en sterk

toenemende rol die emissies uit Azië spelen in de mondiale atmosferische chemie en luchtkwaliteit.

Het onderzoek in dit proefschrift richt zich op de bronnen van sterk verhoogde concentraties van reactieve Cl-KW en dan met name op CH_3Cl, de belangrijkste natuurlijke organische chloorcomponent in de atmosfeer. De best gekwantificeerde grote bronnen van CH_3Cl zijn de oceanen en biomassaverbranding. De schattingen van mondiale emissies van CH_3Cl, met name in de tropen, zijn nog steeds onnauwkeurig, onder andere door gebrek aan waarnemingen. We hebben sterk verhoogde concentraties van CH_3Cl en aanverwante sporengassen (CO, KW en CH_3CN) gerelateerd aan biomassaverbranding waargenomen in de marine grenslaag boven de Indische Oceaan. We schrijven dit toe aan het intensieve gebruik van biomassabrandstoffen, zoals restproducten uit de landbouw en gedroogde mest (naast hout) voor huishoudelijk en klein-industrieel gebruik in India en Zuidoost Azië, met de nadruk op de inefficiënte verbranding en de relatief hoge chlorideconcentratie van deze biomassaproducten. Als een gevolg hiervan kan een relatief hoge emissieratio ten opzichte van CO ($\Delta CH_3Cl/\Delta CO$) worden afgeleid van $1.74 \pm 0.21 \times 10^{-3}$ mol mol^{-1}, in vergelijking tot de gemiddelde waarde van 0.57×10^{-3} mol mol^{-1}, die tot dusver gangbaar is in emissieschattingen van de omvang van wereldwijde biomassaverbranding. We tonen aan dat de bijdrage aan CH_3Cl-emissies door het gebruik van biomassa als brandstof mogelijk met 30 - 35% is onderschat voor emissies uit India en Zuidoost Azië.

De gecombineerde mondiale emissieschattingen voor CH_3Cl uit oceanen en biomassaverbranding (inclusief natuurlijke bronnen) kunnen slechts de helft van het totaal gemodelleerde budget van CH_3Cl in de atmosfeer verklaren (circa 4×10^{12} g $jaar^{-1}$). De andere helft moet nog bepaald worden (dit wordt verder behandeld in Hoofdstuk 5). Als we de INDOEX $\Delta CH_3Cl/\Delta CO$ emissiefactor naar mondiale schaal extrapoleren kunnen we ~14% van de nog niet bepaalde CH_3Cl-bronnen verklaren. Naast CH_3Cl emissies hebben we ook aanwijzingen gevonden voor geringe emissies van CH_2Cl_2 en $CHCl_3$ uit biomassaverbranding. Voor emissies van 1,1,1-trichloormethaan of methylchloroform (CH_3CCl_3) zijn geen aanwijzingen gevonden. De bevindingen in Hoofdstuk 3 vergroten ons inzicht in de belangrijke rol die emissies uit biomassaverbranding spelen in de mondiale budgetten van reactieve chloorkoolwaterstoffen.

In Hoofdstuk 4 wordt een grote verscheidenheid aan sporengasmetingen gepresenteerd die zijn verzameld met het Duitse Falcon straalvliegtuig (Deutsches Zentrum für Luft- und Raumfahrt, DLR) opererend vanuit Kreta boven het oostelijk Middellandse-Zeegebied tijdens de augustus 2001 “Mediterranean Intensive Oxidant Study” (MINOS) campagne. In termen van luchtkwaliteit blijkt het oostelijk Middellandse-Zeegebied een van de meest vervuilde regio’s op aarde te zijn. De MINOS campagne had dan ook tot doel ons inzicht te vergroten in de transportprocessen, de chemische mechanismen en de belangrijkste vervuilingsbronnen, die bepalend zijn voor de conditie van de atmosfeer in het oostelijk Middellandse-Zeegebied.

Deze studie richt zich de vrije troposfeer tussen de 6 en 13 km hoogte waarbij gebruik gemaakt wordt van 10-dagen terug-trajectoriën en een gekoppeld chemie-klimaatmodel (ECHAM4) om de herkomst van en de chemische samenstelling van de luchtmassa’s te onderzoeken. De vrije troposfeer wordt in belangrijke mate beïnvloed door lange-afstandstransport. We richten ons met name op een grote pluim van sterk vervuilde lucht die is waargenomen boven het oostelijk Middellandse-Zeegebied tussen 1 tot 12 augustus, die afkomstig is uit India en Zuidoost Azië, en die we de “Azië-pluim” noemen. Deze Azië-

pluim is het resultaat van grootschalig verticaal-transport tijdens de Aziatische moesson gevolgd door een sterke horizontale (anti-cyclonale) circulatie, die deze luchtmassa's van Azië naar het Middellandse-Zeegebied transporteert (onderzoeksdoelstelling 6). Aan de hand van verticale en longitudinale gradiënten van KW, Cl-KW, O_3, NO_y, CH_4, CO, CO_2, aceton, methanol, and CH_3CN hebben we de chemische invloed van de Azië-pluim op de troposfeer onderzocht en deze vergeleken met de westelijke stroming, die vervuilde lucht uit Noord-Amerika aanvoert (de zg. "Amerika-pluim"). In overeenstemming met eerdere bevindingen tijdens de INDOEX-campagne, vinden we wederom een sterke invloed van emissies van biomassaverbranding (met name door gebruik van biomassabrandstoffen) in verhoogde concentraties van CO, C_2H_2, C_6H_6, CH_3CN, en de Cl-KW CH_3Cl and $CHCl_3$. Acetonconcentraties zijn van dezelfde ordegrootte in de Azië-pluim als in de Amerika-pluim en zijn in beide gevallen sterk verhoogd ten opzichte van de achtergrond. Methanolconcentraties zijn duidelijk hoger in de Azië-pluim ten gevolge van emissies van biomassaverbranding. De gemiddelde fotochemische leeftijd van de Azië-pluim is geschat op circa 2 weken, in overeenstemming met trajectorie-analyses. De concentraties van HFC-134a, die voornamelijk voor auto-airco's wordt gebruikt ter vervanging van CFK-11, waren duidelijk lager in de Azië-pluim dan in de Amerika-pluim. Hieruit blijkt dat HFC-134a een geschikte indicator is voor vervuiling van Westerse, in dit geval Amerikaanse vervuiling. We hebben een sterke positieve correlatie gevonden tussen HFC-134a en CO_2 in de Amerikaanse pluim, die duidt op de grote rol van emissies van fossiele brandstoffen uit Noord-Amerika.

Ondanks de hoge concentraties aan O_3-precusors (CO en KW) in de Azië-pluim is de O_3-concentratie relatief laag (~55 ppbv) in vergelijking tot de Amerika-pluim. Er blijkt geen duidelijk verband te bestaan tussen de KW- en de O_3-concentraties, wat wijst op NO_x-gelimiteerde condities in de Azië-pluim (er is netto fotochemische O_3-vorming uit de oxidatie van CO en KW bij voldoende NO_x = NO en NO_2). Deze situatie zal in de toekomst waarschijnlijk veranderen. Modelsimulaties (ECHAM4) tonen aan dat de verwachte sterke toename van NO_x-emissies in Azië in de komende 20 jaar, ten gevolge van de sterke toename van het gebruik van fossiele brandstoffen, de fotochemische O_3-productie in de Azië-pluim met circa 14% kan doen toenemen. Gezien de omvang van de Azië-pluim en het feit dat O_3 een sterk broeikasgas is (het absorbeert langgolvige straling geëmitteerd vanaf het aardoppervlak) kan dit een aantoonbare invloed gaan hebben op de bijdrage van O_3 aan de stralingsforcering op het Noordelijk Halfrond (nu wordt de bijdrage van O_3 geschat op circa 25% ten opzichte van CO_2).

De omvang en locatie van de Azië-pluim tegen de tropopauze aan is een potentieel belangrijke bron voor transport van vervuilde lucht naar de stratosfeer (zoals beschreven in Hoofdstuk 2). We laten metingen zien, die inderdaad wijzen op horizontaal transport van vervuilde lucht uit de Azië-pluim naar de stratosfeer. Dit is een belangrijk onderwerp voor toekomstig onderzoek.

Aansluitend op Hoofdstuk 2 wordt de rol van tropische emissies in de budgetten van de reactieve Cl-KW CH_3Cl, CH_2Cl_2, $CHCl_3$ en C_2Cl_4 verder onderzocht in Hoofdstuk 5 van dit proefschrift. De bijdrage van natuurlijke bronnen aan de wereldwijde budgetten van deze componenten is tot dusver nog maar nauwelijks onderzocht. In dit hoofdstuk presenteren we metingen van KW en Cl-KW in de atmosfeer boven het regenwoud van Suriname uit de "Large-scale Biosphere-atmosphere experiment in Amazonia – Cooperative LBA Airborne Regional Experiment" (LBA/CLAIRE) campagne in maart 1998 (tijdens het droge seizoen).

De metingen zijn verricht aan canister-luchtmonsters, die zijn verzameld aan boord van de Nederlandse Cessna Citation. De meetresultaten zijn geanalyseerd met behulp van gelijktijdige metingen van CO, aceton en CH_3CN (als indicator voor biomassaverbranding).

De hoofddoelstelling van LBA/CLAIRE was om inzicht te krijgen in de mate van uitwisseling van gassen en deeltjes (aerosolen) tussen het uitgestrekte Amazoneregenwoud en de atmosfeer, die van belang zijn voor, onder andere, het ozonbudget in de tropen. We tonen aan dat de vrije troposfeer, op een hoogte van 8 km en hoger, sterk wordt beïnvloed door uitstroom van grenslaaglucht, tengevolge van diepe convectie in de Zuid-Amerikaanse moesson. De met de moesson samenhangende wolkenband lag een paar graden ten zuiden van Suriname. Een belangrijkere ontdekking is dat we een significante positieve gradiënt hebben waargenomen in de concentraties van CH_3Cl, $CHCl_3$ en C_2Cl_4 als functie van de tijd dat de lucht vanaf de Atlantische oceaan boven het oerwoud is geweest, zonder dat er aanwijzingen zijn voor sterke antropogene bronnen. Deze gradiënten wijzen op significante biogene bronnen uit het Surinaamse regenwoud, overeenkomstig recente inzichten in de literatuur over emissies van, met name, CH_3Cl uit tropische vegetatie. Er is geen gradiënt voor CH_2Cl_2 gevonden.

De positieve concentratiegradiënten zijn gebruikt om emissiefluxen te bepalen uit de 1500 m dikke grenslaag (overdag), die representatief zijn voor het Surinaamse regenwoud (als de som van emissies uit microbiologische bodemprocessen, de afbraak van hout door schimmels en directe emissies uit planten) ter grootte van 7.6 ± 1.8 μg CH_3Cl m^{-2} uur^{-1}, 1.11 ± 0.08 μg $CHCl_3$ m^{-2} uur^{-1} en 0.36 ± 0.07 μg C_2Cl_4 m^{-2} uur^{-1}. Geëxtrapoleerd naar mondiale schaal berekenen we een grote potentiële bron van CH_3Cl emissies uit tropische vegetatie ter grootte van $\sim 2 \times 10^{12}$ g $jaar^{-1}$. Deze hoeveelheid kan in zijn geheel het huidige gemis aan niet-geïdentificeerde CH_3Cl-bronnen in het mondiale CH_3Cl-budget verklaren (zie Hoofdstuk 3) en bevestigt dat tropische vegetatie de belangrijkste bron is van organisch chloor naar de atmosfeer. Daarnaast schatten we een potentiële mondiale emissie van C_2Cl_4 uit tropische bosbodems op $57 \pm 17 \times 10^9$ g C_2Cl_4 $jaar^{-1}$, wat gelijk staat aan de helft van de nog niet-gekwantificeerde bronnen van deze stof. Tenslotte laten we zien dat de afname van het tropisch regenwoud over de laatste 20 jaar (door houtkap) de waargenomen dalende trend van CH_3Cl in de atmosfeer over dezelfde periode kan verklaren.

Samenvattend presenteert dit proefschrift een unieke en uitgebreide dataset van KW en Cl-KW, die de beschikbaarheid van nauwkeurige metingen in de troposfeer (met name in de tropen) en lagere stratosfeer sterk vergroot. De KW en aceton metingen uit STREAM verbreden ons begrip ten aanzien van de rol van reactieve organische componenten in de lagere stratosfeer, met name met betrekking tot het OH-radicaal budget. Verder is duidelijker geworden wat de tijdschalen zijn van horizontaal troposfeer-naar-stratosfeer-transport en wat het belang is van dit transport voor de samenstelling van de lagere stratosfeer. De invloed van de Azië-pluim op de samenstelling van de vrije troposfeer op een hemisferische schaal is beschreven en geanalyseerd. Tenslotte is er een belangrijke bijdrage geleverd aan onze kennis ten aanzien van de rol van tropische bronnen in de wereldwijde budgetten van chloorkoolwaterstoffen.

Acknowledgements

Dear Friends and Colleagues,

This is were I lay down my pen and look back on a wonderful time of campaigning, thrilling science and good team spirit. First of all, I'm greatful to Jos Lelieveld (promotor) and Geert-Jan Roelofs (co-promotor), they encouraged me and assisted me in writing up most of this work over the past one-and-a-half year. In addition, I would like to especially thank Horst Fischer, Jonathan Williams, and Laurens Ganzeveld from the MPI-Mainz for many helpfull discussions and for the compassion and interest they showed in my work. I would like to acknowledge Hillion Wegh who set-up first GC-system at Wageningen University in 1994 and was involved with the analyses of the STREAM and LBA/CLAIRE canisters. Later, this work has been continued by Carina van der Veen at IMAU (Utrecht University) for the INDOEX and MINOS campaigns. Michel Bolder has been the mastermind and constructor of the canister sampling system. Without the work of Hillion, Carina, and Michel the research in this thesis would not have been possible.

I think that I could write an additional very thick and funny book based on all the adventures we experienced together with the "STREAM-team" at Schiphol, in the Arctic skies (SHREDDER 1 to tower..), in the Surinam bush, in "outback" Timmins with its rich nightlife (..), on the "pancake" islands of the Maldives. I won't do that here, but I'm sure that I will never forget the wonderful and pioneering campaigns we did as the STREAM-team with the Dutch Citation and later as the "MINOS-team" with the German Falcon on "raki-planet"-Crete.

Campaigning will move on with bigger aircrafts and more sophisticated measurement techniques. I wish everybody in the field the best of luck and good fun with future campaigning. Keep up the team spirit and let us bring a toast (with a good glass of "optical cleaning liquid") to the health of the unforgettable Dr. Parbo and Prof. Matagami !

Ik dank alle IMAU-ers en in het bijzonder mijn collega-chemici voor een geweldige tijd. Ook denk ik nog vaak met bijzonder veel genoegen terug aan de jarenlange samenwerking met de Faculteit Lucht- en Ruimtevaarttechniek aan de TUD (van de Cessna). Bedankt Kees, Cor, Jaap, Hessel, Tjipke, Alwin, Bob en iedereen die ik verder nog vergeten ben.

Rest mij nog om Agnes een dikke kus te geven.

Curriculum Vitae

I was born on March 12, 1966 in Leiden, the Netherlands. I studied at Wageningen University between 1985 and 1991, where I graduated (M.Sc.) in Organic Chemistry (Dr. T. Van Beek and Prof. A. de Groot) and Air Quality (Prof. E. Adema). During my study, I spent five months (in 1991) at the 'Consiglio Nazionale delle Ricerche (CNR) – Istituto sull'Inquinamento Atmosferico' (Institute for Atmospheric Pollution), Rome, Italy. At the CNR, I worked on the development and application of passive measurement techniques for monitoring ozone (O_3) and sulfur dioxide (SO_2) under supervision of Dr. I. Allegrini and Dr. F. De Santis. After my graduation, I spent another 4 months at the CNR as a researcher. From the beginning of 1992 until mid 1993, I joined the group of Prof. S. Slanina at the environmental department of the Energy research Center of the Netherlands (ECN), Petten (Noord-Holland). At the ECN, I was first involved in a study on the effects of aircraft emissions on the atmosphere. After that, I worked a year on the development of wet-chemical measurement techniques (e.g., wet denuder techniques) for monitoring dry and wet acid deposition. By the end of 1993, I joined the group of Prof. J. Lelieveld at the Air Quality Department of Wageningen University (WU) until 1996, and thereafter at the Institute for Marine and Atmospheric research Utrecht (IMAU) at Utrecht University. Under Prof. Lelieveld, I was project-coordinator of several aircraft measurement campaigns (STREAM 1994-1998, ACE-2 1997, LBA-CLAIRE 1998, INDOEX 1999) conducted with the Dutch Cessna Citation II (PH-LAB). In addition, I was involved in the development and application of measurement techniques for airborne monitoring of ozone and air sampling for post-flight analysis (GC-FID/ECD) on non-methane-hydrocarbons and halocarbons. From the beginning of 2000 to 2002, I was employed as an atmospheric chemistry researcher at the IMAU, co-funded by Utrecht University and the Max-Planck-Institute for Chemistry (MPI-C), Mainz, Germany. During the summer of 2001, I participated in the MINOS campaign, where I was responsable for hydrocarbon and halocarbon trace gas measurements in air samples collected onboard the German Falcon aircraft. From the beginning of 2002, I worked on this thesis under supervision of Prof. J. Lelieveld, by then director of the MPI-C, and Dr. G.-J. Roelofs from the IMAU.